



저작자표시-비영리-변경금지 2.0 대한민국

이용자는 아래의 조건을 따르는 경우에 한하여 자유롭게

- 이 저작물을 복제, 배포, 전송, 전시, 공연 및 방송할 수 있습니다.

다음과 같은 조건을 따라야 합니다:



저작자표시. 귀하는 원저작자를 표시하여야 합니다.



비영리. 귀하는 이 저작물을 영리 목적으로 이용할 수 없습니다.



변경금지. 귀하는 이 저작물을 개작, 변형 또는 가공할 수 없습니다.

- 귀하는, 이 저작물의 재이용이나 배포의 경우, 이 저작물에 적용된 이용허락조건을 명확하게 나타내어야 합니다.
- 저작권자로부터 별도의 허가를 받으면 이러한 조건들은 적용되지 않습니다.

저작권법에 따른 이용자의 권리는 위의 내용에 의하여 영향을 받지 않습니다.

이것은 [이용허락규약\(Legal Code\)](#)을 이해하기 쉽게 요약한 것입니다.

[Disclaimer](#)

공학박사학위논문

**Integrated Earthquake Hazard
Assessment System with
Geotechnical Spatial Grid
Information Based on GIS**

GIS 기반 지반공학적 공간그리드 정보를
활용한 지진재해평가 통합시스템

2014년 8월

서울대학교 대학원

건설환경공학부

김 한 샘

Integrated Earthquake Hazard Assessment System with Geotechnical Spatial Grid Information Based on GIS

지도 교수 정 충 기

이 논문을 공학박사 학위논문으로 제출함
2014 년 7 월

서울대학교 대학원
건설환경공학부
김 한 샘

김한샘의 공학박사 학위논문을 인준함
2014 년 6 월

위 원 장 _____ 김 명 모 _____ (인)

부위원장 _____ 정 충 기 _____ (인)

위 원 _____ 박 준 범 _____ (인)

위 원 _____ 선 창 국 _____ (인)

위 원 _____ 김 현 기 _____ (인)

Abstract

Integrated Earthquake Hazard Assessment System with Geotechnical Spatial Grid Information Based on GIS

Kim, Han Saem

Department of Civil & Environmental Engineering

The Graduate School

Seoul National University

Historically, the Korean peninsula has been regarded as a safe region with respect to the hazard of earthquakes due to the characteristics of its seismotectonic location, being classified as a region of moderate seismicity. However, the number of earthquake events keeps increasing every year, and the recent cases of earthquake hazards invoke the necessity of seismic study in Korea, as geotechnical earthquake hazards, such as strong ground motion, liquefaction and landslides, are a significant threat to structures in port or downtown areas built on seismically vulnerable loose and saturated sandy soils. Therefore, a seismic disaster management system (platform) is required to establish effective and appropriate strategies to reduce earthquake hazards.

In this study, an integrated earthquake hazard assessment system with geotechnical spatial grid information was developed based on a geographic

information system (GIS). The developed system built, within the frame of GIS, consists of a database (DB) containing all site information and processed data in the system in the standard data formats, and the system software performing various functions to manage and utilize the data in the database. The system software is functionally divided into an input module, a geostatistical three-dimensional (3D) integration module, a real-time earthquake hazard assessment module, and output or visualization module. The database and these modules of the system software were combined and integrated into a single system to provide a familiar and user-friendly working environment with a standard interface. In addition, the integrated system was imbedded into a Korea Integrated Seismic System (KISS) server to be linked with real-time seismic accelerations.

DB is the backbone of the developed framework. It stores not only primary data such as geography, geotechnical investigation results, man-made structures, and seismic monitoring data which are transmitted in real time from a seismometer server (at KISS), but also secondary data obtained from a geostatistical 3D integration module and real-time earthquake hazard assessment module. It contains alphanumeric datasets according the outcome of data classification and standardization with a geodatabase (GDB). The data stored in the database can be easily utilized in this framework.

Input function provides an effective way to store and organize all collected field data, including electric or non-electric documents, geographic and geotechnical investigations, man-made structures, seismic monitoring, and analysis data, according to a standard data format based on GDB.

Geotechnical spatial grids in the 3D domain are constructed for target

sites with geostatistical methods in a process known as geostatistical 3D integration. This method has three functional modules with the database: an outlier detection module, a geostatistical integration module, and geotechnical spatial grid construction module. Geotechnical investigation results always reflect the level of soil uncertainty. To handle this uncertainty, the outlier detection methods, which optimize the borehole datasets, are conducted. The geostatistical integration method based on indicator kriging is performed using optimized borehole datasets and digitized geophysical tomography results to construct 3D geo-layers. The 3D geo-layers are categorized and subdivided into representative soil profiles with dynamic properties to add 3D geotechnical spatial grid to the database. This step must be conducted as a baseline prior to the occurrence of earthquakes.

The real-time framework for integrated earthquake hazard assessment with geotechnical spatial grid information has three functional modules with the database: a real-time seismic load determination module, a real-time liquefaction hazard estimation module, and a real-time structure fragility evaluation module. In the first, linked with the 3D geotechnical spatial grid, correlations between rock outcrop accelerations and the maximum accelerations of each layer considering the site response characteristics are predetermined. Thus, as earthquake events occur, as soon as monitored rock outcrop acceleration data are transmitted from the accelerometer, the seismic load at each spatial grid is estimated. In the second, the potential damage due to liquefaction is estimated by combining the geotechnical spatial grid and correlated maximum acceleration of each layer based on the simplified liquefaction potential index (LPI) evaluation method in real time. Finally, in

the third, the possibility of structure failure is evaluated by the integration of the geotechnical spatial grid and correlated maximum acceleration based on the structure fragility curve in real time.

The output and visualization module displays all attributive information in the database using tables and graphics according to its characteristics. Also, all data in the database can be output as a chart or a graphic. The graphic functions, such as 2D plane view, 2D sectional view, and 3D view display, interpolated data are shown in several display formats at same time. Specifically, the earthquake hazard assessments results are visualized to 2D or 3D GIS-maps with satellite images, and the seismic damage (composed of the seismic load, liquefaction potential, and structural fragility) of the target structure can be calculated using zonation criteria in real time.

A simulation of the developed system was specifically conducted at Busan port, Korea, using two virtual earthquake scenarios (Uljin and Tohoku Earthquakes) and two actual earthquake events (2013 Baengnyeong and 2014 Taean Earthquakes) of the Incheon port. The simulation results are visualized as a geotechnical earthquake hazard map to verify the computer-aided real-time assessment framework. A verification test of the integrated system was also performed for the Incheon port using data actually transmitted from the accelerometer of the KISS server when two notable earthquake events occurred at the nearby Incheon port.

Keywords: Integrated system, GIS, Real-time earthquake hazard assessment, Outlier detection, Geostatistical 3D integration, Geotechnical spatial grid, Site-specific seismic response, Liquefaction hazard, Structure fragility

Student Number: 2008-21020

TABLE OF CONTENTS

Abstract	i
TABLE OF CONTENTS.....	vi
LIST OF TABLES	x
LIST OF FIGURES	xiv
LIST OF SYMBOLS	xxi
1 . Introduction.....	1
1.1 Background	1
1.2 Objectives	4
1.3 Structure of Dissertation	7
2 . Literature Review	11
2.1 Introduction.....	11
2.2 Geotechnical Information System.....	13
2.2.1 Geographic information system	13
2.2.2 Geotechnical outliers and detection methodologies	17
2.2.3 Geostatistical interpolation methodologies	24
2.2.4 Previous geotechnical information systems	31
2.3 Earthquake Hazard Management System	44
2.3.1 Earthquake hazard assessment approaches	44
2.3.2 Previous Earthquake hazard management systems	49
2.4 Summary	61

3 . Real-time Framework for Earthquake Hazard

Assessment	63
3.1 Concept of Real-time Framework for Earthquake Hazard Assessment.....	63
3.1.1 Real-time framework procedure.....	63
3.1.2 Methodologies for real-time earthquake hazard assessment	66
3.2 Systematic Database for Integrated Framework	70
3.2.1 Database schema of integrated framework	70
3.2.2 Detailed information of database	72

4 . Geostatistical 3D Integration for Geotechnical Spatial

Grid	74
4.1 Construction Procedure of Geotechnical Spatial Grid.....	74
4.2 Outlier Analysis of Borehole Datasets	76
4.2.1 Proposed outlier detection methods to soil stratification	70
4.2.2 Verification of suggested methods.....	83
4.3 Geostatistical 3D Intergration of Borehole and Geophysical Datasets	90
4.3.1 Geostatistical integration procedure of geotechnical datasets	90
4.3.2 Optimization of borehole datasets using outlier detection methods.....	95
4.3.3 Assumption of geomaterial classification criteria	99
4.3.4 Indicator kriging to construct the three-dimensional stratified geo-layers	103
4.3.5 Verification of the assumed classification criteria using cross-validation.....	108
4.4 Geotechnical 3D Spatial Grid Construction	114

4.4.1 Representative soil profiles	114
4.4.2 Representative dynamic properties	118
4.5 Summary and Conclusions	120
5 . Real-time Earthquake Hazard Assessment.....	123
5.1 Systematic Procedure for Real-time Earthquake Hazard Assessment.....	123
5.2 Real-time Seismic Load Determination.....	125
5.2.1 Real-time seismic load determination method	125
5.2.2 Preceded site response analysis.....	129
5.2.3 Statistical correlation for seismic load	133
5.3 Real-time Liquefaction Hazard Estimation	137
5.4 Real-time Structure Fragility Evaluation.....	143
5.4.1 Fragility curve for structure.....	143
5.4.2 Real-time fragility evaluation method.....	145
5.5 Summary and Conclusions	150
6. Integrated System for Real-time Earthquake Hazard Assessment.....	152
6.1 System Design	152
6.1.1 System requirements	153
6.1.2 System overview	155
6.1.3 Database design.....	158
6.1.4 Database structure	160
6.2 Program for System Modules	173
6.2.1 Management program	173

6.2.2 Input module	176
6.2.3 Geostatistical 3D integration module	184
6.2.4 Real-time earthquake hazard assessment module	187
6.2.5 Output and visualization modules	191
6.3 Summary and Conclusions	196
7 . Application and Verification of System	198
7.1 Simulation Condition	198
7.2 Geotechnical Spatial Grid	204
7.3 Spatial Liquefaction Hazard	218
7.4 Structure Fragility	220
7.5 Verification of System.....	224
7.5.1 Condition of verification	224
7.5.2 Verification results	226
7.6 Summary and Conclusions	230
8 . Conclusions and Recommendations	231
8.1 Conclusions.....	231
8.2 Recommendations.....	235
References.....	238
Appendices	255
A.1 Detailed Standard Data Format of Database.....	251
A.2 Detailed Management module of geotechnical investigation information.....	287

LIST OF TABLES

Table 3.1 Database schema of integrated framework based on geodatabase platform	71
Table 3.2 Procedure for substitution of geotechnical datasets based on digital elevation model (DEM).....	73
Table 4.1 Root mean squared errors of each estimation for the validation points	89
Table 4.2 Conventional geomaterial classification criteria based on P-wave velocity V_P	94
Table 4.3 Assumed geomaterial classification criteria with P-wave velocity	101
Table 4.4 Representative dynamic properties by soil type	119
Table 5.1 General information and acceleration data of input earthquake motions	131
Table 5.2 Deviation of correlated acceleration with frequency from field application results based on the geotechnical spatial grid	137
Table 5.3 Criteria for liquefaction severity categories assessed by the LPI	142
Table 5.4 Definition of damage levels of seismic fragility curves for gravity quay wall (KORDI, 2013)	144
Table 5.5 Definition of damage levels of seismic fragility curves for gantry crane (KORDI, 2013)	145
Table 5.6 Definition of damage levels of seismic fragility curves for unreinforced concrete structure (FEMA, 2003).....	145
Table 5.7 Seismic damage levels of gravity quay wall.....	148
Table 5.8 Seismic damage levels of gantry crane.....	149
Table 5.9 Seismic damage levels of unreinforced concrete structure.....	149
Table 6.1 Environment of system development.....	159

Table 6.2 Types of geographic information in the developed system.....	163
Table 6.3 Type of geodatabase for geotechnical investigation information.....	164
Table 6.4 Type of geodatabase for structure information	164
Table 6.5 Type of geodatabase for seismic monitoring information.....	165
Table 6.6 Type of geodatabase for geostatistical 3D integration results...	165
Table 6.7 Type of geodatabase real-time earthquake hazard assessment results.....	165
Table 6.8 Details of the T_Site table.....	166
Table 6.9 Tables for geotechnical investigation information in the developed system.....	168
Table 6.10 Tables for structure information in the developed system	169
Table 6.11 Data format of earthquake event according to KISS	170
Table 6.12 Tables for seismic monitoring information in the developed system	170
Table 6.13 Tables for geotechnical spatial grid information in the developed system.....	171
Table 6.14 Tables for real-time earthquake hazard information in the developed system.....	172
Table 7.1 General information and acceleration-time histories for simulation	202
Table 7.2 Typical ground stratification of the target site with classifications of each soil strata based on the borehole data.....	203
Table 7.3 Earthquake events information and measured results (Reference: Korea Meteorological Administration).....	226
Table A.1 Details of the T_Borehole_Info table.....	256
Table A.2 Details of the T_Layer table.....	257
Table A.3 Details of the T_SPT table	258
Table A.4 Details of the T_RQD table.....	258
Table A.5 Details of the T_CPT table.....	259

Table A.6 Details of the T_CPTu table.....	260
Table A.7 Details of the T_CPTu_Data table	261
Table A.8 Details of the T_FVT table.....	261
Table A.9 Details of the T_FVT_Data table	262
Table A.10 Details of the T_Vs table.....	262
Table A.11 Details of the T_CTX table	263
Table A.12 Details of the T_RC table.....	263
Table A.13 Details of the T_RC_Data table	264
Table A.14 Details of the T_Borehole_Sum table	264
Table A.15 Details of the T_Test table.....	266
Table A.16 Details of the T_Test_Info table.....	267
Table A.17 Details of the T_Test_Data table	268
Table A.18 Details of the T_Geophysical_Info table.....	269
Table A.19 Details of the T_Geophysical_Result table.....	269
Table A.20 Details of the T_Geophysical_Tomography table.....	270
Table A.21 Details of the T_Structure_Info table.....	272
Table A.22 Details of the T_Structure_Shape table.....	273
Table A.23 Details of the T_Seismological_Observatory table.....	274
Table A.24 Details of the T_Seismic_Monitoring table	275
Table A.25 Details of the T_Earthquake_Event table.....	275
Table A.26 Details of the T_Indicator_kriging table	276
Table A.27 Details of the T_3D_GeoLayer table	277
Table A.28 Details of the T_Geotechnical_Spatial_Grid table.....	278
Table A.29 Details of the T_Corr_Eq table	279
Table A.30 Details of the T_Corr_Graph table.....	280
Table A.31 Details of the T_Shake table	281
Table A.32 Details of the T_Corr_PGA table	281
Table A.33 Details of the T_Corr_layer_PGA table	281
Table A.34 Details of the T_CRR table	282

Table A.35 Details of the T_CSR table.....	283
Table A.36 Details of the T_FS_Liquefaction table	283
Table A.37 Details of the T_LPI table	283
Table A.38 Details of the T_Fragility table	284
Table A.39 Details of the T_Fragility_Grade table.....	285
Table A.40 Details of the T_Fragility_Damage table	285
Table A.41 Details of the T_Integrated_Damage table.....	286

LIST OF FIGURES

Figure 1.1 Schematic flow of integrated earthquake hazard assessment system with geotechnical spatial grid information	6
Figure 2.1 GIS architectures (Esri, 2006).....	15
Figure 2.2 GIS data in the geodatabase (GDB) (Esri, 2006)	16
Figure 2.3 Taxonomy of previous outlier detection methodologies	20
Figure 2.4 Distribution-based method.....	21
Figure 2.5 Definition of the polygonized spatial units for the Moran scatterplot method.....	23
Figure 2.6 Moran scatterplot for the testing data.....	24
Figure 2.7 Concept of typical geostatistical analysis methods (Clayton and Andre, 1997).....	31
Figure 2.8 Map panel in GeoLibrary (Jankowski et al., 2001).....	33
Figure 2.9 GeoFrance 3D client interface for spatial query and visualization (Guillen et al., 2001)	33
Figure 2.10 Visualization example of 3D model in GeoFrance 3D (Guillen et al., 2001).....	34
Figure 2.11 Interactive creation of SPOT image overlaid on terrain surface (Huang and Lin, 2002).....	34
Figure 2.12 System architecture diagram for GeoInfoSys (Kunapo et al., 2005).....	35
Figure 2.13 Main web interface of GeoInfoSys (Kunapo et al., 2005)	36
Figure 2.14 History of development of Gibase	38
Figure 2.15 Locations of boreholes for sampling and soil testings in Gibase39	
Figure 2.16 Main screen of GeoInfo.....	40
Figure 2.17 Management program of IMSSG (Chun et al., 2005).....	41

Figure 2.18 Schematic flow-chart for 3D modelling through data integration (Andrea et al., 2009).....	43
Figure 2.19 Systematic procedure of HAZUS (FEMA, 2003).....	50
Figure 2.20 Flowchart for the integrated earthquake damage assessment methodology (Cinicioglu et al., 2007).....	52
Figure 2.21 Framework of hazard analysis, risk assessment and loss estimation methodology in TELES.....	54
Figure 2.22 Approach for assessing the accuracy of individual modules of REDARS	55
Figure 2.23 Process of UrEDAS.....	56
Figure 2.24 Analysis report of ANSS	58
Figure 2.25 An example of NDMS.....	60
Figure 3.1 Schematic concept for real-time assessment of the geotechnical earthquake hazard based on GIS.....	65
Figure 3.2 Integrated framework with geotechnical earthquake hazard assessment procedures	69
Figure 3.3 Substitution of geotechnical datasets using borehole before earthwork (ex. reclamation).....	73
Figure 4.1 Construction procedure of geotechnical spatial grid.....	76
Figure 4.2 Photograph of the testing site and the borehole locations	78
Figure 4.3 Variogram of the original data based on the exponential model	79
Figure 4.4 The measured soil depth to the bedrock vs. the estimated values by the cross-validation method.....	80
Figure 4.5 Distribution of the defined subsets for the GEVD-based method	82
Figure 4.6 The cumulative distribution of the maximum values of the spatial subsets (solid dots) and the fitted GEVD curve (dotted line).....	83
Figure 4.7 Spatial distributions of the soil depth to the bedrock estimated with or without the suspected outlying measurements (red dots	

outlined bold line).....	86
Figure 4.8 The measured soil depth to the bedrock versus the estimated values by the outlier analysis.....	88
Figure 4.9 Flow diagram for computer-based geostatistical integration method for underground stratification with outlier analyses	91
Figure 4.10 Digital terrain map of the study area with locations of boreholes and seismic refraction wave tests at target site.....	93
Figure 4.11 Variogram of the original borehole datasets for depth to weathered rock and depth to soft rock.....	97
Figure 4.12 Cross-validation based outlier detection method for the depth values to (a) the weathered rock and (b) the soft rock from the boring data.....	99
Figure 4.13 Scatter plot for d_1 (borehole) versus $d_1(V_p)$ and d_2 (borehole) versus $d_2(V_p)$ at borehole locations.....	103
Figure 4.14 Example of indicator variogram for assumed $d_1(V_p = 1500 \text{ m/s})$ and $d_2(V_p = 2000 \text{ m/s})$ referenced from design specification A and B listed in Table 4.2	106
Figure 4.15 Example of two-dimensional spatial distribution of geomaterials for assumed $d_1(V_p = 1500 \text{ m/s})$ and $d_2(V_p = 2000 \text{ m/s})$ referenced from design specification A and B listed in Table 4.2	107
Figure 4.16 Locally-specified classification criteria of V_p for d_1 and d_2 ..	110
Figure 4.17 Three-dimensional spatial distribution of geomaterials and the cross-sectional view along the line A-A' with the verification borehole points	113
Figure 4.18 Conceptual components for the categorization and grouping of representative soil profiles with their dynamic properties.....	117
Figure 4.19 Subdivision for region occupied by structure of a higher grade of seismic capacity.....	118

Figure. 5.1 Systematic procedure architecture for real-time earthquake hazard assessment.....	125
Figure 5.2 Procedure for real-time seismic load determination classified into the database, preceded site response analysis and nonlinear optimization of a regression model to compute seismic loads in real-time.....	128
Figure 5.3 An example of correlation between the rock outcrop acceleration and maximum acceleration of each layer based on the nonlinear optimization of a regression model at particular cell (classified into SP according to the USCS) of the specific geotechnical spatial grid (Grid ID: 1).....	135
Figure 5.4 Procedure for real-time liquefaction hazard estimation	138
Figure 5.5 Procedure for real-time fragility evaluation method	146
Figure 5.6 An example of fragility curve and damage state for unreinforced concrete structure modified from FEMA (2003)	148
Figure 6.1 System overview	156
Figure 6.2 Key data classes and relations of the GDB for the developed system: Primary information	161
Figure 6.3 Key data classes and relations of the GDB for the developed system: Processed information	162
Figure 6.4 Systematic procedure of real-time earthquake hazard assessment according to system program.....	174
Figure 6.5 Main management program and detailed function.....	175
Figure 6.6 Management module of site information	177
Figure 6.7 Management module of borehole information.....	178
Figure 6.8 Management module of geophysical testing information	179
Figure 6.9 Management module of structure information–structure resource information	180
Figure 6.10 Management module of structure information–design report	

information	181
Figure 6.11 Management module of seismic monitoring information– seismological observatory information.....	182
Figure 6.12 Management module of seismic monitoring information– seismic monitoring information.....	183
Figure 6.13 Management module of seismic monitoring information– earthquake event information	184
Figure 6.14 Geostatistical 3D integration module–construction of geotechnical spatial grid	186
Figure 6.15 Geostatistical 3D integration module–indicator kriging	187
Figure 6.16 Automated real-time earthquake hazard assessment wizard module	188
Figure 6.17 Real-time seismic load determination module	189
Figure 6.18 Real-time liquefaction hazard estimation module.....	190
Figure 6.19 Real-time structure fragility evaluation module.....	191
Figure 6.20 3D visualization module–geotechnical spatial grid.....	193
Figure 6.21 3D visualization module– V_s	194
Figure 6.22 Real-time earthquake hazard reporting module	195
Figure 7.1 Simulation conditions for earthquake scenarios for the Busan port, Korea.....	199
Figure 7.2 Condition of geotechnical spatial grid for the target port. 156 cells (13×12 cells) of the geotechnical spatial grid.....	205
Figure 7.3 Two-dimensional spatial distribution of the geotechnical characteristics based on the geotechnical spatial grid for the study area of Busan port	208
Figure 7.4 Three-dimensional projected figure with cross sectional view for the current ground conditions based on the geotechnical spatial grid in the study area.....	211
Figure 7.5 Three-dimensional projected figure with cross sectional view for	

the current ground conditions based on the geotechnical spatial grid combined with the amax calculated based on real-time seismic load correlation equation for the Uljin earthquake scenario in the study area.....	213
Figure 7.6 Three-dimensional projected figures with cross sectional view for the current ground conditions based on the geotechnical spatial grid combined with the results of real-time liquefaction hazard estimation for the Uljin earthquake scenario in the study area.....	217
Figure 7.7 Liquefaction severity zonation maps for the target port for two earthquake scenarios.....	219
Figure 7.8 An example of seismic fragility curve of 50t-gantry crane modified from KORDI (2013).....	221
Figure 7.9 Structure fragility zonation maps of <i>Near collapse</i> damage level for the target port for two earthquake scenarios	223
Figure 7.10 Verification tests conditions for earthquake scenarios for the Incheon port, Korea.	225
Figure 7.11 Earthquake event map (Reference: Korea Meteorological Administration).....	226
Figure 7.12 Liquefaction severity zonation maps for two earthquake events	227
Figure 7.13 Structure fragility zonation maps of <i>Slight</i> damage level for the two earthquake events.....	229
Figure A.1 Management module of geotechnical investigation information– Geo-layer information	288
Figure A.2 Management module of geotechnical investigation information– SPT and RQD/TCR information.....	289
Figure A.3 Management module of geotechnical investigation information– CPT and CPTu information	290
Figure A.4 Management module of geotechnical investigation information–	

FVT information	291
Figure A.5 Management module of geotechnical investigation information– shear wave velocity test information	292
Figure A.6 Management module of geotechnical investigation information– cyclic triaxial test information	293
Figure A.7 Management module of geotechnical investigation information– Resonance column test information.....	294
Figure A.8 Management module of geotechnical investigation information– engineering parameters.....	295
Figure A.9 Management module of geotechnical investigation information– user-defined test information	296
Figure A.10 Management module of geotechnical investigation information–geophysical test condition information.....	297
Figure A.11 Management module of geotechnical investigation information–geophysical tomography information	298

LIST OF SYMBOLS

English

a	Effective range of a variogram model
a	ground acceleration
a_i	Coefficient of drift polynomial
a_{max}	Maximum acceleration of each layer
a_{rock}	Rock outcrop acceleration
C_i	Strength of the structure for damage level i
c_1	Attenuation coefficient
c_2	Attenuation coefficient
c_3	Attenuation coefficient
D	Effect of the load by an earthquake
d_1	Depth to weathered rock
d_2	Depth to soft rock
$d_1(\text{borehole})$	Depth to weathered rock with optimized borehole
$d_2(\text{borehole})$	Depth to soft rock with optimized borehole
$d_1(V_P)$	Depth to weathered rock with P-wave velocity
$d_2(V_P)$	Depth to soft rock with P-wave velocity
d_{i0}	Distance between the prediction and measured locations
dz	Increment of depth
$E[(x)]$	Mathematical expectation

f	Function
$F(z)$	Weighting function with $FS_{\text{liquefaction}}$
h	Lag distance
$i(u; s_k)$	Indicator at location u for category s_k
L	Lag distance
$m(x)$	Local drift
N	Number of measured points
$(N_1)_{60}$	N value corrected for hammer efficiency and the effective overburden stress
$N(h)$	Number of lag distance
P	Parameter
$P_f(s)$	Damage probability of structure at s
PF_{ij}	Probability of exceeding i level for the earthquake in the intensity of j
R	Epicentral distance
$R(x)$	Residual between $Z(x)$ and drift $m(x)$ at x point
s	PGA of the earthquake
\bar{s}	Median of PGA at ground surface
S_a	Spectral acceleration
S_d	Spectral displacement
s_k	particular category for the categorical variable $S(u)$
u	Given spatial location
V_P	P-wave velocity
$(V_P)_{cr}$	Conventional classification criteria of P-wave velocity
$(V_P)_I$	V_P between the weathered soil and the weathered rock

$(V_P)_2$	V_P between the weathered rock and the soft rock
V_S	Shear wave velocity
w_{ij}	Spatial weight matrix
$W(z)$	Weighting function with depth
$X(x)$	Random field
x_i	Measured value
\hat{x}_i	Estimated value by kriging
z	Depth (0–20 m)
z_i	Standardized measurement
$z_{i_neighborhood}$	z_i of the neighboring spatial units
$Z(x_0)$	Predicted value for location x_0
$Z(x_i)$	Measured value at location x_i

Greek

α	Correlation coefficient
β	Correlation coefficient
β	Standard deviation of log value of PGA at ground surface
κ	Function parameter
σ	Function parameter
σ_v	Total vertical stress
σ_v'	Effective vertical stress
μ	Function parameter
γ_d	Stress reduction factor
$\gamma(h)$	Variogram value at lag distance h
λ_i	Weight assigned to measured points
β_k	Unknown weights
$\Phi[]$	Gaussian cumulative log-normal distribution function

Abbreviation

1D	One-dimensional
2D	Two-dimensional
3D	Three-dimensional
CAD	Computer-Aided Design
CPT	Cone Penetration Test
CRR	Cyclic resistance ratio
CRR _{6.5}	CRR for an earthquake magnitude (M) of 6.5
CSR	Cyclic stress ratio
CTX	Cyclic Triaxial
DB	Database
DBMS	Database Management System
DEM	Digital Elevation Model
FS _{liquefaction}	Factor of safety against liquefaction per layer
FVT	Field Vane Test
GDB	Geodatabase
GDBMS	Geodatabase Management System
GEVD	Generalized Extreme Value Distribution
GIS	Geographic Information System
GPS	Global Positioning System
GTIS	Geotechnical Information System
GUI	Graphic User Interface
GWL	Ground Water Level
IBC	International Building Code

IDW	Inverse Distance Weighted interpolation
KISS	Korea Integrated Seismic Monitoring
LAN	Local Area Network
LPI	Liquefaction Potential Index
MAE	Mean Average Error
MSE	Mean Squared Error
MSF	Magnitude scaling factor
NEHRP	National Earthquake Hazard Reduction Program
OK	Ordinary kriging
PGA	Peak Ground Acceleration
RC	Resonance Column
RDBMS	Relational Database Management System
RMSE	Root Mean Squared Error
SCM	Successive Correction Method
SDB	Spatial Database
SDBMS	Spatial Database Management System
SPT	Standard Penetration Test
SQL	Structured Query Language
TIN	Triangular Irregular Network
TM	Traverse Mercator
UBC	Uniform Building Code
UK	Universal kriging
USCS	Unified Soil Classification System

1. Introduction

1.1 Background

Historically, the Korean peninsula has been regarded as a safe region with respect to the hazard of earthquake due to the characteristics of its location, being classified as a region of moderate seismicity. Recently, there have been some large earthquakes among surrounding states of Korea and they are causing a considerable damage: 2008 Sichuan (M 8.0); 2008 Honsu (M 6.9); 2005 Kashmir (M 7.3); and 2011 Tohoku (M 9.0) earthquakes. Korean peninsula also had some earthquakes lately and these are raising concerns among the society and also on a nationwide scale: 2007 Odaesan (M 4.8), 2013 Shinan (M 4.9), 2013 Baengnyeong Island (M 4.9), and 2014 Tae'an (M 5.2) earthquakes. Because the Korean peninsula is located in the inner part of Eurasian Plate, earthquakes and earthquake hazard didn't occur frequently in the earthquake records in the past decades, such as Japan, Taiwan and other neighboring countries belonging to circum-pacific seismic zone.

However, the number of earthquake events keeps increasing every year, and recent cases of earthquake hazards invoke the necessity of seismic study in Korea, as geotechnical earthquake hazards, such as liquefaction and landslides, are a significant threat to structures in port or downtown built on seismically vulnerable loose and saturated sandy soils. Therefore, evaluation of the geotechnical earthquake hazards has been recently emphasized in Korea.

Seismic disaster management and mitigation are required to establish effective and appropriate strategies to reduce earthquake hazards. However, these are not easy tasks, and require considerable resources and analyses (Drabek and Hoetmer, 1991; Xu and Liu, 2009). Their complexity dictates the use of an integrated seismic damage assessment methodology based on a computer-aided system, such as the geographic information systems (GIS) tool. GIS supports spatial decision-making based on multiple georeferenced datasets, and thereby makes possible spatial earthquake hazard assessment for reducing or mitigating damage caused by earthquake shaking (Papadimitriou et al., 2008; Schneider and Schneider, 2006; Vahidnia et al., 2010). Comprehensive frameworks for seismic damage scenarios and risk analysis, including GIS-based evaluation tools, have been developed and proposed as part of major loss estimation systems: HAZUS (FEMA, 2003); RADIUS (RADIUS, 1999); Risk-UE (Mouroux and Le, 2006); DBELA (Crowley et al., 2004). Moreover, evaluation of reliable site-specific seismic response characteristics in an entire area of interest is best handled on a GIS platform, because the geotechnical earthquake hazard is seriously affected by local site effects. Accordingly, the effective construction of a spatial database system is considered in this dissertation for reliable earthquake hazard zonation mapping using GIS techniques.

Although appropriate for earthquake hazard assessment over the long term, GIS can provide immediate and rapid estimation of the earthquake hazard over a target area, and is essential to minimize damage and effective emergency control due to the unexpected and sudden nature of earthquakes (Kim et al., 2012a). Thus, real-time assessment considering the site-specific

geotechnical earthquake hazard using GIS is appropriate for supporting rapid emergency response in certain target areas.

For site-specific geotechnical earthquake hazard assessment, construction of reliable geotechnical database is essential considering spatial uncertainty or errors of geotechnical properties. These are known as “outliers” or “outlying observations” in statistics (Barnett and Lewis, 1994; Grubbs, 1969). To reduce or remove outliers in measurements, appropriate geostatistical methods are necessary. And, in case of using only boring data, geotechnical information is provided as one-dimensional (1D) soil profiles point by point. Therefore, the geophysical and boring datasets can be integrated to construct the three-dimensional (3D) continuous geotechnical spatial information structures based on geostatistical methods (Kupfersberger and Deutsch, 1999; Weissmann et al., 1999; Koltermann et al., 1996).

In this dissertation, the integrated earthquake hazard assessment system with geotechnical spatial grid information based on GIS was developed to response earthquake events in near real-time. The integrated system consists of a database and systematic modules. The sub-modules execute various functions on managing and utilizing information in the database with connection to the database; input of data, geostatistical 3D integrated data based on input data, real-time earthquake hazard data, and output of data. Furthermore, a real-time assessment of the geotechnical hazards were conducted for the Busan port and Incheon port, Korea, based on a computer-based spatial information system to verify the applicability of the developed system.

1.2 Objectives

The purpose of this dissertation is to development of integrated earthquake hazard assessment system with geotechnical spatial grid information, which can predict the reliable liquefaction and structure failure in near real-time. And specific objectives of this study are as following:

- 1) Database: Geographic data, geotechnical data, structure data, and seismic monitoring data were standardized connected with spatial information based on geodatabase.
- 2) Input Function: Input function provides an effective way to store and arrange all collected field data and analysis data, according to database schema.
- 3) Geostatistical 3D integration for geotechnical spatial grid function: This method has three functional modules with the database: Outlier detection method, geostatistical integration method, and construction method of geotechnical spatial grid.
- 4) Real-time earthquake hazard assessment function: The real-time framework has three functional modules with the database: real-time seismic load determination, real-time liquefaction hazard estimation, and real-time structure fragility evaluation.
- 5) Output Function: The output function displays all attributive information in the database by using tables and graphics according to its characteristics either, on screen or as a document. The earthquake hazard can be visualized and forecasted as 2D or 3D maps overlain by satellite images in near real-time, as earthquake events occurred.

The graphical schematic flow of integrated earthquake hazard assessment system with geotechnical spatial grid information (composed of systematic functions for 3D geotechnical spatial grid and real-time earthquake hazard information) was described in Figure 1.1.

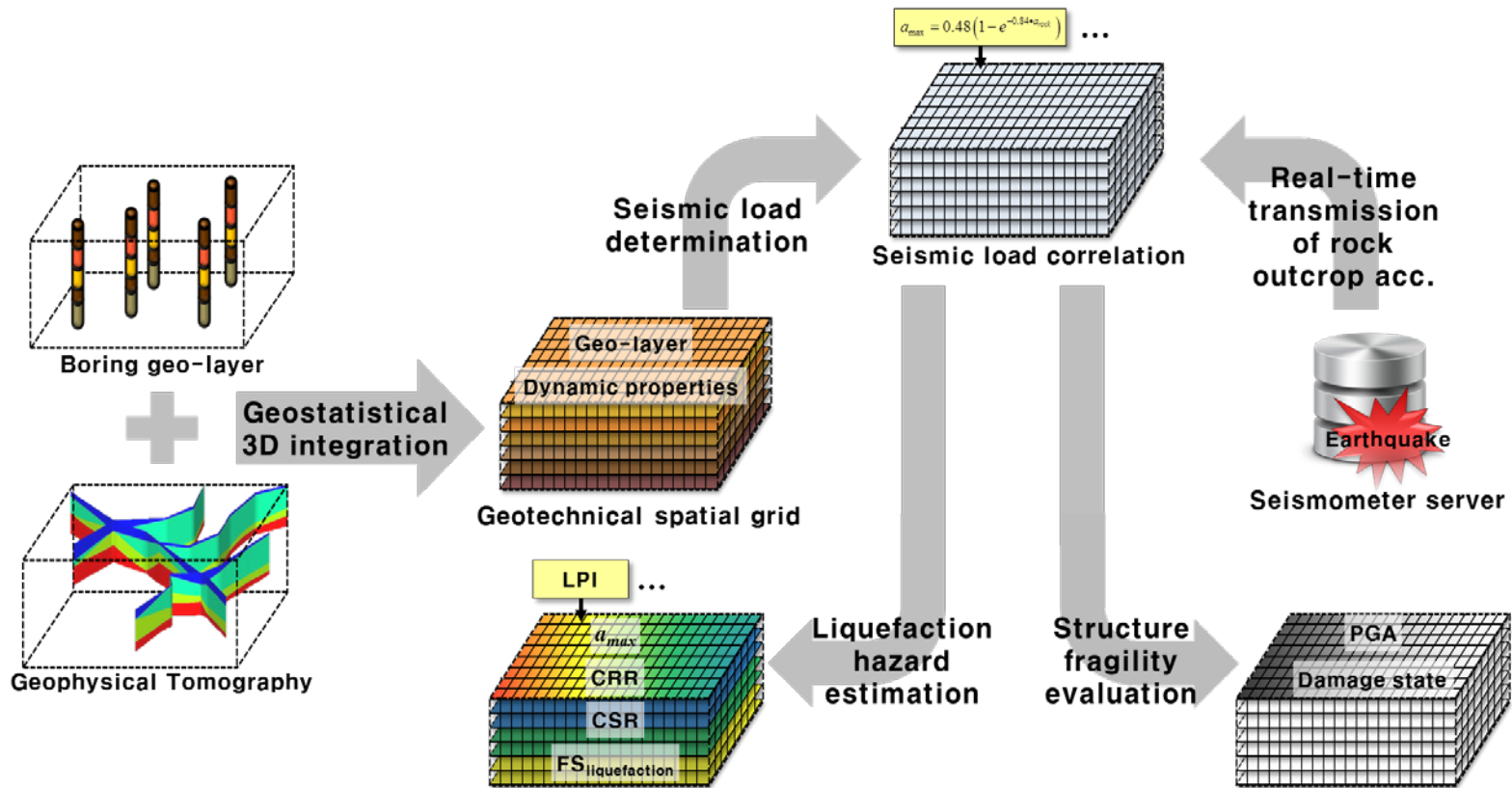


Figure 1.1 Schematic flow of integrated earthquake hazard assessment system with geotechnical spatial grid information

1.3 Structure of Dissertation

This dissertation documents the development of integrated earthquake hazard assessment system with geotechnical spatial grid information based on GIS, its systematic framework (and proposed methodologies), system program and earthquake hazard simulations, and consists of eight chapters.

Chapter 1. Introduction

Research background and research objectives were presented, and organization of this dissertation is described.

Chapter 2. Literature Review

Literature reviews for GIS and reviews for previously developed GTISs are described. In addition, earthquake hazard assessment approaches and previous earthquake hazard management systems are reviewed. Previous all GTISs and earthquake hazard management systems described has some disadvantage that result from incomplete data standardization with spatial data and not fully probabilistic evaluation in the decision making process for earthquake hazard assessments. And the GTIs and earthquake hazard management systems focused only the input and output functions of geotechnical datasets or earthquake hazard.

Chapter 3. Real-time Framework for Earthquake Hazard Assessment

The integrated framework consists of a database and systematic modules. The database contains all field data and processed data in the system. The sub-modules execute various functions on managing and utilizing information in the database with connection to the database; input of data, geostatistical 3D integrated data based on input data, real-time earthquake hazard data, and output of data. The framework includes all these functions or modules: input module; geostatistical 3D integration module for geotechnical spatial grid; real-time earthquake hazard assessment module; output module.

Chapter 4. Geostatistical 3D Integration for Geotechnical Spatial Grid

To figure out reliable geotechnical characteristics of site having seismic risk potential, geostatistical 3D integration using geophysical tomography and soil profile of borehole is established based on GIS platform. The construction procedures of geotechnical spatial grid are composed of three phases: outlier analysis of borehole datasets, geostatistical 3D integration of borehole and geophysical datasets and 3D geotechnical spatial grid construction.

Chapter 5. Real-time Earthquake Hazard Assessment

A systematic framework for real-time assessment of the earthquake hazard was developed to consider local site response characteristics for target areas. According to the framework, three interrelated assessment procedures

were incorporated in a database on a real-time basis: real-time seismic load determination, real-time liquefaction hazard estimation, and real-time structure fragility evaluation. The liquefaction severity class and structure fragility class are forecasted and visualized in satellite map images or digital map in real-time based on the GIS platform. Therefore the integrated earthquake hazard of the target structure is determined considering the liquefaction and fragility grade.

Chapter 6. Integrated System for Real-time Earthquake Hazard

The developed system built within the frame of GIS, consists of the database containing all site information and processed data in the system according to the standard data formats (database schema), and the system software performing various functions to manage and utilize the data in the database. The system software was divided into input module, geostatistical 3D integration module, real-time earthquake hazard assessment module, and output or visualization module, functionally. The database and these modules of the system software were combined integrated in single system and the developed system provides a familiar and user-friendly working environment with a standard interface. And the integrated system was imbedded into KISS server for real-time linking of seismic accelerations.

Chapter 7. Systematic Field Application

The developed system has been specifically applied to the Busan port,

Korea, using two virtual earthquake scenarios based on the GIS platform. The simulation results were visualized as a geotechnical earthquake hazard map to verify the applicability of the computer-aided real-time assessment framework. And the verification test for the integrated system was also performed for Incheon port using actually transmitted from accelerometer of KISS server, when two noticeable earthquake events occurred at nearby Incheon port.

Chapter 8. Conclusions and Recommendations

Summary and conclusions from this study are described focused on the characteristics and field performances of the developed system and systematic framework for real-time geotechnical earthquake hazard assessment and recommendations for the further study are presented.

2. Literature Review

2.1 Introduction

Seismic disaster management and mitigation are required to establish effective system (or methodologies) for spatial information and earthquake hazard assessment. In this study, the previous geotechnical information system and earthquake hazard management system, which are reflected the recent research trends, were reviewed for integration system for geotechnical earthquake hazard assessment, in this chapter.

Data in geotechnical engineering practices encompass a variety of sources of information from in-situ investigations, laboratory tests, field monitoring, and computer analyses. These huge amounts of data are used by a large variety of professionals with different backgrounds and interests necessitating the use of the computer technology (such as big data). In particular, researchers and practitioners in geotechnical engineering have historically had to deal with problems relating to the storage, manipulation and analysis of geotechnical data, which exist within a spatial time domain (Chun et al., 2005). Substantial improvements in computer hardware and software over the past several decade years have made it much easier to assimilate large volumes of spatial data. Recent advances in computer based geographic information system (GIS) make the data ideally suited to fulfill the needs of geotechnical engineering aspect.

Meanwhile, spatial earthquake hazard assessment studies play a key role

in identifying and mitigating the potential consequences of an earthquake. Observations of the areas which were hit by strong earthquakes in the last decades provided enough evidence to suggest that local soil conditions may alter earthquake waves and amplify certain period bands of ground motion significantly (Borcherdt, 1994). Ground shaking affects the structures by both its direct action and also indirectly by changing the state of the soil (consistency, continuity and rigidity) and thus its constitutive response. In this context, strong ground shaking is considered as the primary damage-causing phenomenon whereas events such as liquefaction, seismic bearing capacity degradation, and landslide are among the main collateral causes of structural damage.

There are several spatial earthquake and damage assessment methodologies applied worldwide (King and Kiremidjian, 1994; ATC-13, 1985). Earthquake damage assessment methodologies are applied mainly for two purposes; as a damage assessment methodology in urban areas and as a land use study in undeveloped areas for the purpose of city planning. However the presented approach is not fully probabilistic but can easily be extended to be so, because the main difference lies in the decision making process. If a fully probabilistic evaluation were used, a set of probabilities would be presented for each damage-causing event.

2.2 Geotechnical Information System

2.2.1 Geographic information system

GIS architectures

The phenomena that can be observed in the real world cannot be represented as such in a computer because the real world is infinitely complex and the storage space and the representation power of a computer are limited. Therefore, it is necessary to define models to represent real world information in a form that is suitable for a computer. A model is an artificial construction in which parts of a domain (i.e., the source domain) are represented in another domain (i.e., the target domain). A model allows developers to simplify and to abstract from the source domain by representing its elements with elements of the target domain. Processes that take place in the source domain can also be represented with operations on elements on the target domain. This allows the user of the model to simulate these processes and predict their outcome by applying operations on elements of the target domain and interpreting the results in the source domain. For the particular case of geographic information, the source domain consists of real world geographic phenomena, and the target domain consists of data elements that are stored in a computer. Manipulation algorithms and visualization techniques are applied upon the data on the computer, and the results are then interpreted as real world geographic phenomena (Figure 2.1).

There are four common geographic information system (GIS) architectures available as shown in Figure 2.1 (Kimmance et al., 1999).

- 1) A Project GIS comprising a single PC with all the required GIS software and data resident on that PC.
- 2) A Departmental GIS comprising a series of linked PCs, with a centrally controlled and updated data and graphics set made available on each of the linked PCs.
- 3) A Divisional or Organizational GIS using a centralized data storage system accessible over a network by client PCs running the GIS software.
- 4) A Client-Web Server GIS where the data and GIS software is hosted solely on a server with client PCs acting as terminals via the Internet/Intranet.

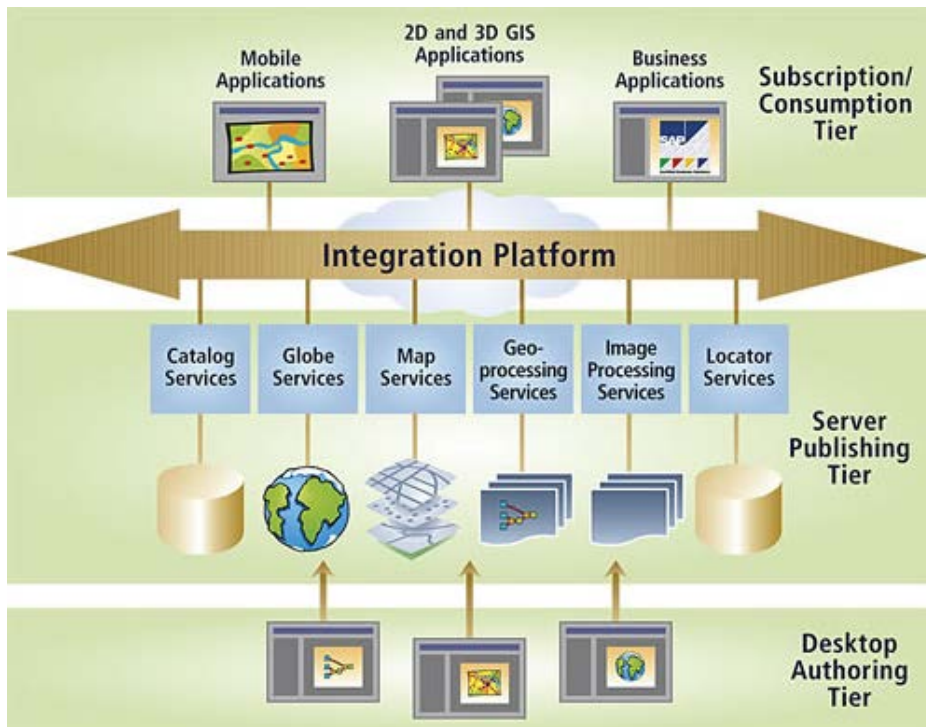


Figure 2.1 GIS architectures (Esri, 2006)

Seismic disaster management and mitigation are required to establish effective spatial information and visualization methodologies. In this dissertation, the integrated system was developed using GIS architectures (building of real-time map services network and 2D / 3D GIS applications) in seismic monitoring and hazard assessment.

Geodatabase management

The geodatabase (GDB) is the common data storage and management framework for ArcGIS. Simply put, it is a container for spatial and attributes data. The geodatabase has been the primary data model for ArcGIS since the

8.0 release. The name combines geo (referring to spatial) with database—specifically, a relational database management system (RDBMS). The term promotes the idea of having all GIS data stored uniformly in a central location for easy access and management.

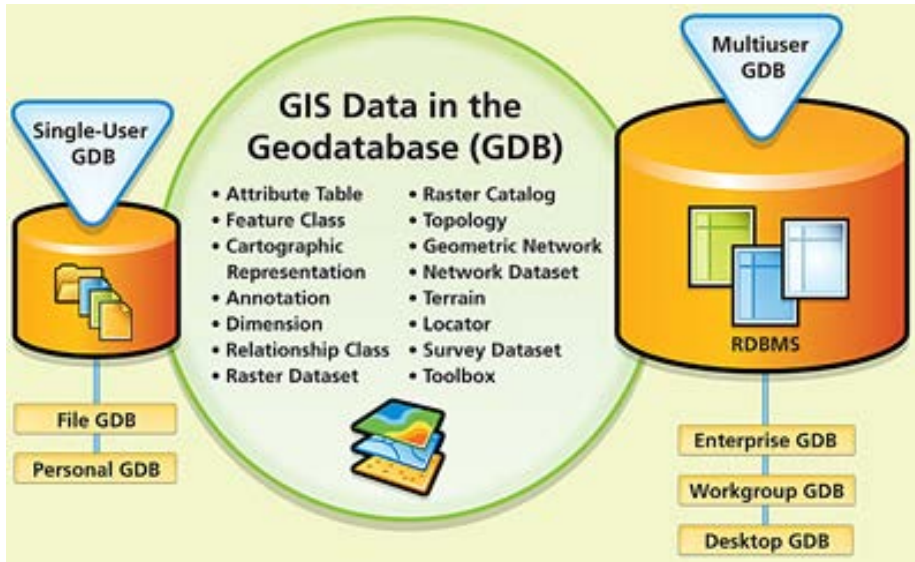


Figure 2.2 GIS data in the geodatabase (GDB) (Esri, 2006)

The geodatabase supports all the different types of GIS data that can be used by ArcGIS, such as attribute data, geographic features, satellite and aerial images (raster data), CAD data, surface modeling or 3D data, utility and transportation network systems, GPS coordinates, and survey measurements. ArcGIS has a comprehensive suite of data conversion tools to easily migrate existing data into the geodatabase. By storing GIS data within a geodatabase, users can take advantage of its superior data management capabilities to leverage spatial information. This can enhance and expand business and GIS

application workflows.

The geodatabase is a more robust and extendable data model compared to shapefiles and coverages. While shapefiles and coverages are outstanding GIS data storage formats, they do not take advantage of the latest data storage technologies. The geodatabase is designed to make full use of the capabilities of ArcGIS Desktop and ArcGIS Server. The geodatabase is not just another spatial data format that can be used by ArcGIS; it is an integral part of the ArcGIS system.

2.2.2 Geotechnical outliers and detection methodologies

Description of outliers in geotechnical datasets

The recently updated design codes of the AASHTO LRFD Bridge Design Specifications (2007), Eurocode 7: Geotechnical Design (2004) and the Reliability Design Table for Port Structures in Korea (2011) specify the manner of selecting the characteristic values or the design values by considering the uncertainty of the given data, the structure significance, the possibility of failure, and other factors.

The spatial uncertainty of geotechnical properties has been discussed and reported extensively thus far (Vanmarke 1977, Asaoka and A-Grivas 1982, DeGroot and Baecher 1993, Lacasse and Nadim 1996, Phoon and Kulhawy 1999, Chun et al. 2005, Yun et al. 2008). Kulhawy (1992) mentions that there are three primary sources of uncertainty in geotechnical design parameters:

the inherent soil variability, the measurement uncertainty, and the transformation uncertainty. The inherent variability is a consequence of natural geologic processes. Measurement uncertainty is caused by equipment, test-operators, and random test effects. Transformation uncertainty is introduced when testing measurements are transformed into design soil properties with empirical or theoretical models. Those uncertainties make the geotechnical design less reliable, making it necessary to reduce or remove “errors” in measurements with appropriate statistical methods. Typically, those erratic measurements are numerically distant from the rest of the data or may deviate significantly from other observations nearby.

These are known as “outliers” or “outlying observations” in statistics (Barnett and Lewis 1994, Grubbs 1969). Typical outlier detection methods can be classified into the univariate methods and the multivariate methods or the parametric methods and the nonparametric methods. Parametric methods assume a known underlying distribution of the observations or they are based on statistical estimates of unknown distribution parameters. These methods consider observations that deviate from the model assumption as outliers. They are often unsuitable for high-dimensional data sets and for arbitrary data sets without prior knowledge of the underlying data distribution. Details can be found in other studies (Zhang et al. 2007, Chandola et al. 2007, Barnett and Lewis 1994, Grubb 1969).

Previous outlier detection methodologies

Outlier detection methods can be divided between univariate methods,

proposed in earlier works in this field, and multivariate methods that usually form most of the current body of research (Figure 2.3). Another fundamental taxonomy of outlier detection methods is between parametric (statistical) methods and nonparametric methods that are model-free (e.g., see (Williams et al., 2002)). Statistical parametric methods either assume a known underlying distribution of the observations (e.g., (Hawkins, 1980; Rousseeuw and Leory, 1987; Barnett and Lewis, 1994)) or, at least, they are based on statistical estimates of unknown distribution parameters (Hadi, 1992; Caussinus and Roiz, 1990). These methods flag as outliers those observations that deviate from the model assumptions. They are often unsuitable for high-dimensional data sets and for arbitrary data sets without prior knowledge of the underlying data distribution (Papadimitriou et al., 2002).

Within the class of non-parametric outlier detection methods one can set apart the data-mining methods, also called distance-based methods. These methods are usually based on local distance measures and are capable of handling large databases (Knorr and Ng, 1997; Knorr and Ng, 1998; Fawcett and Provost, 1997; Williams and Huang, 1997; Mouchel and Schonlau, 1998; Knorr et al., 2000; Knorr et al., 2001; Jin et al., 2001; Breunig et al., 2000; Williams et al., 2002; Hawkins et al., 2002; Bay and Schwabacher, 2003). Another class of outlier detection methods is founded on clustering techniques, where a cluster of small sizes can be considered as clustered outliers (Kaufman and Rousseeuw, 1990; Ng and Han, 1994; Ramaswamy et al., 2000; Barbara and Chen, 2000; Shekhar and Chawla, 2002; Shekhar and Lu, 2001; Shekhar and Lu, 2002; Acuna and Rodriguez, 2004). Hu and Sung (Hu and Sung, 2003), whom proposed a method to identify both high and low density

pattern clustering, further partition this class to hard classifiers and soft classifiers. The former partition the data into two non-overlapping sets: outliers and non-outliers. The latter offers a ranking by assigning each datum an outlier classification factor reflecting its degree of outlyingness. Another related class of methods consists of detection techniques for spatial outliers. These methods search for extreme observations or local instabilities with respect to neighboring values, although these observations may not be significantly different from the entire population (Schiffman et al., 1981; Ng and Han, 1994; Shekhar and Chawla, 2002; Shekhar and Lu, 2001; Shekhar and Lu, 2002; Lu et al., 2003).

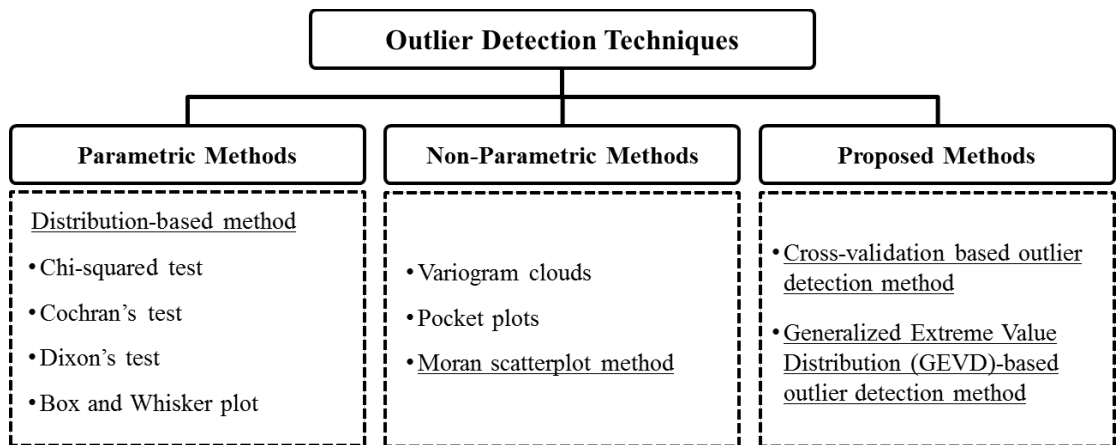


Figure 2.3 Taxonomy of previous outlier detection methodologies

1) Distribution based method

Distribution-based methods are based on the assumption that the measurements follow a standard statistical distribution model such as a normal distribution, a lognormal distribution, or a Poisson distribution. They

determine whether an extreme data point is classified as an outlier depending on how far it is located from the mean or the median in the given distribution, using methods such as the Chi-squared test, Cochran's test, Dixon's test, Grubbs' test, and the Box and Whisker plot method (Dixon 1950, Snedecor and Cochran 1980, Rorabacher 1991, Grubbs 1950, Tukey 1977). However, those methods have a common limitation in that they were developed for scalar-type observations and can therefore be erroneous when analyzing spatially measured vector-type data, which usually have spatial correlations with respect to the measurement locations.

First, the cumulative distribution density curves for all of the soil depth measurements are given in Figure 2.4. In this study, the highest five percent (thicker than 38m) and the lowest five percent (thinner than 17m) of the measurements in the distribution are selected as outliers.

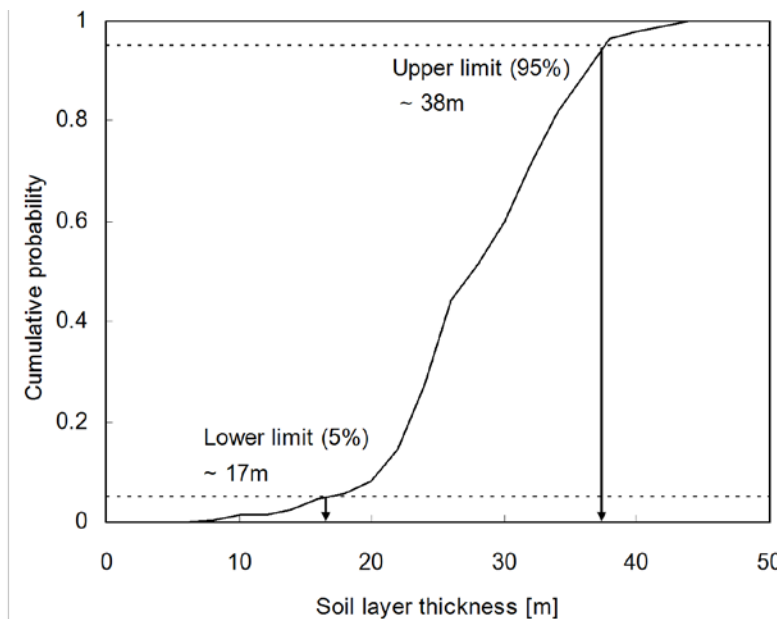


Figure 2.4 Distribution-based method

2) Moran scatterplot method

Anselin's Moran scatterplot (Anselin et al. 2004) represents the spatial correlation of a measurement with the neighboring measurements. The scatterplot depicts a standardized measurement z_i on the x -axis versus the summary of the neighboring spatial units and its standardized measurement z_i neighborhood on the y -axis.

$$z_i = \frac{x_i - \mu_x}{\sigma_x} \quad (4.1)$$

$$z_{i_neighborhood} = \frac{\sum_j (x_{ij} - \mu_x) w_{ij}}{\sigma_x} \quad (4.2)$$

That summary is calculated through a spatial weight matrix, which can take various forms. In this study, the spatial weight matrix is defined by the adjacency criteria. The element of the spatial weight matrix w_{ij} is 1 if the location unit i shares an edge with the location unit j , and 0 otherwise, as shown in Figure 2.5. Figure 2.5 shows the definition of the polygonized spatial unit for the soil depth. Here, the spatial weight matrix is defined in row-standardized form, where the row elements sum to one. The calculated scatterplot for the testing data is shown in Figure 2.6.

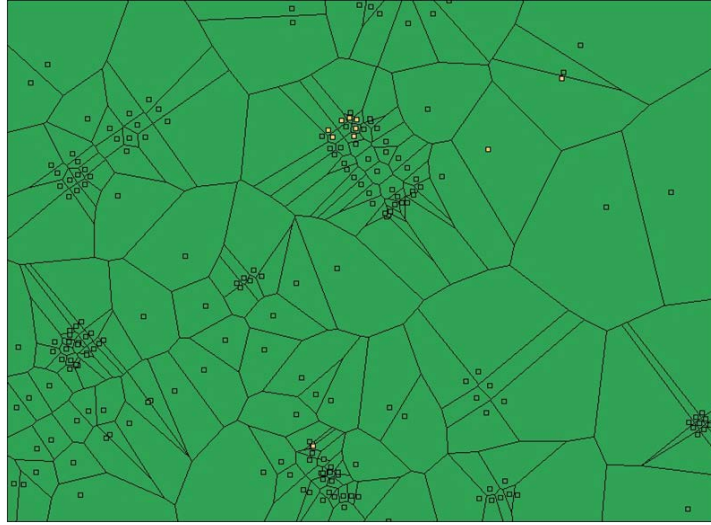


Figure 2.5 Definition of the polygonized spatial units for the Moran scatterplot method

Measurements further from the regression line in the scatterplot are more difficult to estimate via neighboring measurements (Shekhar et al. 2003). The distance between a point and the regression line is used to evaluate its local reliability. In Figure 2.6, the solid line is the regression line and the dotted lines are drawn as outlier criteria for the testing data to select the furthest twenty data points from the regression line.

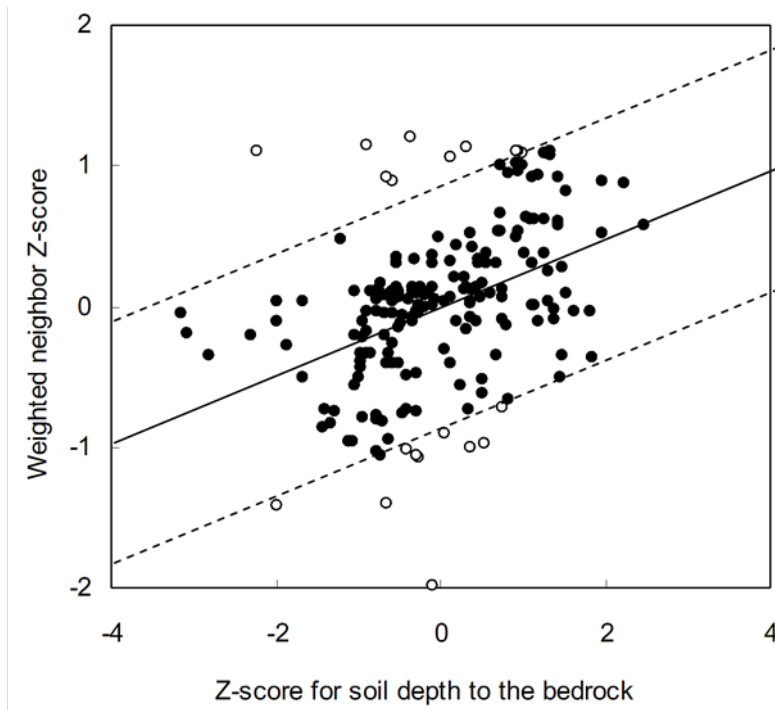


Figure 2.6 Moran scatterplot for the testing data

The negative slope in the scatterplot suggests a negative spatial autocorrelation of low values surrounded by neighboring high values, or high values surrounded by neighboring low values. In contrast, the positive slope indicates a positive spatial autocorrelation of low values surrounded by neighboring low values, or high values surrounded by neighboring high values.

2.2.3 Geostatistical interpolation methodologies

Spatial uncertainties of geotechnical datasets

Recently, several cases of dam structure failure were reported, which were caused by ground settlement or landslide during earthworks in emergency spillway construction: DMAD dam failure in U.S., 1983 (Curtis and Wayne 1988), Soyang River dam failure in South Korea, 2006 (Shin et al. 2007) and Montedoglio dam failure in Italy, 2010 (Moramarco et al. 2013). The emergency spillway is a part of the dam to regulate the passage of flows around the dam structure at floods.

Generally, it is recommended for the emergency spillway to be located at soft rocks with a good quality for the stability. One of the reasons why such failures occurred is that geotechnical engineers designed them on unstable soil deposits without enough information on subsurface profiles, which could cause the lack of stability under construction and management. In most cases, the subsurface information is interpreted based on the boring data which show one-dimensional soil profiles point by point. Engineers should have inevitable limitation to understand the continuous spatial distribution of soil properties (Jaime et al. 1990, Joh et al. 2006). Such a lack of information can mostly be solved by conducting a construction of three-dimensional spatial geotechnical information structures (Kupfersberger and Deutsch 1999, Weissmann et al. 1999, Koltermann et al. 1996). Specially, in case of the emergency spillways, it is challenging to conduct borings at the right locations, because they are usually on too stiff slope faces of mountainous area. Therefore, it is necessary to integrate all the available subsurface information to determine the adequate three-dimensional continuous spatial distribution of soil properties.

And also, in many cases, the borehole data are believed to be true values

of the geomaterials. However, even the borehole data have the uncertainties caused by the inherent soil variability, the measurement uncertainty, and the transformation uncertainty (Kulhway 1992). Those uncertainties make the geotechnical design less reliable, making it necessary to reduce or remove “errors” in measurements with appropriate statistical methods. Typically, those erratic measurements are numerically distant from the rest of the data or may deviate significantly from other observations nearby. These are known as “outliers” or “outlying observations” in statistics, and should be properly controlled for more reliable assessment of the geomaterials (Barnett and Lewis 1994, Grubbs 1969).

Previous geostatistical interpolation methodologies

Geostatistics is a mathematical method to develop efficient spatial networks based on discrete data transformed from continuous values, binary values or categorical data (Deutsch 2002). It can be regarded as a collection of numerical techniques that deal with the characterization of spatial relationships, employing primarily random models (Olea 1999). Some previous studies attempted to obtain a two-dimensional distribution of soil properties analyzing one-dimensional borehole data with the geostatistics techniques (Ozturk 2002, Ryu et al. 2003). Geophysical tests such as seismic refraction prospecting and electrical resistivity surveys are conducted to present soil properties for all the locations within the given area using tomographic inversion.

However, the geophysical methods also have limitation that the

tomographic inversion result does not guarantee the real values of geomaterial. Some approaches to integrate several geophysical testing results or the one-dimensional boring data with the multi-dimensional soil profiles obtained by the geophysical methods were proposed (Kim et al. 2012b, Gallerini and Donatis 2009, Oh et al. 2004, Gomez-Hernandez and Mohan 1990).

Geostatistics is a branch of statistics focusing on spatial or spatiotemporal datasets. Developed originally to predict probability distributions of ore grades for mining operations, it is currently applied in diverse disciplines including petroleum geology, hydrogeology, hydrology, meteorology, oceanography, geochemistry, geography, forestry, environmental control, landscape ecology, soil science, and agriculture. Geostatistical algorithms are incorporated in many places, including geographic information systems (GIS) and the statistical environment (Kriging D.G., 1951).

It is important in geosciences to estimate the structure of large scale fields using limited observational records. The dynamic or statistical methods are often used in interpolation on irregular grids and regular grids. Most of the interpolation methods are designed based on regular grids such as spline, wavelet interpolation, cubic convolution interpolation, etc. (Li et al., 2000). In meteorology, some simple interpolation methods in terms of the distance are widely used, such as inverse distance weighted interpolation (IDW) and successive correction method (SCM).

And kriging is one of the most important parts in geostatistics. Comparing to traditional interpolations, including IDW method, the kriging deals with irregular grids, and has the capability to combine other information in interpolation. Moreover, the kriging is a spatial analysis method in addition

to an interpolation method, because its pre-estimation of errors is considered (Chang et al., 2004).

There are typical geostatistical analysis methods: IDW, spline and kriging interpolation (Figure 2.7).

1) Invers distance weighted interpolation (IDW)

IDW explicitly implements the assumption that things that are close to on one another are more alike than those are farther apart. The value at an unsampled point can be predicted as a weighted average of values at points within a certain cut-off distance, or from a given number of the closest points. Weights are usually inversely proportional to a power of distance (Burrough, 1986; Watson, 1992).

The general formula is

$$Z(x_0) = \sum_{i=1}^N \lambda_i Z(x_i) \quad (2.1)$$

$$\lambda_i = \frac{d_{i0}^{-P}}{\sum_{i=1}^N d_{i0}^{-P}}, \quad \sum_{i=1}^N \lambda_i = 1 \quad (2.2)$$

where $Z(x_0)$ is the predicted value for location x_0 , $Z(x_i)$ is the measured value at location x_i , N is the number of measured points surrounding the prediction location that will be used in the prediction, λ_i is the weight assigned to measured points, d_{i0} is the distance between the prediction location and each of the measured locations and P is a parameter.

2) Spline

The spline, especially B-spline, in which a polynomial is used to fit a surface, is developed in engineering and widely used to meet high accuracy requirement. In general, a polynomial function with an order less than or equal to the 3rd order is used to fit a field. The spline interpolation has, at least, a continuous derivation at order 2 at interpolating result. In general, it is applied in smooth surface interpolation.

3) Kriging

Geostatistics is one of statistical methods, which accounts for a spatial correlation of physical variables. The regionalized variables in geostatistics are usually of closed quantities in many natural phenomena. According to the satisfaction to the stationary assumptions, kriging is divided into simple kriging, ordinary kriging (OK) and universal kriging (UK). For the OK method, the stationary assumption or intrinsic assumption should be satisfied (Li et al., 2000), that is, there should be a constant expectation in the whole field or at least in a sampling area. In addition to the OK method, the stationary assumption is not necessary for the UK method which supposes that the mathematical expectation is a function of a spatial location. Evidently, the UK method is suitable for non-stationary cases. The kriging interpolation can be expressed as

$$Z(x_0) = \sum_{i=1}^N \lambda_i Z(x_i) \quad (2.3)$$

where $Z(x_0)$ is the predicted value for location x_0 , $Z(x_i)$ is the measured value at location x_i , N is the number of measured points surrounding the prediction location that will be used in the prediction, λ_i is the weight

assigned to measured points, and can be solved by following OK system:

$$\begin{cases} \sum_{i=1}^N \lambda_i \gamma(x_i, x_j) + \mu = \gamma(x_j, x_0) & j = 1, 2, \dots, n, \\ \sum_{i=1}^N \lambda_i = 1 \end{cases} \quad (2.4)$$

The corresponding estimated error of the OK method is

$$\sigma_{OK}^2 = \sum_{i=1}^N \lambda_i \gamma(x_i, x_0) + \mu \quad (2.5)$$

where $\gamma(h)$ is the variogram value at lag distance h , and $N(h)$ is the number of lag distance. In practice, one needs to make an experimental variogram curve via sampling values and then fits it with one or more specific analytic functions. For the UK method, its expectation is a function of the spatial locations,

$$\begin{aligned} E[Z(x)] &= m(x), \\ Z(x) &= m(x) + R(x) \end{aligned} \quad (2.6)$$

where $E[Z(x)]$ is the mathematical expectation, and $R(x)$ is the residual between $Z(x)$ and the drift $m(x)$ at x point. The $m(x)$ is usually fitted by a N th-order polynomial:

$$m(x) = \sum_{i=1}^N a_i x^i \quad (2.7)$$

where a_i is the coefficient of drift polynomial. Since interpolation is always a local calculation, $m(x)$ is the local drift. In general, a linear or quadratic polynomial is enough to depict the drift. The variogram of $Z(x)$ is solved by $R(x)$ and the weights are assigned by the UK system:

$$\begin{cases} \sum_{i=1}^N \lambda_i \gamma(x_i, x_j) + \sum_{k=1}^N \mu_k x_i^k = \gamma(x_j, x_0), & i = 1, 2, \dots, n, \\ \sum_{i=1}^N \lambda_i x_i^k = x_0^k, & k = 1, 2, \dots, n \end{cases} \quad (2.8)$$

where the second expression is non-bias condition. The corresponding estimated error of the UK method is written as

$$\sigma_{UK}^2 = \sum_{i=1}^N \lambda_i \gamma(x_i, x_0) - \gamma(x_0, x_0) + \sum_{k=0}^N \mu_k x_0^k. \quad (2.9)$$

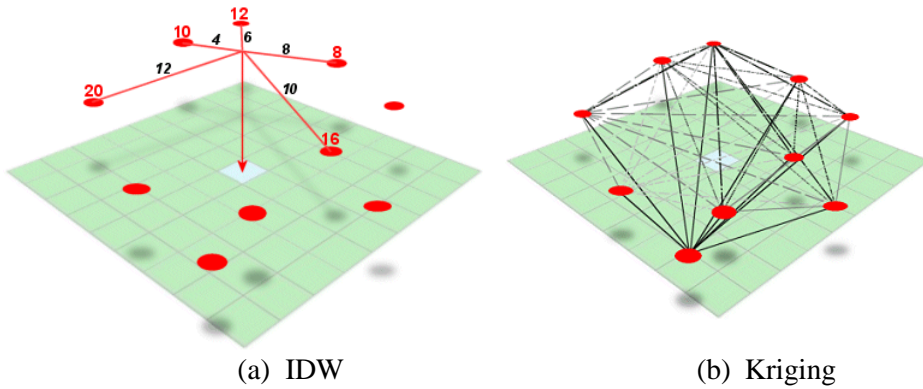


Figure 2.7 Concept of typical geostatistical analysis methods (Clayton and Andre, 1997)

2.2.4 Previous geotechnical information systems

Spatial data in geotechnical engineering has more complex data structures depending on their sources and suppliers. Thus, geotechnical information system (GTIS) demand more sophisticated data standardization

than GISs for other engineering practices. These factors have imposed limitations on the application of GIS in geotechnical engineering. In geotechnical practice, GIS can be used in at least four ways: data integration, data visualization and analysis, planning and summarizing site activities, and data presentation.

In this section, representatives of previous GTISs to utilize geotechnical investigation data, structure data, and real-time basis field monitoring data, which are closely related to the developed system in this dissertation, are arranged and reviewed to set up the basic concepts of the developed system. The reviews focus on architectures, database structures, functions, advantages and disadvantages of previous GTISs.

GeoLibrary, GeoFrance 3D and GeoVR

These systems are serviced on WWW (World Wide Web) with an internet browser. And they were developed based on a commercial program, ArcGIS by Esri. GeoLibrary was to manage geological data and GeoFrance 3D was for geological data and geophysical prospecting data. GeoVR is an interactive toolkit to create a 3D model from topographic data. Figures 2.8, 2.9, 2.10, and 2.11 show the representative examples of these systems.

These systems focus on only input and output, including 3D visualization. Therefore, essential analysis tools for geotechnical or geological dataset are not considered, and limited applications are possible for geotechnical engineering practices.

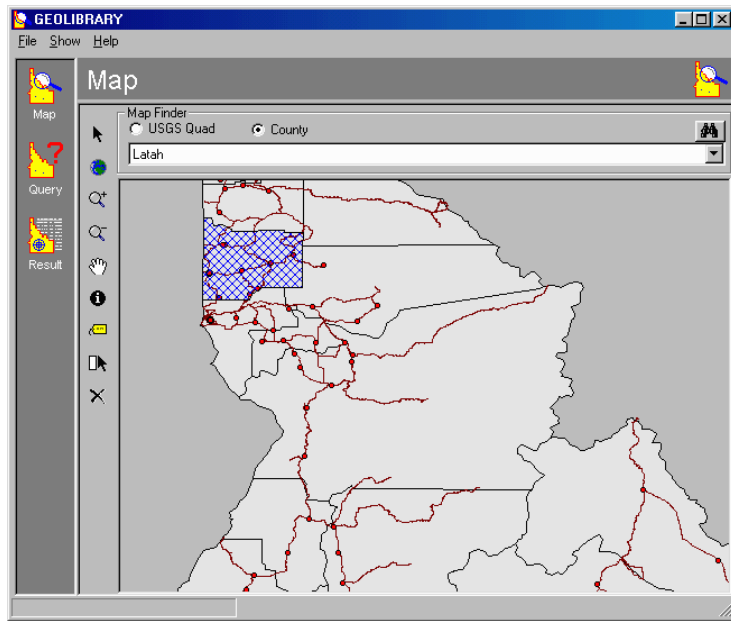


Figure 2.8 Map panel in GeoLibrary (Jankowski et al., 2001)

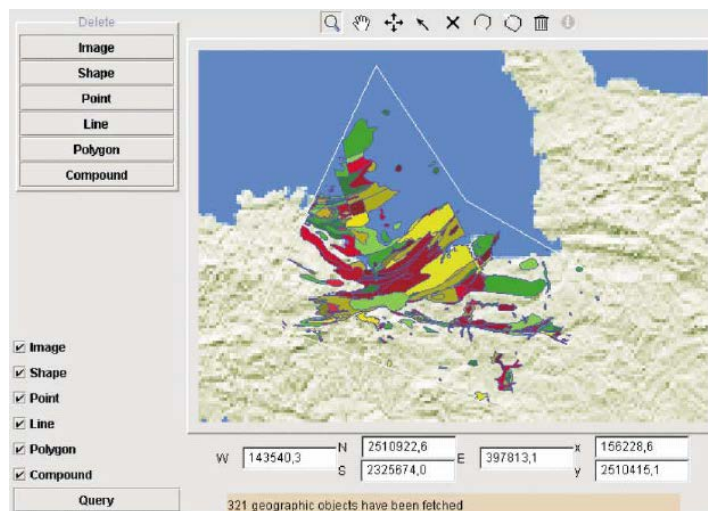


Figure 2.9 GeoFrance 3D client interface for spatial query and visualization (Guillen et al., 2001)

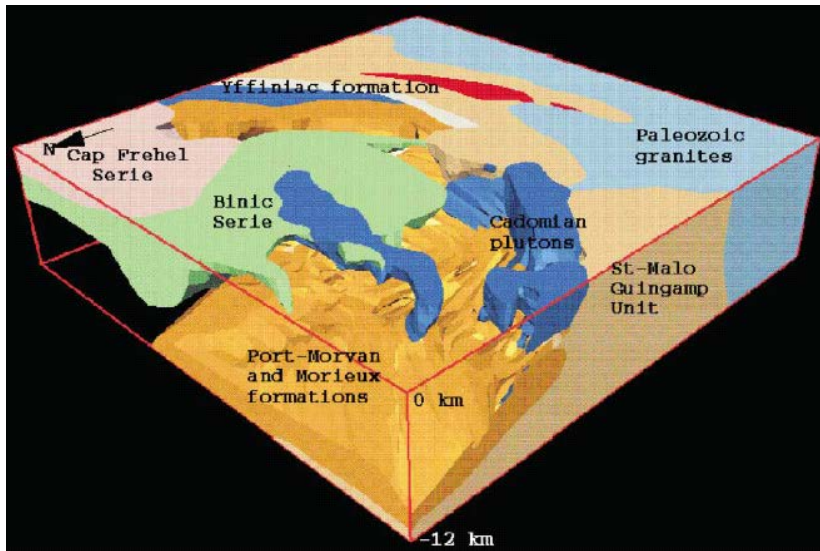


Figure 2.10 Visualization example of 3D model in GeoFrance 3D (Guillen et al., 2001)

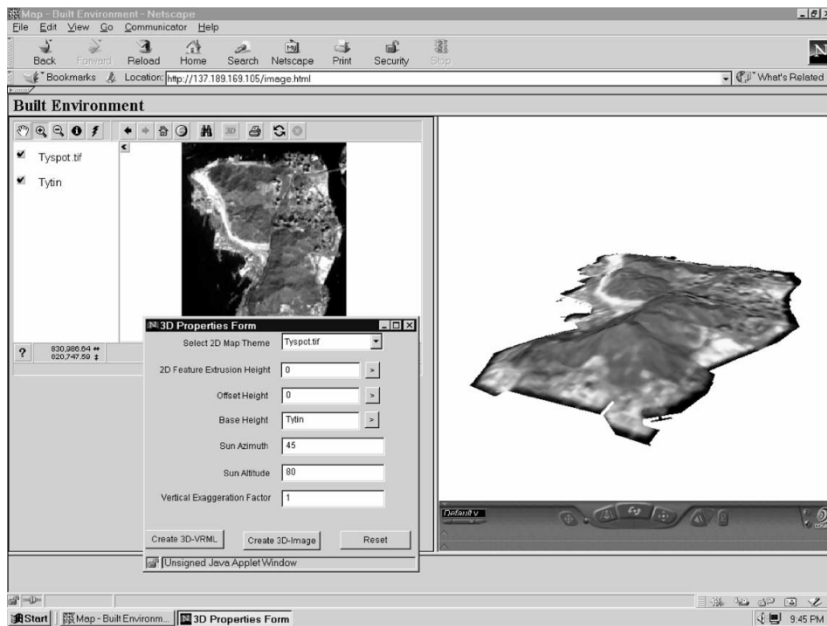


Figure 2.11 Interactive creation of SPOT image overlaid on terrain surface (Huang and Lin, 2002)

GeoInfoSys (Geotechnical Information System)

The development of the geotechnical information system (GeoInfoSys) includes (Figure 2.12): (1) design of the database based on a standard geotechnical data structure; (2) efficiently digitizing and archiving nationwide borehole data; (3) optimizing data analysis and visualization options by interfacing Web-GIS; (4) development of software to support online generation of boring logs and cross sections; (5) providing digital downloadable borehole data (in standard format) for downstream analysis; and (6) Exploring the geotechnical database for future research goals.

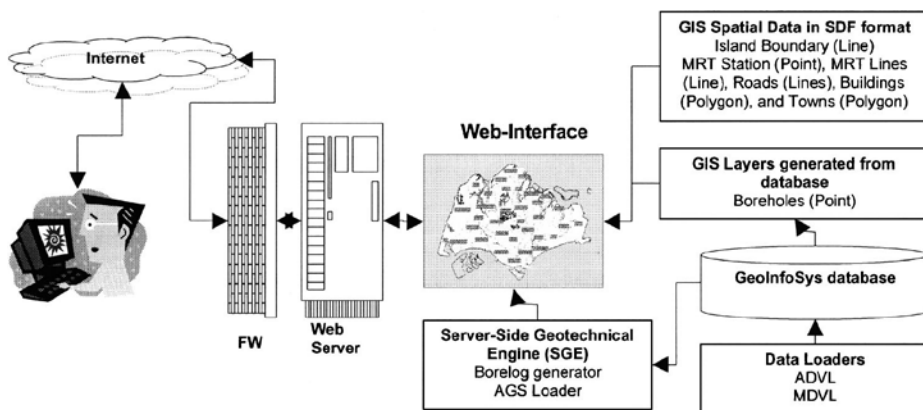


Figure 2.12 System architecture diagram for GeoInfoSys (Kunapo et al., 2005)

The system provides easy-to-use functions to locate boreholes of interest on a map using search tools and geotechnical spatial queries. The system was integrated with a payment module to enable users to purchase boreholes online, to view boring logs, and to download AGS files of purchased boreholes. The digital AGS data generated from GeoInfoSys can be directly input into various geotechnical softwares for use in downstream analysis.

Storing of digital information in a relational database, rather than as images, not only has allowed the distribution of boring logs over the Internet, but also has provided the opportunity to explore the geotechnical database using GIS. It is possible to generate vertical cross sections of soil profiles along an arbitrary line. It is also possible to query the database to get valuable information that can be of immense value in the planning stage of construction projects.

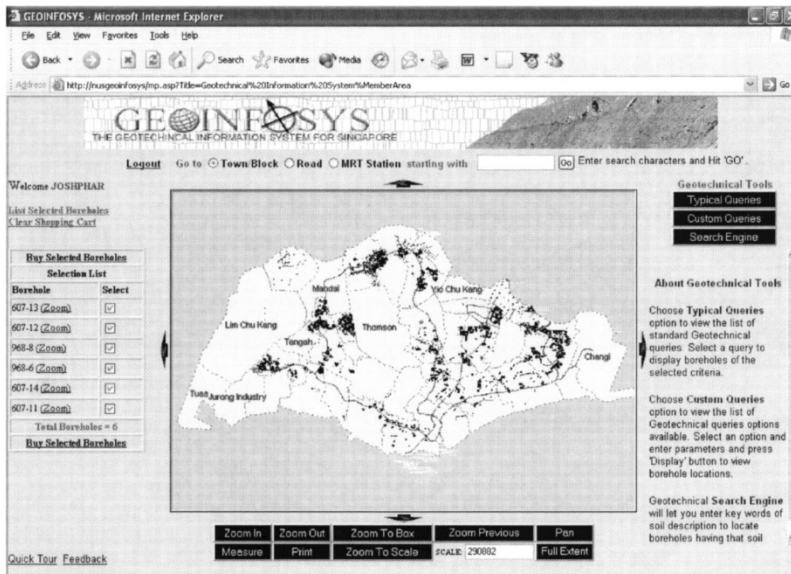


Figure 2.13 Main web interface of GeoInfoSys (Kunapo et al., 2005)

Kansai Gibase (Kansai Geo-Informatics Database)

Kansai geo-informatics database (Gibase) was constructed to gather a very large amount of borehole investigation data obtained in many projects of urban constructions in Kansai regions. Gibase was constructed by using DIG

(Database for Information of Ground) system that was developed by Geo-Research. The system used for DIG was constructed with a core management system assembling boring data with its inherent format by extending the concept of RDB. It is composed of the following four functions:

- 1) Function of total control (Host DB)
- 2) Function of data input control (Local DB)
- 3) Function of data extraction and processing (AP)
- 4) Function of data addition (Layer DB)

GIbase includes the detailed contents of investigation reports, so as to provide various geotechnical informations. The necessary handling functions for managing the Geo-database, DIG consists of five components, such as references, extraction, processing, analysis and indication. The fundamental functions of DIG are as follows:

- 1) Indicating the location of each boring on map and selecting the optional ones using mouse operation.
- 2) Referring the boring on optional condition.
- 3) Creating cross-sectional view of the ground by processing selected borings.
- 4) Creating the summarizing table for soil properties and experimental results.
- 5) Processing experimental data and indicating the distribution chart, correlation chart, etc.

In addition to such basic functions, DIG also interacts with application

programs for the extraction of regional ground characteristics or the examination as liquefaction and so on. GIbase is comprised of over 40,000 borehole data of geotechnical investigation around the Osaka Bay. Figure 2.14 shows the historical developments of GIbase. And Figure 2.15 shows the locations of boreholes for undisturbed sampling and various kinds of soil testing.

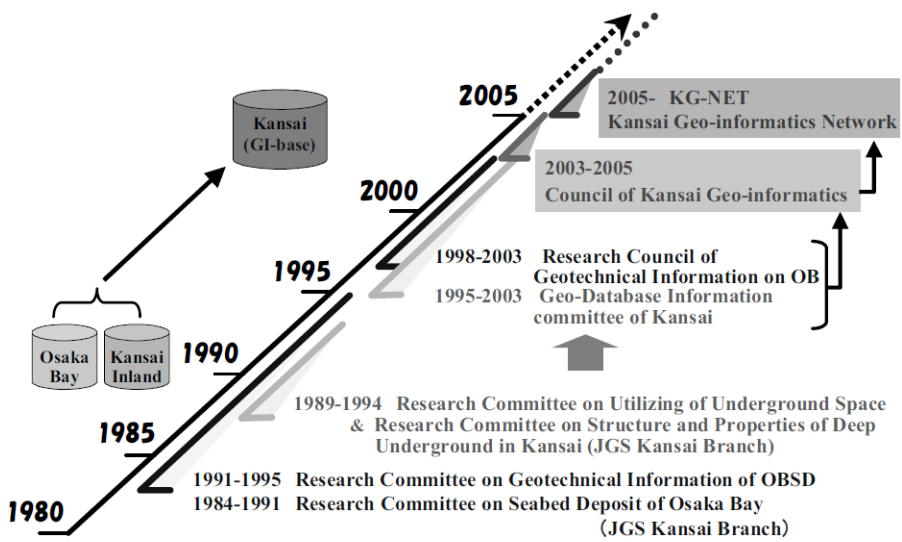


Figure 2.14 History of development of GIbase

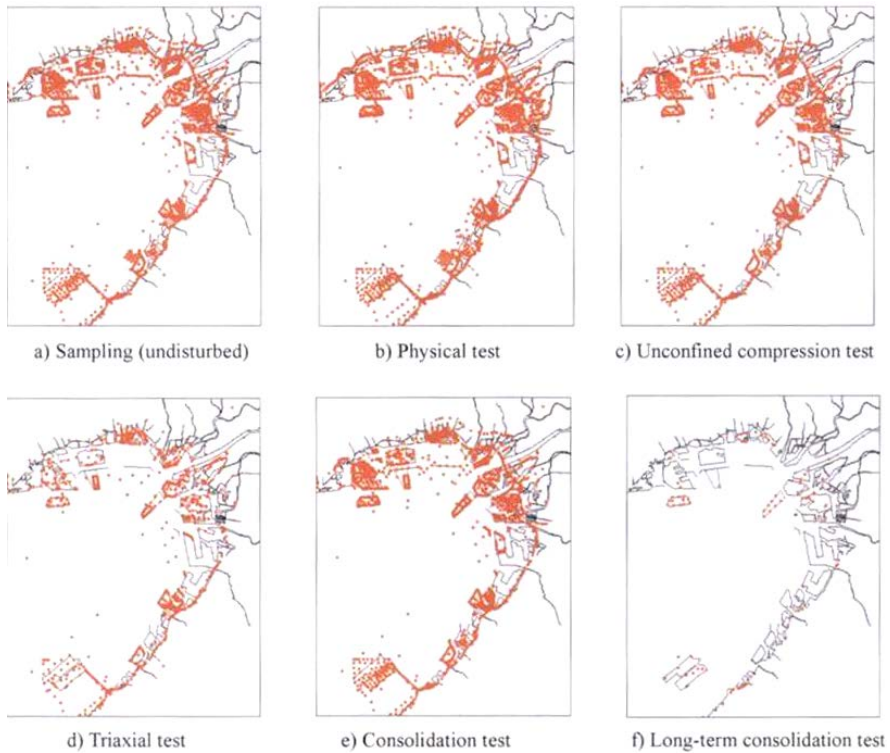


Figure 2.15 Locations of boreholes for sampling and soil testings in Gbase

GeoInfo

GeoInfo was developed to manage and utilized site investigation data over whole domestic land in Korea. The data in this system is mainly acquired from construction sites for roads, railroads and highways. This is a web-based system for public services as shown in Figure 2.16. The first characteristic of this system is well-defined standard data formats to deal with site investigation data including borehole logs, in-situ tests and laboratory tests. And the second characteristic is that it supports not only fundamental functions of the Gbase but also user-defined cross-sectional views for

multiple boreholes. The last characteristic is to categorize the borehole data into soil borehole data and rock borehole data. This system adopted a RDMS considering the scalability and the RDB of this system is structured briefly. The detailed database structure is similar to that of Gbase and well described in KICT's final research report (KICT, 2001). Figure 2.16 shows the main screen of this system, which shows the spatial location of site investigation data.

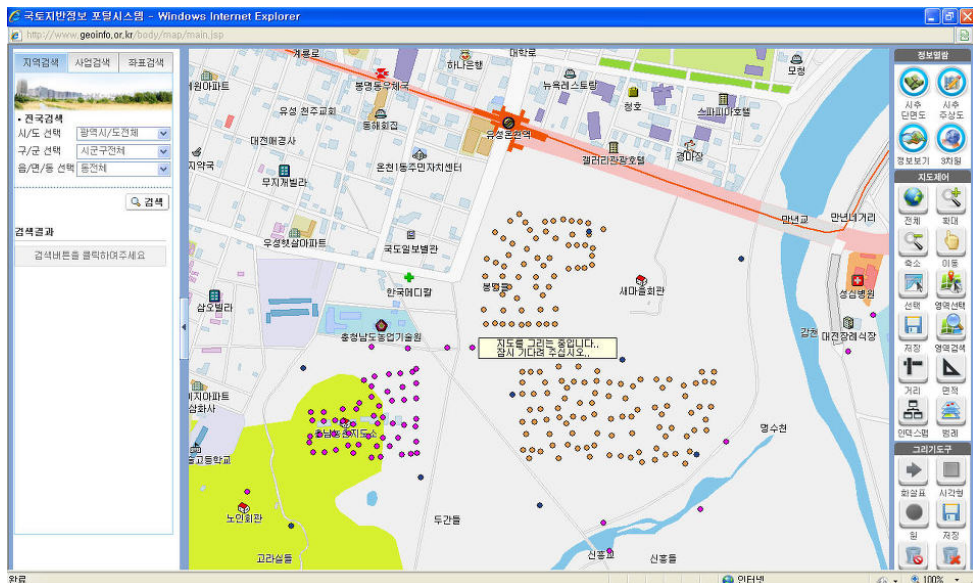


Figure 2.16 Main screen of GeoInfo

IMSSG (Integrated construction Management System on Soft Ground sites)

Integrated construction management system on soft ground sites (IMSSG) was developed based on GIS concepts. The system consists of the database and the system software. The system software performs various functions to

manage, utilize, analyze and display data in the database with connection to the DB sever.

The database is a crucial element of GIS and it contains all collected filed data and processed data in the system. The database of the system was established based on well-defined standard data formats resulting from data standardization. That is, all available filed data and processed data were structured relating to their geographic information. The database and sub-modules of the system were combined integrated in single system and the system provides a familiar and user-friendly working environment with a standard Windows interface.

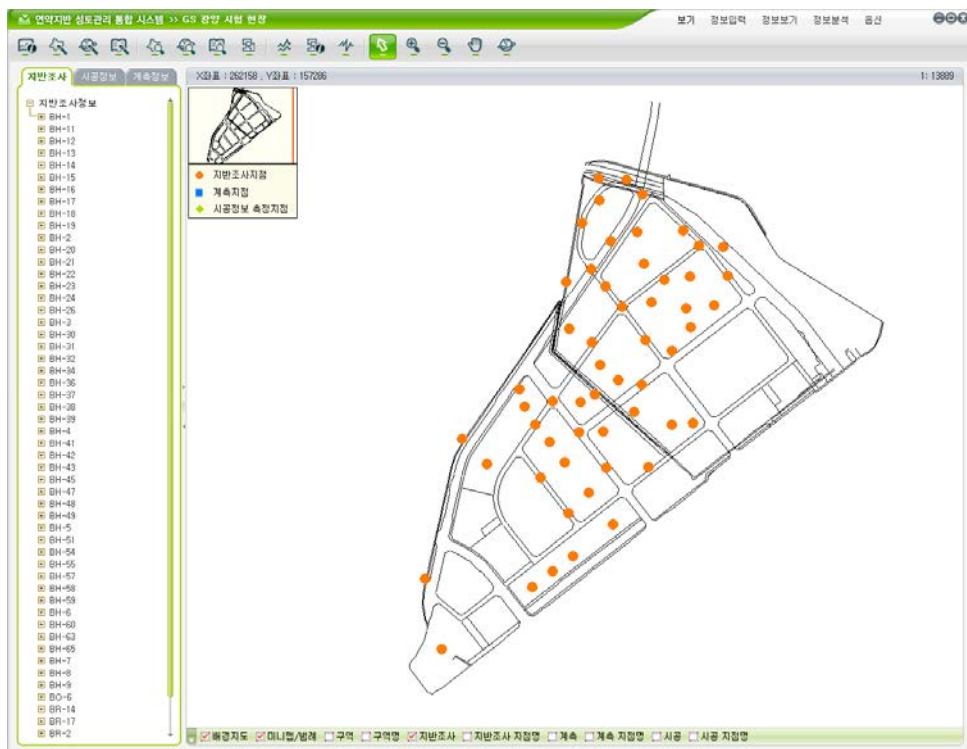


Figure 2.17 Management program of IMSSG (Chun et al., 2005)

3D reconstruction system of complex geological bodies

Cartographic geological and structural data collected in the field and managed by geographic information systems (GIS) technology can be used for 3D reconstruction of complex geological bodies. Using a link between GIS tools and Cad contents, stratigraphic and tectonic surfaces can be reconstructed taking into account any geometrical constraint derived from field observations. Complex surfaces can be reconstructed using large data sets analyzed by suitable geometrical techniques. Three main typologies of geometric features and related attributes are exported from a GIS-geodatabase:

- 1) Topographic data as points from a digital elevation model;
- 2) Stratigraphic and tectonic boundaries, and linear features as 2D polylines;
- 3) Structural data as points.

After having imported the available information into GIS platform, the following steps should be performed:

- 1) Construction of the topographic surface by interpolation of points;
- 2) 3D mapping of the linear geological boundaries and linear features by vertical projection on the reconstructed topographic surface;
- 3) Definition of geometrical constraints from planar and linear outcrop data;
- 4) Construction of a network of cross-sections based on field observations and geometrical constraints;
- 5) Creation of 3D surfaces, closed volumes and grids from the constructed objects.

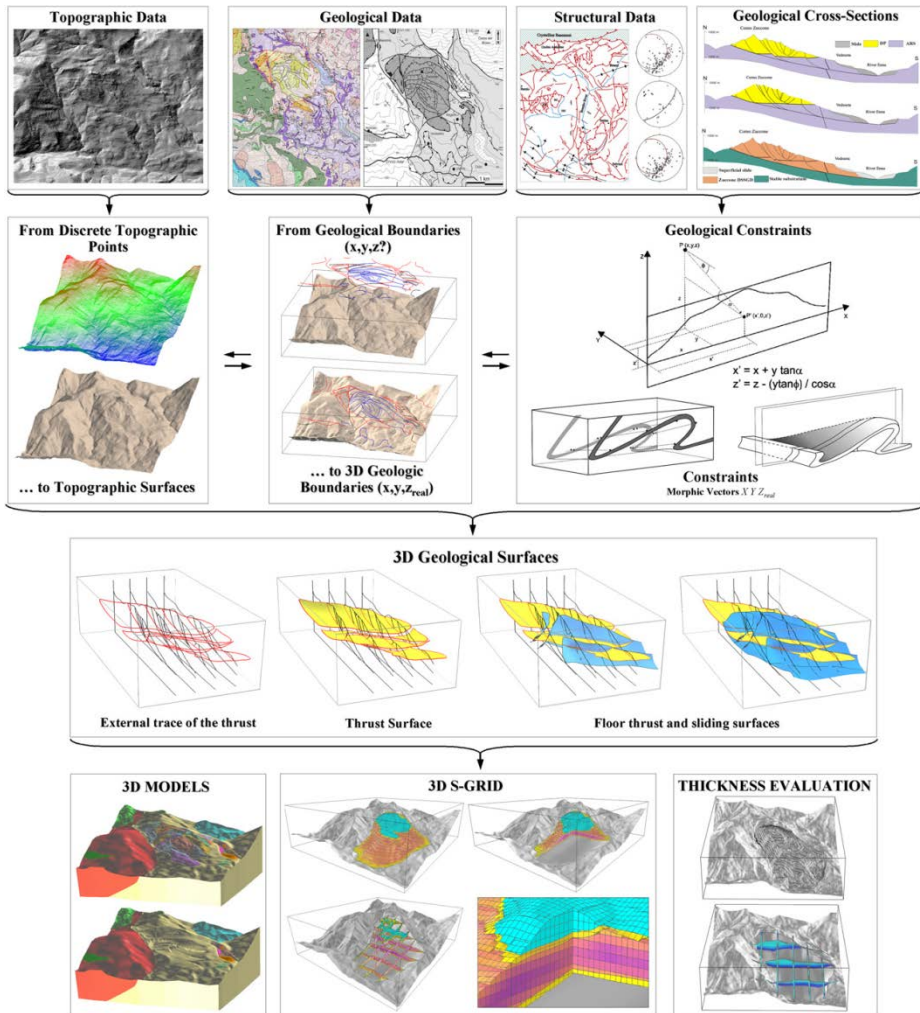


Figure 2.18 Schematic flow-chart for 3D modelling through data integration (Andrea et al., 2009)

2.3 Earthquake Hazard Management System

2.3.1 Earthquake hazard assessment approaches

The earthquake hazard is defined as the probabilistic measure of ground shaking associated to the recurrence of earthquakes. Earthquake hazard maps depict the levels of chosen ground motions that likely will, or will not, be exceeded in specified exposure times. Earthquake hazard assessment commonly specified a 10% chance of exceedance (90% chance of non-exceedance) of some ground motion parameter for an exposure time of 50 years, corresponding to a return period of 475 years.

Seismic disaster management and mitigation are required to establish effective and appropriate strategies to reduce earthquake hazards of vulnerability. However, these are not easy tasks, and require considerable resources and analyses (Drabek and Hoetmer, 1991). Their complexity dictates the use of an integrated seismic damage assessment methodology based on a computer-aided system, such as the geographic information systems (GIS) tool. GIS supports spatial decision-making based on multiple georeferenced datasets, and thereby makes possible earthquake hazard assessment for reducing or mitigating damage caused by earthquake shaking (Papadimitriou et al., 2008; Schneider and Schauer, 2006; Vahidnia et al., 2010). Comprehensive frameworks for seismic damage scenarios and geotechnical seismic risk analysis, including GIS-based evaluation tools, have

been developed and proposed as part of major loss estimation systems: HAZUS (FEMA, 2003); RADIUS (RADIUS, 1999); Risk-UE (Mouroux and Le, 2006); DBELA (Crowley et al., 2004). Moreover, evaluation of reliable site-specific seismic response characteristics in an entire area of interest is best handled on a GIS platform, because the geotechnical hazard is seriously affected by local site effects. Accordingly, the effective construction of a spatial database system is considered in this dissertation for reliable geotechnical earthquake hazard zonation mapping.

Previous studies of liquefaction hazard estimation

Liquefaction can be triggered by the rapid loading invoked by seismic shear wave energy when there is insufficient time for excess pore-water pressure to dissipate through natural drainage (Kim et al., 2012a). Liquefaction can also be triggered by rapid straining along discrete horizons, such as landslides and lateral spreading. Any type of rapid loading situation that serves to elevate the pore-water pressure can result in cyclic softening of fine-grained soil materials or liquefaction in porous materials of relatively low density with little or no cohesion (Luna and Frost, 1998). Various types of liquefaction damage, such as landslides, lateral spreading, and sand boil events, have occurred in port areas constructed by earthwork, such as dredging and reclamation. Extensive liquefaction-induced damage has frequently been observed in recent earthquake events, such as the 1964 Niigata, 1983 Nihonkai-chubu, 1993 Hokkaido-nansei-oki, 1995 Hyogoken-nanbu, 1999 Kocaeli, 1999 Duzce, 2010 Haiti, 2010 Chile, and 2011 Tohoku

earthquakes (Green, 2001; Kim et al., 2012a; Green et al., 2011; Bhattacharya et al., 2011; Sumer et al., 2007; PIANC, 1997).

Assessing the liquefaction potential is an important issue in geotechnical earthquake engineering. Several methods have been proposed to evaluate the liquefaction potential of sandy soils for which insufficient geotechnical data exist. In-situ tests, such as the standard penetration test (SPT), cone penetration test (CPT), Becker penetration test (BPT), and field measurements of the shear wave velocity (V_s), have been used as empirical tools to evaluate the liquefaction resistance of soil layers that may liquefy during an earthquake (Youd and Perkins, 1987; Finn, 2002; Zhao et al., 2007). A simplified procedure based on SPT- N values is commonly used in liquefaction assessments in most countries (Seed and Idriss, 1971), including Korea.

The original simplified procedure based on empirical rules has been modified and improved over the years (Youd and Perkins, 1987; Seed et al., 1985; Youd and Perkins, 1978). And Iwasaki et al. (Iwasaki et al., 1982) proposed the liquefaction potential index (LPI), which evaluates liquefaction potential over the length of a boring or a CPT. Toprak and Holzer (2003) also published a field assessment study of the LPI using CPT soundings at sites that had already experienced liquefaction. Elkatib et al. (Elkatib et al., 2003) discussed the site-specific effects of soil heterogeneity and methods of geotechnical evaluation, including liquefaction of the local ground condition. Baise et al. (Baise et al., 2006) evaluated the liquefaction potential based on the stratigraphic layer; however, the depth dependence was ignored within single layers.

Several researchers have applied GIS tools to describe the liquefaction

potential results based on the simplified procedure to determine the LPI (Luna and Frost, 1998; Elkateb et al., 2003; Baise et al., 2006; Dawson and Baise, 2005). However, most previous applications have focused on one-dimensional (1D) or two-dimensional (2D) evaluations of liquefaction. Luna and Frost (Luna and Frost, 1998) considered the three-dimensional (3D) geologic ground conditions of the liquefaction hazard of Treasure Island in San Francisco Bay during the 1989 Loma Prieta earthquake by comparing individual two-foot slices. Similarly, most research that integrates GIS and earthquake hazard estimation has been restricted to 3D spatial modeling rather than producing cartographic depictions (Andre and David, 2003). And earthquake disaster modeling has long been in need of an integrated framework for effective real-time assessment. In short, there are no proposed applications to estimate the liquefaction potential in real-time for the entire continuous areas, with the utilization of seismic monitoring information.

Previous studies of structural seismic fragility analysis

The fragility of a structure or component is defined as the conditional frequency of failure given a value of the response parameter. The response parameter x could be the force on the component or structure that is induced by a wind, the stress due to an earthquake, etc. The conditional frequency of failure F_0 given x_0 is the fragility of the component at that level. In other words, the fragility curve is the cumulative distribution function of the component's capacity to withstand the imposed stress x . In many seismic risk studies, the response parameter x is the peak horizontal ground acceleration

measured in units of g , the gravitational acceleration. Furthermore, the fragility curve is usually a lognormal distribution (other distributions have also been considered, like the truncated lognormal and the normal distribution).

The time-variant reliability problem in its wider terms is the problem of computing the probability that a nonlinear system with random properties exposed to random, time-varying actions ceases to satisfy a number of requirements, whose definition is also subject to uncertainty. In seismic reliability it is common to obtain the abovementioned probability conditional on an intensity measure of the input ground motion, the so-called fragility function. To compute the unconditional probability that, at a given site and in a given period of time, the structure fails to perform satisfactorily, the uncertainty in the seismic intensity is reintroduced by means of the hazard function (complementary cumulative distribution function (CDF) of the intensity) by convolving the derivative of this latter with the fragility function, leading to what is usually called seismic risk.

A large number of methods have been proposed to compute fragility functions in the last 20 years, ranging from expert judgment (ATC 1985), to data analysis on observed damages (Singhal and Kiremidjian, 1998; Shinozuka et al., 2000), to fully analytical approaches, as, for example, in Cornell et al. (2002); Gardoni et al. (2002, 2003); Au and Beck (2003); Schotanus et al. (2004); and Lupoi et al. (2004). General reviews can be found, for example, in Kiureghian, D. A. (1996) and Pinto et al. (2004). A feature common to most of the analytical approaches is the use of a reduced number of simulations to compare probabilistically the maximum structural responses

with the corresponding capacities. The difference among them lies essentially in their balance between cost and accuracy, i.e., in their ability to account economically for all the aspects entering the reliability problem. These latter include:

- 1) The possibility of the structure reaching collapse in more than one failure mode (system reliability problem), as it is common for civil engineering structures such as multistory buildings and bridges;
- 2) The dependence among the possible failure modes;
- 3) The uncertainty in the capacity of the structure, due to the approximate nature of the models and to the variability of the system parameters; and
- 4) The influence on the dynamic response of the variability of the system parameters.

2.3.2 Previous earthquake hazard management systems

HAZUS (Hazard U.S.)

USA has built a seismic disaster evaluation system by carrying out studies on seismic damage prediction and is utilizing it in establishing the plan to cope with seismic disasters. Representatively, HAZUS (Hazard United State) which was developed by FEMA (Federal Emergency Management Agency) and NIBS (National Institute of Building Sciences) in 1997 for the first time is equipped with a GIS (Geographic Information System) based extensive database (vulnerability by building type determined using statistic

values of seismic damage, etc.) and can predict the damage on not only residential area, commercial facility and school buildings but also on essential facilities like hospitals, fire stations and roads through ground response analysis (Ground Shaking and Ground Failure) based on input values such as the location of occurrence, magnitude and faults of historic earthquakes, virtual earthquakes or actually measured earthquakes (Figure 2.19). Also, it predicts social factors to be considered such as estimation of disaster refuge facilities and displaced households, and magnitude of economic loss such as estimation of restoration expenses.

However, it has some limitations in applying to other region except for U.S. for the reason of that HAZUS was developed for disaster estimation in U.S. based on the data which contains characteristics of soil and earthquake movement in U.S. And it has advantages to estimate damage roughly for extensive area but it is hard to apply for specific area or special structures like port.

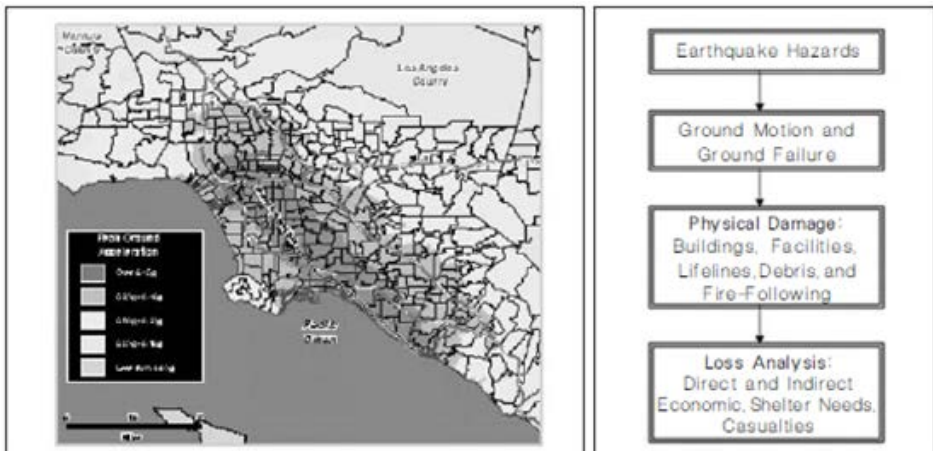


Figure 2.19 Systematic procedure of HAZUS (FEMA, 2003)

Integrated earthquake damage assessment methodology

Integrated earthquake damage assessment studies consider the combined consequences of primary and collateral effects. Risk estimation projects implemented in earthquake-prone areas worldwide show great variety both in terms of the sophistication of application and the parameters included. To date there is no standardized approach for spatial damage assessment analysis. Theoretical developments and experimental justification, which increase the understanding of fundamental behavior, change this route towards more definitive and representative methodologies. To ally with this trend, an integrated damage assessment methodology is developed (Cinicioglu et al., 2007). Ground shaking, liquefaction, seismic bearing capacity degradation and landslides are considered as the damage-causing phenomena in the developed methodology. The risk from each of these damage-causing effects is evaluated separately at a reasonably rigorous level and then integration is made. Assessment of damage levels for individual events separately is necessary in order to know which component of the phenomena should merit the most time and resource allocation for mitigation. The main steps of the integrated earthquake damage assessment methodology can be followed through the flow chart given in Figure 2.20. The basic features of the proposed methodology can be summarized as:

- 1) Each effective phenomenon is considered separately and in combination;
- 2) Quantitative interpretation is made at all levels of analysis;
- 3) Seismic bearing capacity degradation has been acknowledged as a damage-causing phenomenon in this paper and forms one of the

components of the integrated damage assessment;

- 4) The methodology requires analyses for each component of the approach to be carried out to the best possible level that could be expected from a spatial analysis;
- 5) The proposed approach is applicable anywhere in any earthquake prone area;
- 6) The methodology inherently carries soil-structure interaction concept by combining site-specific geotechnical and structural evaluations.

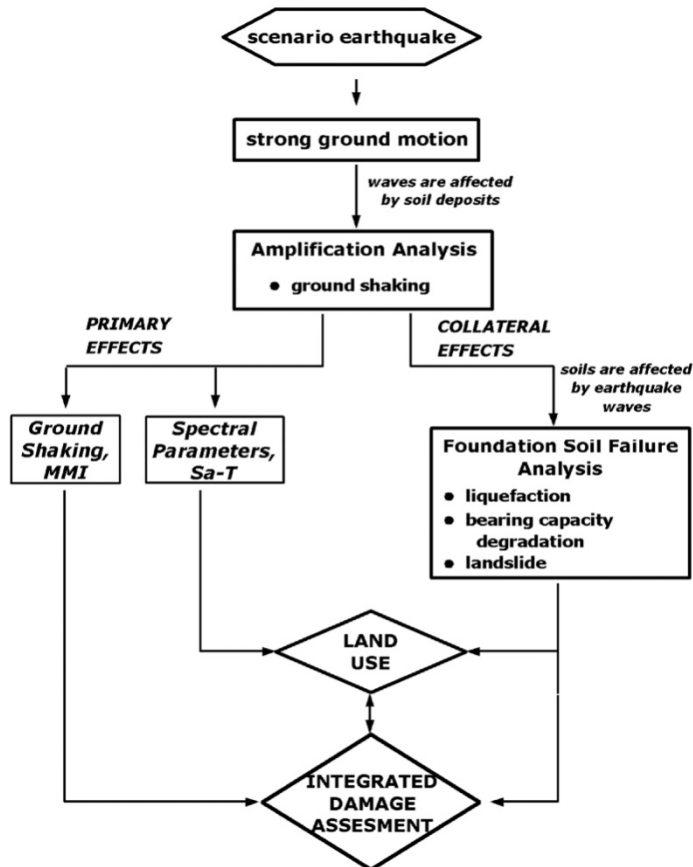


Figure 2.20 Flowchart for the integrated earthquake damage assessment methodology (Cinicioglu et al., 2007)

TELES

The methodology and associated application software are contained in HAZUS (RMS, 1997). Essentially, the Taiwan Earthquake Loss Estimation System (TELES) program follows a similar approach used in HAZUS97. But, to accommodate the special environment and engineering practices in Taiwan, minor modifications in analysis models and parameters have been made.

The results of the TELES program can be used to plan and stimulate efforts for earthquake hazard mitigation, to prepare for emergency response and recovery from an earthquake. In other words, it serves as a decision support system for pre-earthquake mitigation and post-disaster management. It also provides a standard seismic risk assessment and loss estimation methodology. Expected benefits of a standard methodology include: consistency of approach, more economic use of available resources, improved sharing of the state-of-the-art knowledge, more consistent measurement of performance and progress in hazard mitigation efforts, and more effective means to set local, regional and national priorities in hazard mitigation.

To achieve the aforementioned goals, TELES is developed according to the following criteria:

- 1) Standardize data classification system and analysis methodology;
- 2) Provide user-friendly application software;
- 3) Accommodate various user needs and different levels of funding;
- 4) Use modular approach and balance the input/output accuracy;
- 5) Utilize state-of-the-art analysis models and parameters, which are non-proprietary.

Figure 2.21 shows the framework of methodology used in TELES. The analysis modules contain potential earth science hazard (PESH) analysis, direct/indirect physical damage assessment and direct/indirect social and economic loss estimation.

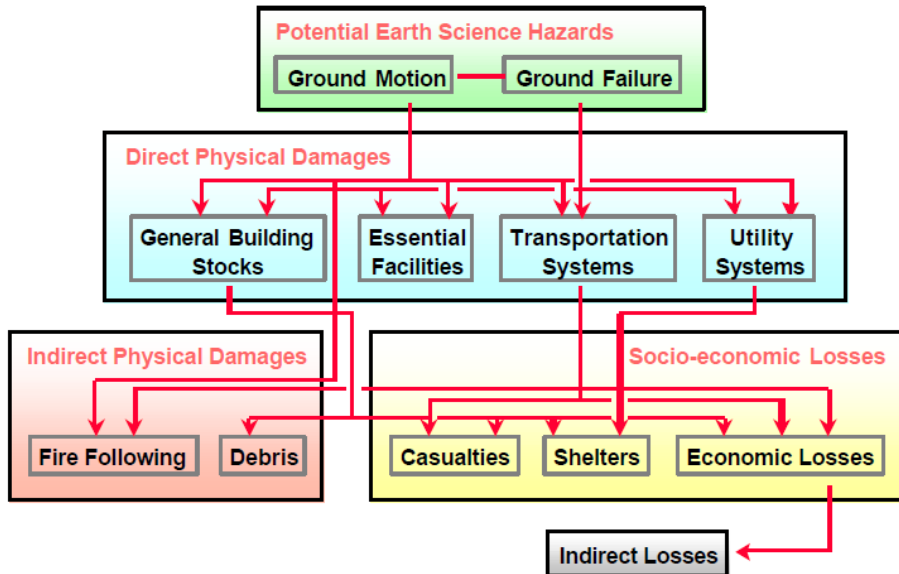


Figure 2.21 Framework of hazard analysis, risk assessment and loss estimation methodology in TELES

REDARS (Risk from Earthquake Damage to Road way System)

Risk from earthquake damage to road way system (REDARS) was built for the purpose of comprehensively informing the damage condition of bridges and road systems when a seismic disaster occurs and supporting decision making for restoration, and it is targeting highways in western United States (LA and California). Seismic damage prediction techniques such as

liquefaction, surface fault rupture and earthquake hazard of ground motions are applied to predict the seismic damage condition of road system and the extent of influence of seismic damage on traffic system service and economic expense loss are predicted. Figure 2.22 shows the approach for assessing the accuracy of individual modules of REDARS.

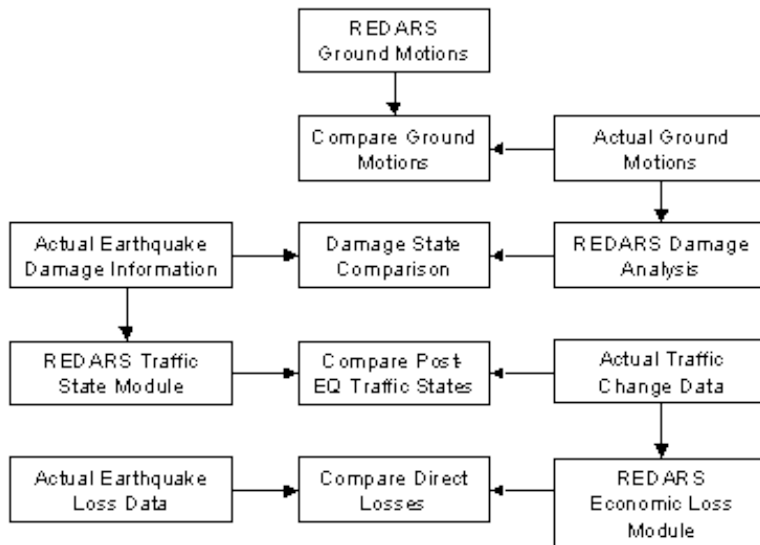


Figure 2.22 Approach for assessing the accuracy of individual modules of REDARS

UrEDAS (Urgent Earthquake Detection and Alarm System)

Japan has built a database of earthquake generated all over Japan and the history of seismic damage as well as ground characteristics of those locations and established UrEDAS (Urgent Earthquake Detection and Alarm System) which processes the information about the location where an earthquake has occurred together with its magnitude in real-time (Figure 2.23).

UrEDAS is the first real-time P-wave alarm system in practical use in the world. It is able to process digitized waveforms step by step without storing the waveform data. As the amount of processing does not differ whether or not an earthquake occurs, system failure due to overload will not occur.

There are two types of UrEDAS at present; UrEDAS and Compact UrEDAS. Function of the UrEDAS is estimating magnitude and location of earthquake by P-wave and issuing the alarm to places which may cause damage. Compact UrEDAS will evaluate whether the earthquake will be destructive or not, and will alarm if need. UrEDAS and Compact UrEDAS can issue the alarm in case of earthquakes within range of 200 km and 20 km, respectively.

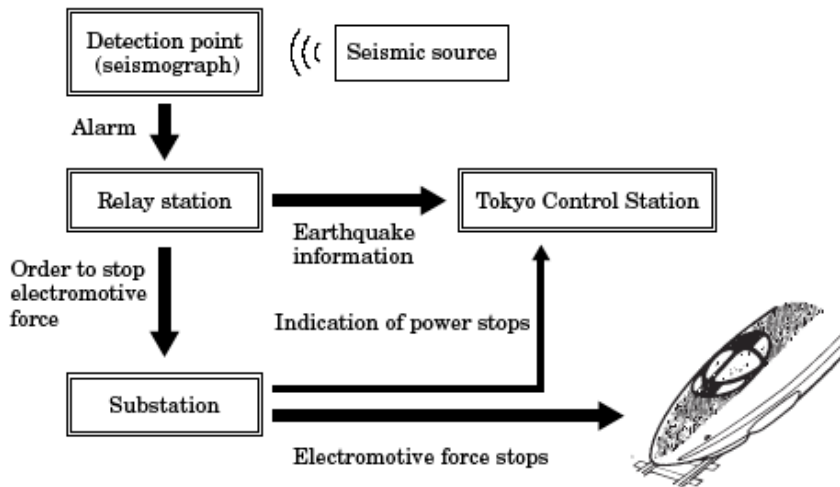


Figure 2.23 Process of UrEDAS

ANSS (Advanced Nation Seismic System)

The mission of ANSS is to provide accurate and timely data and

information products for seismic events, including their effects on buildings and structures, employing modern monitoring methods and technologies. This mission serves a basic function of the national earthquake hazards reduction program (NEHRP) , and drives the four basic goals of the planned system:

- 1) Establish and maintain an advanced infrastructure for seismic monitoring throughout the United States that operates with high performance standards, gathers critical technical data, and effectively provides information products and services to meet the Nation's needs. An Advanced National Seismic System should consist of modern seismographs, communication networks, data processing centers, and well-trained personnel; such an integrated system would constantly record and analyze seismic data and provide timely and reliable information on earthquakes and other seismic disturbances.
- 2) Continuously monitor earthquakes and other seismic disturbances throughout the United States, including earthquakes that may cause a tsunami or precede a volcanic eruption, with special focus on regions of moderate to high hazard and risk.
- 3) Thoroughly measure strong earthquake shaking at ground sites and in buildings and critical structures. Focus should be in urban areas and near major active fault zones to gather greatly needed data and information for reducing earthquake impacts on buildings and structures.
- 4) Automatically broadcast information when a significant earthquake occurs, for immediate assessment of its impact. Where feasible, for sites at distance from the epicenter, broadcast an early warning

seconds before strong shaking arrives. Provide similar capabilities for automated warning and alert for tsunamis and volcanic eruptions.

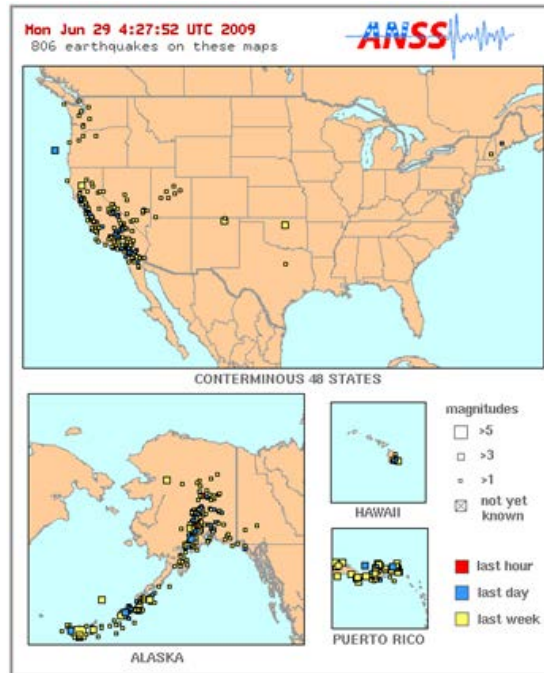


Figure 2.24 Analysis report of ANSS

NDMS (National Disaster Management System)

Korea has analyzed the characteristics of disaster information system mainly using HAZUS of USA and disaster prevention system of Japan as objects and reviewed applicability to Korea. Recently, a study on establishment of a system adequate for domestic situation is being carried out, which includes project to establish a pilot system to cope with national disaster management system (NDMS) promoted by National Emergency

Management Agency (NEMA) of Korea. The NDMS of NEMA is targeting buildings in the city area as objects of system construction and is playing the role of a comprehensive disaster prevention business system which includes prediction of damage on buildings, and selection and search of dangerous buildings and refuge facility.

NEMA has started its construction since 2005 and this system has been updated continuously. It is the system which constructs intensity distribution map based on the information such as occurrence time, epicenter and magnitude and estimates loss of human lives and buildings or damage to lifeline facilities when an earthquake occurs. In this system, fragility functions which are applicable to Korea are developed and adopted to improve estimation accuracy of the system. However fragility functions for harbor structures have not been suggested and empirical formulas using height and site classification by soil map are used to calculate amplification coefficient of the ground. Furthermore the size of the grid is 2 km by 2 km, so that it can make a mistake to estimate seismic damage of small area such as port site.



Figure 2.25 An example of NDMS

2.4 Summary

In this chapter, basic concepts of GIS and reviews for previously developed GRISs are described. In addition, earthquake hazard assessment approaches and previous earthquake hazard management systems are reviewed.

- 1) For development of integrated system, construction of systematic geodatabase is essential, which must be well designed because it is crucial to efficiency, applicability and scalability of GTISs.
- 2) However, previous all GTISs and earthquake hazard management systems described in this chapter has some disadvantage that result from incomplete data standardization with geographic data and not fully probabilistic evaluation in the decision making process for earthquake hazard assessments.
- 3) Most of the previous GTISs were developed for a specific geotechnical practice and they are based on commercial GIS software, which support an easy-to-use GIS environment by providing tools for managing spatial data, performing spatial analysis and displaying data.
- 4) Previous GTISs are difficult to apply to other geotechnical practices and need large amount of effort to overcome the functional boundaries of commercial GIS software.
- 5) The GTIs and earthquake hazard management systems focused only the input and output functions of geotechnical datasets or earthquake

hazard. Consequently, there are limitations: handling small scale database; one-way data processing; lack of analysis function (such as real-time earthquake hazard analysis tool); limited geotechnical information.

- 6) The development of GIS-based real-time system in this study started from the considerations: data modeling to construct the well-defined standard data formats; real-time seismic monitoring and hazard assessments; complementary data processing; geostatistical modeling.
- 7) And the database of the developed system in this study was constructed based on generalized standard data formats.
- 8) The application program of the developed system, which performs various functions to manage, utilize and analyze all data stored in the database, was developed independently, not based on commercial GIS software, with consideration on applications of other practices.

3. Real-time Framework for Earthquake Hazard Assessment

3.1 Concept of Real-time Framework for Earthquake Hazard Assessment

3.1.1 Real-time framework procedure

A methodology was proposed for near real-time earthquake hazard assessment using the schematic concept shown in Figure 3.1. The arrows represent the sequential data processing. This framework functions as a database for geographic, geotechnical, and structure data and is able to receive automatic transmissions of seismic monitoring data. The database was constructed based on geographic information system (GIS) platform, and the attribute data of target site having earthquake hazard potential is related with spatial information. And this framework was comprised two fundamental methods: geostatistical 3D integration and real-time earthquake hazard assessment.

The geostatistical 3D integration method was established to consider the reliable continuous geotechnical information using database. The integration method was composed of outlier detection methods (the cross-validation based method and the generalized extreme value distribution based method) to optimize the borehole datasets, and 3D integration method based on indicator

kriging to obtain 3D geo-layer information. By using the integration method, the site-specific criteria of geomaterial are determined. After all, the 3D geotechnical spatial grid considering dynamic properties can be constructed in database from 3D geo-layer.

By assigning 3D geotechnical spatial grid in database, initial state of the seismic load can be monitored as rock outcrop acceleration records automatically obtained from accelerometers and transmitted to the framework in real-time. The accelerometers are installed on nearby outcrops of bedrock at target site and measure the rock outcrop acceleration. The records from either downhole accelerometers placed below the layer having earthquake hazard potential or on nearby outcrops of bedrock are used to predict ground motions. Seismic waves are amplified as they pass through soil deposits according to site-specific response characteristics (Kim et al., 2012a; Youd and Perkins, 1978). And the site-specific liquefaction hazard can be evaluated in real-time based on geotechnical spatial grid. At the same time, the structure seismic damage correlated with fragility curve can be estimated in real-time.

Ultimately, the earthquake damage due to liquefaction and structure fragility affecting target structures can be evaluated by simulating synthetically the amplified seismic load and 3D dynamic ground properties for the current state of target area on a real-time basis. For the real-time approach, the systematic framework includes an integrated earthquake hazard assessment composed of sequential sub-procedures. The interrelated assessment procedures are incorporated with the database on a real-time basis, interpreted, and presented as reliable 2D and 3D visualizations of geo-layer and geotechnical earthquake parameters.

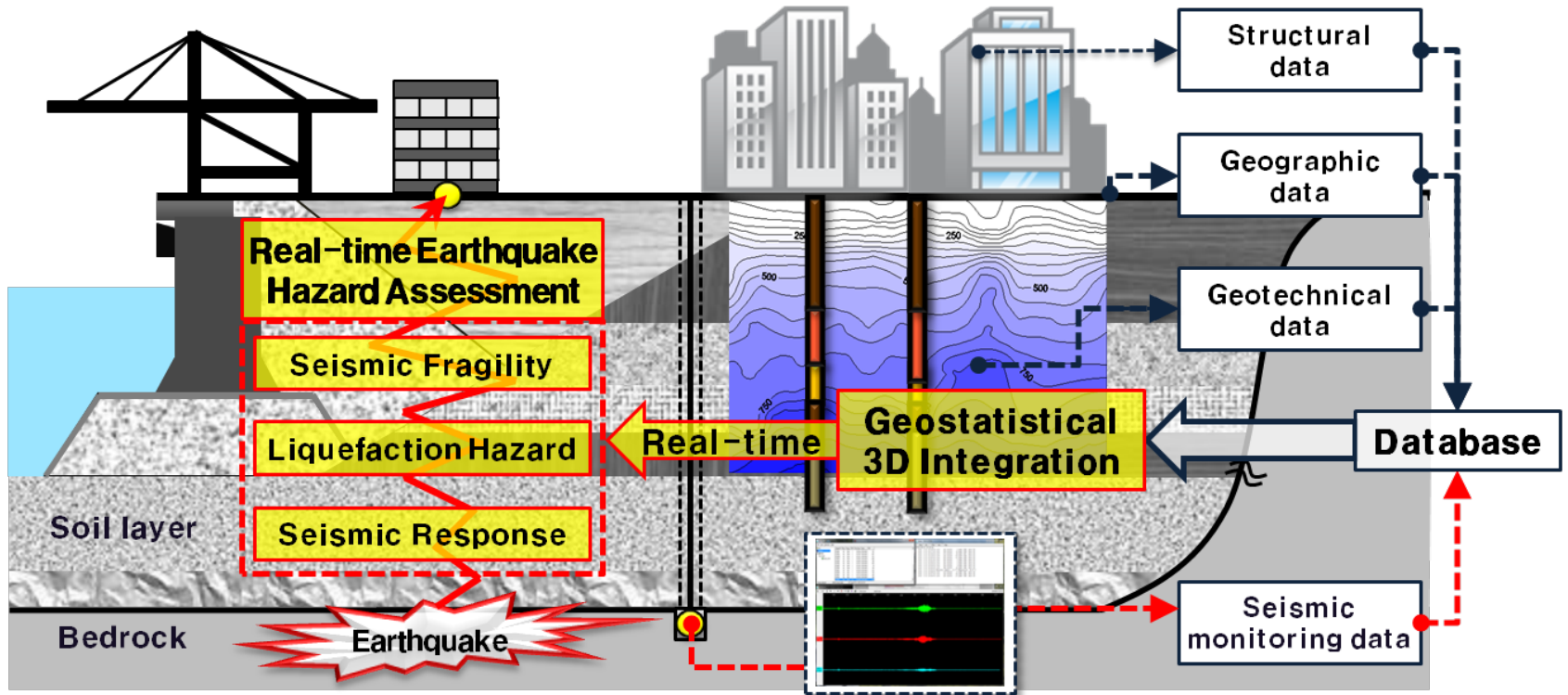


Figure 3.1 Schematic concept for real-time assessment of the geotechnical earthquake hazard based on GIS

3.1.2 Methodologies for real-time earthquake hazard assessment

The integrated framework consists of a Database (DB) and systematic modules. The database contains all field data and processed data in the system. The sub-modules execute various functions on managing and utilizing information in the database with connection to the database; input of data, geostatistical 3D integrated data based on input data, real-time earthquake hazard data, and output of data. The framework including all these functions focuses on user-friendliness and real-time applications. The following is an explanation of the details of the integrated framework (Figure 3.2).

1) Database (DB): DB is the backbone of the developed framework. It stores not only primary collected data such as geography, geotechnical investigation, structure, and real-time based transmitted seismic monitoring data from seismometer server (from KISS; Korea Integrated Seismic System) but also secondary processed data obtained from geostatistical 3D integration and real-time earthquake hazard assessment. It contains all data as alphanumeric values according to standard data formats, which are the outcome of data classification and standardization with geographic data. The data stored in the database can be easily utilized in the framework.

2) Input Function: Input function provides an effective way to store and arrange all collected field data including electric or non-electric documents, geographic, geotechnical investigation, structure, seismic monitoring, and analysis data, according to a standard data format based on geodatabase (GDB).

3) Geostatistical 3D integration for geotechnical spatial grid function: This function constructs distributed 3D geotechnical data over a selected domain from input data acquired from the target site by applying the geostatistical methods. This method has three functional modules with the database: Outlier detection method, geostatistical integration method, and construction method of geotechnical spatial grid. Geotechnical investigation results always reflect a level of soil uncertainty. To determine the uncertainty, the outlier detection methods, which optimize the borehole datasets, is conducted. And geostatistical integration method based on indicator kriging is performed using optimized borehole and digitized geophysical tomography to construct 3D geo-layer. The 3D geo-layer are categorized and subdivided to representative soil profile and dynamic properties to assign 3D geotechnical spatial grid into the database. This step must be conducted as a baseline prior to the occurrence of earthquakes.

4) Real-time earthquake hazard assessment function: The real-time framework has three functional modules with the database: real-time seismic load determination, real-time liquefaction hazard estimation, and real-time structure fragility evaluation. The first phase, linked with the 3D geotechnical spatial grid, correlations between rock outcrop acceleration and maximum acceleration of each layer considering site response characteristics are predetermined. Thus, as earthquake events occur, as soon as monitored rock outcrop acceleration data are transmitted from the accelerometer, seismic load at each spatial grid is estimated. The second phase, the potential damage due to liquefaction is estimated by integration of the geotechnical spatial grid and correlated maximum acceleration of each layer based on the simplified LPI

evaluation method in real-time. And the third phase, the structure failure is evaluated by integration of the geotechnical spatial grid and correlated maximum acceleration based on the structure fragility curve in real-time.

5) Output Function: The output function displays all attributive information in the database by using tables and graphics according to its characteristics either, on screen or as a document. Also, all data in DB can be output as a chart or a graphic. The graphic functions, such as 2D plane view, 2D sectional view, and 3D view display interpolated data with field data over an arbitrary domain at same time. All of the charts, graphs and drawings can then be printed. Especially, the earthquake hazard can be visualized and forecasted as 2D or 3D maps overlain by satellite images. And the seismic severity (composed of seismic load, liquefaction, and structure fragility) of the target structure can be determined using zonation criteria in real-time.

In this proposed framework, the computer-based method for 3D geotechnical information and real-time assessment of spatial earthquake hazard was embedded based on a stand-alone system developed using Microsoft Visual BASIC, the Esri ArcGIS developer tool (Esri, 2006; Lee and Wong, 2001), and the GSLIB of Stanford University (Clayton and Andre, 1997). The ArcGIS developer tool was mainly used for development of the database, evaluation of the results, and spatial visualization. In addition, a sophisticated kriging interpolation program based on Visual BASIC code was developed and adopted by the spatial analysis component of the GSLIB.

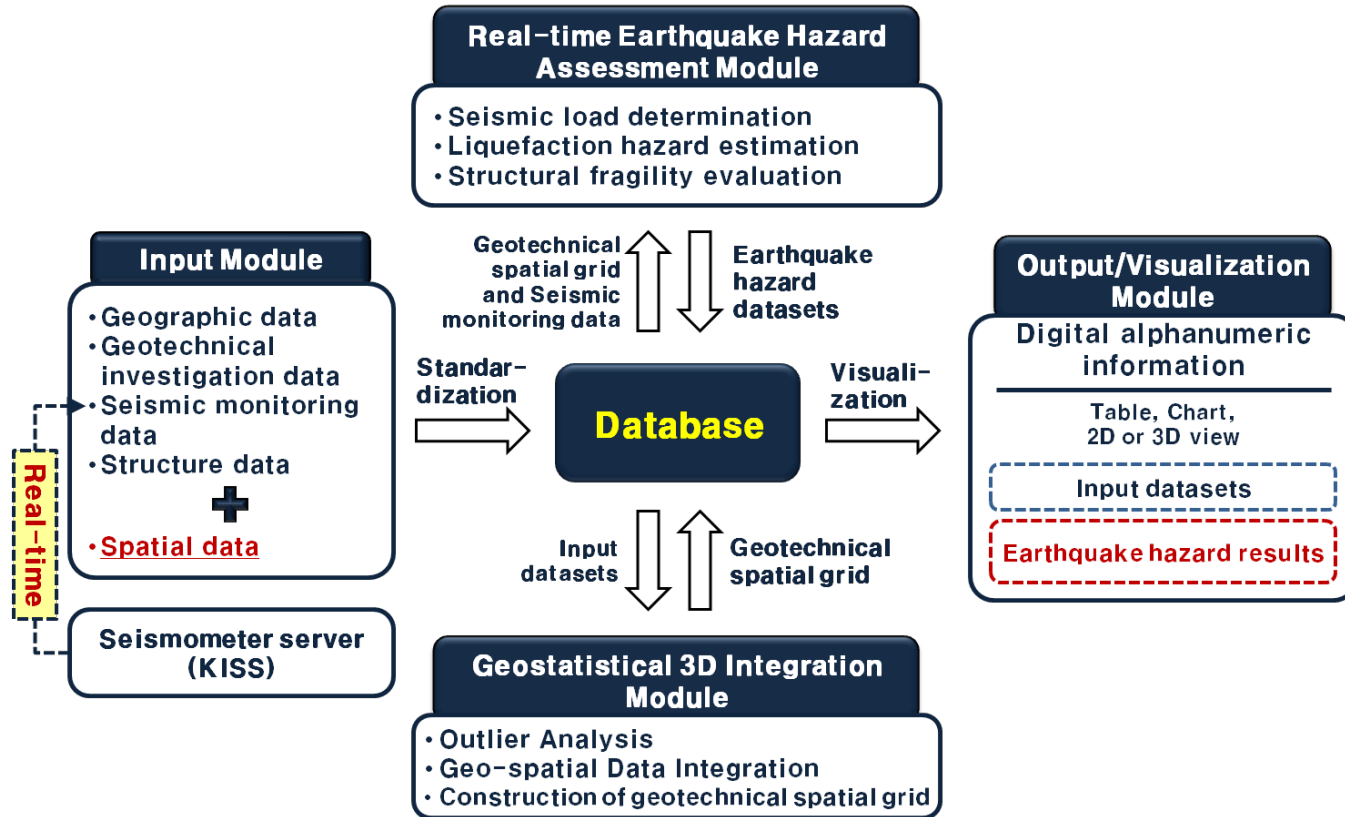


Figure 3.2 Integrated framework with geotechnical earthquake hazard assessment procedures

There are several assumption conditions and preceded assessments to estimate the possible geotechnical earthquake hazard for a target site in real-time, as soon as the earthquake occur. Especially, the preceded procedures consist of the building of database, geotechnical spatial grid construction and site response analysis in order to consider site-specific seismic response overall target area, prior to the occurrence of earthquake. As an earthquake occurs nearby target site, the possible liquefaction hazard can be estimated in real time by linking with the rock outcrop acceleration data monitored from accelerometer.

Thus it is possible to rapidly understand the inherent geotechnical seismic failure on target site, which are invisible to the naked eye. Through simulation of the developed systematic framework, it is potentially useful for stabilizing work to prevent secondary disasters and immediate rehabilitation of the transportation lifelines to improve the accessibility of relevant areas. For this reason, this newly developed systematic framework can be effectively utilized for the decision-making necessary to provide earthquake risk management and develop optimized evacuation paths and restoration plans for target structures.

3.2 Systematic Database for Integrated Framework

3.2.1 Database schema of integrated framework

The first step for systematic earthquake hazard assessment is construction of database from input module. To build a reliable database for the current ground conditions of the target area, it is necessary to consider the geographic conditions as well as the dynamic geotechnical properties from site investigations and earthwork records.

Table 3.1 Database schema of integrated framework based on geodatabase platform

Database	List of collected data
Geographic data	<ul style="list-style-type: none"> • Digital map • Satellite image map, aerial photograph and digital elevation model (DEM) data • Soil map and geology map
Geotechnical data	<ul style="list-style-type: none"> • Borehole investigation (current + initial ground condition) • Ground water level (GWL) records • Geophysical investigation (digitized tomography) • Geotechnical test results • Design and construction reports for earthwork
Structural data	<ul style="list-style-type: none"> • Structure information • Seismic performance evaluation results (→ discriminatory set-up of grid size)
Seismic monitoring data (Real-time)	<ul style="list-style-type: none"> • Acceleration-time series data • Rock outcrop acceleration data

After selection of the target area having earthquake hazard potential, the

database is built as listed in Table 3.1. The database is composed of the four components consisting of geographic data (borehole data, geophysical test data), structure data, and seismic monitoring data. The collected site condition datasets are incorporated in the database in advance.

3.2.2 Detailed information of database

The attribute datasets of collected information are incorporated with spatial information based on a spatial coordinate system. The geographic data is the basic information for GISs to refer to attribute information, and to correlate and analyze various information spatially. Geographic information of the framework was established based on a 3D coordinate system.

The one-dimensional soil profiles obtained from the boring logs and two-dimensional geophysical tomography data are included in the geotechnical data with corresponding digitized spatial information. The borehole data are collected from soil report to obtain current ground condition by complementary calibrating the initial and current geo-layer of boring log. In Figure 3.3, the borehole datasets before earthwork such as reclamation are substituted based on the GIS platform (Table 3.2). And geophysical tomography dataset (seismic refraction test data, resistivity test data etc.) are digitized and stored in database.

Additionally, the spatial distribution characteristics of structures related to seismic performance is taken into account to estimate the seismic damage

potential likely to affect the structures.

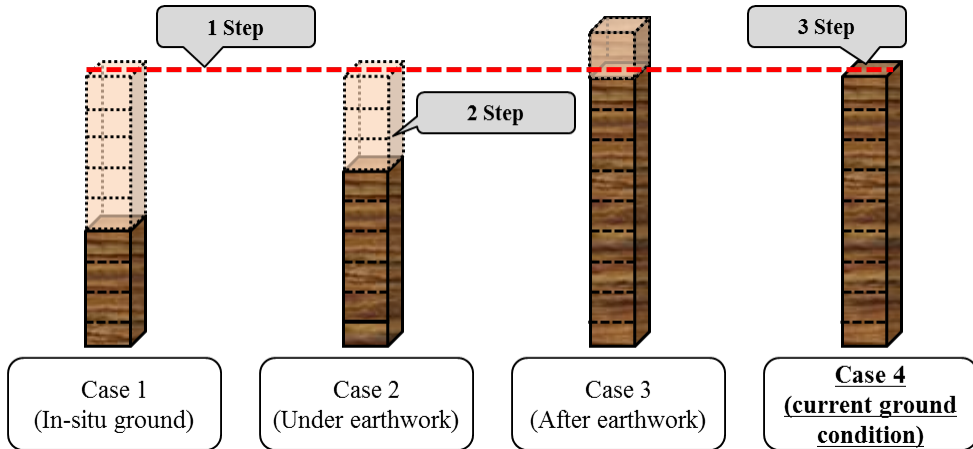


Figure 3.3 Substitution of geotechnical datasets using borehole before earthwork (ex. reclamation)

Table 3.2 Procedure for substitution of geotechnical datasets based on digital elevation model (DEM)

Step	Working details for each step
1st	Calibration of elevation based on digital numerical model
2nd	Substitution of geo-layer based on standard stratum
3rd	Building database for pseudo borehole of current ground condition

Especially, when an earthquake occurs at a target area, the rock outcrop accelerations are recorded from the accelerometers (installed on nearby outcrops of bedrock at target site), transmitted, and stored in this database in real-time. The detailed database schema is explained in ‘6.3.2 Database structure’.

4. Geostatistical 3D Integration for Geotechnical Spatial Grid

4.1 Construction Procedure of Geotechnical Spatial Grid

In the integrated framework, to figure out reliable geotechnical characteristics of site having seismic risk potential, spatial integration of feasible geotechnical investigation datasets which are geophysical tomography involved in continuous ground characteristics and soil profile of borehole, are possible based on GIS. The construction procedures of geotechnical spatial grid are composed of three phases: outlier analysis of borehole datasets, geostatistical 3D integration of borehole and geophysical datasets and 3D geotechnical spatial grid construction (Figure 4.1). In the procedure, database was preferentially constructed for borehole and geophysical information and also digital terrain map used to determine and calibrate site survey datasets.

The first phase is outlier analysis of borehole datasets. Typical geotechnical testing results reflect the level of soil uncertainty, which requires statistical corrections of the data for an appropriate engineering decision. So, to optimize the soil profile, outlier detection method was proposed to detect outlying data points using the cross-validation based method and the generalized extreme value distribution based method, and applied for borehole datasets.

In the second phase, framework for geostatistical three-dimensional

strata modeling of optimized borehole and geophysical datasets considering local variability was established. For geophysical tomography, the digitizing and classification for criterion of geophysical values was performed for stratification. On the basis of the built datasets, 3D integration with local trends using non-linear indicator transform was utilized based on the indicator kriging. And the cross-validation is performed using the borehole measurements sequentially excluded one borehole data in accordance with the indicator kriging to verify the assumed classification criteria.

The third phase is 3D geotechnical spatial grid construction. Based on the 3D stratified geo-layers, the geotechnical information for real-time earthquake hazard assessment was categorized with representative soil profiles and dynamic properties.

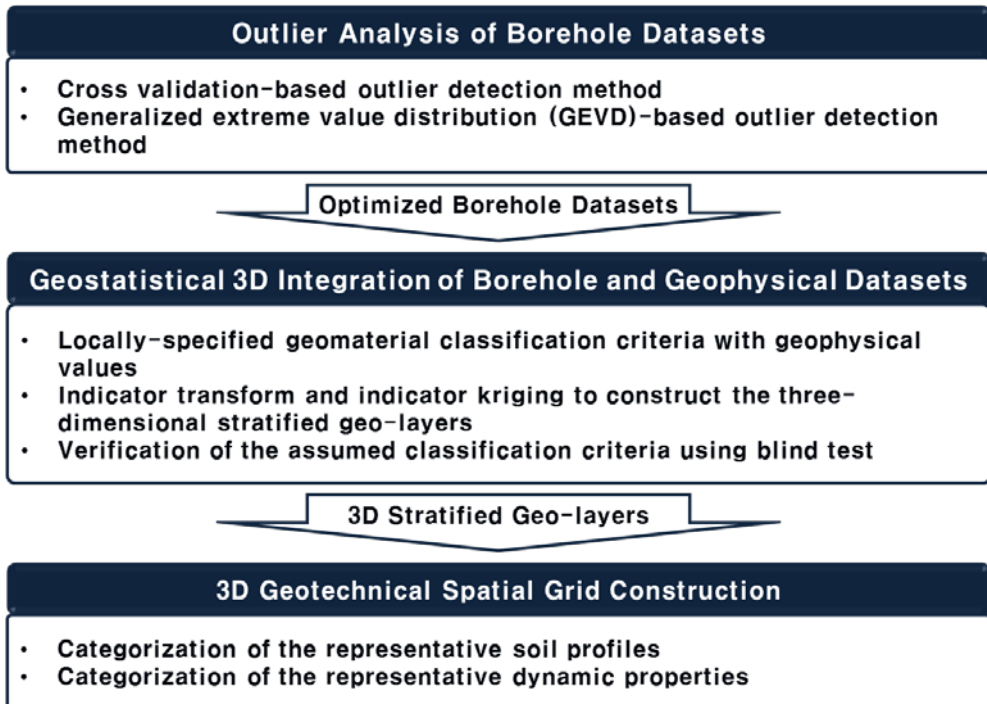


Figure 4.1 Construction procedure of geotechnical spatial grid

4.2 Outlier Analysis of Borehole Datasets

4.2.1 Proposed outlier detection methods to soil stratification

It is difficult to define absolute outliers from geotechnical testing data, but it is possible to indicate the least predictable or relatively outlying data points using statistical tools. Accordingly, the two methods are proposed in this integrated framework to analyze geotechnical testing data and detect less

reliable data points based on statistical processes to obtain a more reliable geotechnical database for designs: Generalized extreme value distribution based outlier detection method and cross-validation based outlier detection method. This dissertation highlights how to detect outlying data points using these two methods and compares the results with the conventional outlier detection techniques, specifically the distribution-based method and the Moran scatterplot method. In this study, the outlier threshold having relatively least reliable data points was determined with 10% (5% too high and 5% too low) of entire borehole. The spatial distribution of the soil depth to the bedrock in a central area of Seoul, South Korea, which has relatively many boring datasets, is assessed to validate the methods.

Testing site descriptions

This study examines the proposed methods to detect outlying observations with boring data obtained from a central area of Seoul, South Korea selected from entire Seoul area, because there are enough many borehole datasets for exclusion of outliers from original datasets. Standard penetration tests are conducted for the 188 points in total, and the local soil depth to the bedrock is measured at each point. The locations of the boring points are shown in Figure 4.2. To verify the methods, the soil depth is measured at ten additional points, the locations of which are also shown as the rectangular points in Figure 4.2. The proposed methods are utilized to select the twenty least predictable measurements defined as outliers in this study. This represents about ten percent of the original 188 measurements. The

twenty measurements consist of ten soil depth measurements that are too high and ten that are too low.



Figure 4.2 Photograph of the testing site and the borehole locations

Cross-validation-based outlier detection method

Cross-validation is a type of blind test to determine whether the target point has the tendency of the surrounding base values using kriging. This method was developed to evaluate the susceptibility of variogram models or kriging models (Isaaks et al. 1989, Delfiner 1976, David 1976, Knudsen and Kim 1978). It is adapted to evaluate the local reliability of the measured properties in this study. The local reliability for each observation is evaluated based on the difference between measured and estimated values with the

following procedure.

- 1) Compute an experimental variogram from the entire set of sample data and fit a plausible model to it.
- 2) Estimate the value at each sampling point by kriging sequentially after excluding the measured target value there.
- 3) Calculate the difference between the estimated value and the measured value.

The variogram for the testing data is presented with the exponential model in Figure 4.3. It is calculated considering the effects of a spatial trend on the variogram. The correlation length of original measurements without trend effects is 110m.

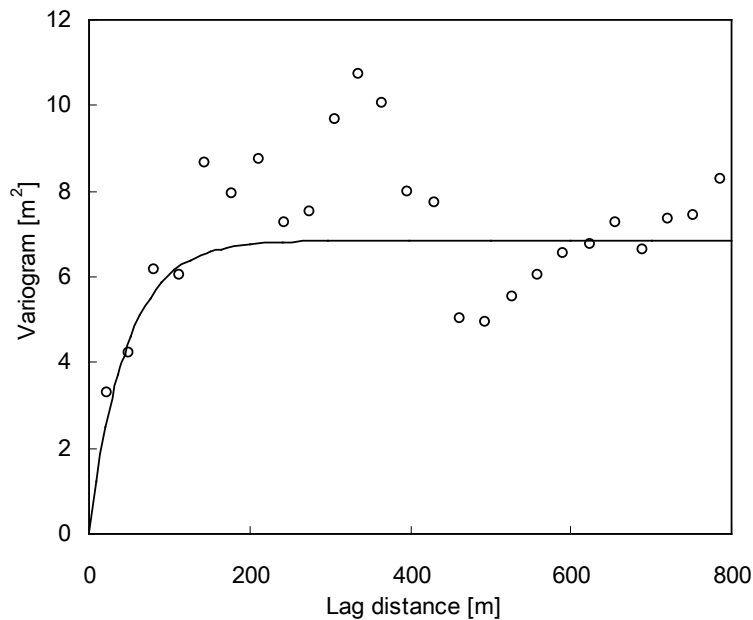


Figure 4.3 Variogram of the original data based on the exponential model

The cross-validation-based outlier detection method is applied to the testing data, and the measured values and the estimated values by the cross-validation are compared in Figure 4.4. The solid line in Figure 4.4 is the line where the estimated values are equal to the measured values, and the dotted lines are outlier criteria to select the least predictable 10% data points with the other measurements. The hollow points are the outliers as determined by this method.

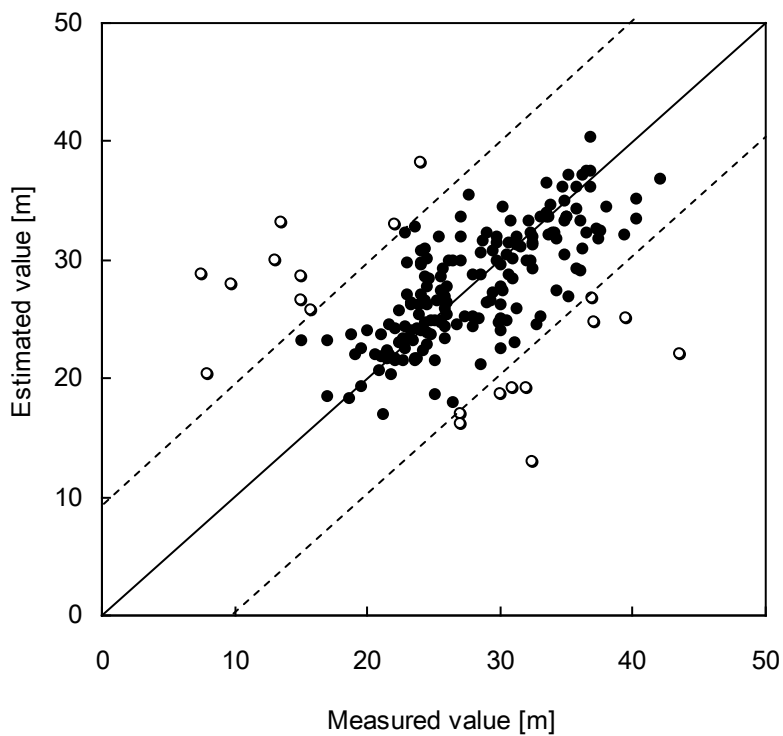


Figure 4.4 The measured soil depth to the bedrock vs. the estimated values by the cross-validation method

Generalized extreme value distribution (GEVD)-based outlier detection method

This study adopts the outlier detection technique using an extreme value distribution to select the outlying data points (Oh et al. 2008, Park and Sohn 2006). The procedures are summarized below. Additional descriptions about this method can be found in Kim et al. (2012b):

- 1) Suppose that the given data are classified into n numbers of subsets $\{x_1, x_2, \dots, x_n\}$.
- 2) Select the maximum (or minimum) values from each subset as the most relevant statistics for the tail distribution.
- 3) The maximum (or minimum) of each subset can be modeled using the following generalized extreme value distribution (GEVD; Park and Sohn 2006, Kotz and Nadarajah 2000, Jenkinson 1955). Estimate the function parameters, κ , σ and μ , corresponding to the best-fit GEVD:

The pdf of the maximal generalized extreme value distribution is given by

$$f(x|\kappa, \lambda, \delta) = \left(\frac{1}{\delta}\right) \exp\left[-\left\{1 - \kappa \frac{x - \lambda}{\delta}\right\}^{\frac{1}{\kappa}}\right] \left(1 - \kappa \frac{x - \lambda}{\delta}\right)^{-1 + \frac{1}{\kappa}} \quad (4.3)$$

The pdf of the minimal generalized extreme value distribution is given by

$$f(x|\kappa, \lambda, \delta) = \left(\frac{1}{\delta}\right) \exp\left[-\left\{1 + \kappa \frac{x - \lambda}{\delta}\right\}^{\frac{1}{\kappa}}\right] \left(1 + \kappa \frac{x - \lambda}{\delta}\right)^{-1 + \frac{1}{\kappa}} \quad (4.4)$$

- 4) Establish a threshold value for a certain confidence level to detect outliers.

Equally separated circular areas with a radius of 110m, the correlation length of the original measurements as shown in Figure 4.5, are defined as the spatial subsets for the testing data in this study, as shown in Figure 4.5. The measured soil depth is converted to the local soil depth ratio, which is the ratio of the soil depth to the arithmetic mean value of the measurements in each subset.

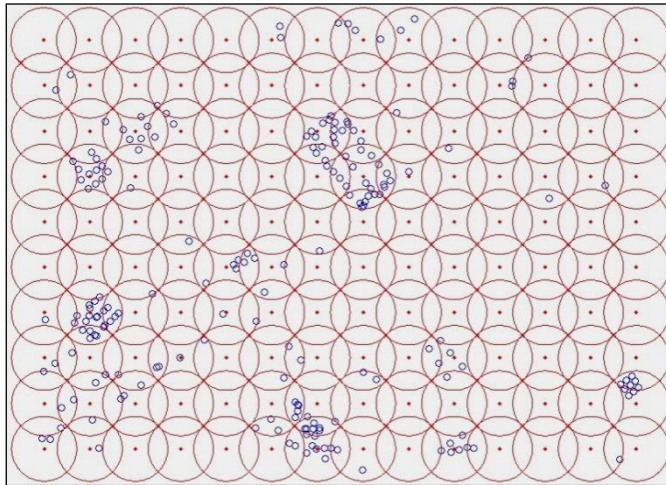


Figure 4.5 Distribution of the defined subsets for the GEVD-based method

The maximum values of each subset are extracted and fitted to the GEVD (Figure 4.6), after which the threshold is defined to select the top five percent of the measurements, all of which are suspected to be too high in this

study, and vice versa for the minimum values of each subset.

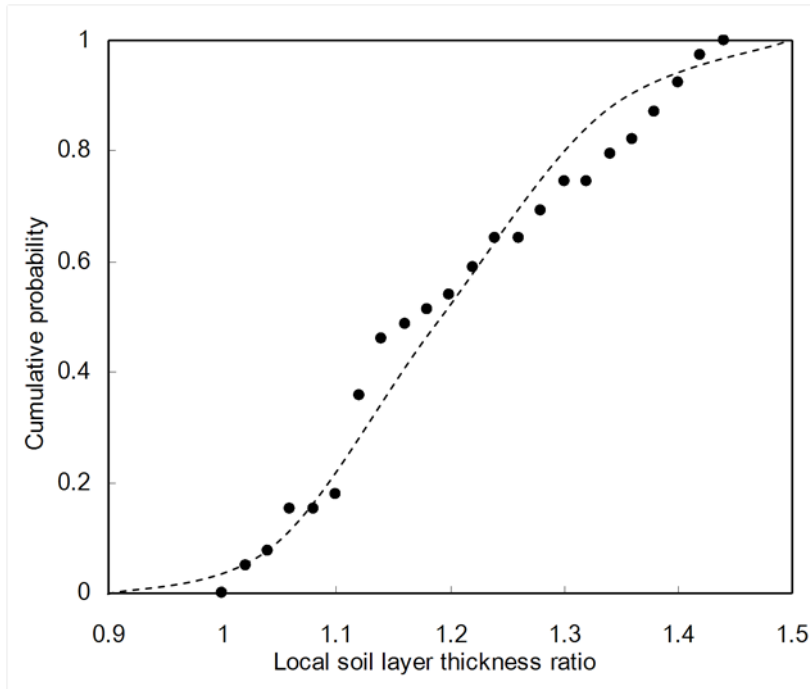
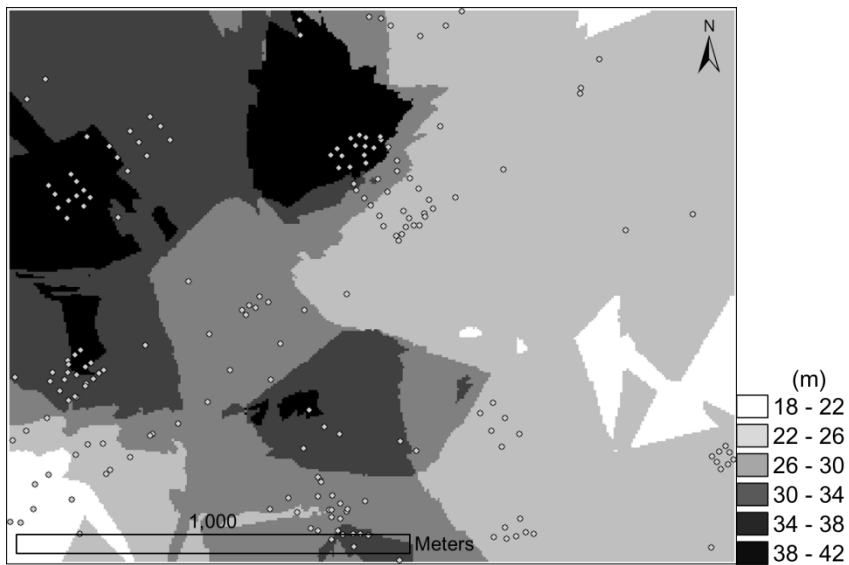


Figure 4.6 The cumulative distribution of the maximum values of the spatial subsets (solid dots) and the fitted GEVD curve (dotted line)

4.2.2 Verification of statistical geo-spatial information technology

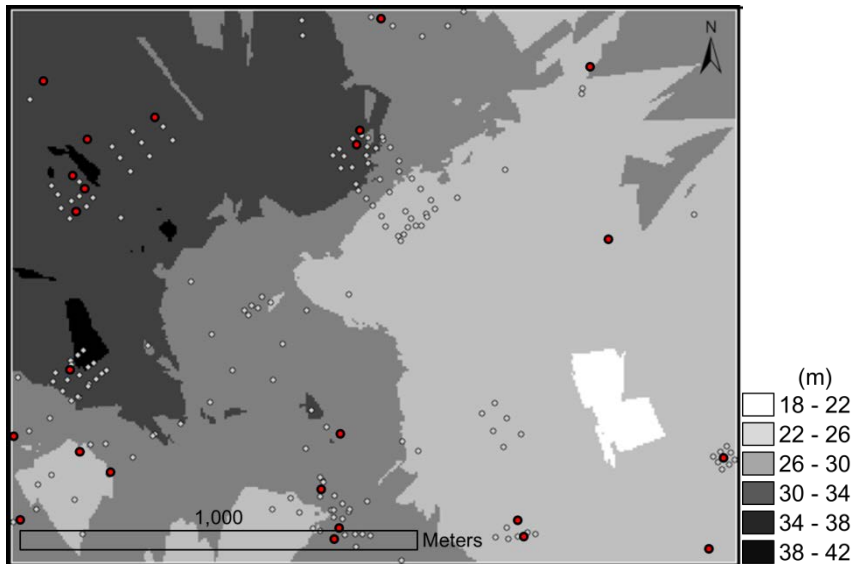
The proposed outlier detection methods (cross-validation-based method and GEVD-based method) are verified with conventional methods (distribution-based method and moran scatterplot method) using testing datasets based on blind test. Figure 4.7 shows the spatial distributions of the soil depth computed using ordinary kriging using (a) the entire measurements,

(b) the measurements without the data points selected by the distribution-based method, (c) the measurements without the data points selected by Moran scatterplot method, (d) the measurements without the data points selected by the cross-validation-based method, and (e) the measurements without the data points selected by the GEVD-based method. A darker color indicates a thicker soil layer. L is the correlation length.

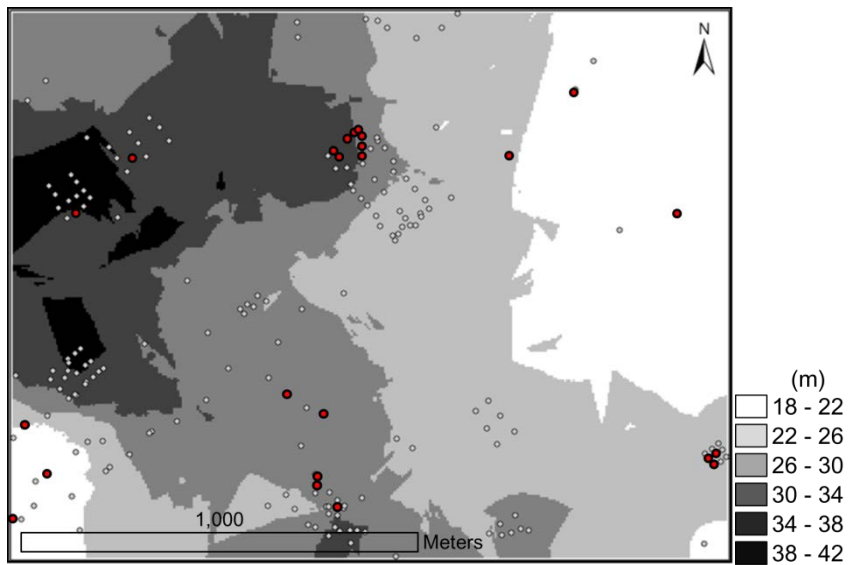


(a) Krigged with the entire measurements ($L = 110$ m)

[Continued]

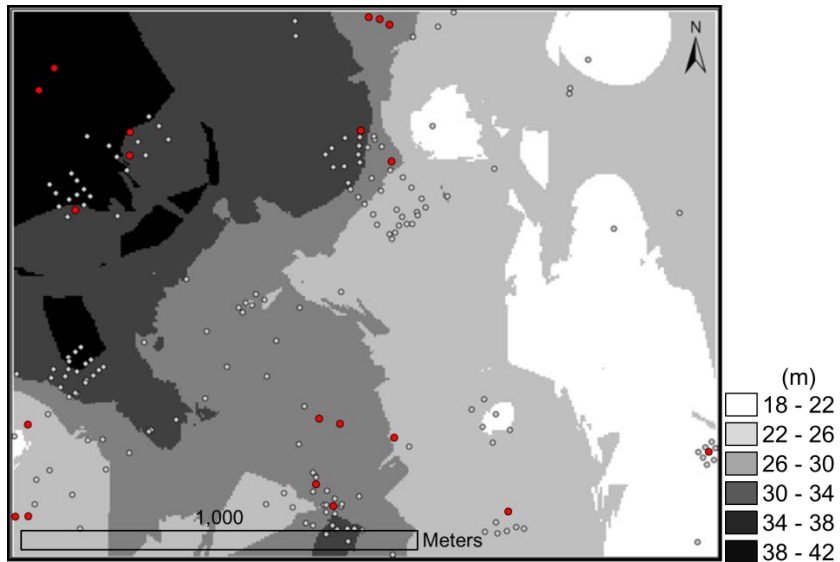


(b) Existing method: distribution-based method ($L = 98$ m)

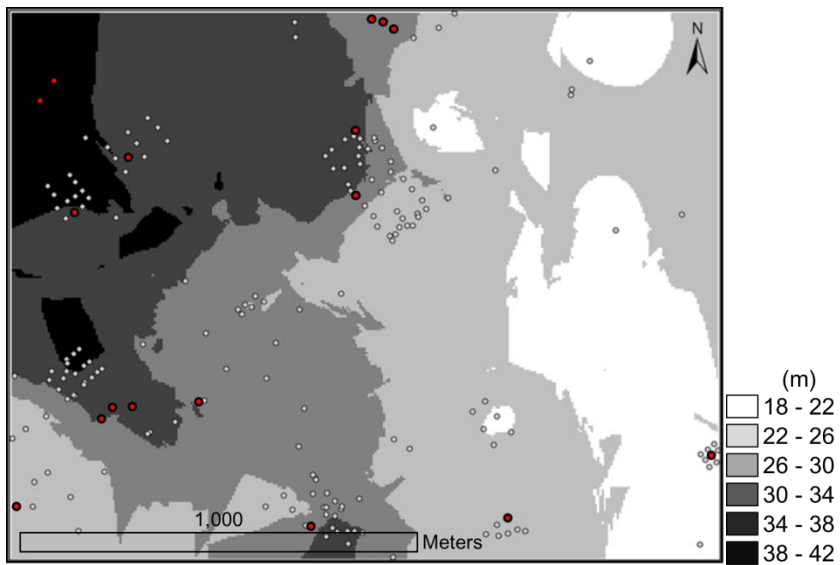


(c) Existing method: Moran scatterplot method ($L = 112$ m)

[Continued]



(d) Proposed method: cross-validation-based method ($L = 70$ m)



(e) Proposed method: GEVD-based method ($L = 79$ m)

Figure 4.7 Spatial distributions of the soil depth to the bedrock estimated with or without the suspected outlying measurements (red dots outlined bold line)

The validation test is conducted using the ten additional measurements,

as shown in Figure 4.2. In the previous sections, the least reliable ten percent of the measurements are selected by the four different detection techniques of the two conventional methods (the distribution-based method and the Moran scatterplot method) and the two proposed methods (the cross-validation-based method and the GEVD-based method). It is recommended to conduct the additional tests at the locations where the measurements are considered to have significant errors in order to confirm feasibility of the outlier selections. At this time, the soil depth at the additional borehole locations is estimated by ordinary kriging after excluding the outliers detected by each technique, after which it is compared to the measurement for validation, as shown in Figure 4.8. Boxed data correspond to the circled point in the map.

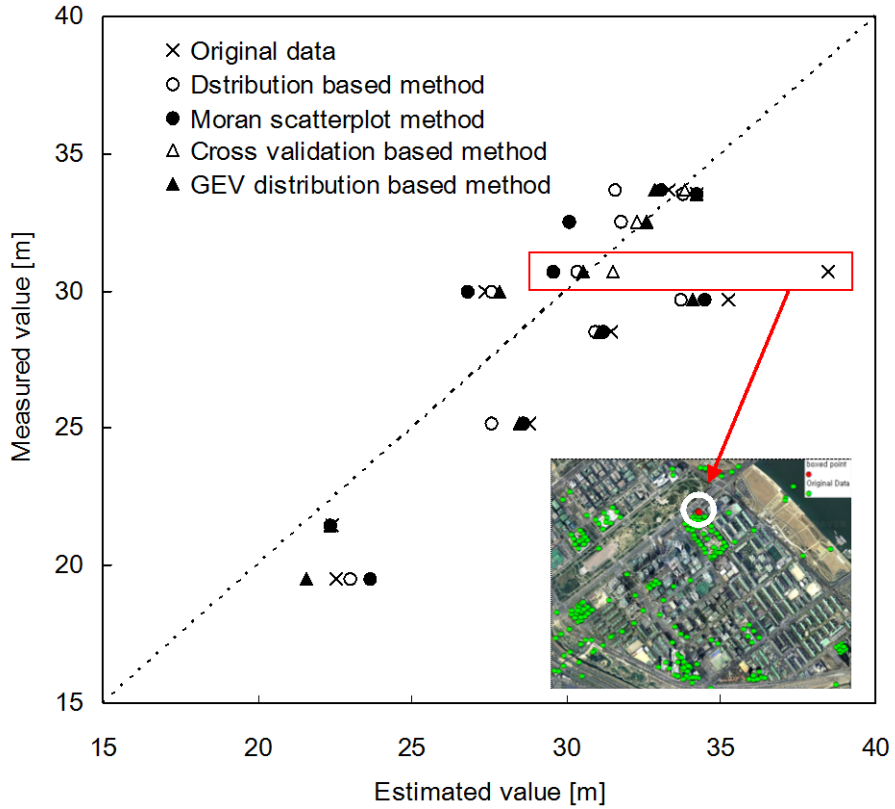


Figure 4.8 The measured soil depth to the bedrock versus the estimated values by the outlier analysis

The several statistics of mean average error (MAE), root mean squared error (RMSE) and mean squared error (MSE) are computed in Table 4.1. The more accurate estimates make MAE, RMSE and MSE closer to zero value.

$$RMSE = \sqrt{\frac{1}{N_v} \sum_{i=1}^{N_v} (x_i - \hat{x}_i)^2} \quad (4.5)$$

$$MAE = \frac{1}{N} \sum_{i=1}^N (x_i - \hat{x}_i) \quad (4.6)$$

$$MSE = \frac{1}{N} \sum_{i=1}^N \frac{x_i - \hat{x}_i}{\sigma_i} \quad (4.7)$$

Here, N is the number of points to be used for verification. At point i , x_i is the measured value, and \hat{x}_i is the estimated value by kriging.

Table 4.1 shows that the values estimated without the suspected outliers are much closer to the measurements than the values estimated by the entire measurements, which is absolutely correct for the boxed data in Figure 4.8. The methods proposed in this study (Cross-validation based method and GEVD-based method) show the less RMSE values than the conventional methods, which reflects our proposed methods can select the least predictable data points considering the spatial correlation of the testing data. However, more case studies are required to conclude our proposed methods are more feasible for outlier detection than conventional methods.

Table 4.1 RMSE, MAE and MSE of each estimation for the validation points

	Original data	Distribution based method	Moran scatterplot method	Cross-validation based method	GEVD-based method
RMSE (m)	4.41	2.27	2.80	2.17	2.17
MAE (m)	5.23	4.20	3.92	3.02	3.05
MSE (m)	5.11	3.55	3.12	2.29	2.31

4.3 Geostatistical 3D Integration of Borehole and Geophysical Datasets

4.3.1 Geostatistical integration procedure of geotechnical datasets

Geo-spatial data integration method

A geostatistical method to integrate borehole and geophysical data considering local uncertainty is proposed as shown in Figure 4.9. In this study, indicator kriging which is characterized by geostatistical non-linear procedures to model the variability of spatial attributes, is utilized to construct the three-dimensional stratified geo-layers.

First, the geo-spatial database is prepared with the borehole data and the seismic refraction results. The depth values in the database are calibrated using the digitized elevation map. Second, the outlier analysis named the cross-validation based method (Kim et al., 2012c), is applied to reduce the uncertainty of the boring data. Third, varying degree of geomaterial classification criteria based on P-wave velocity are assumed to define the two-dimensional underground profiles. Fourth, the geotechnical test datasets are transformed to a set of binary values [0,1] for indicator kriging. Fourth, the optimized boring data and digitized geophysical values at tomography are non-linear transformed to a set of binary values for indicator kriging. Fifth, indicator kriging is utilized using the optimized borehole data and the transformed P-wave velocity profiles. Sixth, the cross-validation is performed using the borehole measurements sequentially excluded one borehole data in

accordance with the indicator kriging to check the validity of the assumed classification criteria. The computer software is developed based on the proposed method with ArcGIS developer tool (Esri 2006, Lee et al. 2001) and GSLIB (Clayton et al. 1997, Deutsch et al. 2002).

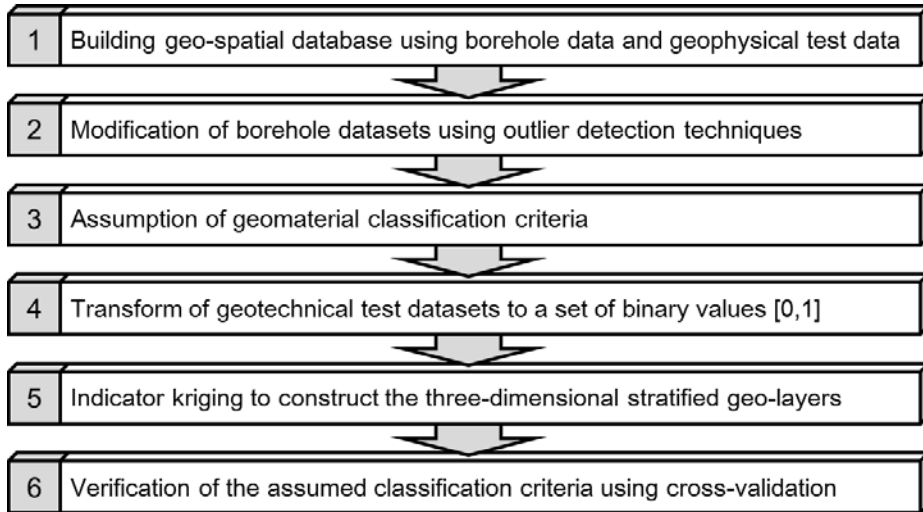


Figure 4.9 Flow diagram for computer-based geostatistical integration method for underground stratification with outlier analyses

The datasets for geostatistical integration method is composed of the three components: borehole information, seismic refraction test information and digital terrain information. The one-dimensional soil profiles obtained from the boring logs and two-dimensional V_p tomography data are included in the database with corresponding digitized spatial information. In this study, the depth values from the ground surface to the weathered rock and the soft rock at each location are assigned as the target variables analyzed with the proposed method.

This method presents a more reliable result by taking care of outlying

measurements in the boring test results from section “4.2.3 Proposed outlier detection methods to soil stratification”.

Testing Site Descriptions

It was applied at a construction site of an emergency spillway in South Korea to develop the local criteria to determine the depth to weathered rock and the depth to soft rock, because there are enough many borehole datasets and intercrossed geophysical testing datasets in testing site considered site-specific density of collected information.

This study examines the proposed methods to classify the geomaterials of an emergency spill way construction site located in Gyeongsangbuk-do, South Korea with the twenty-one boring data and the twelve seismic refraction testing results as shown in Figure 4.10. The site investigation covers an area of $252,000 m^2$ ($720 m$ west to east \times $350 m$ north to south) with an elevation variation from 45 m to 150 m. In this study, not only twenty-one boreholes, but also the twelve seismic refraction tests are conducted to assess the spatial distribution of the P-wave velocity in the target area.

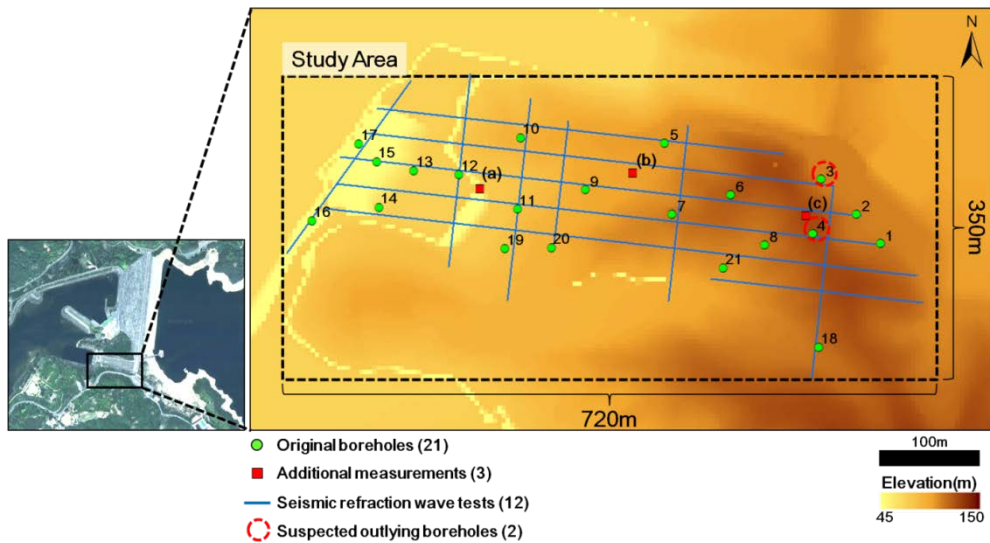


Figure 4.10 Digital terrain map of the study area with locations of boreholes and seismic refraction wave tests at target site.

Conventional geomaterial classification criteria based on P-wave velocity

V_P

The Table 4.2 shows various classification criteria used in Korea to identify the geomaterials based on P-wave velocity (V_P). The values shown in the Table 4.2 indicate the typical values of P-wave velocity for each geomaterial. However, the values listed in the table are not the same, which makes the designers get confused. P-wave velocity is not determined only by the geomaterial type but also many other mechanical or physical characteristics such as applied stresses, unit weight, composition and so on.

Table 4.2 Conventional geomaterial classification criteria based on P-wave velocity V_P

Design specification	V_P [m/s]				
	Soil Deposit	Weathered Rock	Soft Rock	Normal Rock	Hard Rock
A, B	<1,500	1,500– 2,500	2,000– 3,200	3,000– 4,200	4,000– 5,000
C, D	-	< 1,200	1,200– 2,500	2,500– 3,500	3,400– 4,500
E, F	< 2000	2,000– 3,500	3,500– 4,000	4,000– 4,500	> 4,500
G	-	700– 1,200	1,000– 1,900	1,900– 2,900	2,900– 4,200
H	<1,500	1,500– 3,000	3,000– 3,700	3,700– 4,300	4,300– 6,000

A: Geotechnical investigation handbook (Seoul metropolis, 2006).

B: Construction estimate manual (Korea Ministry of Land, Infrastructure and Transport, 2012).

C: Soil investigation manual (Korea Engineering and Consulting Association, 2004).

D: Soil investigation manual (Korea Train Express Corporation, 1995).

E: Road design handbook (Korea Highway Corporation, 2009).

F: Site investigation report (Seoul Metropolitan Subway Corporation, 2001).

G: Soil investigation guideline (Korea Land Corporation, 2002).

H: ISRM suggested methods (International Society for Rock Mechanics, 1981).

The proposed method integrates the boring data and the geophysical results to provide the appropriate values of P-wave velocity for each geomaterial, which are derived site-specifically to classify the local geomaterials comparing with the Table 4.2. The proposed methods are utilized to select the least predictable two measurements defined as outliers in this study. This represents about ten percent of the original twenty-one

measurements. To verify the results, three additional boring tests are conducted, the locations of which are also shown as the rectangles in Figure 4.10 – (a), (b) and (c).

4.3.2 Optimization of borehole datasets using outlier detection methods

As mentioned above previous section (“4.2.3 Cross-validation-based outlier detection method”), some erratic information can be included even in the boring data. Although the outliers at boring data are often considered as an error or noise, they may carry important information. Detected outliers are candidates for aberrant data that may otherwise adversely lead to model misspecification, biased parameter estimation and incorrect results. It is therefore important to identify them prior to modeling and analysis (Williams et al., 2002; Liu et al., 2004). Relatively outlying data points are extracted from the analyzed data set to reduce the uncertainty using cross-validation based outlier detection method (Kim et al. 2012b). Cross-validation is a test to evaluate the susceptibility of variogram models or kriging models (Isaaks et al. 1989, Delfiner 1976, David 1976, Knudsen and Kim 1978). It is adapted to evaluate the local reliability of the measured properties in this study. The local reliability for each observation is evaluated based on the difference between measured and estimated values with the following procedure to optimize borehole datasets by removing outliers.

- 1) Compute an experimental variogram from the entire set of sample data and fit a plausible model to it.
- 2) Estimate the value at each sampling point by kriging sequentially after excluding the measured target value there.
- 3) Calculate the difference between the estimated value and the measured value.

The variogram for the testing datasets with exponential model is presented in Figure 4.11. The conventional variograms for the geotechnical testing datasets with exponential model has a peak, and the phenomenon related to the trend of the variable (soil layer thickness). Accordingly, the variogram was calculated by reducing the effects of a spatial trend of geolayer. The corresponding correlation lengths (or range), which indicate the distance between locations beyond that observations appear independent, are 62.4 m for the depth to the weathered rock and 68.2 m for the depth to the soft rock.

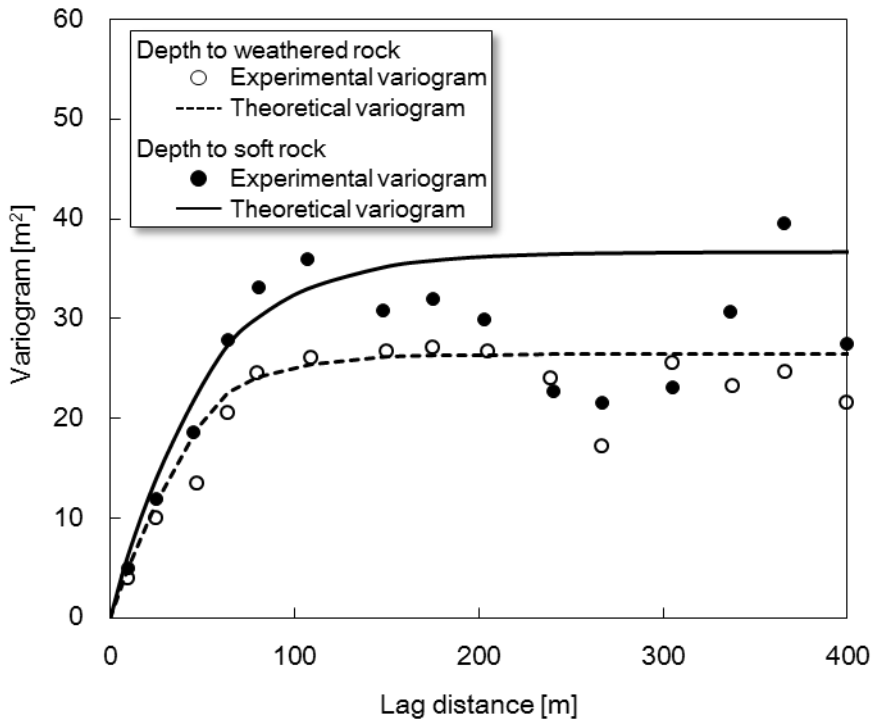
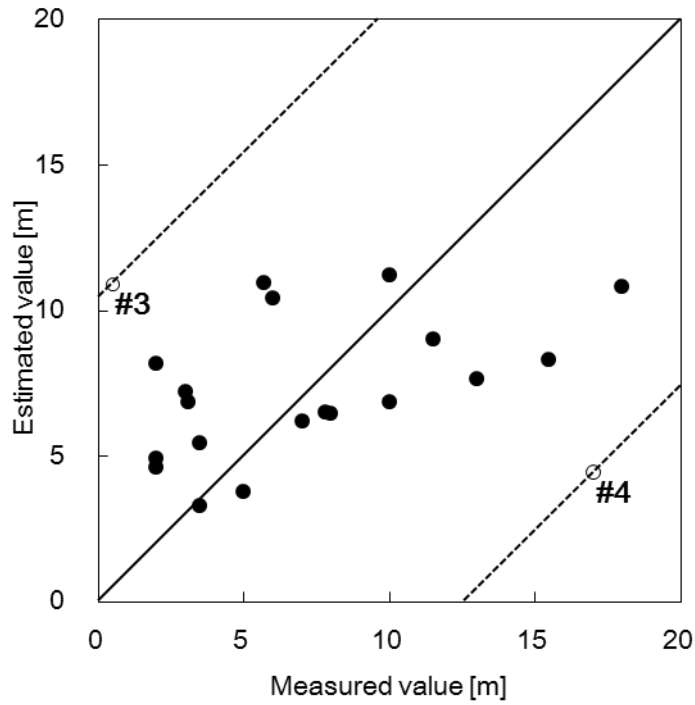


Figure 4.11 Variogram of the original borehole datasets for depth to weathered rock and depth to soft rock

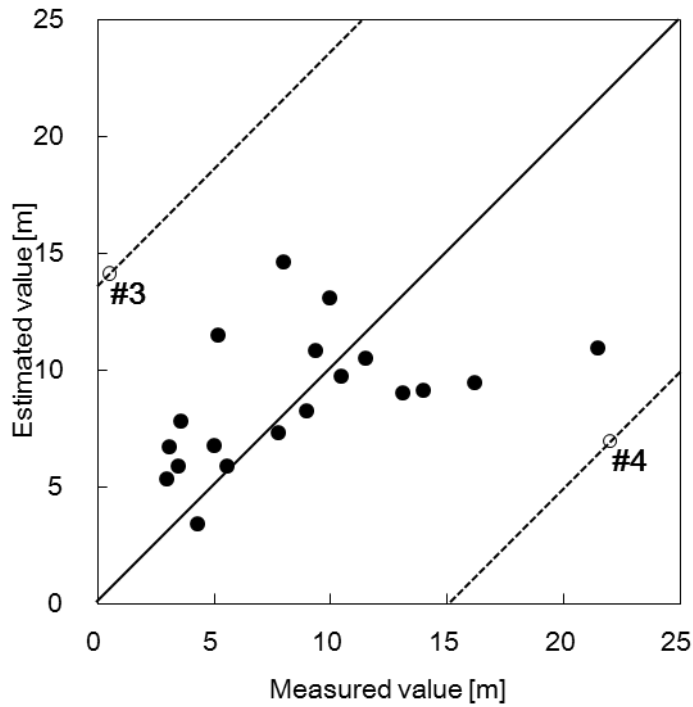
The cross-validation-based outlier detection method is applied to the boring data, and the measured values and the estimated values by the cross-validation are compared in Figure 4.12. The proposed methods are utilized to select the 2 least predictable measurements defined as outliers in this study. This represents about 10% of the original 21 measurements. The 2 measurements consist of 1 (boring #3) that are too high and 1 (boring #4) that are too low. The solid line in Figure 4.12 is the reference to indicate that the estimated values are equal to the measured values. The cross-validation-based outlier detection technique selects the two least predictable measurements (boring #3 and #4) defined as outliers. This represents about 10% of the

original total number of measurements. The two excluded measurements are the boring #3 and the boring #4 as shown in Figures 4.12 (a) and (b).



(a) Depth to weathered rock

[Continued]



(b) Depth to soft rock

Figure 4.12 Cross-validation based outlier detection method for the depth values to (a) the weathered rock and (b) the soft rock from the boring data

The optimized borehole datasets are stored into database, and play a role as indicator threshold. In this integration procedure, the cross-validation-based outlier detection method is replaceable as GEVD-based method.

4.3.3 Assumption of geomaterial classification criteria

Based on the indicator kriging, preceded determination of indicator

threshold is essential to conserve the geotechnical characteristics based on borehole datasets. The twelve two-dimensional seismic refraction tomography inversion results are digitized based on a spatial coordinate system. Accordingly, the variation of P-wave velocity with the depth was quantified along the prospecting lines in a transverse mercator (TM) map projection. According to Table 1, the design specifications A and B defines that the geomaterial with $V_p < 1500$ m/s is a soil deposit and the geomaterial with $V_p > 2000$ m/s is a soft rock.

When spatial measurements of a variable are transformed to binary indicators (i.e., 1 if equal a given threshold value and 0 if different) and the resulting indicator variogram is modeled, indicator kriging produces the probability of the measured variable to exceed the threshold value. In the study, the seven assumed criteria of V_p for soil deposits, weathered rocks and soft rocks are tested: 3/5(60%), 3/4(75%), 7/8(88%), 100%, 9/8(112%), 6/5(120%) and 5/4(125%) of the conventional criteria (A and B in table 1) as listed in Table 2. Based on the assumed classification criteria, the given two-dimensional seismic refraction tomography inversion results are stratified and integration with boring data is conducted using indicator kriging to identify which is the most site-specifically fitted criteria to classify the local geomaterials. And these criteria work like indicator threshold for indicator kriging.

Table 4.3 Assumed geomaterial classification criteria with P-wave velocity

	$(V_P)_1^b$ (m/s)	$(V_P)_2^c$ (m/s)
$3/5 (V_P)_{cr}$	900	1200
$3/4 (V_P)_{cr}$	1125	1500
$7/8 (V_P)_{cr}$	1313	1750
$(V_P)_{cr}^a$	1500	2000
$9/8 (V_P)_{cr}$	1688	2250
$6/5 (V_P)_{cr}$	1800	2400
$5/4 (V_P)_{cr}$	1875	2500

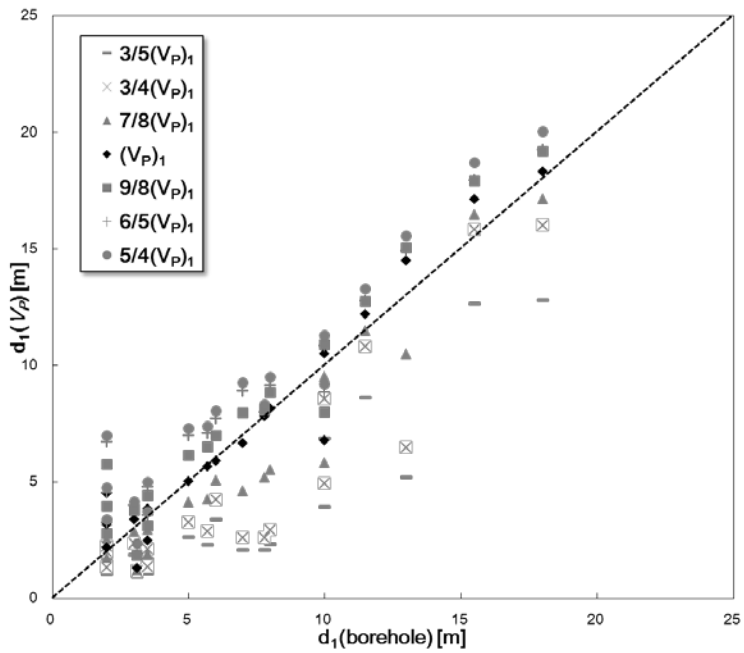
^a Classification criteria of P-wave velocity (V_P) at the design specifications A and B listed in Table 4.2

^b V_P between the weathered soil and the weathered rock

^c V_P between the weathered rock and the soft rock

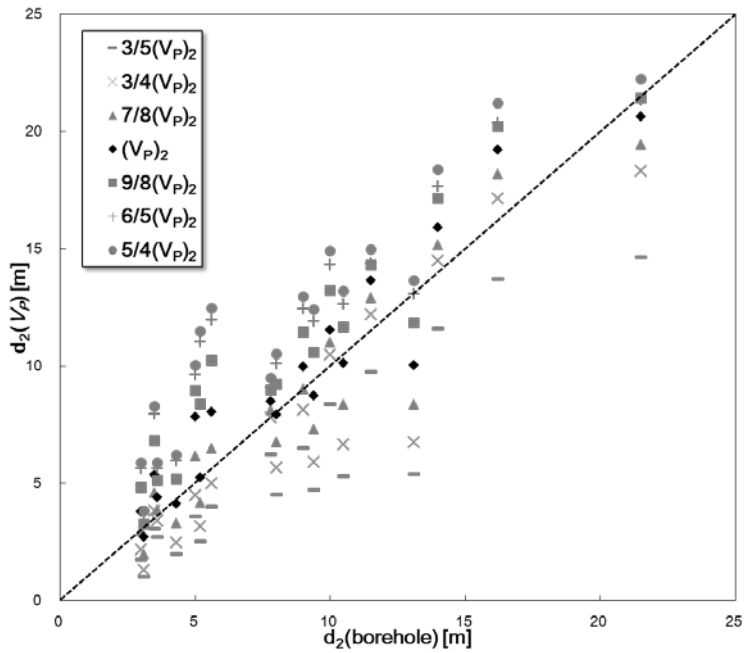
To verify the assumed geomaterial classification criteria, geo-layers of borehole datasets were compared with those of V_P . Figure 4.13 displays the scatter plot at each borehole locations for optimized depth to weathered rock ($d_1(\text{borehole})$) and depth to soft rock ($d_2(\text{borehole})$) of borehole datasets versus corresponding classified depth to weathered rock ($d_1(V_P)$) and depth to soft rock ($d_2(V_P)$) from assumed geomaterial classification criteria with V_P (Table 4.3) based on simple kriging. The correlation for classification criteria of V_P at the design specifications A and B ($(V_P)_{cr}$) was expressed as black color symbol whereas others displayed as gray color symbol. In these correlations, the outlying boreholes were excluded. The overall pattern is not significantly different from correlation regardless of criterion for depth to weathered rock and soft rock. This represents that the assumed indicator thresholds for geomaterial classification are closely related with soil profile

measured from boreholes measurements. However, this example shows that d_1 values defined by the design specifications A and B in Table 4.2 seem reasonable, but d_2 values overestimated by the specifications, which reflects that the locally-specified classification criteria are required to be derived for more reliable stratification of geomaterials.



(a) Correlation of $d_1(\text{borehole})$ and $d_1(V_p)$

[Continued]



(b) Correlation of $d_2(\text{borehole})$ and $d_2(V_p)$

Figure 4.13 Scatter plot for $d_1(\text{borehole})$ versus $d_1(V_p)$ and $d_2(\text{borehole})$ versus $d_2(V_p)$ at borehole locations

4.3.4 Indicator kriging to construct the three-dimensional stratified geo-layers

Linear kriging may be used to infer the parameters of a Gaussian probabilistic model, while indicator kriging, a non-linear kriging method, is used to build a discrete approximation of a generic probabilistic model. Indicator kriging is characterized by geostatistical non-linear procedures to model the variability of spatial attributes. These procedures are used to infer a

discreet approximation to the model of distribution of probability of the attribute, which is used to model uncertainties of its value.

Indicator kriging estimator is a linear kriging estimator applied on a set of elements which attributes values have been modified according to a non-linear transform. Indicator kriging requires a non-linear transform, called indicator transform, which transforms each value of the set into indicator values (Deutsch and Journel 1998). And indicator kriging is the incorporation of borehole datasets (soft data), or local information that is a proxy to the variable of interest and need not relate directly, to supplement hard data (Goovaerts 1997). Soft data can help compensate for a lack of spatially exhaustive observations by providing information about predictions where no hard data is available using prior probabilities.

In this study, indicator kriging is performed for the depth to the weathered rock and the soft rock with the optimized borehole data and the geo-layer data from the digitized P-wave velocity profile based on the assumed classification criteria in the previous section. It is effective method to estimate the probability of site-specific geotechnical characteristics, but can also be used to estimate an entire reliable geo-layer spatial distribution. Indicator kriging let us to evaluate a model of local uncertainty by defining the probability of occurrence for each category at each discretized point of the domain (Caers 2001, Goovaerts 1997, Journel 1983). Given a set of k possible categories, indicator coding consists of defining the probability of occurrence $[0,1]$ for each category:

$$E\{I(u; s_k)\} = \text{Prob}\{S(u) = s_k\} = i(u; s_k) \quad (4.8)$$

where u is a given spatial location, s_k is a particular category for the

categorical variable $S(u)$, and $i(u; s_k)$ is the indicator at location u for category s_k . When working with borehole data and P-wave velocity profile, specifically along a core at a given location u , the coding for entire datasets is exclusively defined as

$$i(u; s_k) = \begin{cases} 1 & \text{if } S(u) = s_k \\ 0 & \text{otherwise} \end{cases} \quad k = 1, \dots, n \quad (4.9)$$

In this study, at the locations of the boreholes, one category will be coded as 1 (the actual category), while the remaining categories at P-wave velocity tomography will be coded as 0 which correspond to each indicator threshold value or 0 which is other P-wave velocities. The three-dimensional spatial continuity structure of the categories could be studied by means of the indicator experimental variogram $\gamma_I(h; s_k)$:

$$\gamma_I(h; s_k) = \frac{1}{2N(h)} \sum_{\alpha=1}^{N(h)} [i(u_\alpha; s_k) - i(u_\alpha + h; s_k)]^2 \quad (4.10)$$

where h is the separation vector, $N(h)$ is the number of pairs of data values whose spatial separation is h , s_k is a given category, and $i(u_\alpha; s_k)$ is the indicator at a given location u_α for the category s_k (Deutsch et al. 1998, Seifert et al. 1999).

According to the indicator kriging method, the example of indicator variogram for depth to weathered rock at 1500 m/s ($d_1(V_p = 1500 \text{ m/s})$) and depth to soft rock at 2000 m/s ($d_2(V_p = 1500 \text{ m/s})$) obtained from the assumed geomaterial classification criteria with V_p were calculated by using binary value transformed from geotechnical testing datasets and presented at the Figure 4.14. Corresponding to the seven arbitrarily assumed criteria (indicator threshold value) of V_p for geo-layer, indicator kriging was performed based on

indicator variogram (such as Figure 4.14), and two-dimensional spatial distribution of geomaterials (Figure 4.15) was estimated for assumed $d_1(V_P = 1500 \text{ m/s})$ and $d_2(V_P = 2000 \text{ m/s})$. The darker color indicates a thicker soil layer.

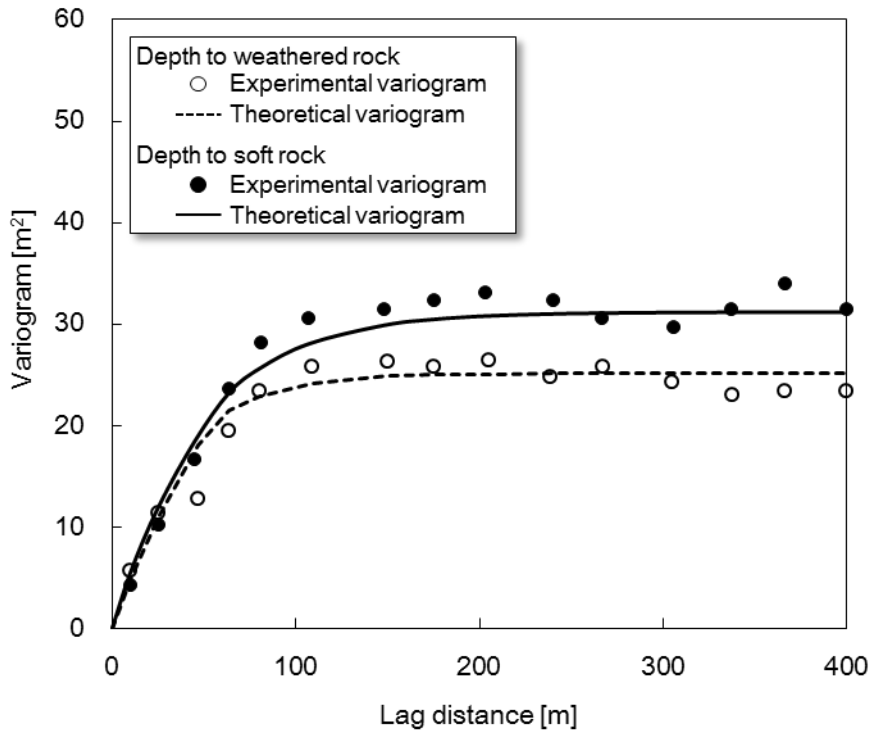
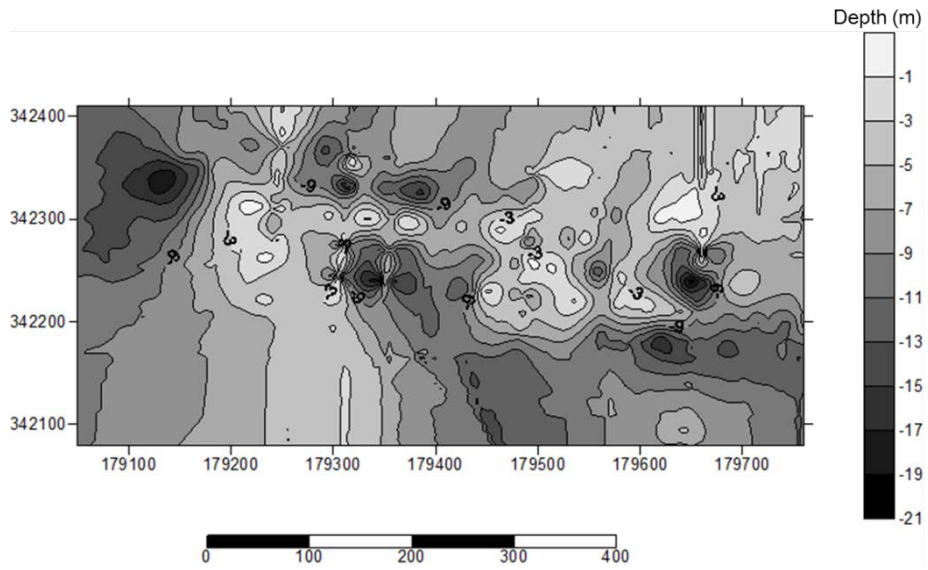
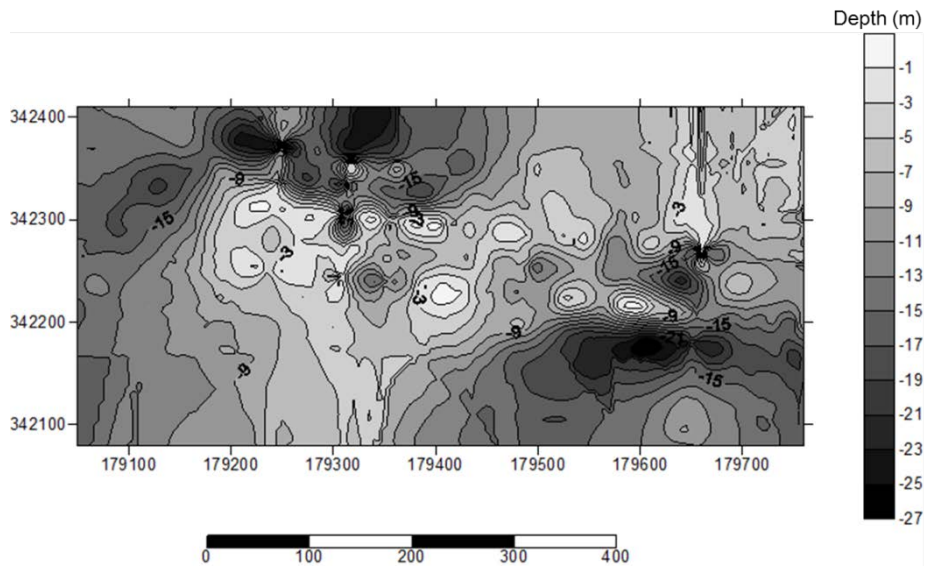


Figure 4.14 Example of indicator variogram for assumed $d_1(V_P = 1500 \text{ m/s})$ and $d_2(V_P = 2000 \text{ m/s})$ referenced from design specification A and B listed in Table 4.2.



(a) $d_1(V_P = 1500 \text{ m/s})$



(b) $d_2(V_P = 2000 \text{ m/s})$

Figure 4.15 Example of two-dimensional spatial distribution of geomaterials for assumed $d_1(V_P = 1500 \text{ m/s})$ and $d_2(V_P = 2000 \text{ m/s})$ referenced from design specification A and B listed in Table 4.2.

After indicator kriging, the 3D spatial distribution of indicator (from 0 to 1) is estimated. This 3D indicator means the conditional probability of that the indicator correspond the assumed geomaterial classification criteria.

4.3.5 Verification of the assumed classification criteria using cross-validation

The validation test is conducted based on cross-validation, which is sequential indicator kriging after excluding the one sample borehole from borehole datasets. According to variable selection of sample borehole, the depth to the weathered rock d_1 and the depth to the soft rock d_2 at the all sample borehole locations are estimated by (1) simple kriging of the geophysical results only, (2) indicator kriging of the geophysical results and the original boring data, and (3) the proposed method, indicator kriging of the geophysical results and the optimized boring data with the outlier analysis. In other word, errors between estimated and measured geo-layer depth (d_1 and d_2) are computed using sequential kriging based on three proposed methods at location where one borehole is excluded.

For comparison, the root mean squared errors (RMSE) are computed for all the cases as shown in Figure 4.16. The hollow triangles and circles correspond to the proposed method results (combination of indicator kriging and outlier analysis). The RMSE is defined as Equation (4.5), and RMSE becomes closer to a zero for the more accurate estimate. The hollow triangles

and circles in Figure 4.16 are for the proposed method (indicator kriging + outlier analysis). In both cases for depth to the weathered rock and depth to the soft rock, the proposed method shows the least RMSE, which indicates that the proposed method estimates the closest three-dimensional underground profiles to the verification borings. Additionally, RMSE of d_2 is smaller than that of d_1 for all the cases, which supports that the geomaterial classification based on the P-wave velocity is more appropriate for d_2 (weathered rock vs. soft rock) than d_1 (soil deposit vs. weathered rock) in this example.

In this study, a multinomial logistic regression analysis is performed to determine the most locally-specified classification criteria of V_p for d_1 and d_2 . According to the regression analysis results, the locally-specified classification criteria of V_p for d_1 and d_2 are 1400 m/s and 1940 m/s.

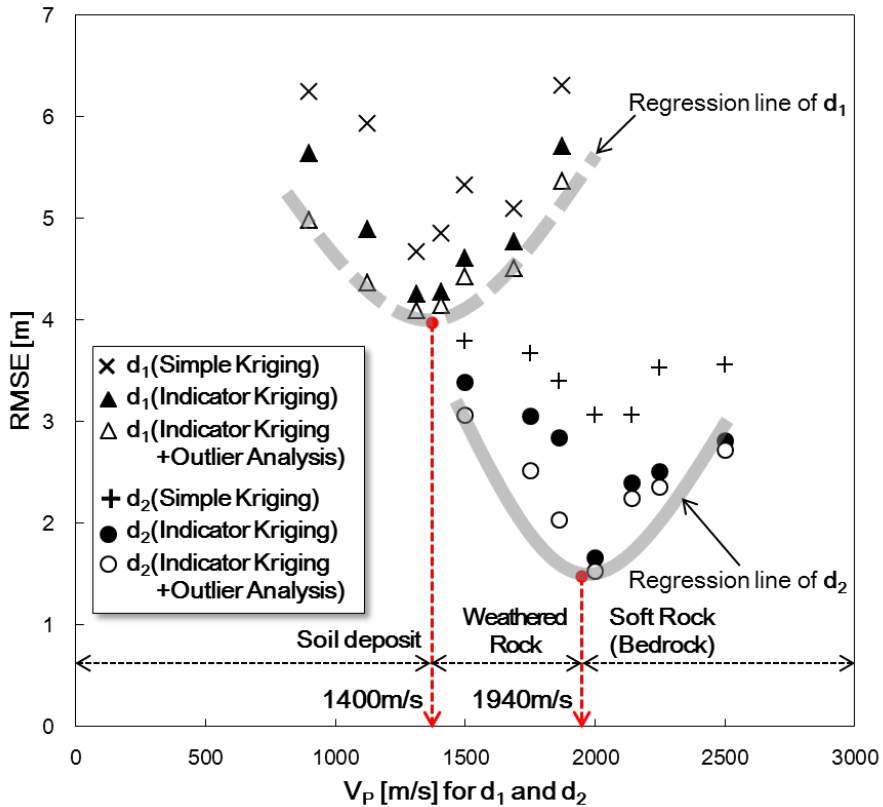


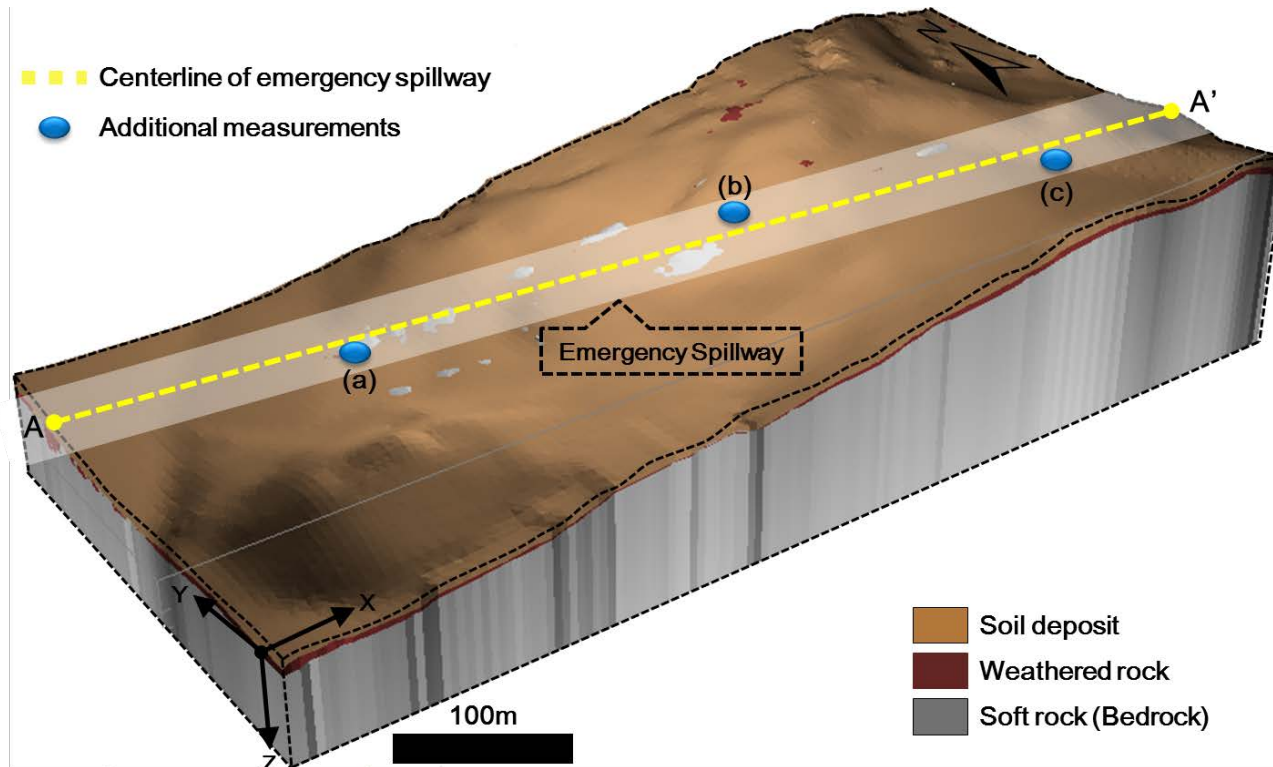
Figure 4.16 Locally-specified classification criteria of V_p for d_1 and d_2

Based on the criteria defined above, the three-dimensional underground profiles are constructed and visualized as shown in Figure 4.17. Geomaterials are classified into a soil deposit, a weathered rock and a soft rock/bedrock. The dotted line A-A' indicates the center line of the planned emergency spillway. On the whole, the depth to weathered rock and depth to soft rock is distributed deeper (d_1 up to 26.9 m, d_2 up to 56.9 m) toward the northwest and more swallows toward the east, where outcrops are located locally. The additional three boreholes for verification of proposed method, as shown in Figure 4.10, are located near the line A-A' in Figure 4.17(a), where the

planned emergency spillway to be constructed.

Figure 4.17(b) compares the proposed method to the conventional methods. $(V_P)_{cr,1}$ and $(V_P)_{cr,2}$ are depth to weathered rock and depth to soft rock according to the conventional design specifications A and B (Table 4.2). It is clear that the profile defined by the proposed method (case 1) is much closer to the verification boring data (case 2) rather than that by the conventional criteria (case 3; A and B in Table 4.2).

And the standard deviation (0.7 m) of proposed geo-layers and actual strata from borehole was decreased as about 13% at verification locations than that (5.3 m) of simple kriging results. Besides, conventional geomaterial classification criteria (A and B in Table 4.2) for d_1 and d_2 was displayed as black dotted line, and demonstrated as unsuitable criteria for site-specific geo-layer beside proposed criteria.



(a) Three-dimensional spatial distribution of geomaterials

[Continued]

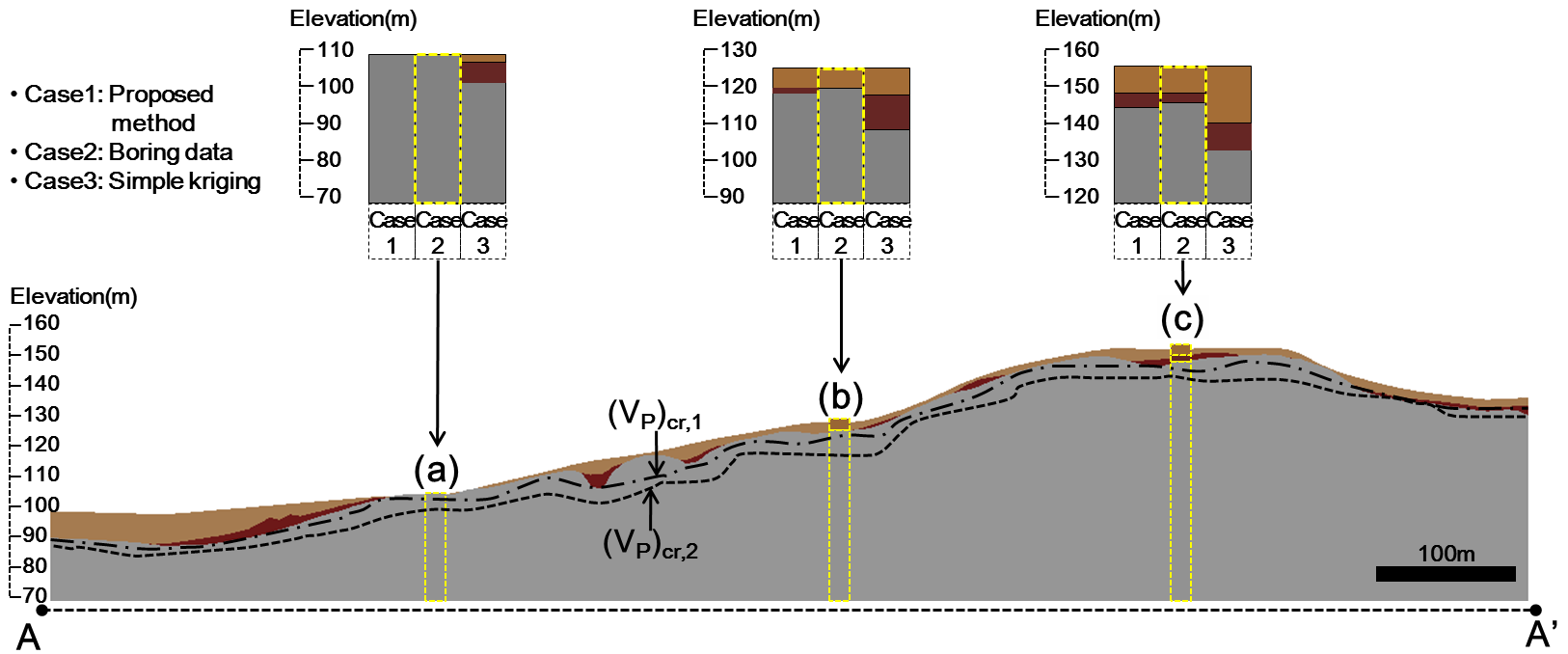


Figure 4.17 Three-dimensional spatial distribution of geomaterials and the cross-sectional view along the line A-A' with the verification borehole points

Generally, it is recommended for the emergency spillway to be located at soft rocks with a good quality for the stability. In the example of this study, soft rocks can be found about 2–13 m below the ground surface along the centerline of the planned emergency spillway. An appropriate soil profile can reduce mistakes of the geotechnical engineers to design the route of the target emergency spillway considering the local variability in soils.

Therefore the geostatistical 3D integration procedure based on indicator kriging was imbedded in integrated framework to incorporate borehole and geophysical datasets. From this procedure, the reliable stratified 3D geo-layers are determined.

4.4 Geotechnical 3D Spatial Grid Construction

4.4.1 Representative soil profiles

Subdivision of geo-layers with representative soil profiles

In the procedure, prerequisite information related to geotechnical zonation is inputted into a 3D spatial database (geotechnical spatial grid) to utilize as primary data for subsequent procedures and to determine the ground conditions to be correlated with the liquefaction potential.

Geostatistical methods are necessary to comprehend all of the ground conditions of the target area because there are spatial constraints to the

collected borehole data, which only provide a 1D profile in 3D space with limited number of data over spacious target area (Ronaldo and David, 1998; NIBS, 1997). Thus, geostatistical 3D integration procedure is applied for the extended area to estimate the spatial distribution of multi-geotechnical profiles with depth according to the widely used Unified Soil Classification System (USCS) (American Society for Testing and Materials, 1985). Accordingly, primary soil profile is interpolated with 3D spatial geometry depending on each soil stratum (fill soil, alluvial soil, and weathered residual soil). On the basis of the 3D primary soil profile, specific soil profile classified with the USCS is interpolated by using 3D kriging.

3D kriging provides the best available linear unbiased estimation with an added ability to estimate certain aspects of the mean trend (Lee and Wong, 2001; Williams et al., 2002; Kim et al., 2012b). The purpose of kriging is to provide the best estimate of a random field between known data points. The basic idea is to estimate $X(x)$ at any point using a weighted linear combination of the values of X at each observation point. Suppose that X_1, X_2, \dots, X_n are observations of the random field $X(x)$ at the points x_1, x_2, \dots, x_n , that is, $X_k = X(x_k)$. Then, the kriged estimate of $X(x)$ at x is given by

$$\hat{X}(x) = \sum_{k=1}^n \beta_k X_k, \quad (4.11)$$

where the unknown weights β_k are to be determined to find the best estimate at point x (Lee and Wong, 2001, Kim et al., 2012b).

After 3D kriging, the typical soil deposits are standardized and categorized with representative soil profile, and the dynamic properties can be correlated with the soil type along the entire interpolated profiles consisting of

3D geotechnical spatial grid, as illustrated in (Figure 4.18). Thus, the effects of spatial trends in the original data can be considered through a trend function, which is used to calculate a best fit line of variogram. The representative soil profile is categorized based upon specific 3D cells (unit cell size: 1 m^3) according to the USCS (American Society for Testing and Materials, 1985). In the procedure, classification criteria of liquefiable geo-layers and non-liquefiable geo-layers can be determined. The geo-layer having liquefaction potential is defined as porous geomaterial below the ground water level (GWL). The classification of liquefiable geomaterial based on the geostatistical integration using V_p has limitation to identify clear site-specific geomaterial classification criteria with distribution of GWL. Accordingly, to construct the reliable 3D geo-layers with dynamic properties, subdivision of geo-layers with representative soil profiles is essential using a number of geophysical tomography and geomaterial classification criteria.

To consider the dynamic ground properties with soil profile obtained from in-situ penetration tests (SPT or CPT), each soil layer is subdivided into specific cells (Figure 4.18).

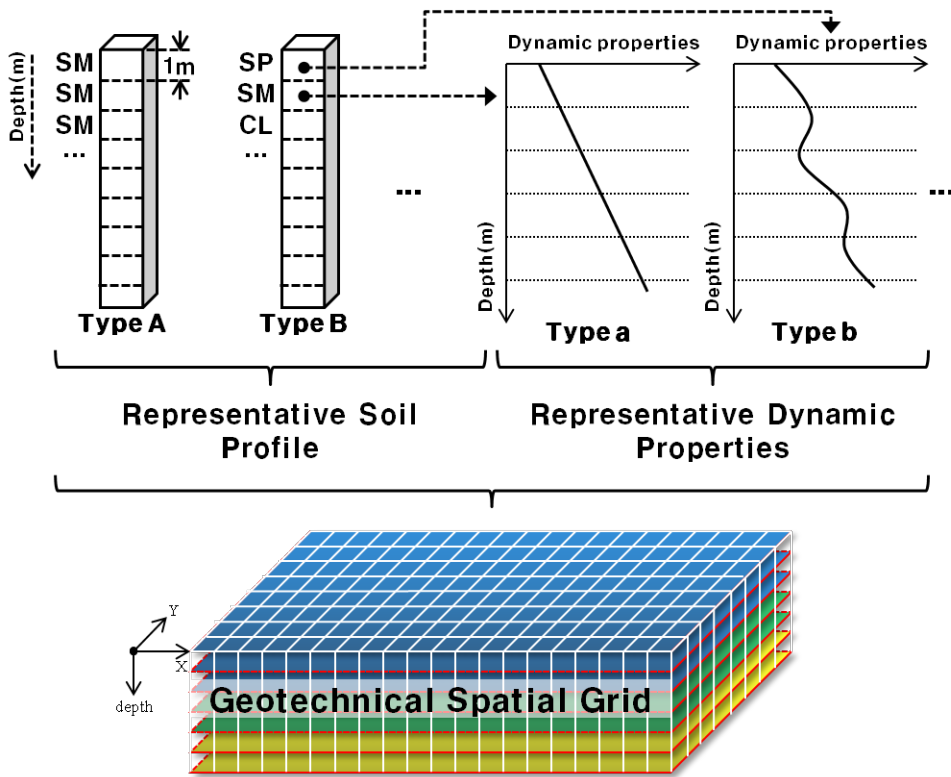


Figure 4.18 Conceptual components for the categorization and grouping of representative soil profiles with their dynamic properties

Determination of grid size considering seismic capacity of the structure

To construct the subdivided 3D geotechnical spatial grid, the grid size is determined considering seismic capacity of the structure. In other words, discriminatory set-up of grid size for geotechnical spatial grid is assessed according to the site-specific seismic capacity of the target structures (Figure 4.19). For example, the spatial grid is further subdivided for a region occupied by construction of a higher grade of seismic capacity. At the area occupied with target structure having 1th seismic priority, the spatial grid over surface

are subdivided as cells of 25m by 25m, while the spatial grid at region of 2th seismic priority are subdivided as cells of 50m by 50m. After determination of grid size, the geotechnical spatial grid for the study area is extracted from the data for the extended target area based on the GIS platform.

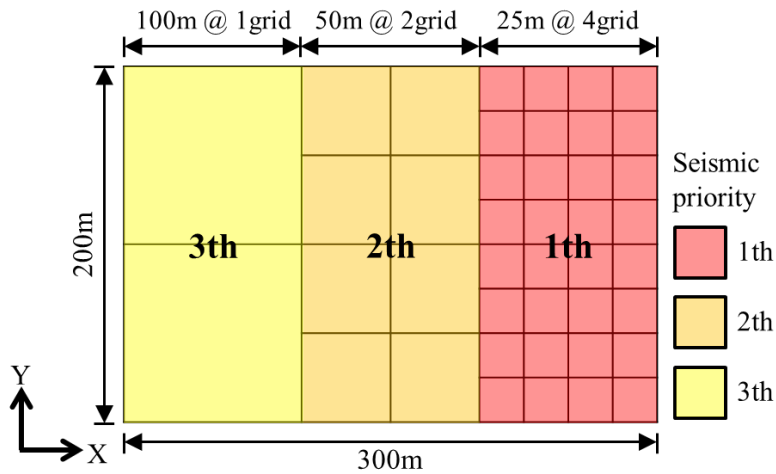


Figure 4.19 Subdivision for region occupied by structure of a higher grade of seismic capacity

4.4.2 Representative dynamic properties

Soil properties depend on different state parameters such as the state of stress, void ratio, confining stress and water content, stress history, strain levels, and drainage condition to name a few. Apart from the influence of the abovementioned parameters, dynamic soil properties are significantly influenced by the dynamic amplitude and frequency of the applied load.

Hence, determination or estimation of the dynamic soil properties requires the consideration of all the influencing parameters: method of sample preparation in laboratory (intact and reconstituted samples), relative density, confining pressure, methods of loading, overconsolidation ratio, loading frequency, soil plasticity, percentage of fines and soil type. Dynamic soil properties can be determined from different field or laboratory tests. However, it is difficult to obtain the dynamic properties by soil type from field or laboratory test.

Therefore representative dynamic properties (Normalized Shear Modulus, Damping ratio, etc.) by soil type are correlated with each classified soil profile and its depth (vertical effective stress) from conventional literature (Figure 4.18). Table 4.4 described the representative dynamic properties by soil type. Finally, the geotechnical spatial grid for the study area is extracted from the data for the extended target site based on the GIS platform.

Table 4.4 Representative dynamic properties by soil type

Representative soil profile	Representative dynamic properties	
	Normalized Shear Modulus (G/G_{max})	Damping ratio (D)
Silty soil	Soil dynamic experiments results	
Sandy soil	Seed and Idriss(1970)	
Clayey soil	Seed & Sun(1989)	Idriss(1990)
Gravel or gravelly soil	Seed et al.(1986)	
Weathered soil	Sun et al.(2005)	
Rock	Schnabel(1972)	

4.5 Summary and Conclusions

In the integrated framework, to figure out reliable geotechnical characteristics of site having seismic risk potential, geostatistical 3D integration using geophysical tomography and soil profile of borehole is established based on GIS platform. The construction procedures of geotechnical spatial grid are composed of three phases: outlier analysis of borehole datasets, geostatistical 3D integration of borehole and geophysical datasets and 3D geotechnical spatial grid construction.

- 1) In the outlier analysis phase, the statistical methods of the cross-validation based method and the generalized extreme value distribution based method are introduced in this study to detect the outlying data points from spatially correlated geotechnical testing results.
- 2) If possible, to point out the outlying observations appropriately, a more reliable spatial distribution of the target physical properties can be guaranteed with additional testing of these locations.
- 3) The results show that the proposed methods enable more reliable spatial distributions to be attained with a quantitative evaluation of local measurement reliability, presenting the less RMSE, MAE, and MSE values than the conventional outlier detection method at the validation test.

And geo-spatial data integration method for three-dimensional underground stratification is proposed. The method is applied at a construction site of an emergency spillway in South Korea to develop the site-specific criteria to determine the depth to the weathered rock and the soft rock. The proposed method integrates the boring data and the geophysical testing results to offer the appropriate values of P-wave velocity, which are derived site-specifically to classify the local geomaterials.

- 1) The boring data are optimized by removing the relatively outlying data points to reduce the uncertainty with above mentioned cross-validation based outlier detection method.
- 2) And also indicator kriging is utilized to construct the three-dimensional stratified geo-layers using the optimized borehole data and the P-wave velocity profiles.
- 3) The validation test for proposed method is conducted by comparing the measured depth with the estimated depth based on the cross-validation. The results suggest the followings.
- 4) The P-wave velocity based geomaterial classification criteria are recommended to be modified locally by the proposed method for more proper stratification results rather than strata by simple kriging of borehole and the conventional classification criteria.
- 5) The geomaterial classification based on the P-wave velocity is more suitable for determining the depth between the weathered rock and the soft rock than the depth between the soil deposit and the weathered rock.

- 6) Indicator kriging is more appropriate for 3D integration method using borehole data and P-wave tomography than general spatial interpolation methods.

The third phase is 3D geotechnical spatial grid construction. Based on the 3D stratified geo-layers, the geotechnical information for real-time earthquake hazard assessment was categorized with representative soil profiles (from USCS) and dynamic properties.

5. Real-time Earthquake Hazard Assessment

5.1 Systematic Procedure for Real-time Earthquake Hazard Assessment

The systematic procedure for real-time earthquake hazard assessment has three functional modules with the database: real-time seismic load determination, real-time liquefaction hazard estimation, and structure fragility evaluation (Figure 5.1). The prepared datasets for real-time earthquake hazard assessment are composed of geographic, geotechnical, structural, and seismic monitoring data of the target site.

Previously, a geotechnical spatial grid is constructed based on the geostatistical 3D integration to confirm the site-specific ground conditions to be correlated with the earthquake hazard potential. This step must be conducted as a baseline prior to the occurrence of earthquakes.

In the first phase, linked with the geotechnical spatial grid, correlations between rock outcrop acceleration and maximum acceleration of each layer (or peak ground acceleration) considering site response characteristics are predetermined. To compute seismic loads causing liquefaction stress and structure failure in real-time, correlations derived previously between the bedrock acceleration transmitted from accelerometers and the maximum acceleration of each layer are assigned into the geotechnical spatial grid. As earthquake events occur, as soon as monitored rock outcrop acceleration data are transmitted from the accelerometer, seismic load at each spatial grid is

estimated

In the second phase, the potential damage due to liquefaction is estimated by integration of the geotechnical spatial grid and correlated maximum acceleration of each layer based on the simplified LPI evaluation method in real-time. As earthquake events occur, the LPI and liquefaction severity class are estimated by correlated with maximum acceleration of each layer in real-time. The liquefaction hazard can be visualized as 2D or 3D maps overlain by satellite images, from which the liquefaction severity of the target structure can be determined using zonation criteria.

In the third phase, the structure failure due to earthquake occurrence is evaluated based on seismic fragility curve. The fragility curve of structure is the function which represents the excess probability of defined damage level for specific earthquake intensity. And the correlated peak ground acceleration is used as intensity index of fragility functions and probabilities of failure are calculated. After all, damage grades of superstructures are determined and they depend on the probabilities of failure.

The liquefaction severity class and structure fragility class are forecasted and visualized in satellite map images or digital map in real-time based on the GIS platform. Therefore the integrated earthquake hazard of the target structure is determined considering the liquefaction and fragility grade.

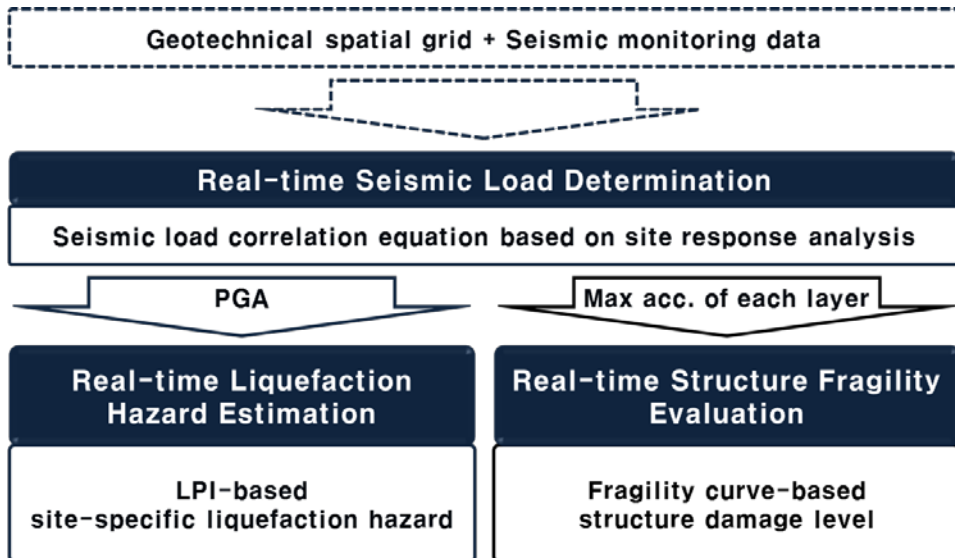


Figure 5.1 Systematic procedure architecture for real-time earthquake hazard assessment

5.2 Real-time Seismic Load Determination

5.2.1 Real-time seismic load determination method

Many researches in moderate seismicity regions over the world including Korea (Sun et al., 2005; Yoon et al, 2006; Lee et al., 2013) have been carried out for evaluating the site-specific seismic amplification using numerical methods of nonlinear (or equivalent-linear) scheme particularly with a number of earthquake excitations considering region-probable motions and various frequency contents. Then, the site amplification coefficients (factors) of

ground surface to bedrock (outcrop or in-layer) according to several period bands have been presented by analyzing peak ground acceleration (PGA) values and spectral shapes from a great number of resultant response spectra (from 0 (free field condition of PGA) to long period of structure), similar to the original approaches for the 1994 NEHRP by Dr. Borchardt or Prof. Dobry.

The amplification coefficients are appropriate to engineers for designing and building structures and facilities at sites having geotechnical investigation data without acceleration monitoring data, thus are incorporated into most of the current international or regional seismic codes. Practically the use of site amplification coefficients may be conservative because of applying several conservative concepts in the procedures to derive the coefficients with several quantified site conditions. In any case, the site coefficients should be determined using the geotechnical investigation-based parameters, representatively the shear wave velocity to a depth of 30 m, and exactly can be applied in the ground surface and correspondent structures.

In the view of practice, it is usual in earthquake engineering applications to adopt a single and simple parameter, the PGA on ground surface, for estimating the severity of an earthquake at a particular location and the surrounding area. With respect to subsurface soil conditions, it is essential to utilize representative profiles of the geotechnical parameters with depth from an engineering point of view: the maximal acceleration a_{\max} profile to bedrock or 20 m in this work of the liquefaction potential evaluation with LPI. As we know, a_{\max} with depth is required to get the CSR for the FS of liquefaction, but any acceleration series data with time or period (frequency), such as acceleration time history and acceleration response spectrum, are unnecessary

to assess the liquefaction hazard. For this reason, the response spectra, kindly sketched in reviewer's comment, was not added in re-revised manuscript.

To compute seismic loads causing site-specific earthquake hazard in real-time, correlations derived previously between the bedrock acceleration transmitted from accelerometers and the maximum acceleration of each layer are assigned into the geotechnical spatial grid. The accelerometers installed on nearby outcrops of bedrock at target site are used to measure the rock outcrop acceleration. Figure 5.2 shows the procedure for real-time seismic load determination consisted with an input database, preceded site response analysis and derivation of seismic load correlation equation (nonlinear optimization of a regression model) (Kim et al., 2012c). This methodology is based on the convincing practice that the seismic monitoring data transmitted and stored in the database are directly correlatable with the seismic loads of earthquake events. First of all, the input dataset should contain the geotechnical spatial grid (soil profile, dynamic soil properties, etc.) to evaluate the likely site response characteristics of the continuous 3D ground conditions of the target area. And various seismic data (e.g., earthquake records, rock outcrop acceleration) are also applied to characterize the normalized seismic trend according to the input seismic load.

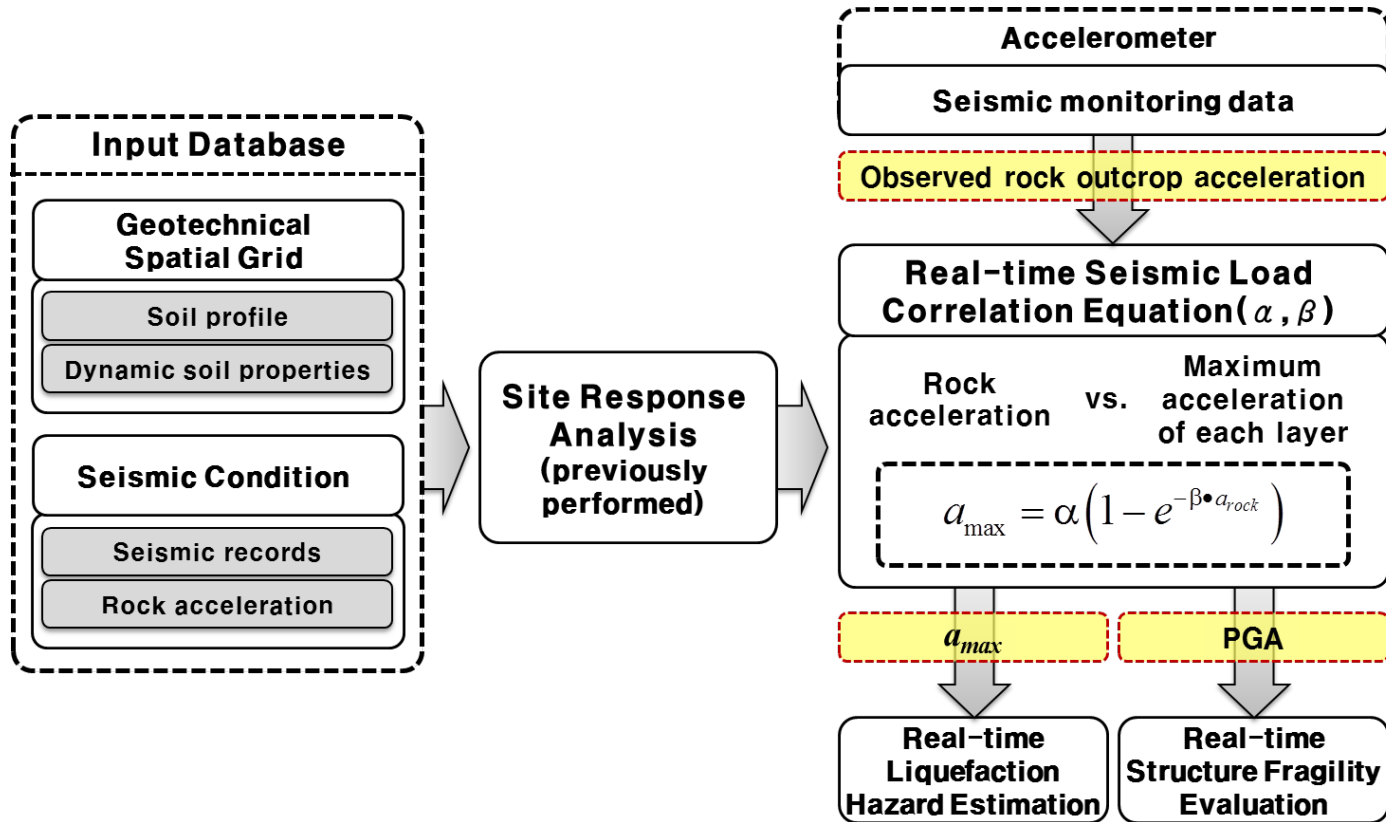


Figure 5.2 Procedure for real-time seismic load determination classified into the database, preceded site response analysis and nonlinear optimization of a regression model to compute seismic loads in real-time

5.2.2 Preceded site response analysis

To determine the site-specific correlation of seismic load determination, the site response analysis is performed previously. The soil profile is input as particular categorized profiles, and the dynamic properties (shear wave velocity, shear modulus, damping ratio, etc.) are applied according to the soil type based on the geotechnical spatial grid. Shear wave velocities, which are of major importance, are determined by a comparative interpretation of seismic refraction tests or the results of the empirical equation for V_S using SPT– N values: $V_S = 65.64N^{0.407}$ given by Sun et al. (Sun et al., 2013). And the nonlinear dynamic curve is determined restrictively through laboratory testing, although limited by sampling of the current conditions in the target area. On this account, typical nonlinear dynamic curves that refer to design and construction reports for earthwork are utilized in this framework.

Nine levels of input rock outcrop acceleration data are used, including six levels ranging from 0.04g to 0.22g by occurrence period, with the addition of 0.30g, 0.40g, and 0.50g to consider major earthquakes, such as the 2011 MW 9.0 Tohoku earthquake. The time history of three types of earthquake records, including Hachinohe and Ofunato plus an artificial synthetic motion, are used to consider the effects of various input-motion frequencies (Table 5.1) (Kim et al., 2012a; Kim et al, 2012d). In Table 5.1, the acceleration time histories are presented together with their elastic response spectra for 5% damping. The two real earthquake motions have similar predominant periods, exactly 0.36 s for Hachinohe motion and 0.38 s for Ofunato motion, despite

the difference of spectral shapes between two motions in mid- to long-period range higher than 0.4 s. On the other hand, the synthetic motion has short predominant period of 0.2 s in wide dominant period band ranging from 0.08 s to 0.42 s.

A site-specific response analysis for the geotechnical spatial grid is previously performed with ProShake (EduPro civil System, 1997). The ProShake is well known as site response analysis computer program using 1D equivalent-linear method, which is probably the most widely used method to perform site response analysis because of its ease of use and conservative results. However, it is well-known that the equivalent visco-elastic approach implemented in ProShake to perform site-response analyses 1) it is not capable of representing changes in soil stiffness and hysteretic damping during the earthquake motion; 2) it is a 1D total stress approach; 3) it is not suitable for wave propagation problems involving high strain levels associated with highly non-linear soil behavior.

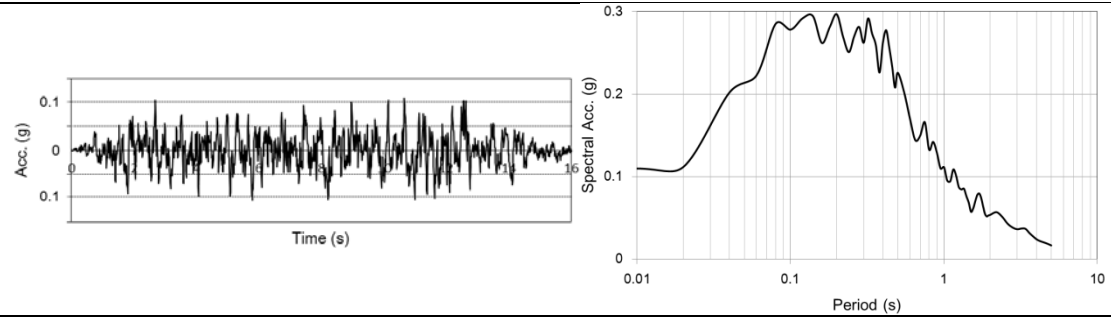
Site response commonly refers to the motion of an elastic wave arriving at the ground surface through rock and soil, and a site response analysis models the propagation characteristics of elastic waves and calculates the ground response (Kim et al., 2012a; Kramer, 1996). However there may be analysis errors under the high strain levels due to nonlinear soil behavior and limitations of only three input earthquake motions with restricted frequency contents. A follow-up study will be conducted based on sophisticated site response analyses using many input motions with various predominant frequencies in domain of 1D as well as of 2D or 3D.

Table 5.1 General information and acceleration data of input earthquake motions

Earthquake	Magnitude	Date	Location	Site Condition*	Acceleration time history	Acceleration response spectrum †
Hachinohe	7.9	May,16, 1968	Tokachi-oki, Japan	S _C		
Ofunato	7.4	Dec.,06, 1978	Miyagik-enoki, Japan	S _D		

[Continued]

Artificial - - - S_B



*: Site conditions are categorized according to the site classification in IBC (International Building Code, 2012).

†: Elastic response spectra are for 5% damping.

5.2.3 Statistical correlation for seismic load

Real-time seismic load correlation equation

From results of preceded site response analysis, a series of ground response values for each geotechnical spatial grid cell are derived from nine levels of rock outcrop acceleration and three types of actual and simulated earthquake records. Then, correlations between the rock outcrop acceleration and maximum acceleration of each layer (having 27 relationships) at particular cell (classified into SP according to the USCS) of the specific geotechnical spatial grid (Grid ID: 1) are determined as represented in Figure 5.3. The thin dotted line describes a one-to-one correlation function of rock outcrop acceleration and maximum acceleration of each layer.

In this respect, vibration characteristics have a relatively small effect upon the site characteristics, although close relationships exist between site-specific seismic vibration characteristics and the frequency components of input earthquake records. Disregarding the influence of earthquake motion, the nonlinear optimization of the regression model is performed considering the nonlinearity of the soil layers. The regression model typically used is the exponential Box–Lucas model (Box and Lucas, 1959).

The correlation between 0–0.3g (red dotted box) is expressed as bold line (to highlight) whereas the correlation over 0.3g is described as dotted line, because the Korean peninsula is classified as a region of moderate seismicity. The correlation between the rock outcrop acceleration and maximum acceleration of each layer (range from 0g to 0.5g) is determined by:

$$a_{\max} = \alpha \left(1 - e^{-\beta \cdot a_{\text{rock}}} \right) \quad (5.1)$$

where a_{\max} denotes maximum acceleration of each layer, a_{rock} represents the measured rock outcrop acceleration, and α and β are correlation coefficients, respectively.

The α and β values relating to the seismic amplification ratio are strongly dependent on not only site condition but input earthquake motion, thus three regression curves in this case would be derived for each grid cell. Nevertheless, unique simple correlation curve was herein determined because wide range of predominant frequency contents of excitations did not apply in the 1D equivalent-linear seismic response analyses. The empirical formulations for estimating seismic load term a_{\max} in this study would be required to be grouped into about 10 levels of predominant periods by performing many analyses using various input motions different frequency contents. The correlation equations averagely considering three motions are assigned into the geotechnical spatial grid. Thus, the maximal acceleration a_{\max} of each layer can be determined in real-time by inputting the measured rock outcrop acceleration to estimate the cyclic stress that causes liquefaction damage.

The site coefficients in this dissertation require further modification for application of more reliable site coefficients in the whole Korean peninsula, and studies on the topographic and basin effects and site classification with surface geology are ongoing.

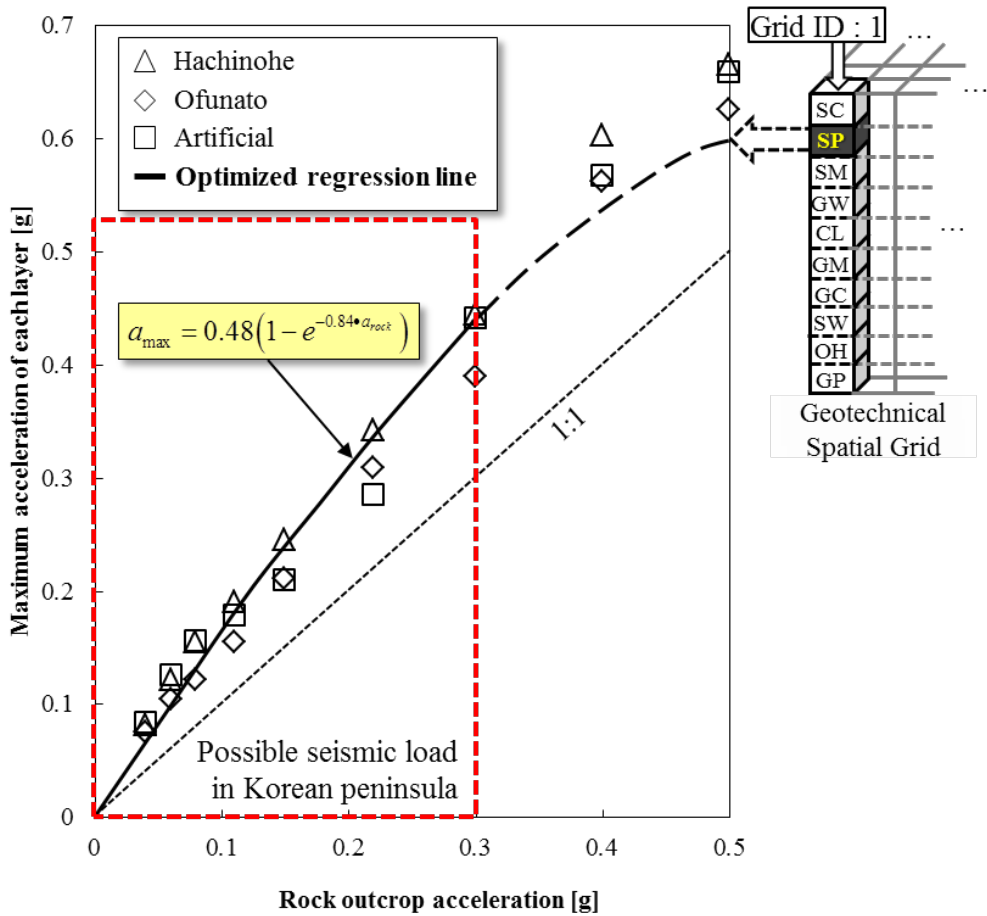


Figure 5.3 An example of correlation between the rock outcrop acceleration and maximum acceleration of each layer based on the nonlinear optimization of a regression model at particular cell (classified into SP according to the USCS) of the specific geotechnical spatial grid (Grid ID: 1)

In the simplified seismic load correlations, the ratio of fundamental site period to predominant excitation period has potential effect on computed a_{max} (Papadimitriou et al., 2008; Kramer, 1996). To consider the effect of nonlinear value of the site period, Papadimitriou et al. (Papadimitriou et al., 2008) computed the peak ground acceleration from empirical relationships. In

this study, the correlations between predominant excitation period and fundamental site period were complied with linear relationship because of the low local variability of geo-layer such as bedrock depth in small reclaimed region of target site (port or downtown). Therefore simplified seismic load correlations assigned into the geotechnical spatial grid can be reasonable to determine the a_{max} , which are not affected by the effect of site period. Additionally, correlation equations considering earthquake scale were established to consider influence of input-motion frequencies in next section.

Correlation equation considering earthquake scale seismic frequency contents

In Figure 5.3, there are some deviations of maximum acceleration of each layer versus rock outcrop acceleration according to the applied seismic frequency contents. Table 5.2 shows the deviation of correlated acceleration with frequency from three field application results based on the geotechnical spatial grid. The average of acceleration deviation with frequency is 6.3%. The effect of frequency contents can be insignificant from the field application.

Additionally, the errors of accelerations by correlation equations are smaller about 20%–57% than these of amplification PGAs. Moreover, correlations have differences by spatial grid but maximum accelerations determined by the correlations is not different significantly, maximum acceleration of each layer by actual site response analysis.

Table 5.2 Deviation of correlated acceleration with frequency from field application results based on the geotechnical spatial grid

Site	Number of grid cell	Deviation from site response curve (%)		
		Avg (COV)	Min (COV)	Max (COV)
Incheon port	1245	6.5	2.2	14.0
Busan port 1	2562	4.2	1.2	10.1
Busan port 2	1542	8.1	2.7	14.5
Avg	-	6.3	2.0	12.9

5.3 Real-time Liquefaction Hazard Estimation

Linked with the geotechnical spatial grid combined with the seismic load correlation equation, LPI-based liquefaction hazard estimation is performed in real-time (Kim et al., 2012c). Initially in this systematic assessment, as depicted in Figure 5.4, the soil profiles and dynamic properties of the geotechnical spatial grid are extracted from a database.

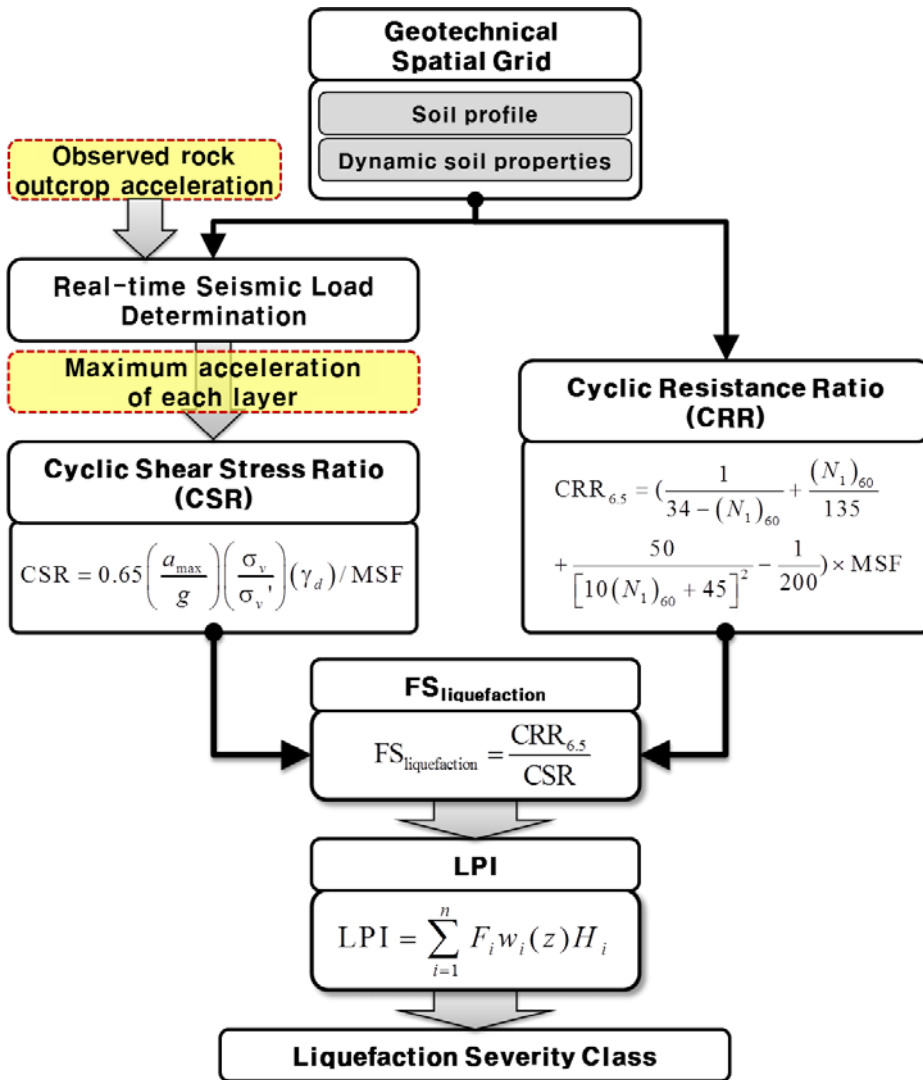


Figure 5.4 Procedure for real-time liquefaction hazard estimation

The basic conditions for the liquefaction-hazard estimation based on borehole drilling logs are as follows: (1) within a depth of 20 m; (2) below the ground water level (GWL); and (3) under 34 blow counts (the corrected SPT blow count, $(N_1)_{60}$ value); (4) under 80% of relative density; (5) under 20% of clayey soil composition (Kramer, 1996; Ishihara, 1996). In the current

standard, the depth of liquefaction can be influenced by the depth to bedrock being shallower than 20 m, although, if necessary, a depth of more than 20 m can be reviewed. To estimate the GWL condition, the highest GWL considering fluctuations, such as the effects of tides and rainfall at the port area, should be selected. The highest daily average GWL during the monitoring period from the annual GWL record at the target port is utilized. The liquefiable geo-layers are selected based on the basic conditions for the liquefaction-hazard estimation and applied to the procedure.

The cyclic resistance ratio (CRR) is then computed using Equations (5.2) and (5.3) based on the ground conditions of the study area. An empirical criterion based on SPT- N values is commonly used in liquefaction assessments in most countries, including Korea. Seed and Idriss (1971) proposed a simplified procedure based on SPT- N values for the evaluation of the liquefaction resistance of soils. This original simplified procedure based on empirical rules has been modified and improved over the years (Ishihara, 1996). Youd et al. (1978, 1987) proposed the following form:

$$CRR_{7.5} = \frac{1}{34 - (N_1)_{60}} + \frac{(N_1)_{60}}{135} + \frac{50}{[10(N_1)_{60} + 45]^2} - \frac{1}{200} \quad (5.2)$$

Here, $CRR_{7.5}$ is the cyclic resistance ratio for an earthquake magnitude (M) of 7.5 and $(N_1)_{60}$ is the value of the field-measured N value corrected for hammer efficiency and the effective overburden stress. $CRR_{7.5}$ is calibrated using the magnitude scaling factor (MSF) (Youd and Perkins, 1987) according to the current seismic design code in Korea with a magnitude (M) of 6.5:

$$CRR_{6.5} = CRR_{7.5} \times MSF \quad (5.3)$$

Here, $MSF = 10^{2.24} / M^{2.56} = 1.44$

Then, the cyclic stress ratio (CSR) is computed using the seismic loads correlated with the transmitted rock outcrop acceleration. The seismic loads are computed by previously derived correlation equations in the geotechnical spatial grid based on the real-time seismic load determination. The CSR is expressed as

$$\text{CSR} = 0.65 \left(\frac{a_{max}}{g} \right) \left(\frac{\sigma_v}{\sigma_v'} \right) (\gamma_d) / \text{MSF} \quad (5.4)$$

where σ_v is the total vertical stress at depth (z), σ_v' denotes the effective vertical stress, a_{max} is the maximum acceleration of each layer (refer to Equation (5.1)), g represents the acceleration of gravity, and γ_d is the stress reduction factor. In this study, the term γ_d is estimated using the following equation formulated by Liao and Whitman (Liao and Whitman, 1986):

$$\gamma_d = 1.0 - 0.00765 \times z \quad \text{for } z \leq 9.15\text{m} \quad (5.5)$$

$$\gamma_d = 1.174 - 0.0267 \times z \quad \text{for } 9.15\text{m} < z \leq 23\text{m} \quad (5.6)$$

The factor of safety against liquefaction per layer, $\text{FS}_{\text{liquefaction}}$, is calculated as the ratio of $\text{CRR}_{6.5}$ to the CSR based on a deterministic procedure widely known as the ‘simplified procedure’ (Seed and Idriss, 1971; Seed et al., 1985; Youd and Perkins, 1978):

$$\text{FS}_{\text{liquefaction}} = \frac{\text{CRR}_{6.5}}{\text{CSR}} \quad (5.7)$$

The conditions of $\text{FS}_{\text{liquefaction}} > 1$ and $\text{FS}_{\text{liquefaction}} < 1$ indicate that the soils are classified as non-liquefiable and liquefiable, respectively, whereas $\text{FS} = 1.0$ represents the limiting equilibrium. The $\text{FS}_{\text{liquefaction}}$ value as determined from the conventional procedure is not a sufficient tool by itself for the evaluation of the liquefaction hazard. The severity of foundation damage

caused by soil liquefaction cannot be accessed directly by the FS, specifically in cases that depend on the severity of liquefaction.

In order to evaluate the liquefaction potential of the ground surface, Iwasaki et al. (Iwasaki et al., 1978; Iwasaki et al., 1982) proposed the use of an index proportional to the thickness of the liquefiable layer and the value of the factor of safety against liquefaction of each layer. A weighting function gives higher values to the layers closest to the ground surface, and decreases linearly to zero at a depth of 20 m. The LPI defined by Iwasaki et al. (Iwasaki et al., 1978; Iwasaki et al., 1982) can be expressed as follows:

$$\text{LPI} = \int_0^{20} F(z)W(z)dz \quad (5.8)$$

$$F(z) = 1 - \text{FS} \quad \text{for } \text{FS}_{\text{liquefaction}} < 1.0 \quad (5.9a)$$

$$F(z) = 0 \quad \text{for } \text{FS}_{\text{liquefaction}} \geq 1.0 \quad (5.9b)$$

$$W(z) = 10 - 0.5z \quad \text{for } z \leq 20m \quad (5.10a)$$

$$W(z) = 0 \quad \text{for } z > 20m \quad (5.10b)$$

Here, z denotes the depth (0–20 m), dz denotes the increment of depth, and $F(z)$ represents the liquefaction severity, which is a function of the $\text{FS}_{\text{liquefaction}}$ defined in Equations (5.9a) and (5.9b). Finally, $W(z)$ is the weighting function as defined in Equations (5.10a) and (5.10b).

This study used a discretized form (Luna and Frost, 1998; Hashemi and Alesheikh, 2011; Alesheikh et al., 2006) of Equation (5.11) to find the LPI, given as

$$\text{LPI} = \sum_{i=1}^n F_i(z)W_i(z)H_i \quad (5.11)$$

where n denotes the number of discretized layers, H_i is the thickness of the discretized layer, and F_i denotes the liquefaction severity for layer i .

Iwasaki et al. (1982) calibrated the LPI values with the severity of liquefaction-induced damage using data mostly for sandy soils, as provided by 87 SPT borings in liquefied and non-liquefied sites in Japan. Iwasaki et al. (1978, 1987) found that severe or minor liquefaction is likely to occur whenever the LPI is greater than 15 or less than 5, respectively. The LPI value is inversely proportional to $FS_{\text{liquefaction}}$ and the depth of the upper layer in saturated zone; the higher the index, the greater the potential for liquefaction. The categories of the liquefaction severity class were modified by Luna and Frost (1998, 2006) and Chung et al. (2011), and are summarized in Table 5.3. The category adopted in this paper was proposed considering the regional seismic characteristics in Korean port areas: none, low, high, and extreme.

Table 5.3 Criteria for liquefaction severity categories assessed by the LPI

LPI	<i>Iwasaki et al. (1982)</i>	<i>Luna and Frost (1998)</i>	<i>Chung et al. (2011)</i>	<i>This study (2013)</i>
0	Not likely	Little to none	None	None
$0 < \text{LPI} \leq 5$	Minor	Minor	Little to none	Low
$5 < \text{LPI} \leq 15$	-	Moderate	Moderate	High
$15 < \text{LPI} \leq 100$	Severe	Major	Severe	Extreme

5.4 Real-time structure fragility evaluation

5.4.1 Fragility curve for structure

Description of fragility curve

Fragility function of structure is the function which represents the excess probability of defined damage level for specific earthquake intensity. Intensity index which means earthquake intensity is needed to represent damage probability. Spectral acceleration (S_a) and spectral displacement (S_d) are usually used as intensity index by characteristics of structure. It is convenient to calculate damage probability of structure instant by using peak ground acceleration (PGA) as intensity index.

Damage probability of superstructure is expressed as

$$PF_{ij} = PROB[D \geq C_i | EQ_j] \quad (5.12)$$

where PF_{ij} is the probability of exceeding i level for the earthquake in the intensity of j , D denotes effect of the load by an earthquake, and C_i is strength of the structure for damage level i .

Indexes which properly represent structural damage should be selected. Fragility is cumulative log-normal distribution function and normally expressed as

$$P_f(s) = \phi \left[\frac{\ln s - \ln \bar{s}}{\beta} \right] \quad (5.13)$$

where $P_f(s)$ is damage probability of structure at s , $\phi[\]$ denotes Gaussian

cumulative log-normal distribution function, \bar{s} is Median of PGA at ground surface, s is PGA of the earthquake, random variable, and β is standard deviation of log value of PGA at ground surface.

Fragility curve of port structure

Port structures are usually located at soft near the coast and because the type of port structures are various, not only location, ground condition, probability of liquefaction and structure characteristics but also importance of structures should be considered to evaluate earthquake hazard. Port facilities are classified into counter facilities, berthing facilities, buildings, crane and bridges etc.

In this study, fragility functions of gravity quay wall, gantry crane and concrete frame with unreinforced masonry infill wall (concrete frame) are applied to real-time structure fragility evaluation method and the median and standard deviation of fragility functions are depicted in Table 5.4–5.6.

Table 5.4 Definition of damage levels of seismic fragility curves for gravity quay wall (KORDI, 2013)

Damage level	<i>Disorder</i>	<i>Slip failure</i>	<i>Collapse</i>
Mean value (\bar{s})	0.518	0.819	1.013
Standard deviation (β)	0.129	0.146	0.216
Damage state	10cm in lateral displacement	10cm in slip	30cm in lateral displacement

Table 5.5 Definition of damage levels of seismic fragility curves for gantry crane (KORDI, 2013)

Damage Level	<i>Near Collapse</i>	<i>Collapse</i>
Mean value (\bar{s})	0.61	1.01
Standard deviation (β)	0.21	0.2
Damage State	30% increase in strain	50% increase in strain

Table 5.6 Definition of damage levels of seismic fragility curves for unreinforced concrete structure (FEMA, 2003)

Damage Level	<i>Slight</i>	<i>Moderate</i>	<i>Extensive</i>	<i>Complete</i>
Mean value (\bar{s})	0.2	0.4	0.8	1.6
Standard deviation (β)	0.64	0.67	0.66	0.66
Damage State	8%	40%	80%	100%

5.4.2 Real-time fragility evaluation method

To evaluate structure susceptibility in real-time, the fragility function is used as threshold of structure failure, linked with geotechnical spatial grid (assigned with correlation equations for seismic load determination). The superstructure for seismic fragility evaluation can be simply classified with two groups: structure above soil layer and structure above rock (Figure 5.5).

The fragility of structure above soil layer is evaluated based on peak ground acceleration linked with seismic load correlation, to consider site-specific site response characteristics. Meanwhile, the fragility of structure above rock, where seismic wave is passed on directly, is evaluated linked with rock outcrop acceleration transmitted from accelerometer.

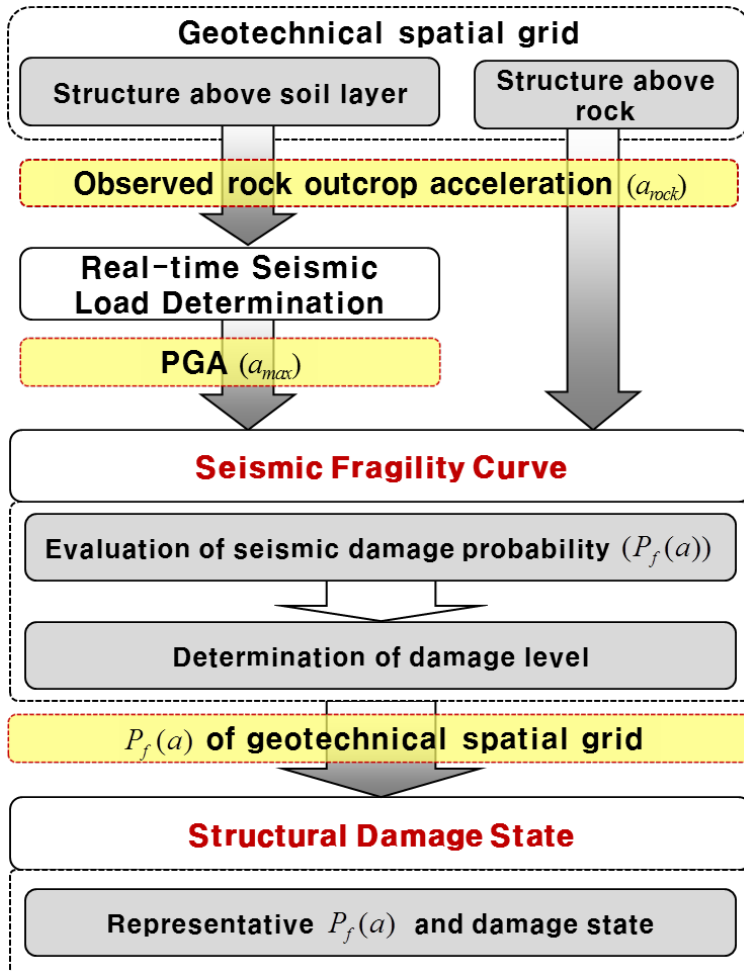


Figure 5.5 Procedure for real-time fragility evaluation method

Damage level of structure when an earthquake occurs is represented as probability of failure by fragility function. In this study, it is applied that the method of determination of damage grade which is based on the probability of failure at each damage level to estimate the seismic damage of structures. First, the failure probability of each structure is calculated by transmitted rock outcrop acceleration from accelerometer or correlated PGA based on statistical correlation for seismic load (from “5.2.3 Statistical correlation for seismic load”). Damage level and state of gravity quay wall, gantry crane and concrete frame are subjected to Table 5.7–9.

Second, the seismic damage probability ($P_f(a)$) with geotechnical spatial grid is determined by transmitting the a_{rock} or PGA in the seismic fragility function. It is assumed that the damage grade is confirmed when the probability of each damage level is over 50%. Damage grade of structure depends on the most severe damage grade when more than 2 damage grades are confirmed. For example, in the case of concrete frame, the probabilities of ‘Slight’ and ‘Moderate’ level are both over 50% then the damage grade of the structure is confirmed as ‘Moderate’ (Figure 5.6).

Third, the structural damage state (or class) for target structure is evaluated considering occupied area ratio of geotechnical spatial grids having $P_f(a)$ value. If the occupied area ratio of $P_f(a)$ determined as damage state (ex. Slight, Moderate, etc.) is more than 50%, the structural damage state of target structure is ‘Failure’ corresponding to the damage level.

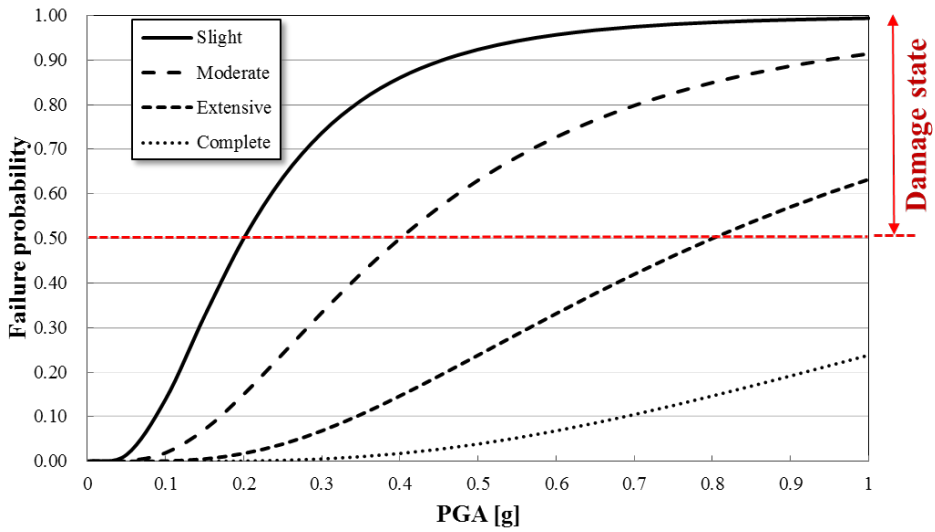


Figure 5.6 An example of fragility curve and damage state for unreinforced concrete structure modified from FEMA (2003)

Damage grades of each structure, dealt in this study, are suggested in Table 5.7–5.9.

Table 5.7 Seismic damage levels of gravity quay wall

	Disorder	Slip Failure	Collapse	State
Failure Probability	<0.5	<0.5	<0.5	<i>Safe</i>
	>0.5	<0.5	<0.5	<i>Disorder</i>
	>0.5	>0.5	<0.5	<i>Slip Failure</i>
	>0.5	>0.5	>0.5	<i>Collapse</i>

Table 5.8 Seismic damage levels of gantry crane

	Near Collapse	Collapse	State
Failure Probability	<0.5	<0.5	<i>Safe</i>
	>0.5	<0.5	<i>Near Collapse</i>
	>0.5	>0.5	<i>Collapse</i>

Table 5.9 Seismic damage levels of unreinforced concrete structure

	Slight	Moderate	Extensive	Complete	State
Failure Probability	<0.5	<0.5	<0.5	<0.5	<i>Safe</i>
	>0.5	<0.5	<0.5	<0.5	<i>Slight</i>
	>0.5	>0.5	<0.5	<0.5	<i>Moderate</i>
	>0.5	>0.5	>0.5	<0.5	<i>Extensive</i>
	>0.5	>0.5	>0.5	>0.5	<i>Complete</i>

5.5 Summary and Conclusions

A systematic framework for real-time assessment of the earthquake hazard was developed to consider local site response characteristics for target areas. According to the framework, three interrelated assessment procedures were incorporated in a database on a real-time basis: real-time seismic load determination, real-time liquefaction hazard estimation, and real-time structure fragility evaluation.

- 1) Previously, the geotechnical spatial grid was constructed based on 3D kriging of geotechnical data to constitute the 3D seismic ground conditions to be correlated with the liquefaction potential.
- 2) First, the previously derived correlation equations between the maximum acceleration of each layer and the rock outcrop acceleration were incorporated in the geotechnical spatial grid to consider site-specific response characteristics.
- 3) As earthquake events occur, as soon as monitored rock outcrop acceleration data are transmitted from the accelerometer, the liquefaction hazard can be evaluated by integration of the geotechnical spatial grid with liquefaction parameters using the simplified real-time LPI evaluation method.
- 4) The correlated peak ground accelerations are linked with fragility functions and probabilities of failure are calculated. Seismic damage grades of superstructures are determined and they depend on the probabilities of failure.

- 5) The liquefaction severity class and structure fragility class are forecasted and visualized in satellite map images or digital map in real-time based on the GIS platform.
- 6) The integrated earthquake hazard of the target structure is determined considering the liquefaction and fragility grade.

6. Integrated System for Real-time Earthquake Hazard

6.1 System Design

The integrated system consists of a database (DB) and systematic modules. The sub-modules execute various functions on managing and utilizing information in the database with connection to the database; input of data, geostatistical 3D integrated data based on input data, real-time earthquake hazard data, and output of data. The system program including all these functions focuses on user-friendliness and real-time applications. And the main management program corporates sub-modules.

In this proposed framework, the computer-based method for 3D geotechnical information and real-time assessment of spatial earthquake hazard was embedded based on a stand-alone system developed using Microsoft Visual BASIC, the Esri ArcGIS developer tool, and the GSLIB of Stanford University. The ArcGIS developer tool was mainly used for spatial development of the database, evaluation of the results, and spatial visualization. In addition, a sophisticated kriging interpolation program based on Visual BASIC code was developed and adopted by the spatial analysis component of the GSLIB.

The system including all these functions focuses on user-friendliness and real-time applications. Also, the system can service the multi-client's information needs with network connection to a single server with a database.

6.1.1 System requirements

The initial required elements for the GIS-based integrated system for real-time earthquake hazard assessment are categorized into systematic and functional parts.

Systematic requirements

- 1) Construction of an optimal GDB for all collected filed data and system data throughout data standardization
 - Data standardization of all available filed data and system data
 - Construction of a relational database based on the results from data standardization
- 2) System accessibility without limitations of time and space
 - Connection between clients and a database server on the network
- 3) Scalability in data, users and analysis procedures
 - Storage capability of a database
 - Flexibility of a database for new complex data
 - Supplying simultaneous services to multiple users
 - Applicability of further analysis
- 4) User-friendliness
 - Predefined standard output formats according to characteristics

of data

- Easiness to learn and subsequently use

Functional requirements

- 1) Pre- and post-data processing with graphic visualization
 - Inputting, importing and updating of filed information
 - Viewing of the data by standard database tools or predefined formats
 - 2-dimensional plane views and sectional views
 - 3-dimensional views
- 2) Geostatistical 3D integration for geotechnical spatial grid
 - Optimization of borehole datasets based on the proposed outlier detection methods (Cross-validation-based outlier detection method, Generalized extreme value distribution (GEVD)-based outlier detection method)
 - Geostatistical 3D integration of optimized borehole datasets (geo-layers) and digitized geophysical tomography to construct 3D geo-layers
 - Geotechnical 3D geotechnical spatial grid construction by categorizing the representative soil profile and dynamic properties
 - Supplying reliable 3D geometric geo-layer having site-specific geotechnical characteristics to support the best method by users and the system

3) Real-time earthquake hazard assessment

- Real-time seismic load determination considering site-specific site response characteristics based on the correlation rock outcrop acceleration and maximum acceleration of each layer
- Real-time liquefaction hazard estimation based on liquefaction potential index
- Real-time structure fragility evaluation based on seismic fragility function
- Supporting user's decision making by displaying spatial distribution of earthquake hazard information

The developed system requires these complex analysis functions and comprehensive displays. Even though database – web server GIS is the most advanced GIS architecture, it does not fully support these requirement because the web server or an application server must handle all things. Therefore an organizational GIS was selected as the architecture of the developed system, which satisfies these requirements and enables the user to access data from widely distributed locations. That is, the developed system consists of a database and system software. Also, this architecture can be transformed into a client-web server GIS if necessary.

6.1.2 System overview

The developed system is hosted on a secure Intranet / local Area Network (LAN), and it follows the client-server model, in which multiple client PCs are request data from a single server with a geodatabase. System software service the client's information needs. The operating schema of the developed system is shown in Figure 6.1.

From the seismic monitoring and response system of Korea Integrated Seismic System, the seismic monitoring datasets which are transmitted from server of seismic accelerometer, are linked to database server for integrated system. And the earthquake hazard datasets analyzed from developed system are forecasted from response system in real-time.

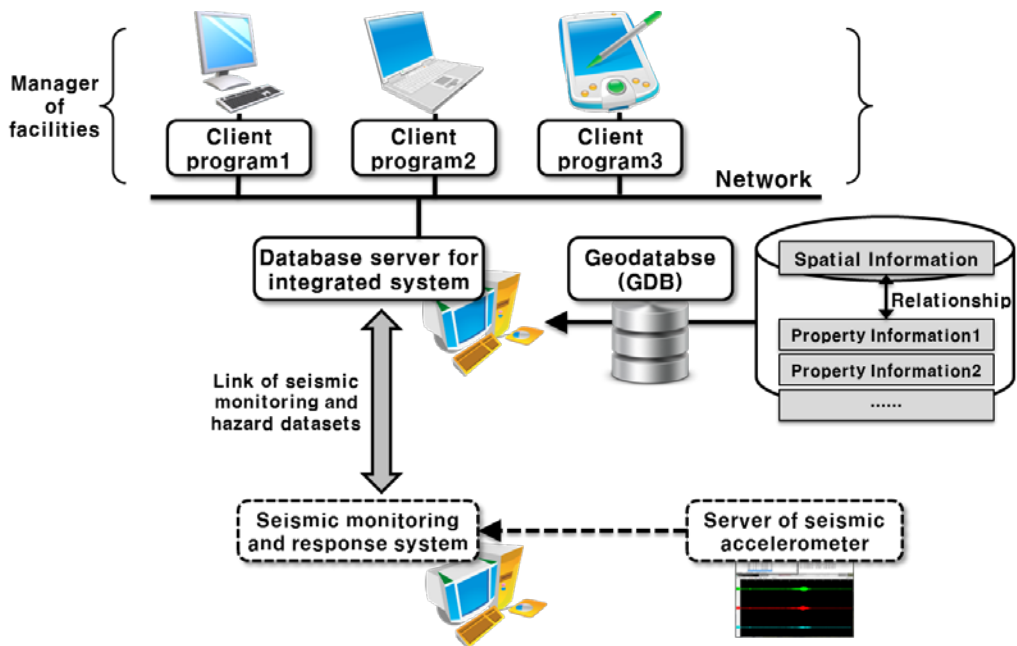


Figure 6.1 System overview

Based on the design schema described above, the system structure

consisting of a GDB and 4 modules was established, as shown in Figure 3.2. The spatial database is the backbone of the developed system. It stores not only primary collected field data such as geographical data, geotechnical data, structure data, and seismic monitoring data, but also secondary processed data obtained from the application of the modules of the system. An input module provides an effective way to store and arrange all collected field data in the GDB according to standard data formats. In the geostatistical 3D integration module, reliable 3D continuous geotechnical information is determined and constructed the geotechnical spatial grid into the database. In the real-time earthquake hazard assessment module, geo-spatial earthquake hazard is estimated in real-time by linking with measured rock outcrop accelerations. The output / visualization module provides functions such as graphs, 2D plane views, 2D sectional views, and 3D views together with tabular formats. Moreover, earthquake hazard can be visualized at the 2D or 3D digital map in real-time.

With system software installed in a client PC, connected to the server by network, a user manages and utilizes the information in the GDB. The system software focuses on user friendly functions and real-time applications. In particular, field data can be entered into the GDB very simply. Once stored in the GDB, all data can be utilized without difficulty in each module of the system software. And the environment of system development is shown in Table 6.1.

Table 6.1 Environment of system development

		Environment of system development
System server		Microsoft SQL Server 2008 Esri ArcSDE
Management program		Microsoft Visual Basic.net Esri ArcGIS Engine
System program	Geostatistical 3D integration module	Microsoft Visual Basic.net GSLIB
	3D visualization module	Microsoft Visual C++ OpenGL

6.1.3 Database design

The key component of a GIS-based system is the spatial data, which must be obtained and accessible. The primary advantage of GDBs already in Chapter 2, over other data storages, is that it allows GIS to build on the existing capabilities of relational database management systems (RDBMS). RDBMSs include the support of the SQL (Structured Query Language) and the ability to generate complex geospatial queries. Also, a database's client-server architecture supports multiple users simultaneously and allows them to view, edit, and query the database without conflict. The GDB design process of the developed system based on the database design concepts is explained in Section 2.2.1.

The detailed design procedure of the GDB for the developed system is:

- 1) Defining the objectives: deciding on the types of data to be stored.

- Geographic data, geotechnical data, structure data, seismic monitoring data, geostatistical 3D integration results data, and earthquake hazard data from system analyses are selected to be stored in a database.
 - From this step, the concept of a database is determined.
- 2) Reviews on current database and information, irrespective of its nature such as paper, electronic documents, reports, etc., and extracting the key types of data such as chart and data formats for borehole logs.
 - 3) Design the data tables needed for 2) above.
 - 4) Identifying and constructing relationships between the tables and records by identifying primary keys across table, such as borehole identities.
 - 5) Developing and applying necessary rules to the data in the tables such that data is consistent such as signs, magnitudes, units, etc.
 - 6) Creating tables according to results from data standardization above in a GDBMS.
 - 7) Creating relationship between tables in the GDBMS.

Stages 1) to 5) are regarded as standardization, which is used to decide the standard data formats. Stages 6) and 7) are setting up a database in the GDBMS software.

6.1.4 Database structure

Microsoft SQL Server was chosen for the GDBMS of the developed system because of the robustness and scalability of its GDBMS. Residing on the DB server, the GDB contains information on all 6 classes: 4 primary collected field data and 3 processed data. The data was standardized by accompanying by establishing a relation between geographic locations and other attribute information as described in section 6.2.2. The primary classes of the data model and relations between these classes are shown in Figures 6.2 and 6.3. The detailed descriptions for standard data structures of all information in the developed system are following below. And detailed database structure contained field, data format and detail function description was included in 'Appendices' section.

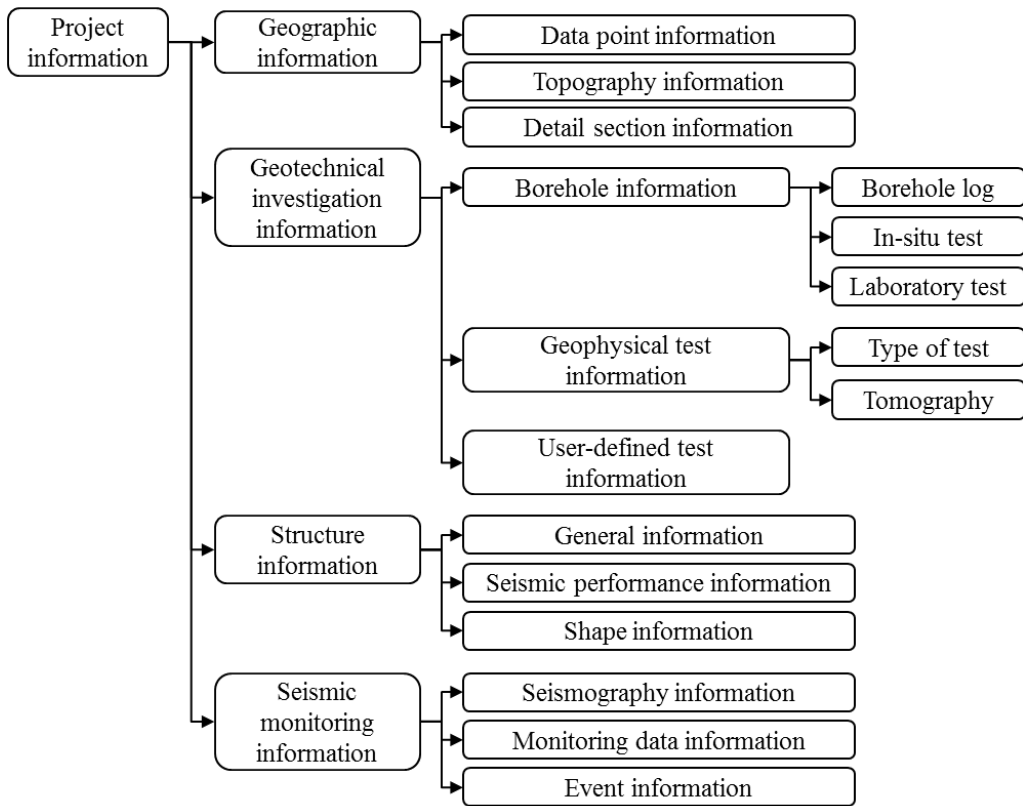


Figure 6.2 Key data classes and relations of the GDB for the developed system: Primary information

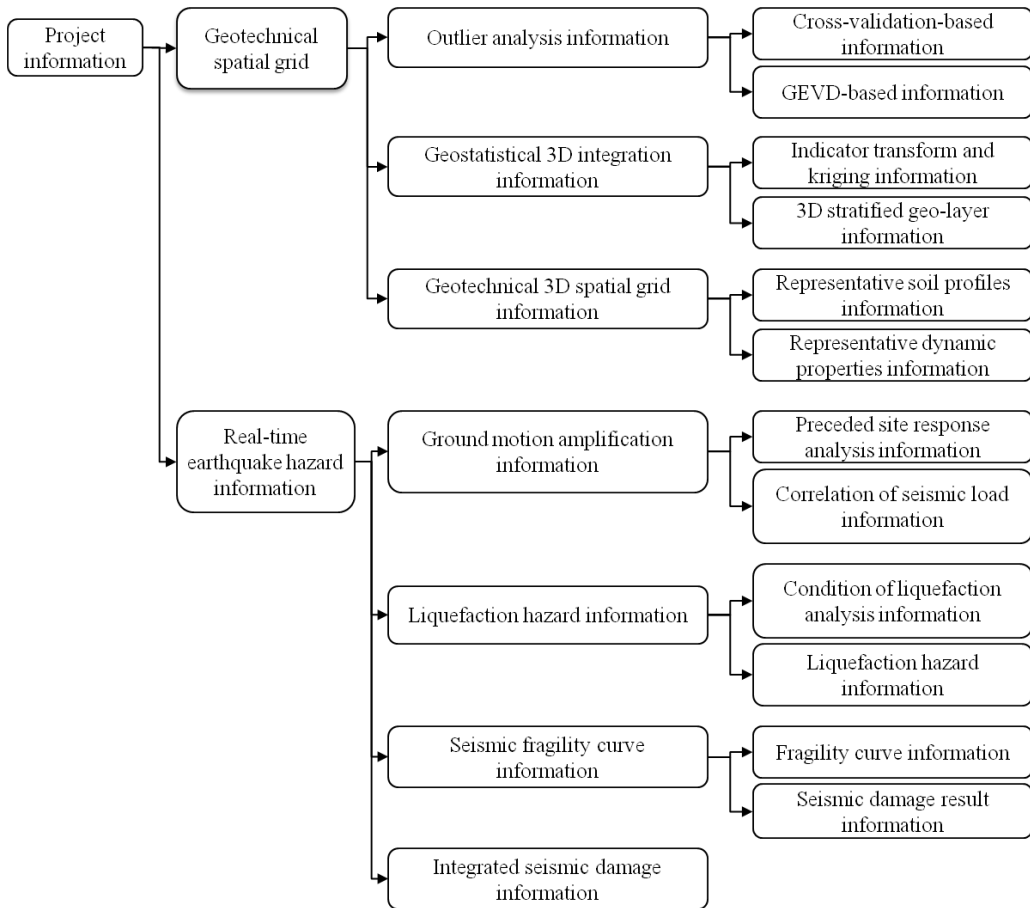


Figure 6.3 Key data classes and relations of the GDB for the developed system: Processed information

Geodatabase (GDB)

Geodatabase (GDB) is the basic data format for GISs to refer to attribute information, and to correlate and analyze various datasets spatially. GDB of the developed system was established based on a 3-dimensional coordinate system. Sub-areas for a wide target area are generally used in fields to promote the efficiency of site-specific earthquake hazard management. Also,

a digital map can be used as basic topographical information of the system because it offers an easy way to construct topographical information for a target area.

GDB is divided according to types as shown in Table 6.2 and shown as a point in the 3-dimensional coordinates, that is, a XYZ coordinates. GDB for topography, sub-areas and structures is the 3-dimensional coordinates for lines and text. Lines represent spatially the shapes and locations of topography, sub-areas and structures and text are descriptions in a digital map and names of structures.

Table 6.2 Types of geographic information in the developed system

Category	Spatial type	Geodatabase type of ArcInfo(ArcSDE)
Attribute information	object	object
Sub-areas	line	line feature
Topography and structures	raster	raster

Type of GDB is arranged as geotechnical investigation information, structure information, seismic monitoring information, geostatistical 3D integration results, and real-time earthquake hazard assessment results (Tables 6.3–6.7).

Table 6.3 Type of geodatabase for geotechnical investigation information

Category	Sub Category	Spatial type	Geodatabase type of ArcInfo(ArcSDE)
Borehole	Boring log	point	point feature
	Layer	object	object
	SPT		
	RQD		
	CPT		
	FVT		
	CTX		
	RC		
	Borehole Summary		
	Additional test		
Geophysical test	General information	object	object
	1D tomography	line	line feature
	2D tomography	raster	raster
	3D tomography	raster	raster

Table 6.4 Type of geodatabase for structure information

Category	Spatial type	Geodatabase type of ArcInfo(ArcSDE)
General information	object	object
Structure shape	polygon	polygon feature

Table 6.5 Type of geodatabase for seismic monitoring information

Category	Spatial type	Geodatabase type of ArcInfo(ArcSDE)
General information	object	object
Seismic observatory	point	point feature
Earthquake event	point	point feature

Table 6.6 Type of geodatabase for geostatistical 3D integration results

Category	Spatial type	Geodatabase type of ArcInfo(ArcSDE)
General information	object	object
Geotechnical spatial grid	raster	raster

Table 6.7 Type of geodatabase real-time earthquake hazard assessment results

Category	Spatial type	Geodatabase type of ArcInfo(ArcSDE)
General information	object	object
Liquefaction hazard information	raster	raster
Structure fragility information		

Site information

Detailed description of table for project information in the developed system is shown in the Table 6.8. The project information is the uppermost category in the hierarchy database system. General information on a target site is stored in the T_Site.

Table 6.8 Details of the T_Site table

Field	Data type	Constraint	Details
site_id	Integer	PK	Serial numbers to manage sites
site_name	Text		Name of the site
project_id	Integer	PK	Serial numbers to manage projects
project_name	Text		Name of the project
project_file	Filestream		Attached file related with target project

Geotechnical investigation information

Geotechnical investigation has been performed to identify the field ground condition and to evaluate engineering parameters of field ground. Quality and quantity of geotechnical investigation are dependent on the importance and reliability of current site condition. But generally types of geotechnical investigation are categorized into boring inspection, in-situ tests, laboratory tests, and geophysical tests.

The boring log, which is the basis of geotechnical investigation data, must be utilized in the GDB. Generally, in the most port or urban area in Korea, CPT (Cone Penetration Test) and FVT (Field Vane Test) among various in-situ tests are very often performed. Therefore, CPT and FVT data are necessary to be pre-defined. Engineering parameters evaluated from in-situ tests and laboratory tests are also important values.

Especially, the dynamic tests such as shear wave velocity test, cyclic triaxial test, and resonance column test, are standardized for consideration of

dynamic properties in target site. Geophysical tests which are composed of seismic refraction test and resistivity test are essential to retain the rational continuous geotechnical properties. Raw test data for in-situ tests, laboratory tests, and earthwork results (design or construction reports) is necessary on occasion.

Therefore, geotechnical investigation information consists of borehole log data, In-situ test data, Dynamic test data, engineering parameters evaluated from various tests, user-defined data and geophysical test data, and standardization for geotechnical investigation data was performed. According to the results from the standardization, the brief database structure to store geotechnical investigation information can be shown as Table 6.9.

Detailed standard data formats of borehole information (T_Borehole_Info, T_Layer, T_SPT, T_RQD, T_CPT, T_CPTu, T_CPTu_Data, T_FVT, T_FVT_Data, T_Vs, T_CTX, T_RC, T_RC_Data, T_Borehole_Sum, T_Test, T_Test_Info and T_Test_Data) and geophysical testing information (T_Geophysical_Info, T_Geophysical_Result, T_Geophysical_Tomography) are shown in 'Appendix A.1.1' section.

Table 6.9 Tables for geotechnical investigation information in the developed system

Category	Sub Category	Comment
Borehole data	General description of boring	Boring data, inspector, address, etc.
	Geo-layer data	Description of each geo-layer
	SPT data	N-value with depth
	RQD/TCR data	RQD and TCR with depth
In-situ test data	CPT data	Summarized and raw data for CPT and CPTu data
	FVT data	Summarized and raw data for FVT data
Dynamic test data	Shear wave velocity test data	Summarized and raw data for shear wave velocity test data
	Resonance column test data	Summarized and raw data for resonance column test data
	Cyclic triaxial test data	Summarized and raw data for cyclic triaxial test data
Soil material properties		Engineering parameters evaluated from various tests
User-defined data		Raw data for laboratory tests and undefined in-situ tests
Geophysical test data		Summarized and raw data for geophysical test data

Structure information

Structure information can be regarded as seismic performance capacity, and obtained from a building register and performance appraisal report. According to the structure data from standardization, the brief database structure to store structure information can be shown as Table 6.10.

Table 6.10 Tables for structure information in the developed system

Category	Comment
Structure information data	Structure type, shape, repair status, structure report, etc.
Structure shape	Spatial coordinate, geometry, etc.

Detailed standard data formats of borehole information (T_Structure_Info and T_Structure_Shape) are shown in ‘Appendix A.1.2’ section.

Seismic monitoring information

Prior to the explanation for data structure of seismic monitoring information, it is necessary to look into operating mechanism of instruments, types of instruments and so on. As the seismic accelerations are transmitted from the Korea Integrated Seismic System (KISS) in real-time, the data format of earthquake event according to KISS is retained to consider the event trigger time and transferred event file. In Table 6.11, data format of earthquake event (belong to KISS server) was arranged previously for port area, Korea. Based on header data field, the earthquake event information such as event trigger time, event file and data alarming message can be provided as fundamental data for transmission of outcrop rock outcrop acceleration.

Table 6.11 Data format of earthquake event according to KISS

	name	type	size	comment						
Header	mtag (message tag)	string	6	message tag, always be <table border="1" style="display: inline-table; vertical-align: middle;"> <tr> <td>K</td> <td>I</td> <td>O</td> <td>S</td> <td>T</td> <td>\0</td> </tr> </table>	K	I	O	S	T	\0
	K	I	O	S	T	\0				
	mtype (message type)	int	4	message type, 1 = event trigger time 2 = event file transfer completed						
mlength (message length)	int	4	real message length followed by header							
Data	data	string	50	ex) mtype=1; 20120808121453 mtype=2; 20120808121453.evt						

In seismic monitoring in real-time basis, seismological observatory data, seismic monitoring data, and earthquake event data are standardized in table 6.12.

Table 6.12 Tables for seismic monitoring information in the developed system

Category	Comment
Seismological observatory data	Station name, type, coordinate, etc.
Seismic monitoring data	Summarized and raw data for seismic monitoring data
Earthquake event data	Summarized and raw data for earthquake event

Detailed standard data formats of borehole information (T_Seismological_Observatory, T_Seismic_Monitoring, T_Earthquake_Event) are shown in 'Appendix A.1.3' section.

Geotechnical spatial grid information

Geotechnical spatial grid information is the results and options of geostatistical 3D integration procedure (Table 6.13). The results are a grid model over a selected domain and the options are information related to geostatistical method and gridding of selected domain which are excluded outliers of borehole datasets.

Table 6.13 Tables for geotechnical spatial grid information in the developed system

Category	Comment
Indicator kriging data	Kriging type, variogram model, etc.
3D Geo-layer data	Summarized and raw data for geostatistical integrated layer data
Geotechnical spatial grid data	Summarized and raw data for geotechnical spatial grid data

Detailed standard data formats of borehole information (T_Indicator_kriging, T_3D_GeoLayer and T_Geotechnical_Spatial_Grid) are shown in ‘Appendix A.1.4’ section.

Real-time earthquake hazard information

Real-time earthquake hazard information consists of earthquake hazard assessment results and analysis options. Earthquake hazard results contain the seismic load correlation determination results, liquefaction estimation results, and structure fragility evaluation results (Table 6.14). And the hazard information are automatically determined and stored in to database with

geotechnical spatial grid information.

Table 6.14 Tables for real-time earthquake hazard information in the developed system

Category	Sub Category	Comment
Seismic load data	Correlation equation data	Correlation coefficient for correlation equation of seismic load
	ProShake results data	Summarized and raw data for ProShake output
	Correlated PGA data	Correlated PGA results
	Correlated PGA of layer data	Correlated PGA of layer results
Liquefaction hazard data	CRR data	Summarized and raw data for cyclic resistance ratio data
	CSR data	Summarized and raw data for cyclic stress ratio data
	FS data	Summarized and raw data for factor of safety for liquefaction data
	LPI data	LPI and liquefaction severity class data
Structure fragility data	Fragility grade data	Structure fragility curve and damage level data
	Fragility damage data	Fragility damage class data
Integrated seismic damage data		Integrated seismic damage associated with liquefaction and fragility class data

Detailed standard data formats of borehole information (T_Corr_Eq, T_Corr_Graph, T_Shake, T_Corr_PGA, T_Corr_layer_PGA, T_CRR, T_CSR, T_FS_Liquefaction, T_LPI, T_Fragility, T_Fragility_Grade, T_Fragility_Damage and T_Integrated_Damage) are shown in ‘Appendix A.1.5’ section.

6.2 Program for System Modules

6.2.1 Management module

Management of input or analysis results data is the fundamental and indispensable function to run the system software based on the SDB. All the collected field data are stored in the GDB with their locations based on the established standard data formats described in previous section. Therefore, prior to input of attribute information, earthquake hazard information must be inputted in the GDB. Manage of data is performed in the independent window form according to the database structure. Based on the management module, sub-modules are combined with automated linking procedure: input modules (geotechnical investigation data input module, structure data input module, and real-time seismic data link module), geostatistical 3D integration module, real-time earthquake hazard assessment module, and output / 3D visualization modules. In Figure 6.4, sequential systematic procedures for earthquake hazard assessment are programmed by integrating the sub-modules.

The main management program has various functions: menu, map view, layer content, visualization tool, site information. From the menu, when users select the menu function, the related sub-modules can be implemented as sharing database. And site information inputted from input modules and geotechnical spatial grid and earthquake hazards estimated real-time framework are visualized on the map view, which display the 2D or 3D spatial distribution of the satellite map.



Figure 6.4 Systematic procedure of real-time earthquake hazard assessment according to system program



Figure 6.5 Main management program and detailed function

6.2.2 Input module

Management of site information

Project information and topographic information of site information are managed in a same window form, because this information generally is used to identify locations of attribute information spatially. Also, digital or satellite map are directly converted into topographic information. Considering the efficiency of data management, input of geographic information for sub-area information and attribute information was designed to be performed in input window forms for attribute information. Geographic information for attribute information is used to display locations of attribute information on topographic map, that is, background map, and to utilize attribute information in geostatistical 3D integration procedure. The window forms for management of geographic information for target site are shown Figure 6.6.

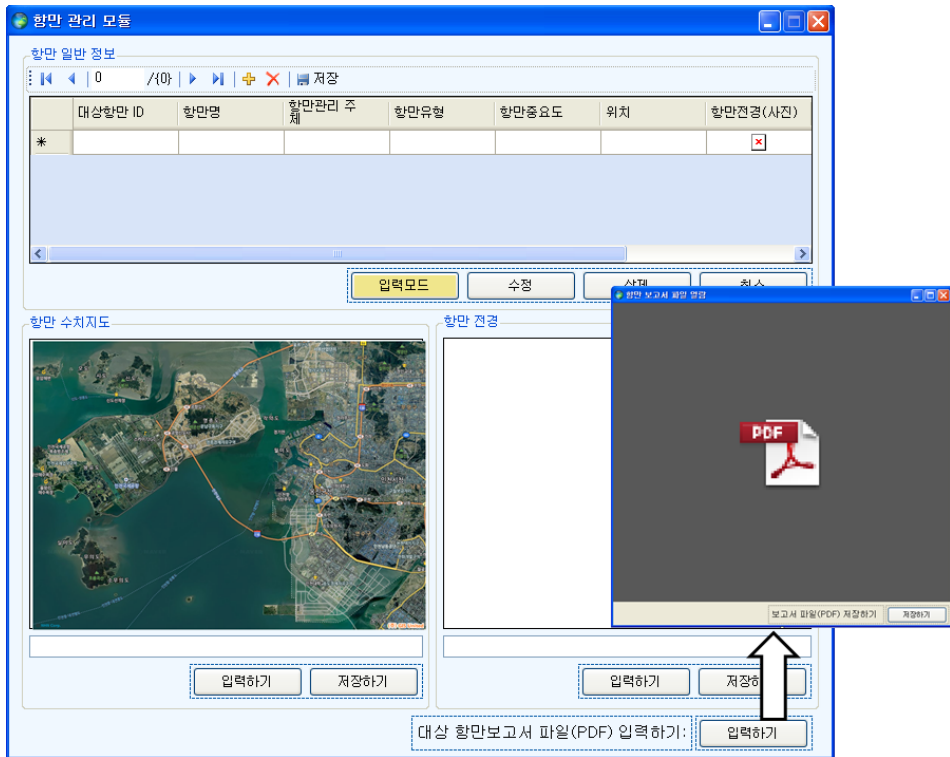


Figure 6.6 Management module of site information

Management of geotechnical investigation information

All geotechnical investigation information is managed in a window form according to sub classes. The management modules of borehole information and geophysical testing are shown in Figures 6.7 and 6.8. General descriptions for borehole including geographic locations and geo-layer information are managed in Figure 6.7. And the detailed screen views for management module of SPT, RQD and TCR information, CPT information, FVT information, shear wave velocity test information, cyclic triaxial test information, resonance column test information, engineering parameters

evaluated from various tests, user-defined test information were included in ‘Appendix A.2’.

Geophysical tomography data is digitized by using digitizing tool of the management module, as shown Figure 6.8. These window forms for management of geotechnical investigation information are designed according to the database structures and the characteristics of the geotechnical investigation information.

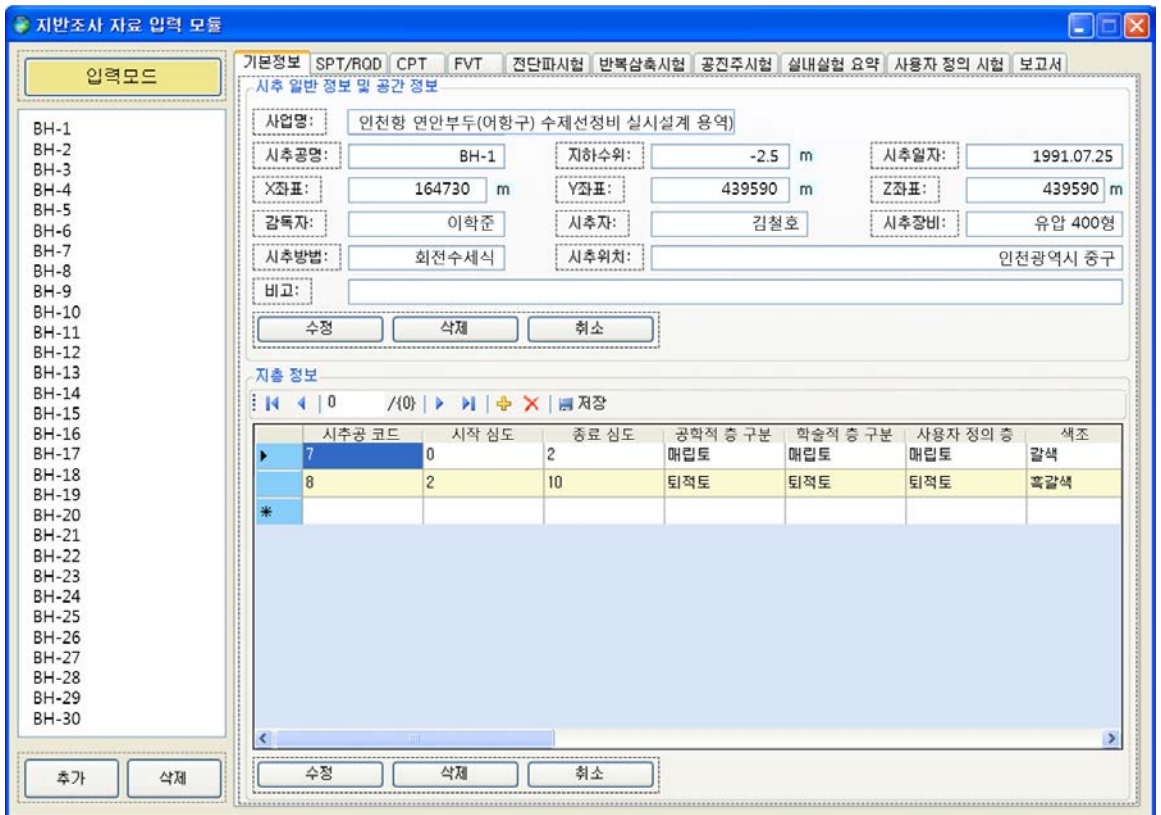


Figure 6.7 Management module of borehole information

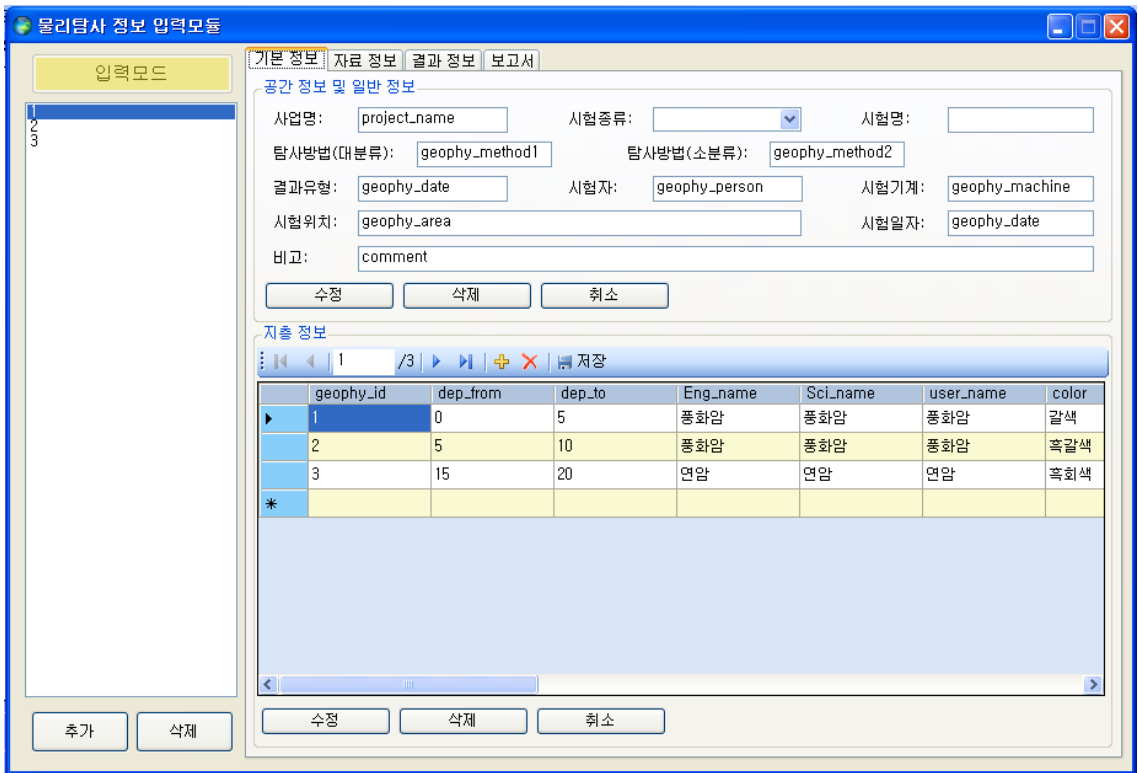


Figure 6.8 Management module of geophysical testing information

Management of structure information

Structure information is stored into the database of integrated system (Figures 6.9 and 6.10). Structure standard data is inputted by using text and image classes, the structure fragility function and design report are automatically transformed to the database.

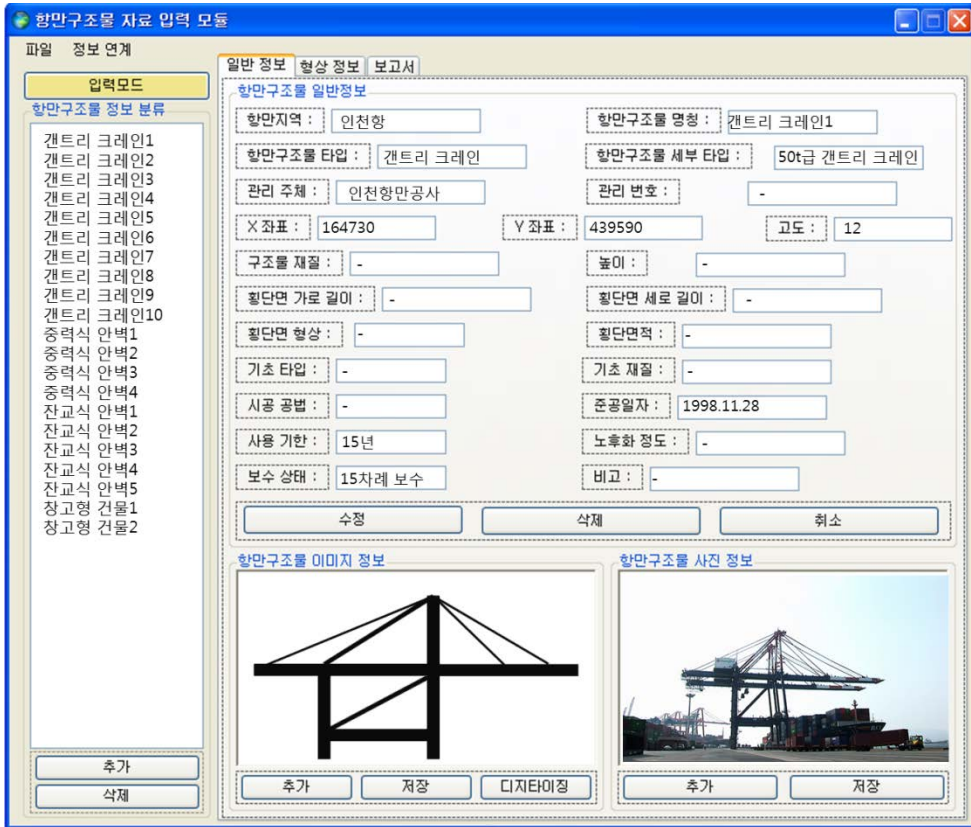


Figure 6.9 Management module of structure information–structure resource information

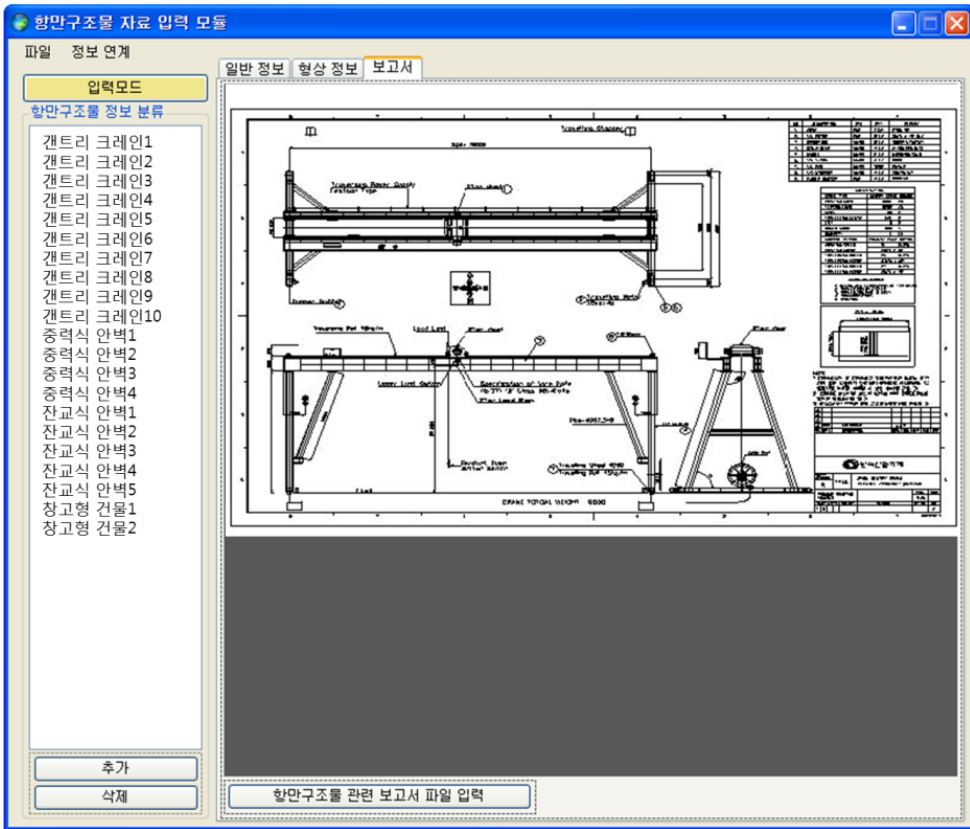


Figure 6.10 Management module of structure information–design report information

Management of seismic monitoring information

All seismic monitoring information is managed in a window format according to sub classes as same as another input modules. Figures 6.11, 6.12 and 6.13 are management screens of seismic monitoring information according to sub classes. Geographic location and types of seismometers for a filed monitoring point are defined in Figure 6.11. The seismic monitoring datasets transmitted from KISS are linked with the nearest accelerometer

located in target site in real-time (Figure 6.12). And the earthquake event information is confirmed as acceleration-time series data and peak rock outcrop acceleration data.



Figure 6.11 Management module of seismic monitoring information–seismological observatory information

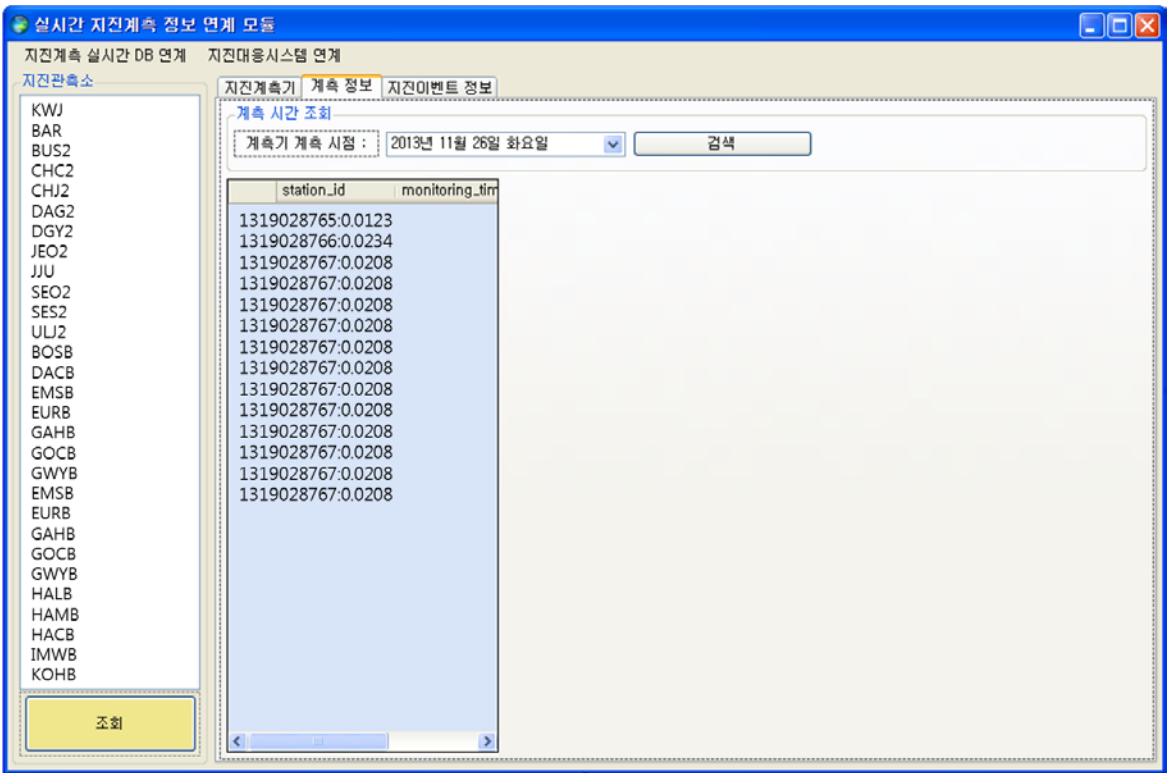


Figure 6.12 Management module of seismic monitoring information–seismic monitoring information

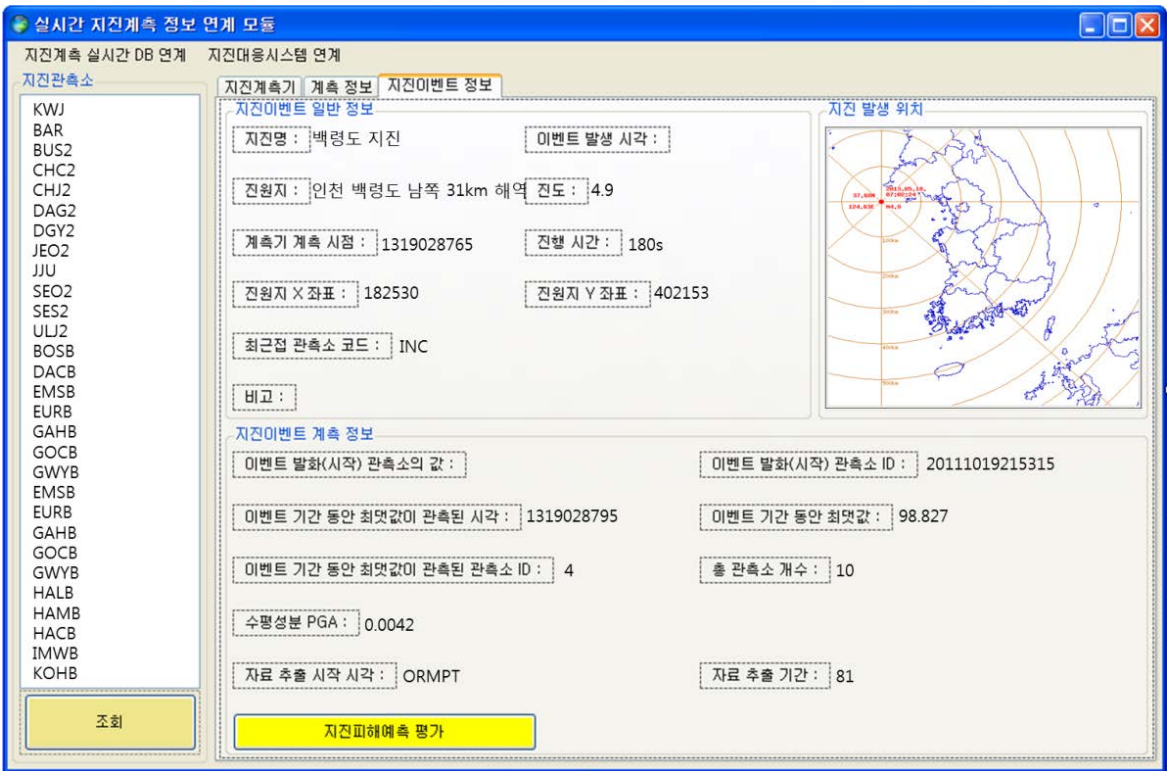


Figure 6.13 Management module of seismic monitoring information–earthquake event information

6.2.3 Geostatistical 3D integration module

A limited number of attribute data is used to determine the reliable continuous geo-layers. A grid model on an attribute value of geotechnical value and earthquake hazard information can provide the spatial distribution of attribute information over a domain graphically, for example, a contour map. Therefore, for effective site-specific geotechnical earthquake hazard

assessment, it is necessary to produce a grid model on the value of interest over a domain from known point values.

As described in Chapter 3, it is known that integration is the best method to produce a grid model from various geotechnical investigation results. Therefore integration is selected as the construction method of geotechnical spatial grid in this system. Geostatistical 3D integration module performs the outlier analysis and geostatistical interpolation to produce an evenly spaced grid of values over a selected domain from the known datasets. Because integration procedure is somewhat complex, it is necessary that users have some knowledge of kriging and variograms. Thus, geostatistical 3D integration module is constructed in a wizard form without knowledge of statistical methods. Also, it is possible to execute integration procedure in detail.

This module can be applied to all attribute information related to their geographic information in the GDB, which are geo-layer data, 3D geotechnical spatial grid, and earthquake hazard assessment results with transmitted seismic monitoring data in real-time, as earthquake events occurred. Figures 6.14 and 6.15 are integration screens according to the order of integration procedure. In the Figure 6.14, the wizard functions for sequential geostatistical integration are arranged. Selection of a domain and gridding of a selected domain for integration are performed. Attribute data for integration is selected. In Figure 6.15, the indicator kriging procedure is performed. After that, the 3D geotechnical spatial grids are determined with selected domain and linked to the database for real-time earthquake hazard assessment module.

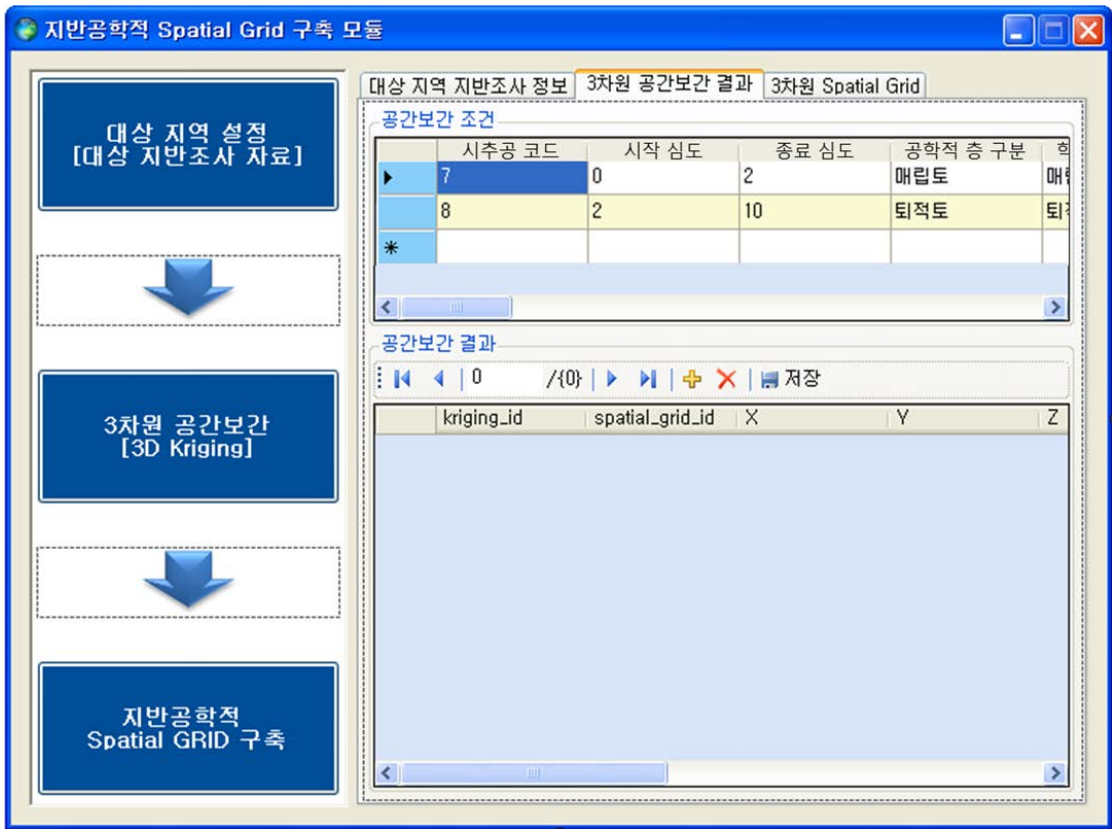


Figure 6.14 Geostatistical 3D integration module—construction of geotechnical spatial grid



Figure 6.15 Geostatistical 3D integration module–indicator kriging

6.2.4 Real-time earthquake hazard assessment module

Even though the earthquake events and earthquake hazards are rapidly occurred at wide region, site-specific earthquake hazard assessment, which is established by considering the reliable seismic load, liquefaction severity, and structure fragility based on geotechnical spatial grid. In Chapter 5, the theoretical procedures are proposed. And these methods are not simply

applied at various site conditions, as providing possible earthquake hazard in every instance. Therefore the wizard functions for sequential real-time earthquake hazard assessment are developed in the integrated system, as shown in Figure 6.16. If the earthquake events are detected and the seismic monitoring data can be transformed in real-time, the determination of seismic load, liquefaction hazard estimation, and structure fragility evaluation are automatically forecast in real-time. And wizard functions upon three procedures were arranged at left-side of window forms (Figure 6.17, 6.18, 6.19).

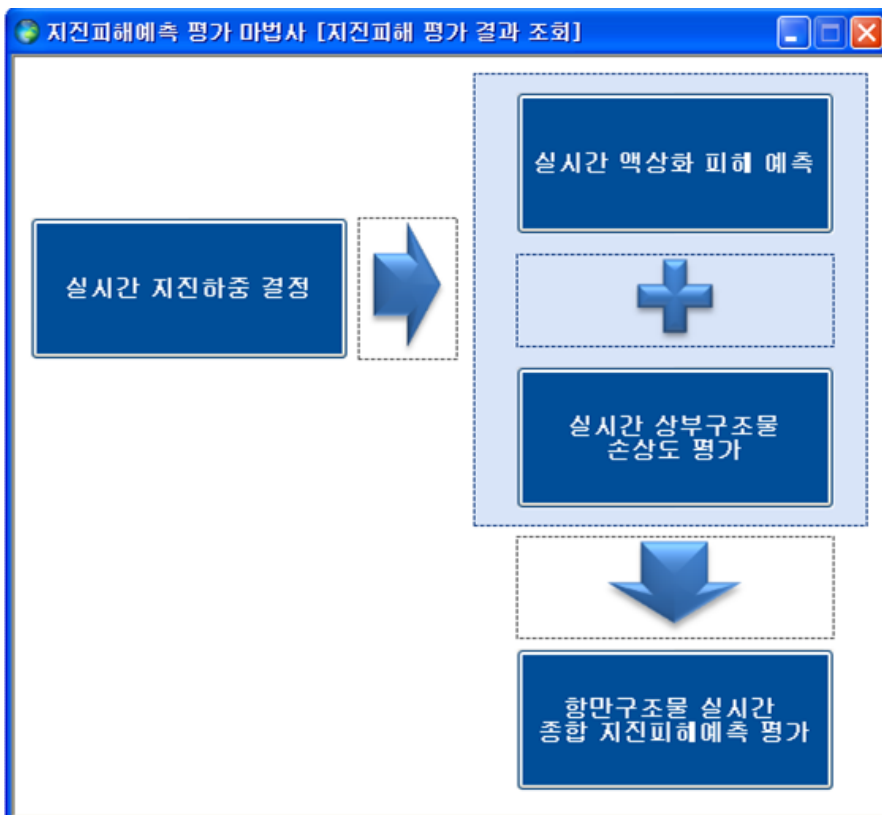


Figure 6.16 Automated real-time earthquake hazard assessment wizard module

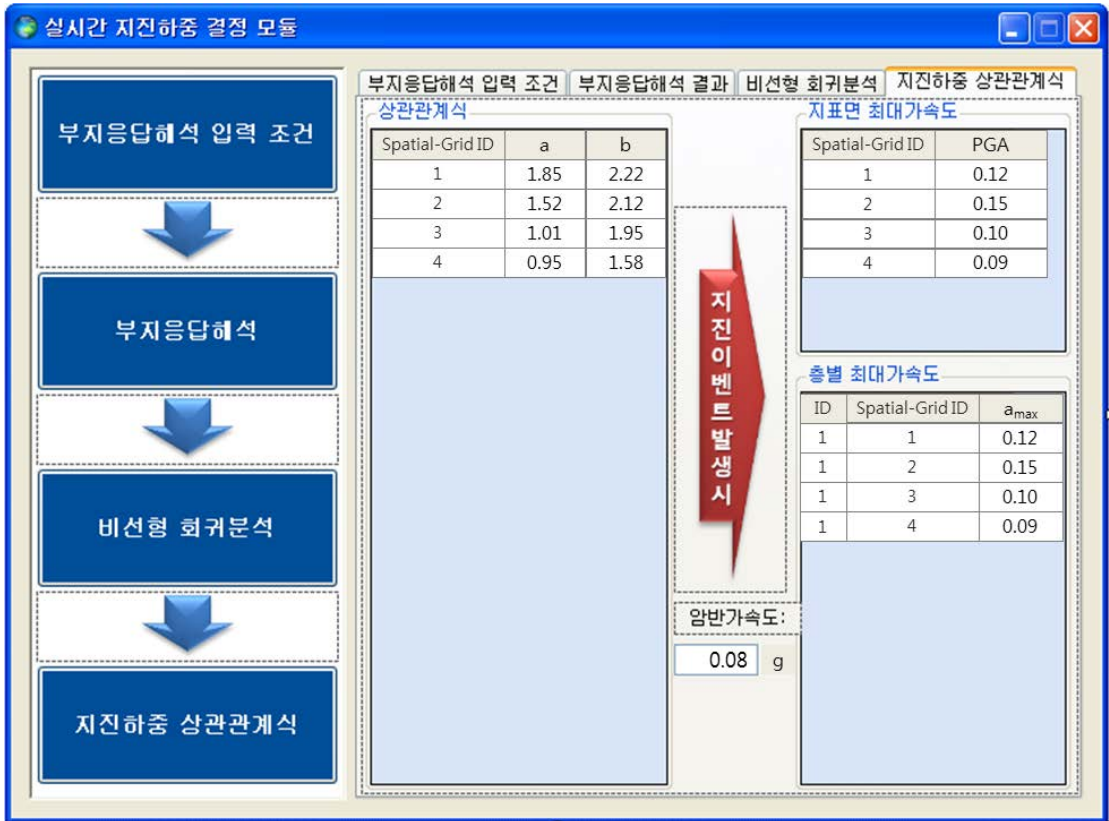


Figure 6.17 Real-time seismic load determination module



Figure 6.18 Real-time liquefaction hazard estimation module



Figure 6.19 Real-time structure fragility evaluation module

6.2.5 Output and visualization modules

Output and 3D visualization modules

Users want to see desired information in the GDB in user-friendly and functional manner. The output of attribute information, which are provided by GUI (Graphic User Interface), can be displayed in a tabular form and graphic form (ex. Graphs, 2D plan views and 2D sectional views). Tabular forms are

generally used to input, edit and view information in the GDB, and graphic forms provide intuitive views of the (Spatial) relationship between attributive information.

Output module displays all attribute information in the GDB by using tables and graphics according to its characteristics and data structures. Also, output module, that is, tables and graphs have been already shown in previous sections of this Chapter. 3D integration results are displayed in 2D plan views, 3D sectional views and 3D views with field information over a selected domain. 3D visualization module is independent program developed considering application in other GISs. This module is designed based on the amount of background researches on previous commercial GIS software such as ArcGIS, GDM, Suffer, EVS, Eardas Imagine, and so on. Also, this module is programmed by a professional programmer based on authors design.

3D visualization module is executed on 3D spatial coordinate system for selecting integrated data, as shown in Figures 6.20 and 6.21, and these views are representative screens of geotechnical spatial grids and real-time basis earthquake hazard results.

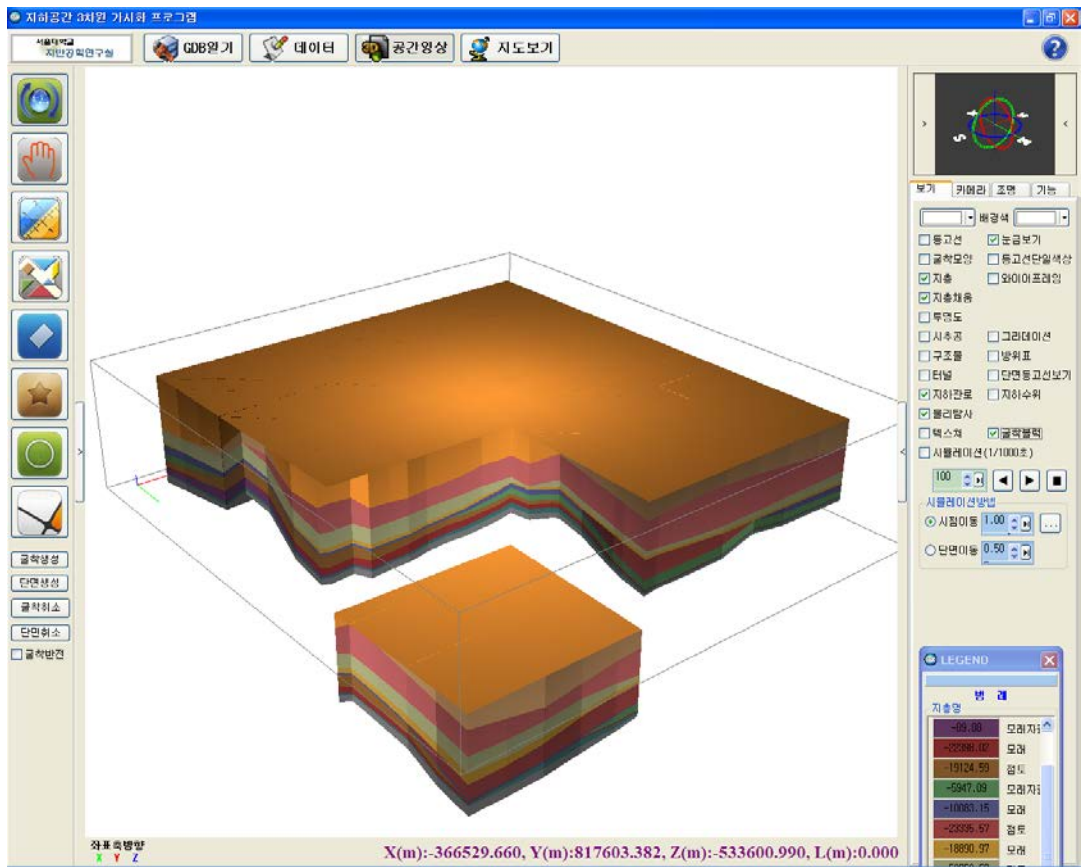


Figure 6.20 3D visualization module—geotechnical spatial grid

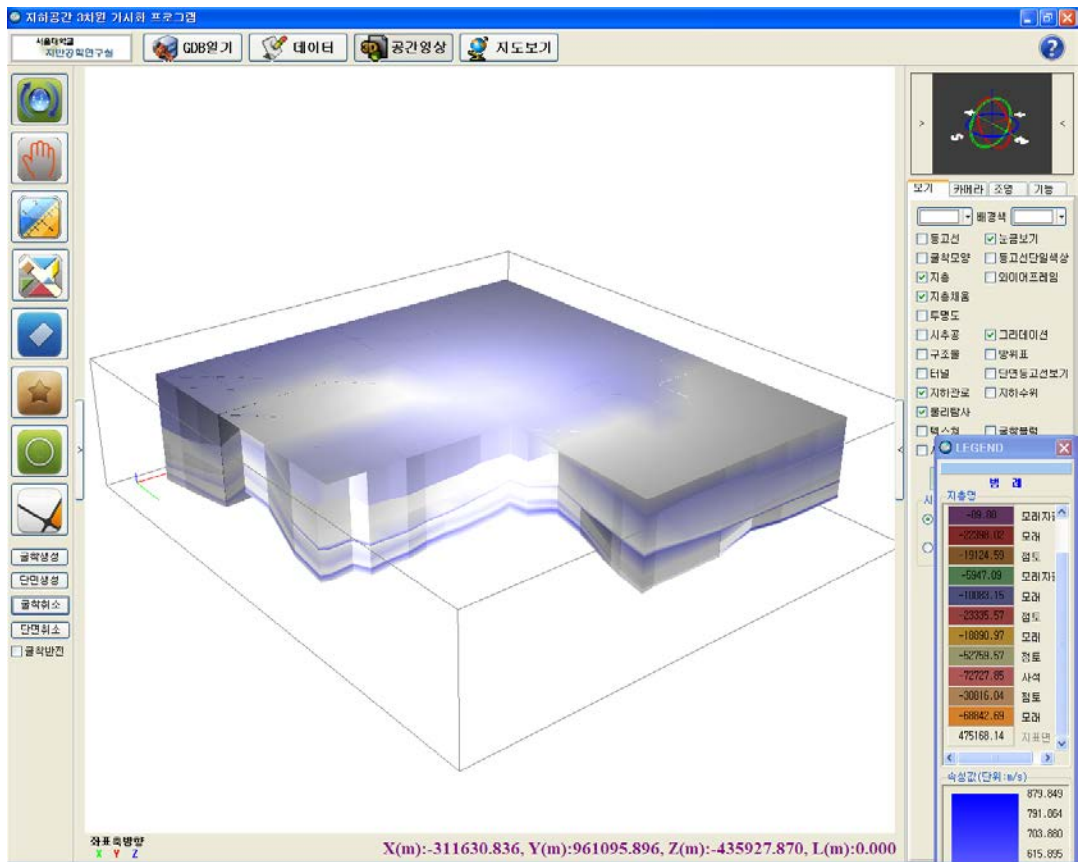


Figure 6.21 3D visualization module– V_S

Real-time earthquake hazard reporting module

Integrated earthquake hazard severity, which is composed on liquefaction severity class and structure fragility class, is forecasted as report type based on the earthquake hazard reporting module, as shown in Figure 6.22. The report contains condition of target site, earthquake events, and predicted damage susceptibility. Furthermore, 2D and 3D sequential hazard zones were expressed as contours or grid patterns on location maps to provide more

reliable liquefaction severity data. Therefore the end-user of the integrated system can be alarmed the earthquake hazard and provided the decision-making report for earthquake risk management in real-time.

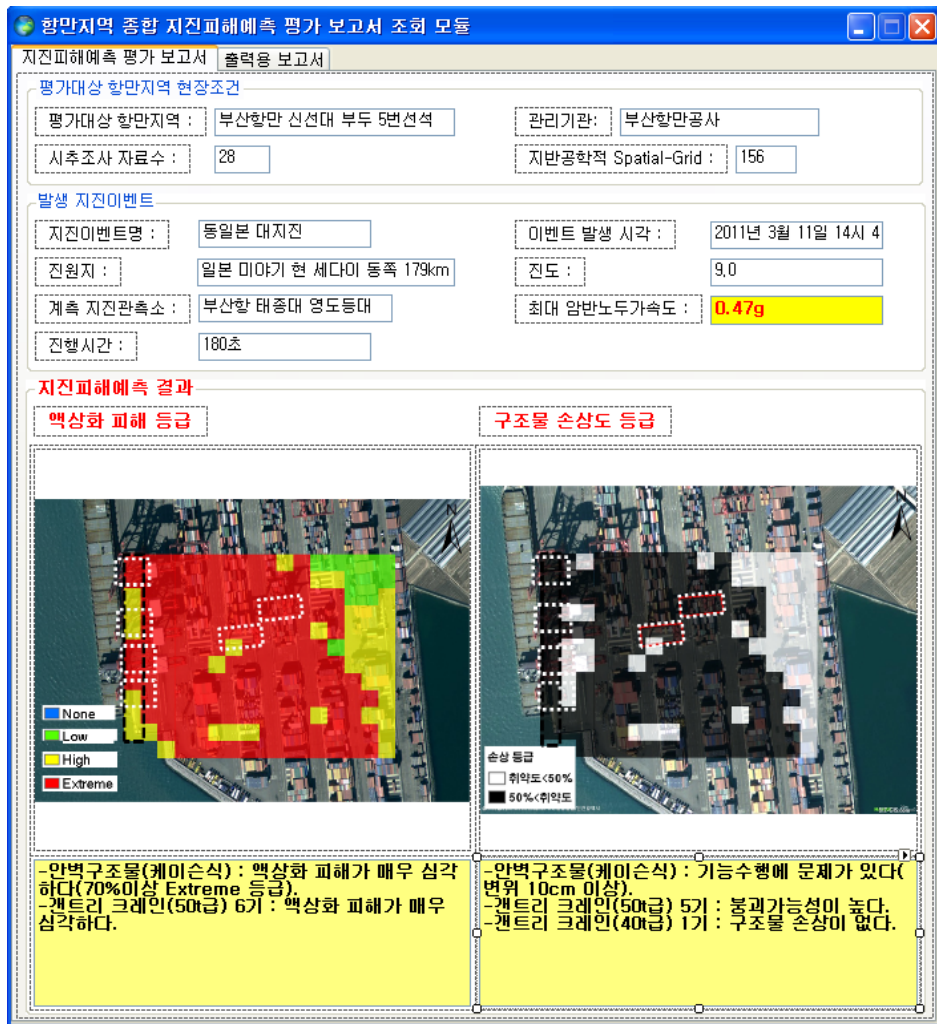


Figure 6.22 Real-time earthquake hazard reporting module

6.3 Summary and Conclusions

The integrated system consists of a DB (Database) and systematic modules. The sub-modules execute various functions on managing and utilizing information in the database with connection to the database; input of data, geostatistical 3D integrated data based on input data, real-time earthquake hazard data, and output of data.

- 1) DB (Database): It stores not only geography, geotechnical investigation, structure, and seismic monitoring data but also geostatistical 3D integration results and real-time earthquake hazard assessment results.
- 2) Input Function: Input function provides an effective way to store and arrange all collected field data and analysis data, according to a standard data format based on geodatabase (GDB).
- 3) Geostatistical 3D integration for geotechnical spatial grid function: This method has three functional modules with the database: Outlier detection method, geostatistical integration method, and construction method of geotechnical spatial grid.
- 4) Real-time earthquake hazard assessment function: The real-time framework has three functional modules with the database: real-time seismic load determination, real-time liquefaction hazard estimation, and real-time structure fragility evaluation.
- 5) Output Function: The output function displays all attributive information in the database by using tables and graphics according to

its characteristics either, on screen or as a document. The earthquake hazard can be visualized and forecasted as 2D or 3D maps overlain by satellite images in real-time.

The database and these modules of the system software were combined integrated in single system and the developed system provides a familiar and user-friendly working environment with a standard interface. And the integrated system is imbedded into KISS server for real-time linking of seismic accelerations. It is potentially useful for stabilizing work to prevent secondary disasters and immediate restoration of the transportation lifelines to improve the accessibility of relevant areas by simulation of the developed system.

7. Application and Verification of System

7.1 Simulation Condition

In this dissertation, to validate the applicability and effectiveness of the integrated earthquake hazard assessment system with geotechnical spatial grid information based on GIS, the systematic field application was performed. The verification testing site is selected port area.

Because international trade and travel have been growing rapidly in recent years, seaports or harbors in coastal areas are increasingly vital to the local and regional sustainability of industries and economies. Further, ports are now being developed into larger areas by reclaiming land from the sea. Port areas that consist of huge facilities, buildings, and yards underlain by various soil deposits have experienced serious disasters from recent earthquakes around the world (Green, 2001). In particular, earthquake-induced liquefaction is a significant threat to manmade structures built on loose and saturated sandy soils (Seo et al., 2012), which are widely distributed in coastal port areas. And the seismic fragility of port structures such as gantry crane and quay wall and so on, which have seismic vulnerability, is not studied and verified.

The integrated earthquake hazard assessment system with geotechnical spatial grid information in real-time basis was applied to the Busan port, Korea, using two virtual earthquake scenarios based on computer-based spatial information to verify the applicability of the proposed framework and

system. Figure 7.1 describes the target area with the real-time transmission of the seismic monitoring data at earthquake event.

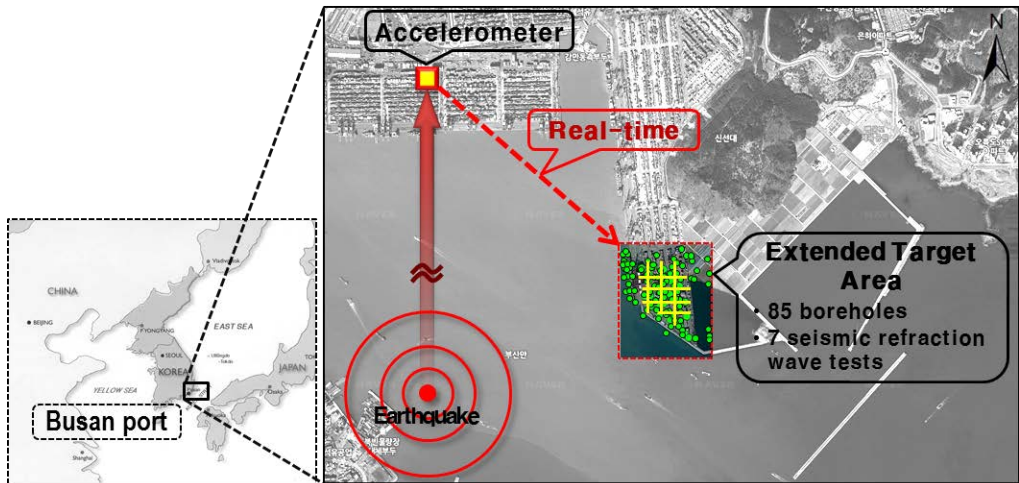


Figure 7.1 Simulation conditions for earthquake scenarios for the Busan port, Korea

In this integrated system, a downhole accelerometer was installed in bedrock at the Busan port, and continuous monitoring of earthquake event has been conducted since 2010. And the accelerometer was imbedded into the KISS server. Unfortunately, as the significant major earthquake events have not been recorded up to now, hypothetical earthquakes were simulated. For the application examples, the 2004 Uljin and the 2011 Tohoku earthquakes were utilized to verify the proposed assessment. For the Uljin earthquake (magnitude 5.2) and the Tohoku earthquake (magnitude 9.0), monitored records at 150 km off from the epicenter were applied. And the input rock outcrop accelerations were respectively determined as 0.08g and 0.37g through the ground motion attenuation relation (Campbell and Bozorgnia,

2003) considering comprehensive trend of ground shakings in Korea. The attenuation equation is represented as

$$\ln a = c_0 + c_1M + c_2 \ln R + c_3R \quad (7.1)$$

where a denotes ground acceleration, M represents the magnitude, R is the epicentral distance, and c_1 , c_2 , and c_3 are attenuation coefficients, respectively. And the waveforms of the two earthquake events are shown in Table 7.1.

Total of 85 borehole datasets and 7 seismic refraction wave test datasets were used for the container terminal area at the Busan port (Figure 7.1). To complementary construct current geo-layer of boring log, 28 current borehole datasets and 57 borehole datasets before earthwork are substituted based on the GIS platform (Table 3.2).

From the design report and a satellite image of the database for the target port, the extended target area (126,000 m²: 300 m west to east × 420 m north to south) included a gravity quay wall and a gantry crane. And the seismic fragility function of these structures was collected. Ground coverage at the Busan port has varied over the last 40 years due to dredging and soil reclamation events (Kim et al., 2012c); thus, the soil conditions have changed over time. The ground coverage conditions for each borehole location based on aerial photographs were described as water later filled by reclamation efforts.

The GWL was determined from the daily average record monitored at a well installed at the Busan port. Fill soils partly cover the extended port area. This soil consisted of mixed materials with reclaimed soil deposits from offshore areas and boulder stone quarried from a nearby mountain. Alluvial soils consist of silty sand or silty clay, which underlie the fill. The underlying

weathered residual soil above weathered rock can be classified as hard sandy materials. Table 7.2 shows typical ground stratification of the target site with classifications of each soil strata. Given these site conditions, the sandy stratum was characterized as a material susceptible to liquefaction, whereas the clayey material was considered to be non-liquefiable (Kim et al., 2012c; Baise et al., 2006). The ground conditions for real-time assessment of the site-specific earthquake hazard do not rely on the soil layer itself, but on the conditions specific to liquefiable soils, such as material properties, and SPT- N value with the GWL.

The integrated earthquake hazard assessment system with geotechnical spatial grid information is imbedded in KISS database server, and linked with the accelerometer server distributed in the entire Korean peninsula. And the above collected various datasets are inputted into the database by using the integrated system program. The field application is applied sequentially in real-time.

Table 7.1 General information and acceleration-time histories for simulation

Earthquake	Magnitude	Date	Station	Acceleration-time history
Uljin	5.2	29 May, 2004	ULJ, Ulsan, Korea	
Tohoku	9.0	11 March, 2011	MYG, Miyagi-oki, Japan	

Table 7.2 Typical ground stratification of the target site with classifications of each soil strata based on the borehole data

Ground stratification	Compositional ordering of USCS	Thickness (m)			Liquefaction susceptibility
		Avg.	Min.	Max.	
Fill soil	SC > CL > GM > SM > SP	10	5	22	Liquefiable layer
Alluvial soil	SM > SP > SC > ML > OL	12	7	28	
Weathered residual soil	SW > GP > GW > GM > GC > OH	8	3	15	Non-liquefiable layer
Soft rock (Bedrock)	-	-	-	-	

7.2 Geotechnical spatial grid

The geotechnical spatial grid was determined considering the site conditions of the target port with regard to the geostatistical 3D integration procedure using the GIS platform, as shown in Figure 7.2. These observation sites were referenced by spatial coordinates determined by the GPS (Sun, 2004; Sun et al, 2008). Because interpolation was expected to produce more reliable spatial predictions than extrapolation, geostatistical integration method was applied to the extended area ($126,000 \text{ m}^2$: 300 m west to east \times 420 m north to south) encompassing the study area ($62,400 \text{ m}^2$: 260 m west to east \times 240 m north to south).

For optimization of borehole datasets, the variogram for the 85 borehole data values was compared with the exponential model; the correlation length without trend effects was found to be 76 m. 87 borehole datasets collected from boring log before and after reclamation were optimized by using outlier detection method. Based on the threshold range of outlier (10%), the 8 boring datasets were excluded from the integration procedure. And geostatistical 3D integration was performed by using optimized 76 borehole datasets and 7 seismic wave tomography datasets (having V_p value). Accordingly, 156 cells (13×12 cells) of the geotechnical spatial grid (covering the ground surface) with constant 20 m intervals were selected for the study area considering the effects of a spatial trend function.

The 3D geotechnical spatial grid classified liquefiable geo-layers and non-liquefiable geo-layers based on basic conditions for the liquefaction-hazard estimation. The geo-layer having liquefaction potential is defined as

porous geomaterial below the ground water level (GWL). The classification of liquefiable geomaterial based on the geostatistical integration using V_p has limitation to identify clear site-specific geomaterial classification criteria with distribution of GWL. In the construction of 3D geotechnical spatial grid for Busan port area, developed system was applied considering the limitation of capability of V_p .

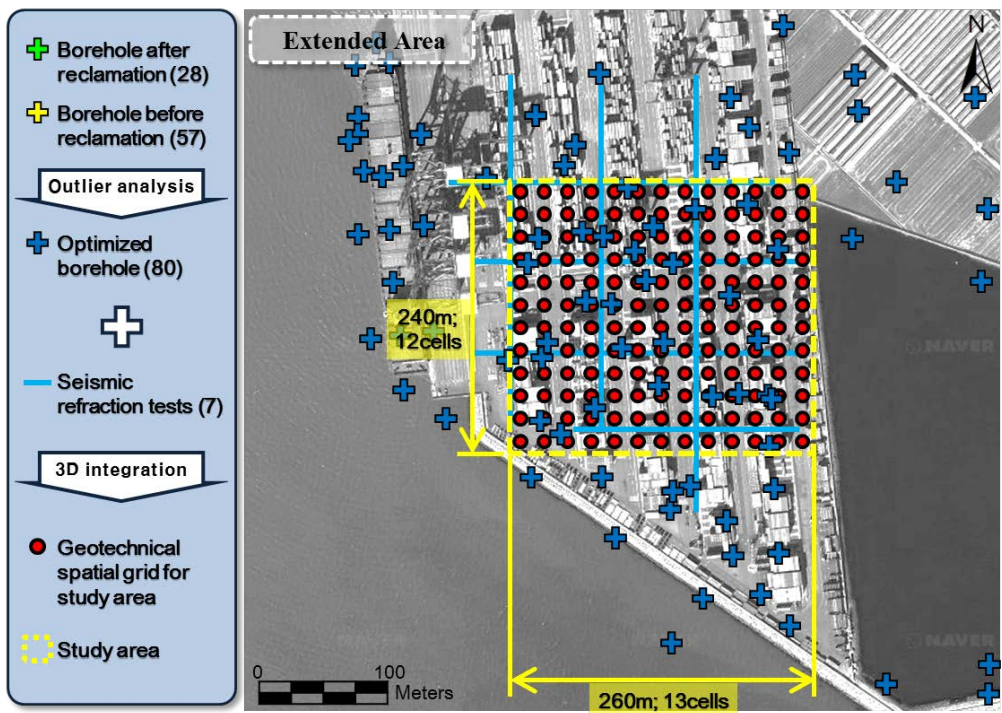
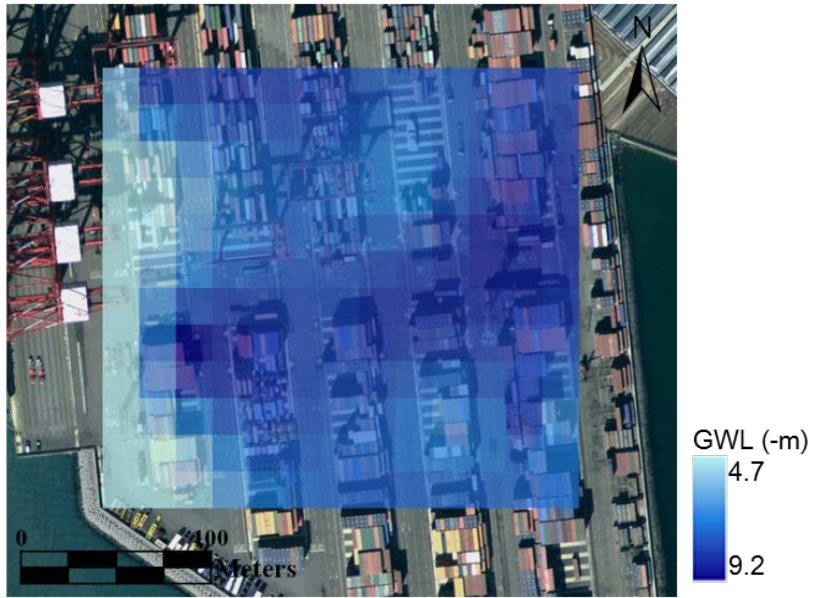


Figure 7.2 Condition of geotechnical spatial grid for the target port. 156 cells (13 × 12 cells) of the geotechnical spatial grid

Based on the geotechnical spatial grid, the assessment results were visualized on a location map to confirm the applicability of the integrated earthquake hazard assessment system with geotechnical spatial grid

information in real-time based on the GIS platform. To confirm the spatial variation of the ground conditions of the study area, Figure 7.3 presents the spatial variation of geotechnical data based on the geotechnical spatial grid, such as the ground water level (GWL), depth to bedrock, soil profile thickness, and liquefiable soil profile thickness (based on the procedure of liquefaction hazard estimation). The GWL affects the liquefiable soil condition and computation of effective stress for the saturated layer. The GWL obtained from boring logs was calibrated based on the daily average highest GWL monitored from the nearby annual GWL records and interpolated on the geotechnical spatial grid. On the whole, the GWL was deeper (9.2 m) toward the northeast (or east), and shallower (4.7 m) toward the coastal gravity wall of the southwest (or west) (Figure 7.3(a)).

When evaluating the seismic ground amplification and the corresponding earthquake hazard, the depth to bedrock is a particularly important geotechnical parameter (Toprak and Holzer, 2003; Sun et al., 2008). Regarding the spatial distribution of the depth to bedrock defined as soft rock and total soil profile thickness, the soil was thicker (45 m) and the depth to bedrock was greater (about 55 m) toward the northwest (or west) (Figures 7.3(b) and 7.3(c)). The liquefiable layer was determined based on the liquefiable soil condition from the original soil layers, and was more susceptible to liquefaction during earthquakes toward the coast (Figure 7.3(d)).

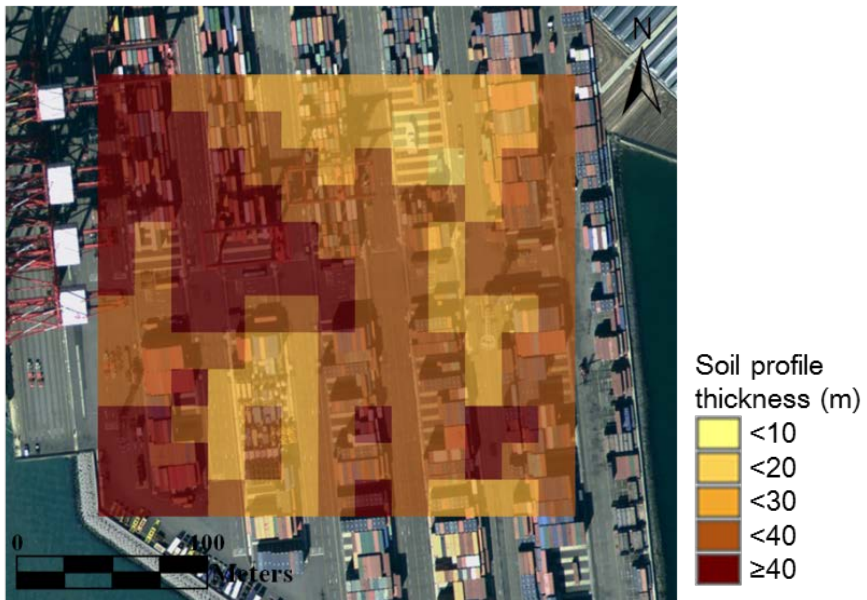


(a) Ground water level (GWL)

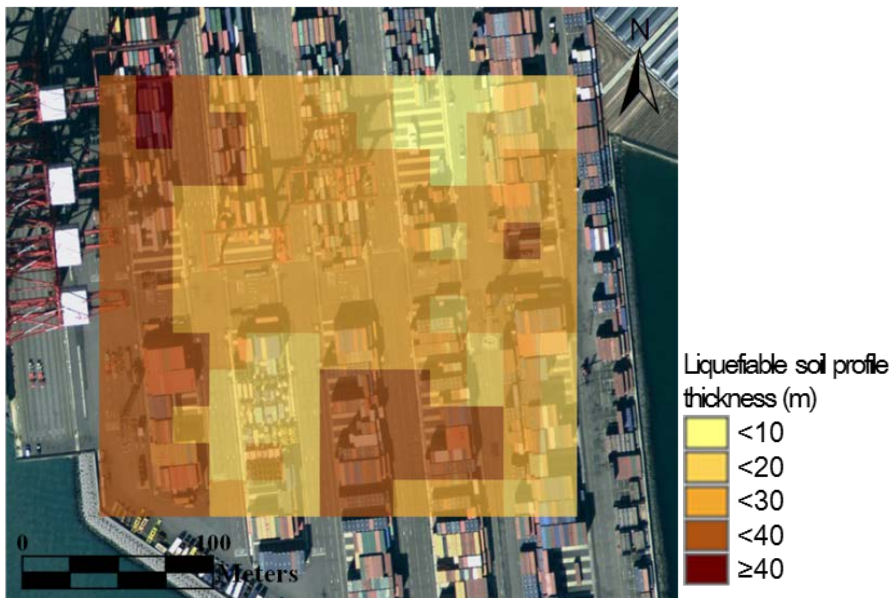


(b) Depth to bedrock

[Continued]



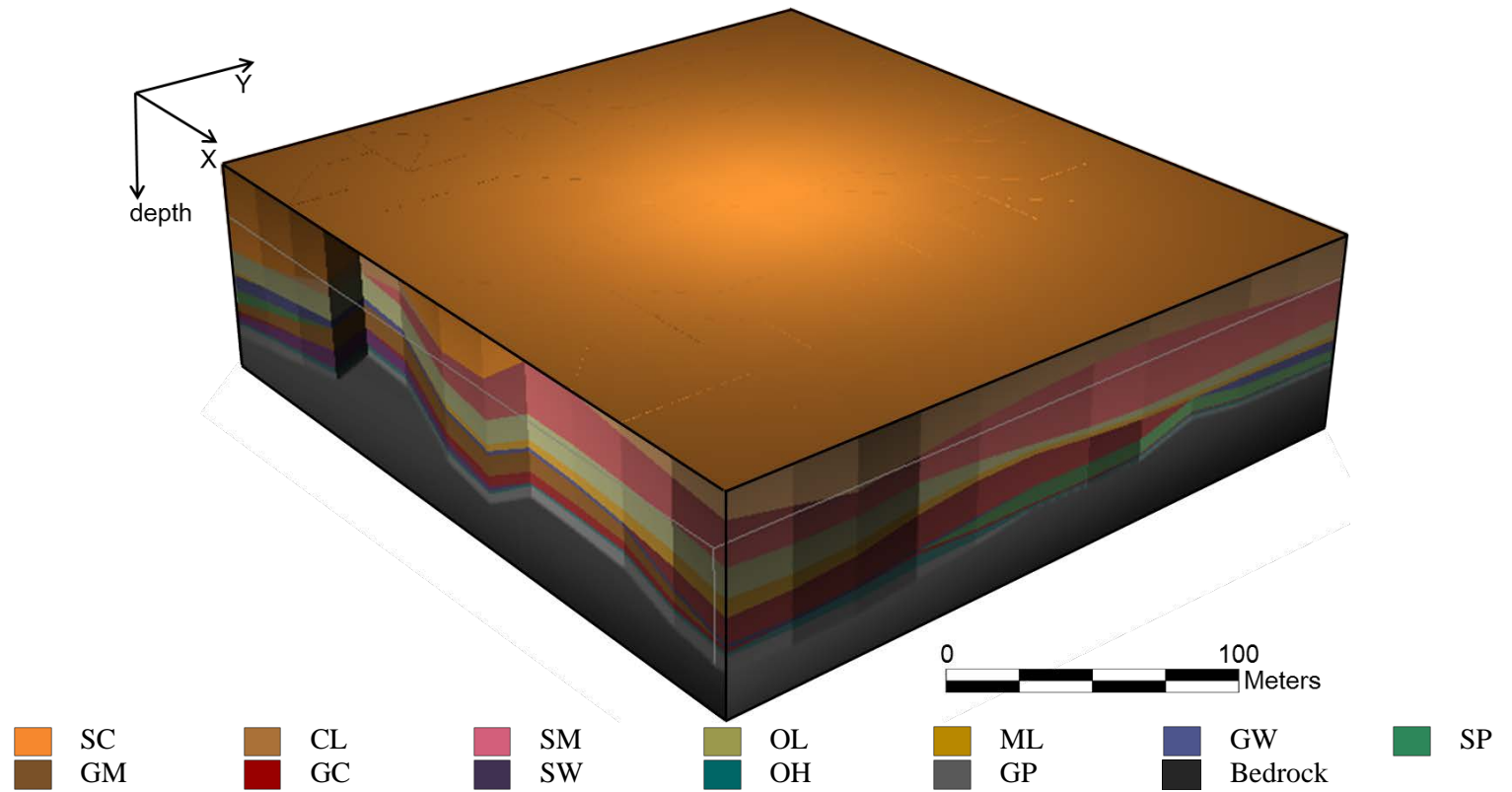
(c) Soil profile thickness



(d) Liquefiable soil profile thickness

Figure 7.3 Two-dimensional spatial distribution of the geotechnical characteristics based on the geotechnical spatial grid for the study area of Busan port

The thickness of the geotechnical layers and the depths to bedrock are usually expressed as contours on corresponding 3D contour maps to provide better realistic ground conditions, as shown Figures 7.4–7.6. In particular, volume cutting of 3D contour maps was applied at the Figure 7.4(b) and Figures 7.5 and 7.6 to confirm the inside view of 3D geotechnical spatial grid (for only soil layers). The 3D spatial distribution of the soil profile containing dynamic properties by soil type was categorized according to the USCS (American Society for Testing and Materials, 1985), and bedrock (such as soft rock, normal rock and hard rock) was classified in accordance with ISRM (International Society for Rock Mechanics, 1981), as shown in Figure 7.4 (a) (Kim et al., 2012d). The soil layers were classified mainly into poorly graded sand (SP) or silty sand (SM). Figure 7.4(b) shows the 3D spatial distribution of the shear wave velocity (V_s) derived from the SPT– N values.



(a) Soil profile classified into 13 soil types based on the Unified Soil Classification System and bedrock
 [Continued]

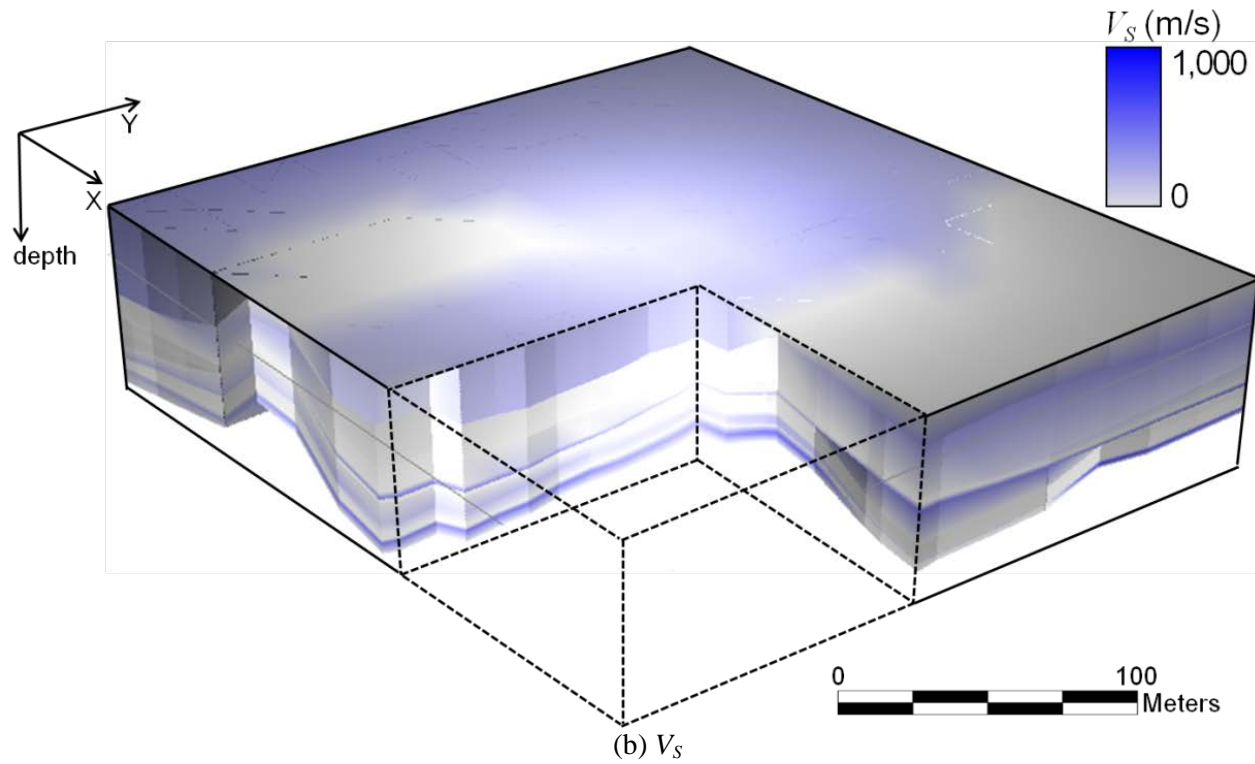


Figure 7.4 Three-dimensional projected figure with cross sectional view for the current ground conditions based on the geotechnical spatial grid in the study area

Consequently, the V_s for the center and northwest zones having thicker soil deposits was generally greater than those for other regions: values generally ranged from about 500 to 750 m/s in the study area. And the normalized shear modulus and damping ratios curves classified by soil type were also included with geotechnical spatial grid according to the representative Korean criteria for site response analysis. The nonlinear curves were adopted based on the criteria: clayey soil from Sun et al. (1988); sandy soil from Seed and Idriss (1970); weathered soil from Sun et al. (2005); rock from Schnabel (1972).

The integrated system was applied for two earthquake scenarios at the study area based on the geotechnical spatial grid for the soil profile. At the Figures 7.5 and 7.6, application results for the Uljin earthquake scenario were presented. The correlations between the rock outcrop acceleration and maximum acceleration of each layer were determined for every 2,326 cells of geotechnical spatial grid based on the real-time seismic load determination. Accordingly, the maximum accelerations for each layer (a_{max}) were calculated (Figure 7.5).

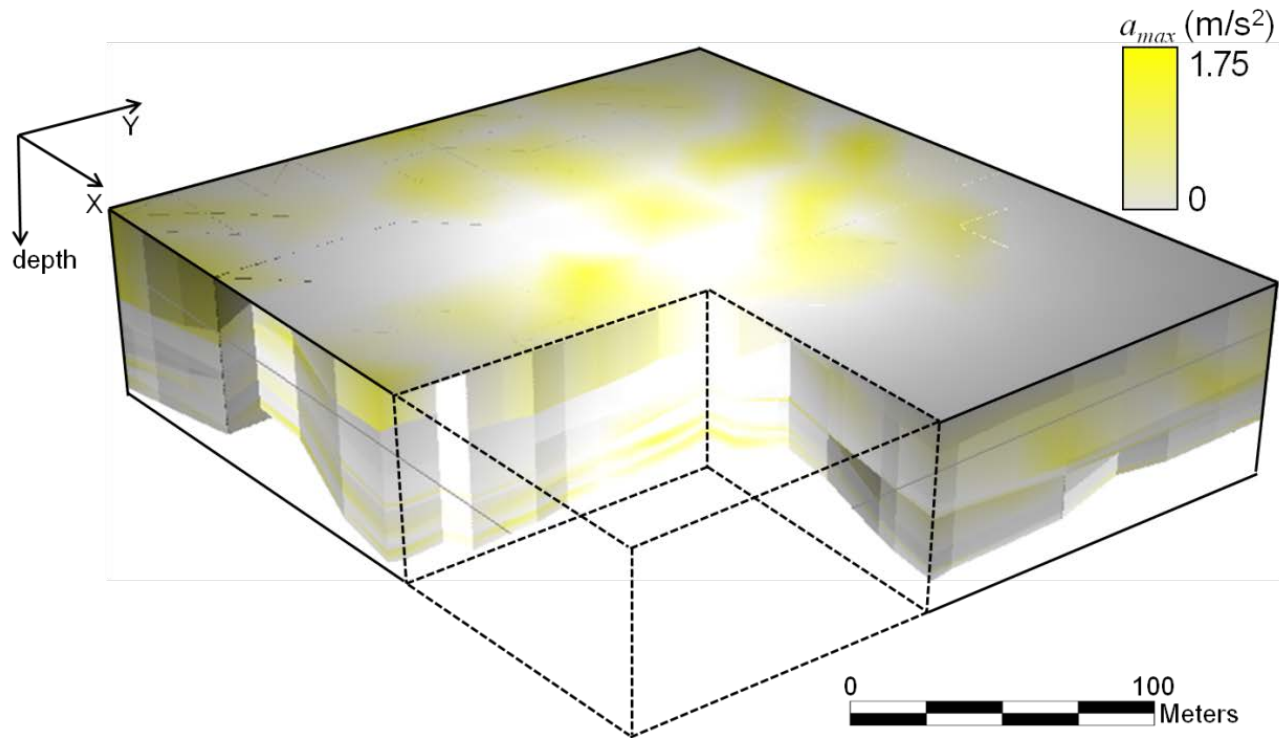
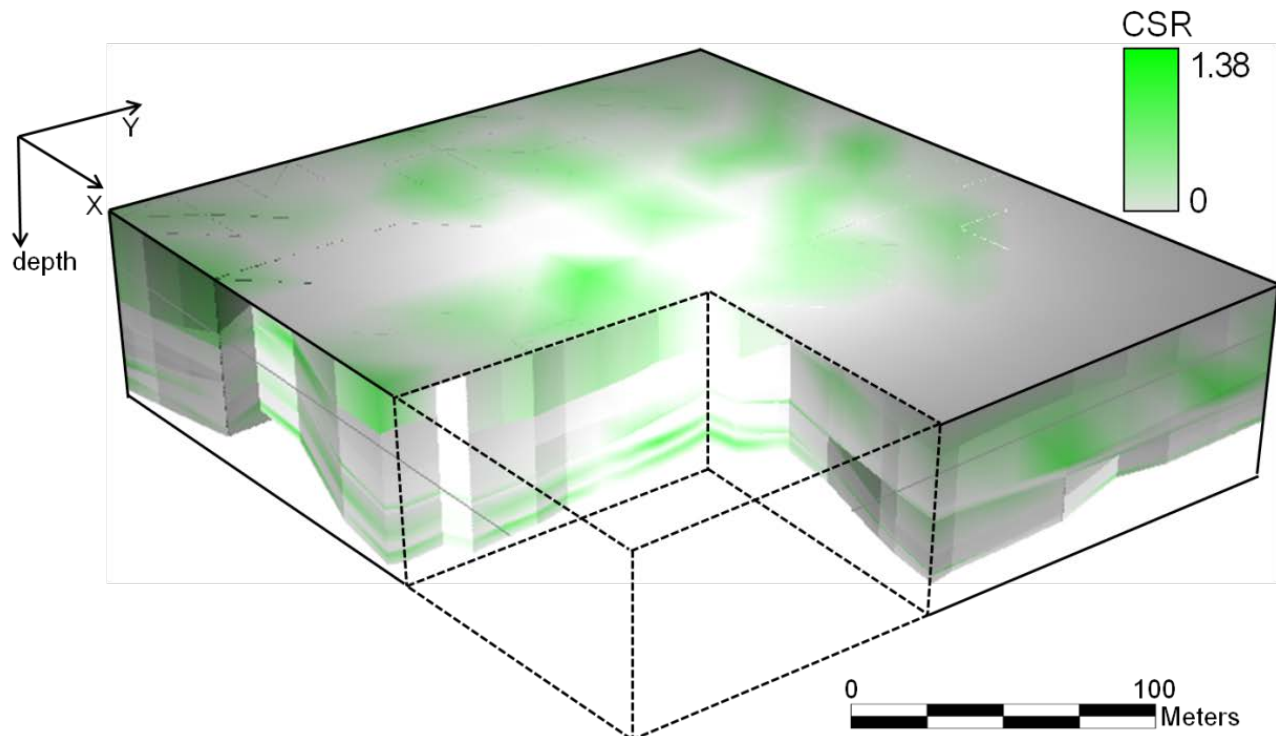
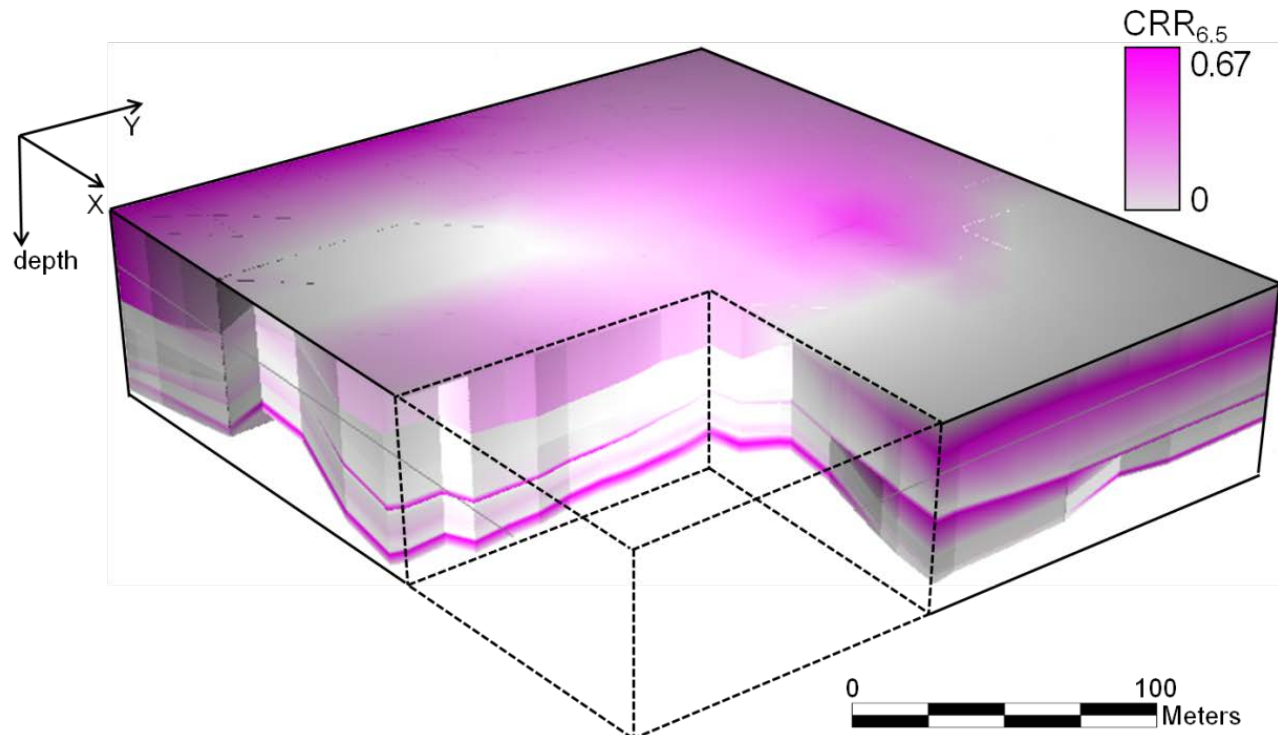


Figure 7.5 Three-dimensional projected figure with cross sectional view for the current ground conditions based on the geotechnical spatial grid combined with the a_{max} calculated based on real-time seismic load correlation equation for the Uljin earthquake scenario in the study area

The CSR for the liquefiable layer was estimated by linking the geotechnical spatial grid for a_{max} (Figure 7.6(a)). Figure 7.6(b) shows the 3D spatial distribution for the $CRR_{6.5}$ computed using the SPT– N values from the geotechnical spatial grid. Therefore, the quantitative $FS_{\text{liquefaction}}$ pertaining to the liquefaction potential of each liquefiable soil layer was analyzed using the geotechnical spatial grid of $CRR_{6.5}$ and CSR, as shown in Figure 7.6(c). For the Uljin earthquake scenario, $FS_{\text{liquefaction}}$ for the entire study area was almost larger than 1. Thus, the geotechnical characteristics and liquefaction parameters resulting from the geotechnical spatial grid for the Uljin earthquake scenario would be less susceptible to a liquefaction hazard than those for the Tohoku earthquake scenario.



(a) CSR
[Continued]



(b) CRR_{6.5}
[Continued]

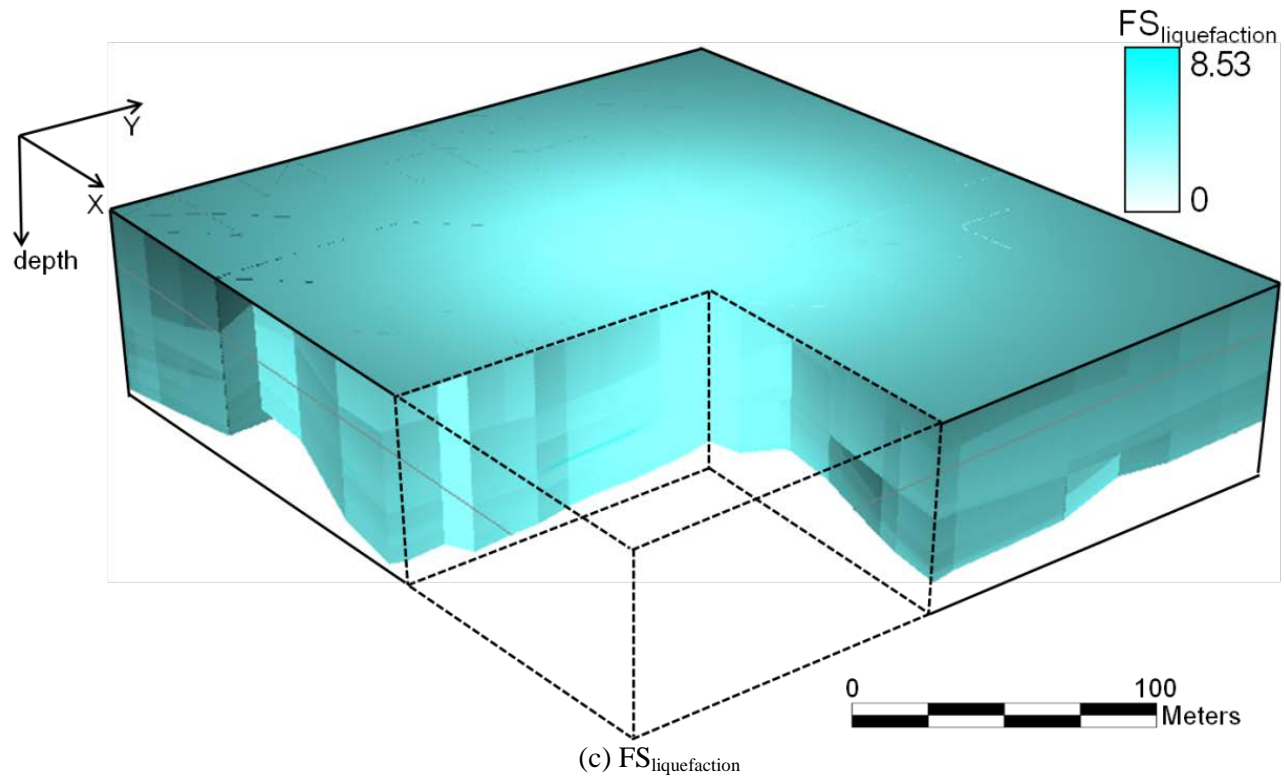
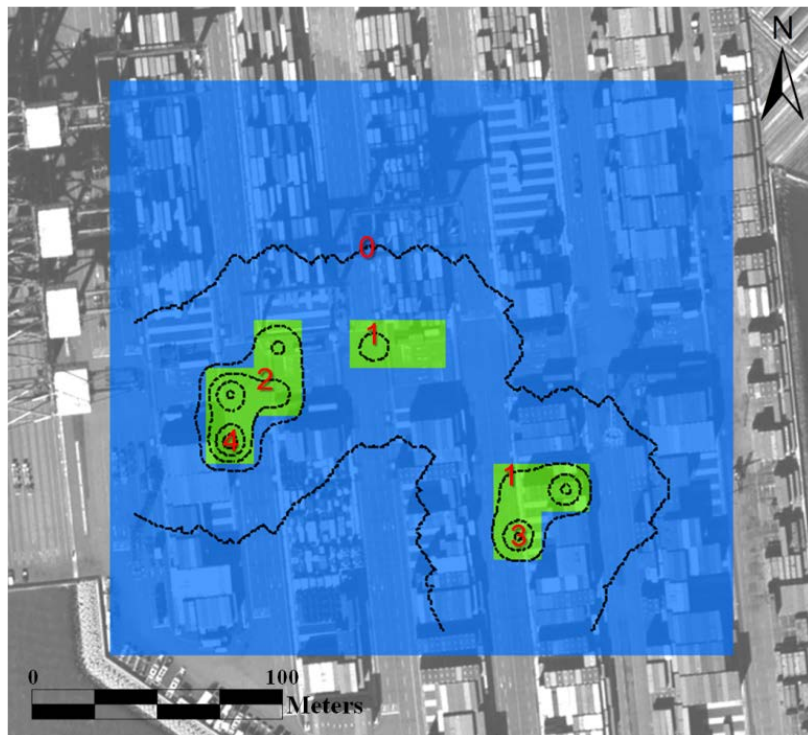


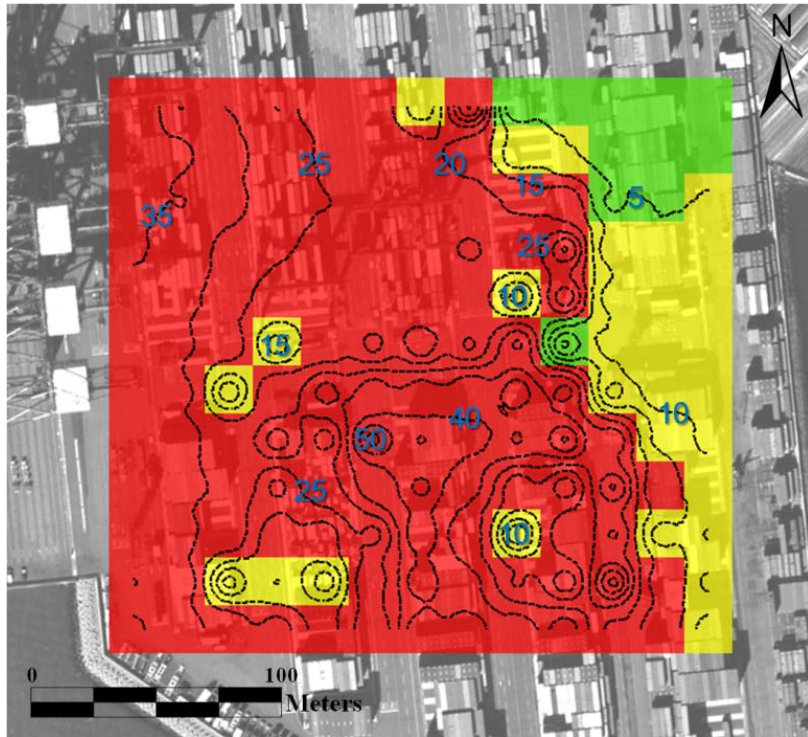
Figure 7.6 Three-dimensional projected figures with cross sectional view for the current ground conditions based on the geotechnical spatial grid combined with the results of real-time liquefaction hazard estimation for the Uljin earthquake scenario in the study area

7.3 Spatial liquefaction hazard

To evaluate the site-specific liquefaction hazard of the study area, quasi-real-time liquefaction hazard estimation was performed for the two earthquake scenarios by integrating the geotechnical spatial grid with soil profiles and correlated seismic load based on the LPI. The liquefaction severity results (visualized as grid zones) were determined for the study area according to the LPI criteria (visualized as dotted contour lines) by compiling the 3D geotechnical spatial grid of $FS_{\text{liquefaction}}$ (Figure 7.7).



(a) The Uljin earthquake
[Continued]



(b) The Tohoku earthquake

(0) (0 < LPI ≤ 5) (5 < LPI ≤ 15) (10 < LPI ≤ 100)

Liquefaction Severity ■ None ■ Low ■ High ■ Extreme

Figure 7.7 Liquefaction severity zonation maps for the target port for two earthquake scenarios

For the Uljin earthquake event, nine cells of the geotechnical spatial grid (which had 156 cells covering the ground surface), on the center region, were classified into the ‘low’ liquefaction severity class, whereas the others belonged to the ‘none’ class. For the 2011 Tohoku earthquake event, the overall study area was ‘extreme’ or ‘high’. The northeast of the study area (with 10 cells covering the ground surface) was regarded as a safe region for the liquefaction hazard, classified as having ‘low’ potential because the topsoil generally consisted of non-liquefiable boulder stone or dredged silty

clay. Consequently, for the Uljin earthquake scenario with relatively low rock outcrop acceleration (0.08g), the central part had a higher probability of a liquefaction hazard than other parts. In comparison, for the Tohoku earthquake scenario with relatively high rock outcrop acceleration (0.37g), the liquefaction hazards were extremely severe for the entire study area except for the northeast or eastern regions.

When an earthquake actually occurs in the port area, the critical classified zonation of the liquefaction hazard will be demonstrated in real-time. Therefore, this newly developed systematic framework can be effectively utilized for the decision-making necessary to provide earthquake risk management and develop optimized evacuation paths and restoration plans for port structures. As a result, it is potentially useful for stabilizing work to prevent secondary disasters and immediate restoration of the transportation lifelines to improve the accessibility of relevant areas by simulation of the developed integrated system. However, more case studies are required to conclude the proposed framework.

7.4 Structure fragility

Based on the real-time structure fragility evaluation module, the fragility function of the gantry crane at study area was determined. The fragility curve was categorized by professional structural engineer based on various seismic numerical analyses, and grouped as representative type of gantry crane. Figure 7.8 shows the seismic fragility curve of 50t-gantry crane which is located in

central zone of study area (Figure 7.9). The damage level is only arranged as *Near collapse*, which means the failure mode by overturn of gantry crane. It is assumed that the seismic failure is confirmed when the probability of *Near collapse* damage level is over 50%.

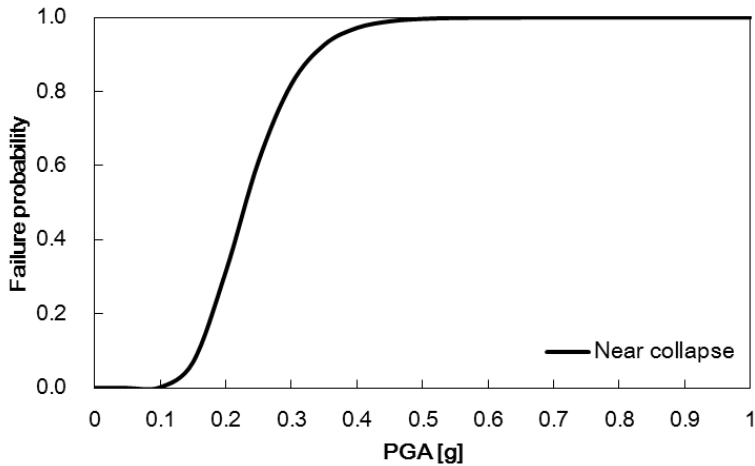
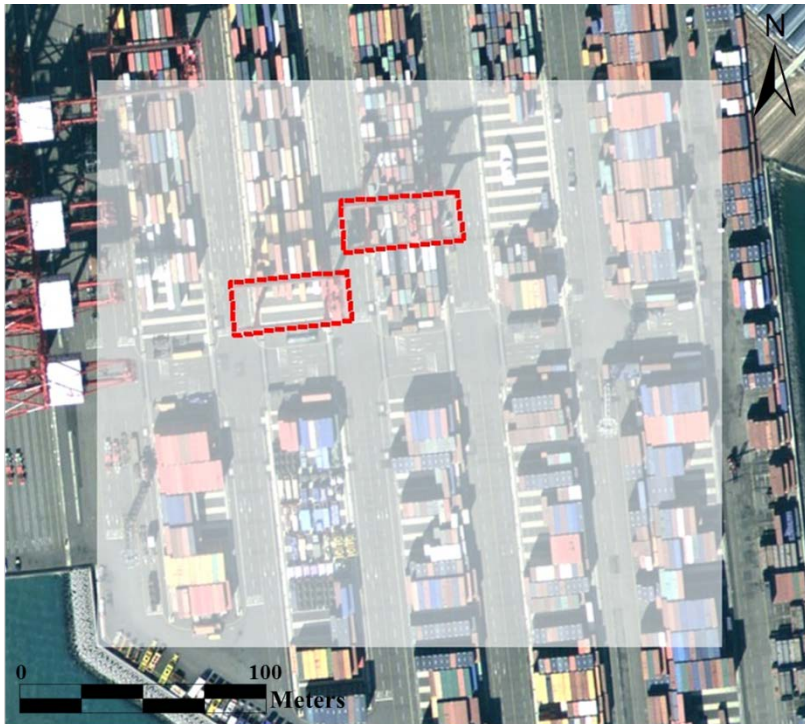


Figure 7.8 An example of seismic fragility curve of 50t-gantry crane modified from KORDI (2013)

Linked with geotechnical spatial grid, which are assigned seismic load correlation equations, the correlated peak ground acceleration (PGA) is determined in real-time. And the failure probability in ‘*Near collapse*’ damage level of gantry crane is calculated by correlated PGA based on geotechnical spatial grid. For the Uljin earthquake event, every cells of the geotechnical spatial grid above geo-layers are evaluated as ‘safe’ of damage state ($0 < \text{Fragility} \leq 50\%$). Therefore, the two-gantry cranes were determined as safe for seismic fragility (Figure 7.9(a)).

Otherwise, for the Tohoku earthquake event, the overall study area (which had 115 cells among 156 cells covering the ground surface) was classified into *failure* damage level. The east of the study area (with 41 cells covering the ground surface) was regarded as a safe region for the structure fragility, classified as having ‘safe’ damage state because the topsoil generally consisted of non-amplifiable boulder stone or dredged silty clay. Therefore, the two-gantry cranes are determined as failure for seismic fragility, because the structure occupied most of the cells evaluated as ‘failure’ damage state (Figure 7.9(b)).



(a) The Ujain earthquake

[Continued]

7.5 Verification Tests of System

7.5.1 Condition of verification tests

The integrated system is installed in seismic monitoring and response system server, which are managed by Korea Institute of Ocean Science and Technology (KIOST), and embedded at Korea Integrated Seismic System (KISS) to manage the seismic risk of major port are in Korea. And continuous monitoring of earthquake event has been conducted since 2010. In 2013 and 2014, the noticeable earthquake events were occurred in waters west of Baengnyeong Island and Taean, and the seismic monitoring datasets were measured from the accelerometers installed at coast pier of Incheon port. At the testing site, two accelerometers are installed to monitor the free-field ground motion (at lock) and structure motion (at passenger terminal) (Figure 7.10).

Therefore, in this dissertation, for verification of the integrated system, the actual earthquake events and monitoring data were applied. The testing site is partial area of coast pier of Incheon, and 12 borehole datasets are stored into the system database. And the distance from accelerometer to extended target area is 0.7 km, and the attenuation effect is negligible. Figure 7.10 shows the verification tests condition for earthquake scenarios.

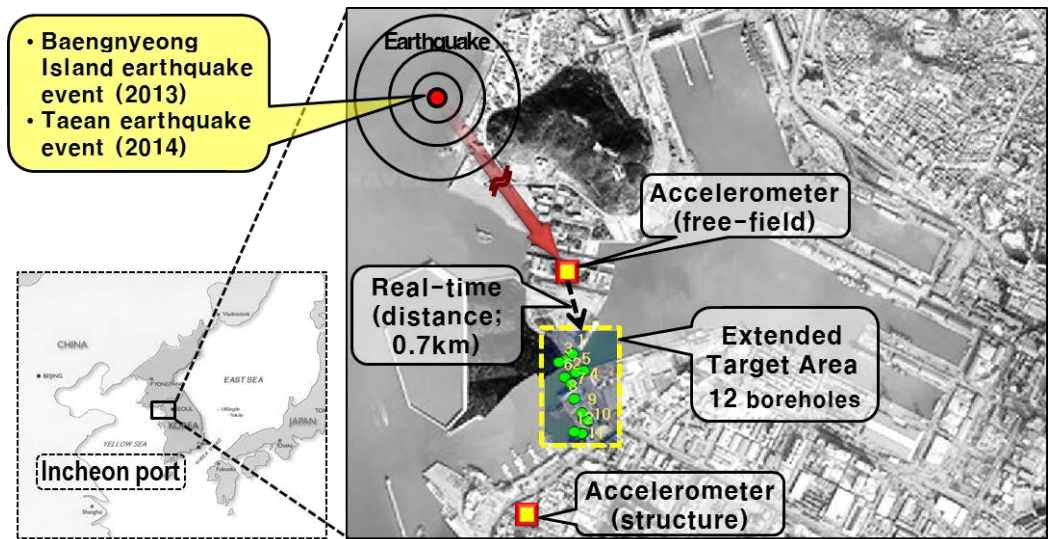
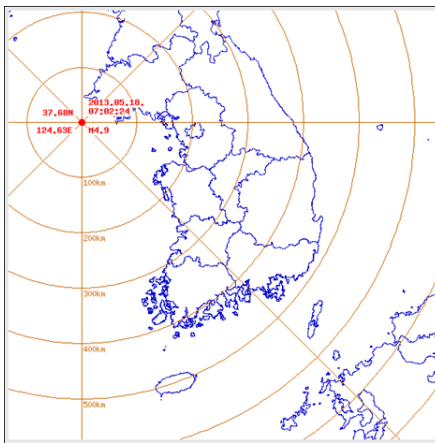


Figure 7.10 Verification tests conditions for earthquake scenarios for the Incheon port, Korea

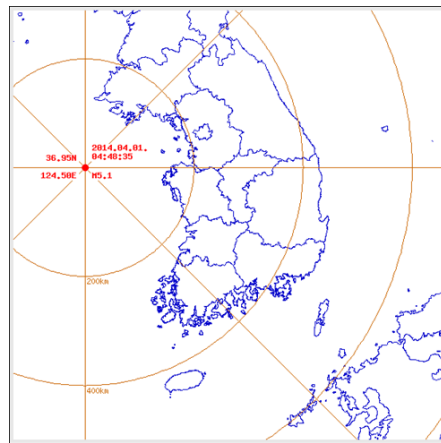
The condition of earthquake events for verification tests is obtained from Korea Meteorological Administration (Table 7.3 and Figure 7.11). The magnitude of Baengnyeong Island earthquake event is 4.9 and the epicenter is located in waters west of Incheon port (distance; about 41km). The magnitude of Taeon earthquake event is 5.1 and the epicenter is located in waters west of Incheon port (distance; about 141km). The Baengnyeong Island earthquake event and Taeon earthquake event are 5th and 4th largest magnitude since seismic monitoring in Korea (1978).

Table 7.3 Earthquake events information and measured results (Reference: Korea Meteorological Administration)

	Baengnyeong Island earthquake event	Tae'an earthquake event
Magnitude	4.9	5.2
Date and Time (KST)	2013.05.18, 07:02:24	2014.04.01, 04:48:35
Location (lat, lon)	37.68, 124.63	36.95, 124.58
a_{rock} (g) at free-field accelerometer	0.0032	0.0035
Acceleration (g) at structure accelerometer	0.0249	0.0255



(a) Baengnyeong Island earthquake event



(b) Tae'an earthquake event

Figure 7.11 Earthquake event map (Reference: Korea Meteorological Administration)

7.5.2 Verification results

Spatial liquefaction hazard

The spatial liquefaction hazards are automatically estimated based on

real-time earthquake hazard estimation module (Chapter. 6.3.6). The actually real-time basis measured and transmitted rock outcrop accelerations are 0.0032g and 0.0035g (Table 7.3). In advance, the geotechnical spatial grids (having 68 cells over surface) were constructed using 12 borehole datasets based on geostatistical 3D integration module. Consequently, near real-time liquefaction hazards were equally estimated using assigned correlated maximum accelerations of each layer, as shown Figure 7.12. The liquefaction severity for entire zone of study area was classified as ‘None’. After the earthquake events, the simple safety test analysis for unreinforced concrete structure at the study area (visualized as dotted red lines at Figure 7.12) concluded that the structure is not affected by liquefaction hazard.

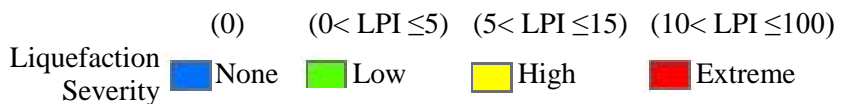
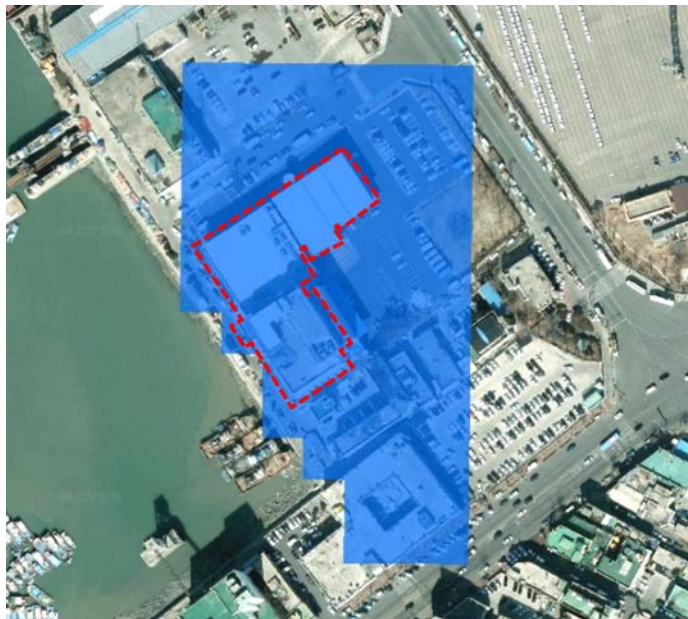


Figure 7.12 Liquefaction severity zonation maps for two earthquake events

Structure fragility

The structure fragilities are automatically estimated based on real-time earthquake hazard estimation module (Chapter. 6.3.6). For unreinforced concrete structure at the study area (visualized as dotted red lines at Figure 7.13), the fragility curve (Figure 7.8) is linked with correlated peak ground accelerations (PGAs) based geotechnical spatial grid. Consequently, the failure probability in *Slight* damage level of unreinforced concrete structure is calculated by correlated PGAs based on geotechnical spatial grid, as shown Figure 7.13. For the two earthquake events, every cells of the geotechnical spatial grid are evaluated as 'safe' of damage state ($0 < \text{Fragility} \leq 50\%$). Therefore, the target structure was determined as safe for seismic fragility. The simple safety test analysis for the target structure concluded that the structure is not affected by structure failure.



($0 < \text{Fragility} \leq 50\%$)

($50\% < \text{Fragility} \leq 100$)

Damage class □ Safe

■ Failure (overturn)

Figure 7.13 Structure fragility zonation maps of *Slight* damage level for the two earthquake events

7.6 Summary and Conclusions

Integrated earthquake hazard assessment system with geotechnical spatial grid information based on GIS was developed to consider local site response characteristics in real-time. Within the context of this dissertation, the developed system has been specifically applied to the Busan port, Korea, using two virtual earthquake scenarios based on the GIS platform.

- 1) The simulation results were visualized as a geotechnical earthquake hazard map to verify the applicability of the computer-aided real-time assessment framework.
- 2) 2D and 3D sequential hazard zones were expressed as contours or grid patterns on location maps based on geotechnical spatial grid to provide more reliable liquefaction severity and structure fragility data.
- 3) The verification test for the integrated system was also performed for Incheon port using actually transmitted from accelerometer of KISS server, when two noticeable earthquake events occurred at nearby Incheon port.
- 4) This systematic application demonstrates that the spatial liquefaction hazard and structure fragility can be determined in real-time to assist with the decision-making required for earthquake risk management in port areas and develop optimized evacuation paths and restoration plans for port structures.

8. Conclusions and Recommendations

8.1 Conclusions

In this study, an integrated earthquake hazard assessment system with geotechnical spatial grid information was developed based on GIS, and the applicability and effectiveness of the developed system for prediction reliable earthquake hazard in near real-time were verified with field simulation. In addition, the real time framework for earthquake hazard assessment (composed of geostatistical 3D integration and real-time earthquake hazard assessment) was suggested and its applicability was also verified.

The developed system built within the frame of GIS, consists of the database containing all site information and processed data in the system according to the standard data formats (database schema), and the system software performing various functions to manage and utilize the data in the database. The system software is divided into input module, geostatistical 3D integration module, real-time earthquake hazard assessment module, and output or visualization module, functionally. The characteristics of the developed system can be summarized as follows.

- 1) All information collected from the site and processed in the system is categorized and standardized in relation to the spatial information based on geodatabase. According to standard data formats, the database was designed and the input module was developed.

Standard data formats encompass site information including geographic information, geotechnical information, structure information, and seismic monitoring information transmitted from accelerometers in real-time and processed information including 3D geotechnical information and geotechnical earthquake hazards. Due to standardization of all site information, the integrated system can manage all site information in various geotechnical applications. Moreover, real-time basis seismic monitoring system and spatial earthquake hazard prediction can be possible by implementing a unique analysis procedure in this stand-alone system.

- 2) Input and output of all site information were designed in consideration of data structures of the existing documents and standard data formats.
- 3) Geostatistical 3D integration method integrates the boring data and the geophysical testing results to offer the appropriate geophysical values, which are derived site-specifically to classify the local geomaterials. The boring data are optimized by removing the relatively outlying data points to reduce the uncertainty with proposed outlier detection methods. And also indicator kriging is utilized to construct the three-dimensional stratified geo-layers using the optimized borehole data and the geophysical profiles. The locally integrated geomaterial classification criteria are more proper stratification results compared to the conventional classification criteria.
- 4) A systematic real-time assessment of the geotechnical earthquake

hazard was developed to consider local site response characteristics for target areas. According to the framework, three interrelated assessment procedures were incorporated in a database on a real-time basis: real-time seismic load determination, real-time liquefaction hazard estimation, and real-time structure fragility evaluation. The liquefaction severity class and structure fragility class are forecasted and visualized in satellite map images or digital map in real-time based on the GIS platform. Therefore the integrated earthquake hazard of the target structure is determined considering the liquefaction and fragility grade.

- 5) The integrated framework consists of a database and systematic modules. The sub-modules execute various functions on managing and utilizing information with connection to the database. The framework including all these functions focuses on user-friendliness and real-time applications. Thus it is possible to rapidly understand the inherent geotechnical seismic failure on target site, which are invisible to the naked eye. Through simulation of the developed systematic framework, it is potentially useful for stabilizing work to prevent secondary disasters and immediate rehabilitation of the transportation lifelines to improve the accessibility of relevant areas. For this reason, this newly developed systematic framework can be effectively utilized for the decision-making necessary to provide earthquake risk management and develop optimized evacuation paths and restoration plans for target structures.
- 6) These functions to manage, utilize and analyze the data in the

database were integrated into the system software. The developed system was complete by interconnecting the database and the system software with internet connection, and it supports multi-user application and user-friendly operation.

- 7) The developed system has been specifically applied to the Busan port, Korea, using two virtual earthquake scenarios based on the GIS platform. The simulation results were visualized as a geotechnical earthquake hazard map to verify the applicability of the computer-aided real-time assessment framework. Furthermore, 2D and 3D sequential hazard zones were expressed as contours or grid patterns on location maps based on geotechnical spatial grid to provide more reliable liquefaction severity and structure fragility data. And the verification test for the integrated system was also performed for Incheon port using actually transmitted from accelerometer of KISS server, when two noticeable earthquake events occurred at nearby Incheon port.

The integrated earthquake hazard assessment system with geotechnical spatial grid information based GIS was imbedded in KISS server for real-time linking of seismic accelerations, and utilized for port structure in major port (Incheon and Busan ports, Korea). It is potentially useful for stabilizing work to prevent secondary disasters and immediate restoration of the transportation lifelines to improve the accessibility of relevant areas by simulation of the developed system.

8.2 Recommendations

In this study, an integrated earthquake hazard assessment system with geotechnical spatial grid information based on GIS was developed reliably with the geostatistical 3D integration and real-time earthquake hazard assessment considering site-specific site response characteristics for prediction of spatial seismic damage in near real-time. And the applicability and effectiveness of the developed system in seismic risk management were confirmed from systematic field simulation of port site. The further researches are recommended to supplement the developed system.

- 1) The outlier threshold having relatively least reliable data points was determined with 10% of entire borehole. To determine the appropriate site-specific outlier threshold considering spatial correlation of borehole datasets, multivariate outlier analysis and can be performed as a follow-up study. And validation test of geostatistical 3D integration using optimized borehole datasets (excluded outliers) is possible based on various case studies.
- 2) There are analysis errors under the high strain levels due to non-linear soil behavior, because the 1D site response analysis performed to determine the seismic load correlation equation. It is well-known that the equivalent viscos-elastic approach implemented in ProShake to perform site response analyses: 1) it is not capable of representing changes in soil stiffness and hysteretic damping during the

earthquake motion; 2) it is a 1D total stress approach; 3) it is not suitable for wave propagation problems involving high strain levels associated with highly non-linear soil behavior. And there may be analysis errors under the high strain levels due to nonlinear soil behavior and limitations of only three input earthquake motions with restricted frequency contents. A follow-up study will be conducted based on sophisticated site response analyses using many input motions with various predominant frequencies in domain of 1D as well as of 2D or 3D.

- 3) In the simplified seismic load correlations, the ratio of fundamental site period to predominant excitation period has potential effect on computed a_{max} . To consider the effect of non-linear value of the site period, Papadimitriou et al. (2009) computed the peak ground acceleration from empirical relationships. In this study, the correlations between predominant excitation period and fundamental site period were almost complied with linear relationship because of the low local variability of geo-layer such as bedrock depth in small reclaimed region of port. Therefore simplified seismic load correlations assigned into the geotechnical spatial grid can be reasonable to determine the a_{max} , which are unaffected by the effect of site period. However, a follow-up study will be conducted by using various cases of seismic frequency to consider influence of input-motion frequencies.
- 4) The developed system was applied to only few field examples. From the application results, the developed system was improved by

removing bugs and shortages. But because there are various field engineers and field conditions, the developed system must be applied to more field examples. More shortcomings may be detected in these field applications and they can be improved to make a more sound and reliable system.

References

1. AASHTO LRFD Bridge Design Specifications (2007). American Association of State Highway and Transportation Officials, American Association of State Highway and Transportation Officials, New York, 15–25.
2. American Society for Testing and Materials (1985). Classification of Soils for Engineering Purpose, Annual Book of ASTM Standards, 4(8), 395–408.
3. Andrea, A., Salvi, F., Zanchetta, S., Sterlacchini, S., and Guerra, G. (2009). 3D reconstruction of complex geological bodies: Examples from the Alps, *Computers and Geosciences*, 35, 49–69.
4. Andre, Z, and David, I. S. (2003). Impediments to using GIS for real-time disaster decision support, *Computers, Environment and Urban Systems*, 27, 123–141.
5. Anselin, L., Kim, Y. W., and Ibnu, S. (2004). Web-based analytical tools for the exploration of spatial data. *Journal of Geographical Systems*, 6, 197–218.
6. Asaoka, A., and A-Grivas, D. (1982). Spatial variability of the undrained strength of clays, *Journal of Geotechnical Engineering, ASCE*, 108(5), 743–756.
7. ATC-13 (1985). Earthquake damage evaluation data for California ATC-13 Report. Applied Technology Council, Redwood City, CA.
8. Au, S. K., and Beck, J. L. (2003). Subset simulation and its application to

- seismic risk based on dynamic analysis, *J. Eng. Mech.*, 129(8), 901–917.
9. Baise, L. G., Higgins, R. B., and Brankman, C. M. (2006) Liquefaction hazard mapping—statistical and spatial characterization of susceptible units, *Journal of Geotechnical and Geoenvironmental Engineering*, 132(6), 705–715.
 10. Barnett, V., and Lewis, T. (1994). *Outliers in Statistical Data*. John Wiley & Sons, 3rd edition, New York, 58–61.
 11. Bhattacharya, S., Hyodo, M., Goda, K., Tazoh, T., and Taylor, C. A. (2011). Liquefaction of soil in the Tokyo Bay area from the 2011 Tohoku (Japan) earthquake, *Soil Dynamics and Earthquake Engineering*, 31, 1618–1628.
 12. Box, G. E. P., and Lucas, H. L. (1959). Design of experiments in non-linear situations. *Biometrika*, 46(1/2), 77–90.
 13. Caers, J. (2001). Geostatistical reservoir modeling using statistical pattern recognition, *Journal of Petroleum Science and Engineering*, 29(3), 177–188.
 14. Campbell, K. W., and Bozorgnia, Y. (2003). Updated near-source ground-motion (attenuation) relations for the horizontal and vertical components of peak ground acceleration and acceleration response spectra, *Bulletin of the Seismological Society of America*, 93(1), 314–331.
 15. Chandola, V., Banerjee, A., and Kumar, V. (2007). *Outlier Detection: A Survey*, Technical Report. University of Minnesota, Minnesota.
 16. Chang, W. Y., Dai, X. G, and Chen, H. W. (2004). A case study of geostatistical interpolation in meteorological fields, *Chinese Journal of*

- Geophysics, 47(6), 1104–1112.
17. Chung, J. W., David, R. J. (2011). Simplified method for spatial evaluation of liquefaction potential in the St. Louis area, *Journal of Geotechnical and Geoenvironmental Engineering*, 137(5), 505–515.
 18. Chun, S. H., Sun, C. G., and Chung, C. K. (2005). Application of geostatistical method for geo-layer information, *Journal of Korean Society of Civil Engineers*, 25 (2C), 103-115.
 19. Clayton, D., and Andre, J. (1997). *GSLIB: Geostatistical Software Library and User's Guide*.
 20. Cornell, A. C., Jalayer, F., Hamburger, R., and Foutch, D. (2002). Probabilistic basis for the 2000 SAC/FEMA steel moment frame guidelines, *J. Eng. Mech.*, 128(4), 526–533.
 21. Crowley, H., Pihnho, R., and Bommer, J. J. (2004). A probabilistic displacement-based vulnerability assessment procedure for earthquake loss estimation, *Bulletin of Earthquake Engineering*, 2(2), 173–219.
 22. Curtis, A. B., and Wayne, J. G. (1988). Assessing the threat to life from dam failure, *Water Resources Bulletin*, 24(6), 1303–1309.
 23. Dawson, K. M., and Baise, L. G. (2005). Three-dimensional liquefaction potential analysis using geostatistical interpolation, *Soil Dynamics and Earthquake Engineering*, 25(5), 369–381.
 24. Drabek, T. E., and Hoetmer, G. J. (1991). *Emergency Management: Principles and Practice for Local Government*, Washington, DC: International City Management Association.
 25. David, M. (1976). The practice of Kriging. In: M. Guarascio, M. David, C. Huijbregts, eds. *Advanced Geostatistics in the Mining Industry*,

- Boston, 31–48.
26. Debbie, R., Hutchison, R., Sanders, R., and Faust, T. (2001). Workshop report: Making USGS information effective in the electronic age, U.S. Geological Survey Open File Report 03-240, 82–83.
 27. Degroot, D.J., and Baecher, G. B. (1993). Estimating autocovariance of in-situ soil properties, *Journal of Geotechnical Engineering*, ASCE, 119(1), 147–166.
 28. Delfiner, P. (1976). Linear estimation of nonstationary spatial phenomena. In: Guarascio, M., David, M., and Huijbregts, C. eds, *Advanced Geostatistics in the Mining Industry*, Boston, 49–68.
 29. Deutsch, C. V., and Journel, A. G. (1998). *GSLIB: Geostatistical Software Library and User's guide* (Oxford University Press. Oxford).
 30. Deutsch, C. V. (2002). *Geostatistical Reservoir Modeling* (Oxford University Press. Oxford).
 31. Dixon, W. J. (1950). Analysis of extreme values, *The Annals of Mathematical Statistics*, 21(4), 488–506.
 32. Dubrule, O. (1983). Cross validation of Kriging in a unique neighborhood, *Mathematical Geology*, 15(6), 687–699.
 33. EduPro civil System (1997). Inc. ProShake User's Manual. Redmonde, Washington.
 34. Elkateb, T., Chalaturnyk, R., and Robertson, P. K. (2003). An overview of soil heterogeneity: quantification and implications on geotechnical field problems, *Canadian Geotechnical Journal*, 40(1), 1–15.
 35. Esri (2006). *ArcGIS 9: Using ArcGIS Desktop* (ESRI Press).
 36. European Committee for Standardization (2004). *Eurocode 7*

- Geotechnical Design. Part 1: General Rules. Final Draft, EN 1997-1:2004 (E), (F) and (G), Brussels., 152–153.
37. FEMA (2003). HAZUS-MH Technical Manual. Federal Emergency Management Agency, Washington, D.C.
 38. Finn, W. D. L. (2002). State of the art for the evaluation of seismic liquefaction potential, *Computers and Geotechnics*, 29(5), 329–341.
 39. Gallerini, G., and Donatis, M. D. (2009). 3D modeling using geognostic data: The case of the low valley of Foglia river (Italy), *Computers and Geosciences*, 35, 146–164.
 40. Gomez-Hernandez, J. J., and Srivastava, R. M. (1990). ISIM3D: An ANSI-C three-dimensional multiple indicator conditional simulation program, *Computers and Geosciences*, 16(4), 395–440.
 41. Goovaerts, P. (1997). *Geostatistics for Natural Resources Evaluation* (Oxford University Press, Oxford).
 42. Gardoni, P., Der Kiureghian, A., and Mosalam, K. M. (2002). Probabilistic capacity models and fragility estimates for RC columns based on experimental observations, *J. Eng. Mech.*, 128(10), 1024–1038.
 43. Gardoni, P., Mosalam, K. M., and Der Kiureghian, A. (2003). Probabilistic seismic demand models and fragility estimates for RC bridges, *J. Earthquake Eng.*, 7 (special Issue 1), 79–106.
 44. Green, R. A. (2001). *Energy-based Evaluation and Remediation of Liquefaction soils*. Ph.D. Dissertation. Virginia Polytechnic Institute and State University 2001. Blacksburg, VA.
 45. Green, R. A., Olson, S. M., Cox, B. R., Rix, G. J., Rathje, E., Bachhuber, J., French, J., Lasley, S., and Martin, N. (2011). *Geotechnical aspects of*

- failures at Port-au-Prince seaport during the 12 January 2010 Haiti earthquake, *Earthquake Spectra*, 2011, 27(S1), S43–S65.
46. Grubbs, F. E. (1950). Sample criteria for testing outlying observations, *Annals of Mathematical Statistics*, 21(1), 27–58.
 47. Grubbs, F. E. (1969). Procedures for detecting outlying observations in samples, *Technometrics*, 11, 1–21.
 48. Guillen, A., Meunier, C., Renaudd, X., and Repousseau, P. (2001). New Internet tools to manage geological and geophysical data, *Computers and Geosciences*, 27(5), 563–575.
 49. Hashemi, M., and Alesheikh, A. A. (2011). A GIS-based earthquake damage assessment and settlement methodology, *Soil Dynamics and Earthquake Engineering*, 31(11), 1607–1617.
 50. He, Z., Deng, S., and Xu, X. (2005). An optimization model for outlier detection in categorical data, *Proceedings of ICIC*, 400–409.
 51. Holzer, T. L., Bennett, M. J., Noce, T. E., Padovani, A. C., and Tinsley, J. C. (2006). Liquefaction hazard mapping with LPI in the Greater Oakland, California, area, *Earthquake Spectra*, 22(3), 693–708.
 52. Huang, B., and Lin, H. (1999). GeoVR: a web-based tool for virtual reality presentation form 2D GIS data, *Computers and Geosciences*, 28(1), 1167–1175.
 53. International Building Code (IBC) (2012). International Code Council. Falls Church, Va.
 54. International Society for Rock Mechanics (1981), *Suggested Methods for the Quantitative Description of Discontinuities in Rock Mass*, ISRM Suggested Methods, Pergamon Press.

55. Issaks, E. H., and Srivastva, R. M. (1989). *An Introduction to Applied Geostatistics* (Oxford University Press, Oxford).
56. Isaaks, E. H., and Srivastava, R. M. (1989). *Applied geostatistics*, New York, 20–35.
57. Iwasaki, T., Tatsuoka, F., Tokida, K., and Yasuda, S. (1978). A practical method for assessing soil liquefaction potential based on case studies at various sites in Japan, 5th Japan Earthquake Engineering Symposium, Japan, 641–648.
58. Iwasaki, T., Tokida, K., Tatsuoka, F., Watanabe, S., Yasuda, S., and Sato, H. (1982). Microzonation for soil liquefaction potential using simplified methods, *Proceedings 3rd International Conference on Microzonation*, Seattle, USA, 1319–1330.
59. Ishihara, K. (1977). Simple method of analysis for liquefaction of sand deposits during earthquakes, *Soils and Foundations*, 17(3), 1–8.
60. Ishihara, K. (1996). *Soil Behaviour in Earthquake Geotechnics*. Oxford science publications.
61. Jaime, J. G. H., and Mohan, S. R. (1990), ISIM3D: An Ansi-C Three-dimensional Multiple Indicator Conditional Simulation Program, *Computers and Geosciences*, 16(4), 395–440.
62. Jankowski, P., Stasik, M., and Jankoska, M. (2001). A map browser for an Internet-based GIS data repository, *Transactions in GIS*, 5(1), 5–18.
63. Jenkinson, A. F. (1955). The frequency distribution of the annual maximum (or minimum) of meteorological elements, *Quarterly Journal of the Royal Meteorological Society*, 81, 158–171.
64. Joh, S. H., Kim, D. S., Kang, T. H., Kim, K. S., Chang, H. S. and Jo, C.

- H. (2006). Comparison of Surface-Wave Techniques in the Spatial Profiling of Subsurface Stiffness, Proceedings of Sessions of GeoShanghai, China.
65. Journel, A. G. (1983). Nonparametric estimation of spatial distributions, *Mathematical Geology*, 15(3), 445–468.
66. Kim, H. -S., Cho, N. -G., and Chung, C. -K. (2012). Real-time LPI-based assessment of the liquefaction potential of the Incheon port in Korea, Proceeding of 15th World Conference of Earthquake Engineering, Lisbon, Portugal, 1120–1131.
67. Kim, H. -S., Kim, H. -K., Shin, S. -Y., and Chung, C. -K. (2012). Application of Statistical Geo-Spatial Information Technology to Soil Stratification in the Seoul metropolitan area, *Georisk*, 6(4), 221–228.
68. Kim, H. -S., Kim, M. -K., Kim, J. -Y., Kim, K.-L., and Chung, C.-K. (2012). Geostatistical Integration of Borehole and Geophysical Data for Design of Offshore-foundation, *Journal of Korean geotechnical Society*, 28(5), 109–120.
69. Kim, H. -S., Yoo, S. -H., Jang, I. -S., and Chung, C. -K. (2012). Real-time seismic damage estimation for harbor site considering ground motion amplification characteristics, *Journal of Earthquake Engineering*, 28(5), 55–65.
70. Kim, J. -Y., Kim, H. -K., and Cho, N. -J. (2010). Probabilistic stratification method for heterogeneous soils using outlier analysis, Proceedings Korean Geotechnical Society Spring National Conference, Gyeonggi, South Korea.
71. Kimmance, J. P. (1999). Geographical information system application to

- construction and geotechnical data management on large project, Proc. Of the 5th Int'l Symposium on Field Measurements in Geomechanics, Singapore, 151–156.
72. King, S. A., and Kiremidjian, A. S. (1994). Regional Seismic Hazard and Risk Analysis through Geographic Information Systems. Blume Center Reports, Report No. 111. Palo Alto, California, U.S.A., Stanford University: 185
 73. Kiureghian, D. A. (1996). Structural reliability methods for seismic safety methods for seismic safety assessment: A review, Eng. Struct., 18(6), 412–426.
 74. Koltermann, C. E., and Gorelick, S. (1996). Heterogeneity in sedimentary deposits: A review of structure-imitating, processimitating, and descriptive approaches, Water Resources Research, 32(9), 2617–2658.
 75. Korea Engineering and Consulting Association (2004). Soil Investigation Manual.
 76. Korea Highway Corporation (2009). Road Design Handbook.
 77. Korea Land Corporation (2002). Soil Investigation Guideline.
 78. Korea Ministry of Land, Infrastructure and Transport (2012). Construction Estimate Manual.
 79. Korea Train Express Corporation (1995). Soil Investigation Manual.
 80. Kotz, S., and Nadarajah, S. (2000). Extreme Value Distributions: Theory and Applications, Imperial college press, London, 61–94.
 81. Knudsen, H., and Kim, Y. C. (1978). Application of geostatistics to roll front type uranium deposits, Society of Mining Engineers of AIME, Denver, Colorado, 78–94.

82. Kramer, S. L. (1996). *Geotechnical Earthquake Engineering*, Prentice Hall: New Jersey.
83. Krige, D. G. (1951). A statistical approach to some basic mine valuation problems on the Witwatersrand, *J. of the Chem., Metal. and Mining Soc. of South Africa*, 52(6), 119–139
84. Kulhawy, F. H., Birgisson, B., and Grigoriu, M. D. (1992). Reliability-based foundation design for transmission line structures, *EPRI. Uncertainties in Soil Property Measurement*, 3, 220–231.
85. Kunapo, J., Dasari, G. R., Phoon, K. K., and Tan, T. S. (2005). Technical Report: Development of a Web-GIS based geotechnical information system, *Journal of Computing in Civil Engineering, ASCE*, 19, 323–327.
86. Kupfersberger, H., and Deutsch, C. V. (1999). Methodology for integrating analog geologic data in 3D variogram modeling, *AAPG Bulletin*, 83(8), 1262–1278.
87. Lacasse, S., and Nadim, F. (1996). Uncertainties in characterizing soil properties. In: Shackelford, C.D., Nelson, P.P. and Roth, M.J.S., eds, *Proceedings of Uncertainty in the Geologic Environment: from Theory to Practice*, ASCE, Madison, WI, 49–75.
88. Lee, J., and Wong, D. W. S. (2001). *Statistical Analysis with ArcView GIS*, John Wiley & Sons, Canada.
89. Li, X., Cheng, G. D., and Lu, L. (2000). Comparison of spatial interpolation methods, *Advances in Earth Sciences*, 15(3), 260–265.
90. Liao, S. S. C., and Whitman, R. V. (1986). Overburden correction factors for SPT in sand, *Journal of Geotechnical Engineering, ASCE* , 112(3), 373–377.

91. Liu, H., Shah, S., and Jiang, W. (2004). On-line outlier detection and data cleaning, *Computers and Chemical Engineering*, 28, 1635–1647.
92. Luna, R., and Frost J. D. (1998). Spatial liquefaction analysis system. *Journal of Computing in Civil Engineering*, 12(1), 48–56.
93. Lupoi, G., Franchin, P., Lupoi, A., and Pinto, P. E. (2004). Seismic fragility analysis of structural systems, *Proc., 13th World Conf. Earthquake Engineering*, Vancouver, Canada, Paper No. 4008.
94. Moramarco, T., Barbetta, S., Pandolfo, C., Tarpanelli, A., Berni, N., and Morbidelli. (2012). The spillway collapse of the Montedoglio dam on the Tiber River (central Italy): data collection and event analysis, *Journal of Hydrologic Engineering*, 18(8), 919–928.
95. Mouroux, P., and Le, B. B. (2006). Risk-UE project: an Advanced approach to earthquake risk scenarios with application to different European towns. In: *Assessing and Managing Earthquake Risk*, Oliveira, C. S. Roca, A., and Goula, X., Eds. Springer, Dordrecht, 479–508.
96. Nakamura, Y. (1996). Research and Development of Intelligent Earthquake Disaster Prevention System urEDAS and HERAS, *Journal of Structural Mechanics and Earthquake Engineering*, Japan Society of Civil Engineers, 531, 1–33.
97. NIBS (1997). *Earthquake Loss Estimation Technology HAZUS*, Federal Emergency Management Agency, Washington D. C.
98. Oh, C. -K., Sohn, H., and Bae, I. -H. (2009). Statistical novelty detection within the Yeongjong suspension bridge under environmental and operational variations, *Smart Materials and Structures*, 18, 1–9.
99. Oh, S. -H., Chung, H. -J., and Lee, D. -K. (2004) *Geostatistical*

- Integration of MT and Borehole Data for RMR Evaluation, *Journal of Korean Society of Earth and Exploration Geophysicists*, 7(2), 121–129.
100. Oh, S. -H. (2008). The Safety Assessment of embankment by three dimensional electrical DC modeling, *Journal of the Korean Earth Science Society*, 29(6), 447–453.
101. Olea, R. A. (1999). *Geostatistics for Engineers and Earth Scientists* (Kluwer Academic Publishers).
102. Ozturk, C. A. (2002). Geostatistical assessment of rock zones for tunneling, *Tunneling and Underground Space Technology*, 17, 275–285.
103. Papadimitriou, A. G., Antoniou, A. A., Bouckovalas, G. D., Marinou, P. G. (2008). Methodology for automated GIS-aided seismic microzonation studies, *Computers and Geotechnics*, 35, 505–523.
104. Papathanassiou, G. (2008). LPI-based approach for calibrating the severity of liquefaction-induced failures and for assessing the probability of liquefaction surface evidence, *Engineering Geology*, 9, 694–704.
105. Park, H. W., and Sohn, H. (2006). Parameter estimation of the generalized extreme value distribution for structural health monitoring, *Probabilistic Engineering Mechanics*, 21, 366–376.
106. Phoon, K. K. and Kulhawy, F.H., 1999. Characterization of geotechnical variability, *Canadian Geotechnical Journal*, 36, 612–624.
107. PIANC (1997) *Seismic Design Guidelines for Port Structures*. Working Group No. 34 of the Maritime Navigation Commission, International Navigation Association, Balkema, Rotterdam, The Netherlands.
108. Pinto, P. E., Giannini, R., and Franchin, P. (2004). *Seismic reliability analysis methods*, IUSS Press, Pavia, Italy.

109. RADIUS (1999). Risk Assessment Tools for Diagnosis of Urban Areas Against Seismic Disasters. United Nations Initiative towards Earthquake Safe cities. Website: <http://www.geohaz.org/radius/>.
110. Ronaldo, L., and David, F. J. (1998). Spatial liquefaction analysis system, *Journal of Computing in Civil Engineering*, 12(1), 350–356.
111. Rorabacher, D. B. (1991). Statistical treatment for rejection of deviant values: critical values of Dixon's "Q" parameter and related subrange ratios at the 95% confidence level, *Analytical Chemistry*, 63(2), 139–146.
112. Ryu, D. W., Kim, T. K., and Heo, J. S. (2003). A Study on geostatistical simulation technique for the uncertainty modeling of RMR, Tunnel and Underground, 13, 87–99.
113. Schnabel, P. B., Lysmer, J., and Seed, H. B. (1972). SHAKE : A Computer program for earthquake reponse analysis of horizontally layered sites. Report EERC 72–12, Earthquake Engineering Research Center, University of California, Berkeley, California.
114. Schneider, P. J., and Schauer, B. A. (2006). HAZUS—Its development and its future, *Natural Hazards Review*, 7, 40–44.
115. Schotanus, M. I. J., Franchin, P., Lupoi, A., and Pinto, P. E. (2004). Seismic fragility analysis of 3D structures, *Struct. Safety*, 26, 421–441.
116. Seed, H. B., and Idriss, I. M. (1970). Soil Moduli and Damping Factors for Dynamics Response Analysis. Report No. EERC 70–10, Earthquake Engineering Research Center, University of California, Berkeley, California.
117. Seed, H. B., and Idriss, I. M. (1971). Simplified procedure for evaluating soil liquefaction potential, *Journal of Soil Mechanics and Foundation*

- Division, ASCE, 97(SM9), 221–235.
118. Seed, H. B., Tokimatsu, L. F., Harder, L. F., and Chung, R. M. (1985). Influence of SPT procedures in soil liquefaction resistance evaluations, *Journal of Geotechnical Engineering*, 111(12), 1425–1445.
 119. Seifert, D., and Lensen, J. L. (1999). Using sequential indicator simulation as a tool in reservoir description: Issues and uncertainties, *Mathematical Geology*, 31(5), 527–550.
 120. Seo, M. –U., Scott, M. O., Sun, C. –G., and Oh, M. –H. (2012). Evaluation of liquefaction potential index along western coast of South Korea using SPT and CPT, *Marine Georesources & Geotechnology*, 30, 234–260.
 121. Seoul Metropolitan Subway Corporation (2001). Site Investigation Report.
 122. Shekhar, S., Lu, C., and Zhang, P. (2003). A unified approach to detecting spatial outliers, *GeoInformatica*, 7(2), 102–121.
 123. Shin, Y. W., Lee, I. K., Park, H. S., Choi, H. S., Park, S. C., Kim, J. K., Lee, M. S., Shin, K. H., and Han, B. H. (2007). A modified design of a large section tunnel as an auxiliary spillway along large faults. *Underground Space – the 4th Dimension of Metropolises: Proceedings of the World Tunnel Congress 2007 and 33rd ITA/AITES Annual General Assembly, Prague, May 2007* (Taylor & Francis).
 124. Shinozuka, M., Feng, M. Q., Lee, J., and Naganuma, T. (2000). Statistical analysis of fragility curves, *J. Eng. Mech.*, 126(12), 1224–1231.
 125. Singhal, A., and Kiremidjian, A. (1998). Bayesian updating of fragilities with application to RC frames, *J. Struct. Eng.*, 124(8), 922–929.

126. Sumer, B. M., Ansai, A., Cetin, K. O., Damgaard, J., Gunbak, A. R., Hansen, N. O., Sawicki, A., Synolakis, C. E., Yalciner, A. C., Yalcin, Y., and Zen, K. (2007). Earthquake-induced liquefaction around marine structures. *Journal of Waterway, Port, Coastal, and Ocean Engineering*, 133(1), 55–82.
127. Sun, C. -G. (2004). Geotechnical Information System and Site Amplification Characteristics for Earthquake Ground Motions at Inland of the Korean Peninsula. Ph.D. Dissertation, Seoul National University: Seoul, Korea.
128. Sun, C. -G., Kim, D. -S, and Chung, C. -K. (2005) Geologic site conditions and site coefficients for estimating earthquake ground motions in the inland areas of Korea, *Engineering Geology*, 81(4), 446–469.
129. Sun, C. -G., Chun, S. -H., Ha, T. -G., Chung, C. -K., and Kim, D. -S. (2008). Development and application of GIS-based tool for earthquake-induced hazard prediction, *Computers and Geotechnics*, 35(3), 436–449.
130. Sun, C. -G., Cho, C. -S., Son, M. -K., and Shin, J. -S. (2013). Correlations between shear wave velocity and in-situ penetration test results for Korean soil deposits. *Pure and Applied Geophysics*, 170(3), 271–281.
131. Sun, J. I., Golesorkhi, R., and Seed, H. B. (1988). Dynamic Moduli and Damping and Damping Ratios for Cohesive Soils. Report No. UCB/EERC–88/15, Earthquake Engineering Research Center, University of California, Berkeley, California.
132. Toprak, S., and Holzer, T. L. (2003). Liquefaction potential index: field assessment, *Journal of Geotechnical and Geoenvironmental Engineering*,

- ASCE, 129, 315–322.
133. Tukey, J. W. (1977). *Exploratory Data Analysis*. Addison-Wesley, New York, 58–63.
134. Vahidnia, M. H., Alesheikh, A. A., Alimohammadi, A., and Hosseinali, F. A. (2010). GIS-based neuro-fuzzy procedure for integrating knowledge and data in landslide susceptibility mapping, *Computers & Geosciences*, 36, 1101–1114.
135. Vanmarcke, E. H. (1977). Probabilistic modeling of soil profiles, *Journal of geotechnical Engineering*, ASCE, 103(11), 1227-1246.
136. Wang, X., Lv, J., Wei, C. and Xie, D. (2009). GIS-based elaborate spatial prediction of soil nutrient elements using ancillary terrain data in Chongqing tobacco planting region, China, *Computer and Computing Technologies in Agriculture II*, 1, 345–356.
137. Weissmann, G. S., Carle, S. F., and Fogg, G. E. (1999), Threedimensional hydrofacies modeling based on soil surveys and transition probability geostatistics, *Water Resources Research*, 35(6), 1761–1770.
138. Werner, S. D. (1998), *Seismic Guidelines For Ports*, Technical Council on Lifeline Earthquake Engineering Monograph, 12, 1–17.
139. Werner, S. D., Lavoie, J. P., Eguchi, R. T., Taylor, C. E. and Moore, J. E. (2003). REDARS1: Demonstration Software for seismic Risk Analysis of Highway System, *Research Progress and Accomplishments 2001-2003*, MCEER-03-SP01, Red Jacket Quadrangle, Buffalo, New York, 17–23.
140. Williams, G. J., Baxter, R. A., He, H. X., Hawkins, S., and Gu, L. (2002).

- A Comparative Study of RNN for Outlier Detection in Data Mining, IEEE International Conference on Data-mining (ICDM'02), Maebashi City, Japan, CSIRO Technical Report CMIS-02/102.
141. Williams, T., Szary, P., Thomann, T., Konnerth, C., and Nemeth, E. (2002). GIS Applications in Geotechnical Engineering. Final Report FHWA 2002-06, Federal Highway Administration, U.S. Department of Transportation.
 142. Xu, L., Liu, G. (2009). The study of a method of regional environmental risk assessment, *Journal of Environmental Management*, 90(3), 290–296.
 143. Youd, T. L. (1978). Perkins DM. Mapping liquefaction-induced ground failure potential. *Journal of the Geotechnical Engineering*, 104, 433–446.
 144. Youd, T. L. (1987). Perkins DM. Mapping of liquefaction severity index. *Journal of Geotechnical Engineering*, 113(11), 1374–1392.
 145. Yun, G. -L., Yun, Y. -W., and Kim, H. -Y. (2008). Characteristic values of design parameters for geotechnical reliability design, *Journal of Korean geotechnical Society*, 24 (5), 27–35.
 146. Zhang, Y., Meratnia, N., and Havinga, P. J. M. (2007). A taxonomy framework for unsupervised outlier detection techniques for multi-type data sets. Technical Report TR-CTIT-07-79, Centre for Telematics and Information Technology, University of Twente, Enschede.
 147. Zhao, H. B., Ru, Z. L., and Yin, S. (2007). Updated support vector machine for seismic liquefaction evaluation based on the penetration tests, *Marine Georesources & geotechnology*, 25(3-4), 209–220.

Appendices

A.1 Detailed Standard Data Format of Database

A.1.1 Geotechnical investigation information

Detailed standard data formats of borehole information are shown in following tables. The T_Borehole_Info table is for general descriptions of the boring inspection as shown Table A.1.

The T_Layer table (Table A.2) contains geo-layer data, which are the classification of geo-layers and detailed descriptions of each geo-layer. Descriptions of each geo-layers are divided into color, density, moisture, fracture, weathering and strength in detail, and additional descriptions are stored in a comment field. And the T_SPT table (Table A.3) contains N-values with depth acquired from SPT (Standard Penetration Test) and T_RQD tables (Table A.4) store RQD (Rock Quality Designation) and TCR (Total Core Recovery) values with depth.

Table A.1 Details of the T_Borehole_Info table

Field	Data type	Constraint	Details
project_id	Integer		Serial numbers to manage projects
borehole_id	Integer	PK	Serial numbers to manage boreholes
borehole_name	Text		Name of the borehole
b_x	Float		X coordinate of a borehole point
b_y	Float		Y coordinate of a borehole point
b_z	Float		Z coordinate of a borehole point
b_gwl	Float		Groundwater elevation at a point
b_date	Date		Boring date
b_inspector	Text		Name of inspector
b_driller	Text		Name of driller
b_machine	Text		Types of boring machine
b_location	Text		Boring location
b_method	Text		Boring method

Table A.2 Details of the T_Layer table

Field	Data type	Constraint	Details
borehole_id	Integer		Serial numbers to manage boreholes
dep_from	Float		Top elevation of each geo-layer
dep_to	Float		Bottom elevation of each geo-layer
Eng_name	Text		Fill, alluvial soul, weathered soil, weathered rock, etc.
Sci_name	Text		USCS
user_name	Text		User-defined geo-layer classification
color	Text		Color
den_from	Text		Density
den_to	Text		
moist_from	Text		Moisture
moist_to	Text		
compo_main	Text		Main components of each geo-layer
compo_sub	Text		Minor components of each geo-layer
fracture_from	Text		Fracture
fracture_to	Text		
weather_from	Text		Weathering
weather_to	Text		
str_from	Text		Strength
str_to	Text		
comment	Text		Additional comments

Table A.3 Details of the T_SPT table

Field	Data type	Constraint	Details
borehole_id	Integer		Serial numbers to manage boreholes
SPT_depth	Float		Testing depth
SPT_N	Integer		N-value
pet_depth	Float		Penetration depth for a N-value

Table A.4 Details of the T_RQD table

Field	Data type	Constraint	Details
borehole_id	Integer		Serial numbers to manage boreholes
dep_from	Float		Top elevation of a test data
dep_to	Float		Bottom elevation of a test data
rqd	Float		Rock Quality Designation
tcr	Float		Total Core Recovery

CPT data consists of penetration test data and dissipation test data. Dissipation test data is divided into summary data and raw data of the test. The T_CPT table (Table A.5) contains the penetration test data, the T_CPTu table (Table A.6) stores the depth and summarized results of dissipation tests, and T_CPTu_Data table (Table A.7) stores the raw test data of dissipation tests.

FVT data consists of summary data and raw test data. The T_FVT table (Table A.8) is for the test depth and summarized results, and the T_FVT_Data table (Table A.9) is for the raw test data.

Table A.5 Details of the T_CPT table

Field	Data type	Constraint	Details
borehole_id	Integer		Serial numbers to manage boreholes
cpt_gwl	Float		Groundwater elevation of a CPT test point
cpt_date	Date		Test date
depth	Float		Testing depth
U	Float		Porewater pressure
U0	Float		Static water pressure
ft	Float		Skin friction
qt	Float		Tip resistance
Rf	Float		Friction ratio
DPPR	Float		DPPR

Table A.6 Details of the T_CPTu table

Field	Data type	Constraint	Details
borehole_id	Integer		Serial numbers to manage boreholes
cptu_id	Integer	PK	Serial numbers to manage CPTu tests
depth	Float		CPTu testing depth
cptu_gwl	Float		Groundwater elevation of a CPTu test point
ui	Float		Initial porewater pressure
ut	Float		Final porewater pressure
u0	Float		Static water pressure
ur	Float		Residual porewater pressure
u	Float		Degree of consolidation
Sf	Float		Skin friction
RRCR	Float		RRCR
T50	Float		Theoretical time factor at t_{50}
R	Float		Radius of cone
U50	Float		Porewater pressure at t_{50}
tt50	Float		Time to 50% dissipation of excess porewater pressure in normalized dissipation curves
Cht	Float		Coefficient consolidation with time
Ch	Float		Coefficient consolidation
L0	Float		Estimating location of porewater pressure

Table A.7 Details of the T_CPTu_Data table

Field	Data type	Constraint	Details
cptu_id	Integer	PK	Serial numbers to manage CPTu tests
cptu_t	Float		Elapsed time
cptu_u	Float		Porewater pressure

Table A.8 Details of the T_FVT table

Field	Data type	Constraint	Details
borehole_id	Integer		Serial numbers to manage boreholes
fvt_id	Integer	PK	Serial numbers to manage FVT tests
depth	Float		FVT testing depth
fvt_type	Float		Types of FVT test apparatus
fvt_size	Float		Size of FVT test apparatus
St	Float		Sensitivity
m_date	Date		Test date
Tester	Float		Tester
UVC	Float		Vane constant under undisturbed condition
RVC	Float		Vane constant under remolded condition
UMaxT	Float		Maximum torque under undisturbed condition
RMaxT	Float		Maximum torque under remolded condition
UFs	Float		Friction under undisturbed condition
RFs	Float		Friction under remolded condition
UShear	Float		Shear strength under undisturbed condition
RShear	Float		Shear strength under remolded condition
USCS	Text		Soil classification

Table A.9 Details of the T_FVT_Data table

Field	Data type	Constraint	Details
fvt_id	Integer	PK	Serial numbers to manage FVT tests
UDeg	Float		Rotation degree under undisturbed condition
UT	Float		Torque under undisturbed condition
USec	Float		Time (second) under undisturbed condition
RDeg	Float		Rotation degree under remolded condition
RT	Float		Torque under remolded condition
RSec	Float		Time (second) under remolded condition

The dynamic test (shear wave velocity, cyclic triaxial test, and resonance column test) data consists of summary and raw test data. The T_Vs table (Table A.10) is for the test depth and shear wave velocity, and the T_CTX table (Table A.11) contain condition and results of cyclic triaxial test. The T_RC table (Table A.12) is for the test depth and summarized results, and the T_RC_Data table (Table A.13) is for the raw test data of resonance column test.

Table A.10 Details of the T_Vs table

Field	Data type	Constraint	Details
borehole_id	Integer	PK	Serial numbers to manage boreholes
Depth	Float		Depth
Vs	Float		Shear wave velocity

Table A.11 Details of the T_CTX table

Field	Data type	Constraint	Details
borehole_id	Integer		Serial numbers to manage boreholes
CTX_id	Integer	PK	Serial numbers to manage cyclic triaxial tests
Depth	Float		Testing depth
Re_Density	Float		Relative density
Dry_Weight	Float		Dry unit weight
Eff_Str	Float		Effective stress
CSR	Float		Cyclic shear stress ratio
Co_Cor	Float		Correction correlation
Cor_CSR	Float		Correction cyclic shear stress ratio
Num_Cycle	Integer		Number of cycle

Table A.12 Details of the T_RC table

Field	Data type	Constraint	Details
borehole_id	Integer		Serial numbers to manage boreholes
RC_id	Integer	PK	Serial numbers to manage resonance column tests
Depth	Float		Testing depth
Re_Density	Float		Relative density
Dry_Weight	Float		Dry unit weight
Tot_Weight	Float		Total unit weight
Wn	Float		Natural water content

Table A.13 Details of the T_RC_Data table

Field	Data type	Constraint	Details
RC_id	Integer	PK	Serial numbers to manage resonance column tests
Strain	Float		Shear strain
G_Gmax	Float		Normalized shear modulus
Damping	Float		Damping ratio

The T_Borehole_Sum table (Table A.14) is designed to store engineering parameters evaluated from in-situ or laboratory tests.

Table A.14 Details of the T_Borehole_Sum table

Field	Data type	Constraint	Details
borehole_id	Integer		Serial numbers to manage boreholes
dep_from	Float		Top elevation of a test sample
dep_to	Float		Bottom elevation of a test sample
m_date	Date		Test date
Wn	Float		Natural water content
Gs	Float		Specific gravity
e0	Float		Initial void ration
rt	Float		Total unit weight
LL	Float		Liquid limit
PI	Float		Plastic Index
PL	Float		Plastic limit
OMC	Float		Optimum moisture content
rdmax	Float		Max relative density
rdmin	Float		Minimum relative density
<i>[Continued]</i>			

CBR	Float		California bearing ratio
qu	Float		Uniaxial strength
qur	Float		
St	Float		Sensitivity
E50	Float		Elastic stiffness
Cc	Float		Compression index
Cr	Float		Recompression index
Pc	Float		Pre-consolidation pressure
kv	Float		Vertical permeability
kh	Float		Horizontal permeability
Cuu	Float		Cohesion under undrained condition
Ccu	Float		Cohesion under drained condition
Phi_cu	Float		Friction angle
C	Float		Cohesion from direct shear test
Phi	Float		Friction angle from direct shear test
No4	Float		Grain size analysis
No10	Float		
No40	Float		
No200	Float		
No002	Float		
USCS	Text		Soil classification

Designing standard data formats for all in-situ and laboratory tests are impossible, because there are many testing methods and new test methods can be developed can. Therefore, if necessary, it is essential to build up new data structures according to user's test data. The developed system supports functions for user-defined data, to define newly data structures according to user's test data and to store raw test data in the GDB. User-defined data

consists of 3 tables: T_Test, T_Test_Info and T_Test_Data tables. T_Test table (Table A.15) contains the setup data for the T_Test_Info table (Table A.16), the T_Test_Info table contains the general information on a test and the setup data for the T_Test_Data table (Table A.17), and the T_Test_Data table contains raw test data of a test.

Table A.15 Details of the T_Test table

Field	Data type	Constraint	Details
borehole_id	Integer		Serial numbers to manage boreholes
test_id	Integer	PK	Serial numbers to manage tests
test_name	Text		Name of a test (ex. Consolidation test)
test_type	Text		Type of a test (optional)
f_num	Integer		Number of real variables to be used
s_num	Integer		Number of test variables to be used
d_num	Integer		Number of date variables to be used
fname1	Text		Name of real variables
...			
fname20			
funit1	Text		Unit or real variables
...			
funit20			
sname1	Text		Name of text variables
...			
sname20			
dname1	Text		Name of date variables
...			
dname5			

Table A.16 Details of the T_Test_Info table

Field	Data type	Constraint	Details
test_id	Integer		Serial numbers to manage tests
test_info_name	Text		Name of a test data (ex. 2 nd stage of consolidation test)
f_num	Integer		Number of real variables to be used
s_num	Integer		Number of text variables to be used
d_num	Integer		Number of date variables to be used
x_col	Integer		Real variables to be used as X axis of a graph
y_col	Integer		Real variables to be used as Y axis of a graph
fname1	Text		Name of real variables
...			
fname20			
funit1	Text		Unit or real variables
...			
funit20			
sname1	Text		Name of text variables
...			
sname20			
dname1	Text		Name of date variables
...			
dname5			
f1	Text		Real variables
...			
f20			
s1	Text		Text variables
...			
s20			
d1	Text		Date variables
...			
d5			

Table A.17 Details of the T_Test_Data table

Field	Data type	Constraint	Details
test_id	Integer		Serial numbers to manage tests
f1	Float		Real variables
...			
f20			
s1	Text		Text variables
...			
s10			
d1	Date		Date variables
...			
d5			

Geophysical datasets are compositely studied in terms of multi-attribute interpretations for the subsurface mappings of tomography, associated with geotechnical geo-layers. Utilizing GIS platform, the attribute data were implemented to a database; a lineament from the satellite image, electrical resistivity and its standard deviation, radioactivity, seismic velocity, and bedrock depth. In an attempt to interpret 1D electrical sounding data in 3D views, 1D data are firstly performed horizontal and vertical interpolation and extrapolation. Reconstruction of a resistivity volume is found to be an effective scheme for tomography mapping.

To obtain the digitized geophysical tomography, the GIS-based digitizing is performed for geophysical image file. In this geophysical datasets schema, 2D or 3D tomography is coordinated based on the 3D coordinate system and attribute datasets are associated with spatial information. T_Geophysical_Info

table (Table A.18) is general information, and T_Geophysical_Result table (Table A.19) is digitized condition. And T_Geophysical_Tomography table (Table A.20) contains digitized geophysical values.

Table A.18 Details of the T_Geophysical_Info table

Field	Data type	Constraint	Details
geophysical_id	Integer	PK	Serial numbers to manage geophysical tests
geophysical_name	Text		Name of a geophysical test data
geophysical_method1	Text		Type of geophysical test
geophysical_method2	Text		Detail type of geophysical test
geophysical_area	Text		Area of geophysical test
geophysical_person	Text		Tester
geophysical_machine	Text		Machine of geophysical test
geophysical_date	Date		Testing date
comments	Text		Additional comments

Table A.19 Details of the T_Geophysical_Result table

Field	Data type	Constraint	Details
geophysical_id	Integer	PK	Serial numbers to manage geophysical tests
shape	Geometry		Geometric data type based on ArcSDE (ex. Line feature, Polygon feature, Raster etc.)
result_Type	Text		Type of geophysical result (ex. 1D, 2D, 3D)
xmin	Float		Minimum X coordinate of a geophysical tomography area

[Continued]

xmax	Float		Maximum X coordinate of a geophysical tomography area
ymin	Float		Minimum Y coordinate of a geophysical tomography area
ymax	Float		Maximum Y coordinate of a geophysical tomography area
zmin	Float		Minimum Z coordinate of a geophysical tomography area
zmax	Float		Maximum Z coordinate of a geophysical tomography area
NoX	Integer		Number of grid lines along X axis
NoY	Integer		Number of grid lines along Y axis
NoZ	Integer		Number of grid lines along Z axis
SizeX	Float		Grid size along X axis
SizeY	Float		Grid size along Y axis
SizeZ	Float		Grid size along Z axis
comments	Text		Additional comments

Table A.20 Details of the T_Geophysical_Tomography table

Field	Data type	Constraint	Details
Geophysical_id	Integer		Serial numbers to manage geophysical tests
Geophysical_order	Integer		Order of a geophysical tomography
Geophysical_X	Float		X coordinate of grid points
Geophysical_Y	Float		Y coordinate of grid points
Geophysical_Z	Float		Z coordinate of grid points
Geophysical_Value	Float		Geophysical value of grid points

A.1.2 Structure information

The T_Structure_Info table (Table A.21) contains structure type, shape, repair status, construction type, deterioration status, and structure fragility curve. The structure fragility curves are standardized according to the above section “5.4.1 Fragility curve” based on filestream data type. To display the spatial distribution of the structure information, the digitized structure geometry obtained from digital map is contained in T_Structure_Shape table (Table A.22).

Table A.21 Details of the T_Structure_Info table

Field	Data type	Constraint	Details
site_id	Integer		Serial numbers to manage sites
structure_id	Integer	PK	Serial numbers to manage structures
owner	Text		Owner or manager of structures
reference_no	Text		Structure management number
structure_type1	Text		Structure type
structure_type2	Text		Structure detail type
height	Float		Height of structure
width	Float		Width of structure
length	Float		Length of structure
section_shape	Text		Cross-sectional shape of structure
section_area	Float		Cross-sectional area of structure
foundation_type	Text		Foundation type of structure
foundation_material	Text		Foundation material of structure
construction_method	Text		Construction method of structure
construction_date	Date		Construction year of structure
used_date	Date		Operation period of structure
aging	Text		Deterioration of structure
repair_status	Text		Status of repair
seismic_fragility	Filestream		Structure seismic fragility curve
structure_report	Filestream		Report file associated with structure
comment	Text		Additional comments

Table A.22 Details of the T_Structure_Shape table

Field	Data type	Constraint	Details
structure_id	Integer		Serial numbers to manage structures
vertex_id	Integer	PK	Serial numbers to manage vertex of structure shape
xmin	Float		Minimum X coordinate of a structure
xmax	Float		Maximum X coordinate of a structure
ymin	Float		Minimum Y coordinate of a structure
ymax	Float		Maximum Y coordinate of a structure
zmin	Float		Minimum Z coordinate of a structure
zmax	Float		Maximum Z coordinate of a structure
shape	Geometry		Geometric data type based on ArcSDE
shape_length	Float		Length of a geometry
shape_area	Float		Area of a geometry

A.1.3 Seismic monitoring information

Data for types of seismometers (Table A.23) includes names of types of seismometers, setup data of each seismometer, setup data of monitoring results, etc. And data for each seismometer contains the general information for a seismometer such as installation data, type of seismometer. Seismic monitoring data (Table A.24) consists of raw reading values of each station, when earthquake events are detected. And earthquake events data (Table A.25)

is summarized and raw data for earthquake event.

Table A.23 Details of the T_Seismological_Observatory table

Field	Data type	Constraint	Details
station_id	Integer	PK	Serial numbers to manage seismological observatories
kiss_id	Integer		Serial numbers to manage sites KISS code
station_kor_name	Text		Name of seismological observatories in Korean
sataion_eng_name	Text		Name of seismological observatories in English
monitoring_type	Text		Type of a seismometer
monitoring_x	Float		X coordinate of a seismometer point
monitoring_y	Float		Y coordinate of a seismometer point
monitoring_z	Float		Z coordinate of a seismometer point
monitoring_depth	Float		Install depth of a seismometer
constructor	Text		Installment company of a seismometer
manager	Text		Management company of a seismometer
construct_date	Date		Install date
location	Text		Location
comment	Text		Additional comments

Table A.24 Details of the T_Seismic_Monitoring table

Field	Data type	Constraint	Details
station_id	Integer		Serial numbers to manage seismological observatories
event_id	Integer	PK	Serial numbers to manage earthquake events
monitoring_time	Float		Monitoring time of earthquake events
rock_acc	Float		Measured rock outcrop acceleration

Table A.25 Details of the T_Earthquake_Event table

Field	Data type	Constraint	Details
event_id	Integer	PK	Serial numbers to manage earthquake events
event_time	Float		Earthquake event time
trigger_val	Float		Trigger time
init_val	Float		Initial trigger value
init_STA	Float		Initial short term averaging
max_time	Float		Time of maximum acceleration
max_val	Float		Maximum velocity
max_STA	Float		Maximum short term averaging
num_STA	Float		Number of short term averaging
non_chan	Float		Number of channel
start_time	Float		Starting time of earthquake event
duration	Float		Duration time of earthquake event

A.1.4 Geotechnical spatial grid information

From the indicator kriging method, the T_Indicator_Kriging table contains the indicator kriging options and the T_3D_GeoLayer table contains the indicator kriging results, as shown in Table A.26 and Table A.27. Finally, the geotechnical spatial grids are constructed by subdividing the 3D geolayers as shown in Table A.28.

Table A.26 Details of the T_Indicator_kriging table

Field	Data type	Constraint	Details
AnalLayer_id	Integer	PK	Serial numbers to manage geostatistical 3D integration analysis
geolayer_type	Integer		Type of geo-layer (ex. Fill, alluvial soil,
kriging_type	Integer		Type of kriging
kriging_model	Integer		Type of variogram model
Nugget	Float		Nugget of variogram model
Range	Float		Range of variogram model
Sill	Float		Sill of variogram model

Table A.27 Details of the T_3D_GeoLayer table

Field	Data type	Constraint	Details
site_id	Integer		Serial numbers to manage sites
AnaLayer_id	Integer	PK	Serial numbers to manage geostatistical 3D integration analysis
AnaLayer_date	Date		Analysis date
geophysical_id	Integer		Serial numbers to manage geophysical tests
geophy_method	Integer		Type of a geophysical test
borehole_num	Integer		Number of borehole for geostatistical 3D integration
AnaLayer_area	Integer		Area of geostatistical 3D integration
AnaLayer_location	Text		Location of geostatistical 3D integration
xmin	Float		Minimum X coordinate of geostatistical 3D integration
xmax	Float		Maximum X coordinate of geostatistical 3D integration
ymin	Float		Minimum Y coordinate of geostatistical 3D integration
ymax	Float		Maximum Y coordinate of geostatistical 3D integration
zmin	Float		Minimum Z coordinate of geostatistical 3D integration
zmax	Float		Maximum Z coordinate of geostatistical 3D integration
NoX	Integer		Number of integrated grid lines along X axis
NoY	Integer		Number of integrated grid lines along Y axis
NoZ	Integer		Number of integrated grid lines along Z axis
SizeX	Float		Integrated grid size along X axis
SizeY	Float		Integrated grid size along Y axis
SizeZ	Float		Integrated grid size along Z axis

Table A.28 Details of the T_Geotechnical_Spatial_Grid table

Field	Data type	Constraint	Details
AnalLayer_id	Integer		Serial numbers to manage geostatistical 3D integration analysis
AnalLayer_order	Integer		Order of integrated grid
Spatial_Grid_id	Integer	PK	Serial numbers to manage geotechnical spatial grids
x	Float		X coordinate of spatial grid cells
y	Float		Y coordinate of spatial grid cells
z	Float		Z coordinate of spatial grid cells
Value	Float		Value of geotechnical spatial grid
SVar	Float		Integration variation of grid points
NVar	Float		Normalized integration variation of grid points

A.1.5 Real-time earthquake hazard information

The standard data format of real-time earthquake hazard information was composed of four categories (real-time seismic load determination information, real-time liquefaction hazard estimation information, real-time structure fragility evaluation information and Integrated seismic damage grad information) according to the systematic procedure for real-time earthquake hazard assessment.

Real-time seismic load determination information

From the procedure of real-time seismic load determination, the T_Corr_Eq table contains the correlation function of seismic load and the T_Corr_Graph table contains the actual regression results for seismic load correlation, as shown in Table A.29 and Table A.30. T_Shake table contained the site response analysis result based on ProShake. And T_Corr_PGA table (Table A.31) is for the correlation of rock outcrop acceleration and PGA, T_Corr_layer_PGA table (Table A.32) indicates the correlation of rock outcrop acceleration (a_{rock}) and the maximum acceleration of each layer (a_{max}).

Table A.29 Details of the T_Corr_Eq table

Field	Data type	Constraint	Details
Spatial_Grid_id	Integer	PK	Serial numbers to manage geotechnical spatial grids
Sei_load_id	Integer		Serial numbers to manage seismic load correlation equations
Corr_a	Float		Correlation coefficient α ($a_{max} = \alpha(1 - e^{-\beta \cdot a_{rock}})$)
Corr_b	Float		Correlation coefficient β ($a_{max} = \alpha(1 - e^{-\beta \cdot a_{rock}})$)

Table A.30 Details of the T_Corr_Graph table

Field	Data type	Constraint	Details
Spatial_Grid_id	Integer		Serial numbers to manage geotechnical spatial grids
Sei_load_id	Integer	PK	Serial numbers to manage seismic load correlation equations
rock_acc1	Float		Rock outcrop acceleration 1
rock_acc2	Float		Rock outcrop acceleration 2
rock_acc3	Float		Rock outcrop acceleration 3
rock_acc4	Float		Rock outcrop acceleration 4
rock_acc5	Float		Rock outcrop acceleration 5
rock_acc6	Float		Rock outcrop acceleration 6
rock_acc7	Float		Rock outcrop acceleration 7
rock_acc8	Float		Rock outcrop acceleration 8
rock_acc9	Float		Rock outcrop acceleration 9
PGA1	Float		Peak ground acceleration 1
PGA2	Float		Peak ground acceleration 2
PGA3	Float		Peak ground acceleration 3
PGA4	Float		Peak ground acceleration 4
PGA5	Float		Peak ground acceleration 5
PGA6	Float		Peak ground acceleration 6
PGA7	Float		Peak ground acceleration 7
PGA8	Float		Peak ground acceleration 8
PGA9	Float		Peak ground acceleration 9
comment	Text		Additional comments

Table A.31 Details of the T_Shake table

Field	Data type	Constraint	Details
Spatial_Grid_id	Integer	PK	Serial numbers to manage geotechnical spatial grids
Sei_load_id	Integer		Serial numbers to manage seismic load correlation equations
shake_file	Filestream		Output zip file from ProShake

Table A.32 Details of the T_Corr_PGA table

Field	Data type	Constraint	Details
Spatial_Grid_id	Integer		Serial numbers to manage geotechnical spatial grids
Sei_load_id	Integer	PK	Serial numbers to manage seismic load correlation equations
rock_acc	Float		Measured rock outcrop accelerations
PGA	Float		Correlated PGA

Table A.33 Details of the T_Corr_layer_PGA table

Field	Data type	Constraint	Details
Spatial_Grid_id	Integer		Serial numbers to manage geotechnical spatial grids
Sei_load_id	Integer	PK	Serial numbers to manage seismic load correlation equations
rock_acc	Float		Measured rock outcrop accelerations
depth	Float		Depth of geotechnical spatial grid
Max_layer_acc	Float		Correlated PGA of each layers

Real-time liquefaction hazard estimation information

From the procedure of real-time liquefaction hazard estimation, the T_CRR table contains the cyclic resistance ratio information, and the T_CSR table contains the cyclic stress ratio information, as shown in Table A.34 and Table A.35. T_FS_Liquefaction table (Table A.36) contained the factor of safety for liquefaction information. And T_LPI table (Table A.37) is for the liquefaction potential index and liquefaction severity class.

Table A.34 Details of the T_CRR table

Field	Data type	Constraint	Details
Spatial_Grid_id	Integer	PK	Serial numbers to manage geotechnical spatial grids
Sei_load_id	Integer		Serial numbers to manage seismic load correlation equations
liquefaction_id	Integer		Serial numbers to manage liquefaction estimation
SPT-N	Float		N-value
CRR	Float		Cyclic resistance ratio

Table A.35 Details of the T_CSR table

Field	Data type	Constraint	Details
Spatial_Grid_id	Integer	PK	Serial numbers to manage geotechnical spatial grids
Sei_load_id	Integer		Serial numbers to manage seismic load correlation equations
liquefaction_id	Integer		Serial numbers to manage liquefaction estimation
layer_thick	Float		Thickness of go-layer
max layer acc	Float		Correlated PGA of each layers
layer_load	Float		Total vertical stress at depth
layer_e_load	Float		Effective vertical stress at depth
CSR	Float		Cyclic stress ratio

Table A.36 Details of the T_FS_Liquefaction table

Field	Data type	Constraint	Details
Spatial_Grid_id	Integer		Serial numbers to manage geotechnical spatial grids
Sei_load_id	Integer		Serial numbers to manage seismic load correlation equations
liquefaction_id	Integer	PK	Serial numbers to manage liquefaction estimation
FS	Float		Factor of safety for liquefaction

Table A.37 Details of the T_LPI table

Field	Data type	Constraint	Details
Spatial_Grid_id	Integer		Serial numbers to manage geotechnical spatial grids
Sei_load_id	Integer		Serial numbers to manage seismic load correlation equations
liquefaction_id	Integer	PK	Serial numbers to manage liquefaction estimation
LPI	Float		Liquefaction potential index
liquefaction_class	Text		Liquefaction severity class (none, low, high, severe)

Real-time structure fragility evaluation information

From the procedure of real-time structure fragility evaluation, the T_Fragility table contains the type of fragility curve and fragility grade, and the T_Fragility_Grade table contains the determined PGA and corresponding failure probability, as shown in Table A.38 and Table A.39. T_Fragility_Damage table (Table A.40) contained the structure seismic fragility class information.

Table A.38 Details of the T_Fragility table

Field	Data type	Constraint	Details
structure_id	Integer	PK	Serial numbers to manage structures
structure_type	Text		Type of structure
fragility_id	Integer		Serial numbers to manage seismic fragility curves
fragility_curve_type	Text		Type of seismic fragility curve
fragility_grade_step	Text		Structure fragility class
fragility_grade_curve1	Integer		Serial numbers to manage structures seismic fragility curve of damage level 1
fragility_grade_curve2	Integer		Serial numbers to manage structures seismic fragility curve of damage level 2
fragility_grade_curve3	Integer		Serial numbers to manage structures seismic fragility curve of damage level 3
fragility_grade_curve4	Integer		Serial numbers to manage structures seismic fragility curve of damage level 4
fragility_grade_curve5	Integer		Serial numbers to manage structures seismic fragility curve of damage level 5

Table A.39 Details of the T_Fragility_Grade table

Field	Data type	Constraint	Details
fragility_id	Integer		Serial numbers to manage seismic fragility curves
fragility_grade_id	Text	PK	Serial numbers to manage structures seismic fragility curve (id; 1-5)
PGA	Integer		PGA
fragility_value	Float		Structure seismic fragility

Table A.40 Details of the T_Fragility_Damage table

Field	Data type	Constraint	Details
Spatial_Grid_id	Integer		Serial numbers to manage geotechnical spatial grids
structure_id	Integer		Serial numbers to manage structures
Sei_load_id	Integer		Serial numbers to manage seismic load correlation equations
fragility_grade_id	Text	PK	Serial numbers to manage structures seismic fragility curve (id; 1-5)
PGA	Float		PGA
fragility_value	Float		Structure seismic fragility
fragility_class	Text		Structure seismic fragility class

Integrated seismic damage grad information

The T_Integrated_Damage table (Table A.41) contains the integrated seismic damage class determined engineering judgment considering synthetically liquefaction hazard class and structure seismic fragility class based on geotechnical spatial grid.

Table A.41 Details of the T_Integrated_Damage table

Field	Data type	Constraint	Details
site_id	Integer		Serial numbers to manage sites
earthquake_id	Integer		Serial numbers to manage earthquake events
structure_id	Integer	PK	Serial numbers to manage structure
Spatial_Grid_id	Integer	PK	Serial numbers to manage geotechnical spatial grid
liquefaction_id	Integer	PK	Serial numbers to manage liquefaction estimation
liquefaction_severity	Text		Liquefaction severity class (none, low, high, severe)
fragility_grade_id	Text	PK	Serial numbers to manage structures seismic fragility curve (id; 1–5)
fragility_class	Text		Structure seismic fragility class
integrated_damage	Text		Integrated seismic damage class

A.2 Detailed Management module of geotechnical investigation information

All geotechnical investigation information is managed in a window form according to sub classes, as shown in Figures A.1–A.11. General descriptions for borehole including geographic locations and geo-layer information in Figure A.1, SPT, RQD and TCR information in Figure A.2, CPT information in Figure A.3, FVT information in Figure A.4, shear wave velocity test information in Figure A.5, cyclic triaxial test information in Figure A.6, resonance column test information in Figure A.7, engineering parameters evaluated from various tests in Figure A.8, user-defined test information in Figure A.8 are managed.

Additionally, the input module of geophysical test information is arranged in Figures A.9 and A.10. Geophysical tomography data is digitized by using digitizing tool of the input module in Figure A.11. These window forms for management of geotechnical investigation information are designed according to the database structures and the characteristics of the geotechnical investigation information.

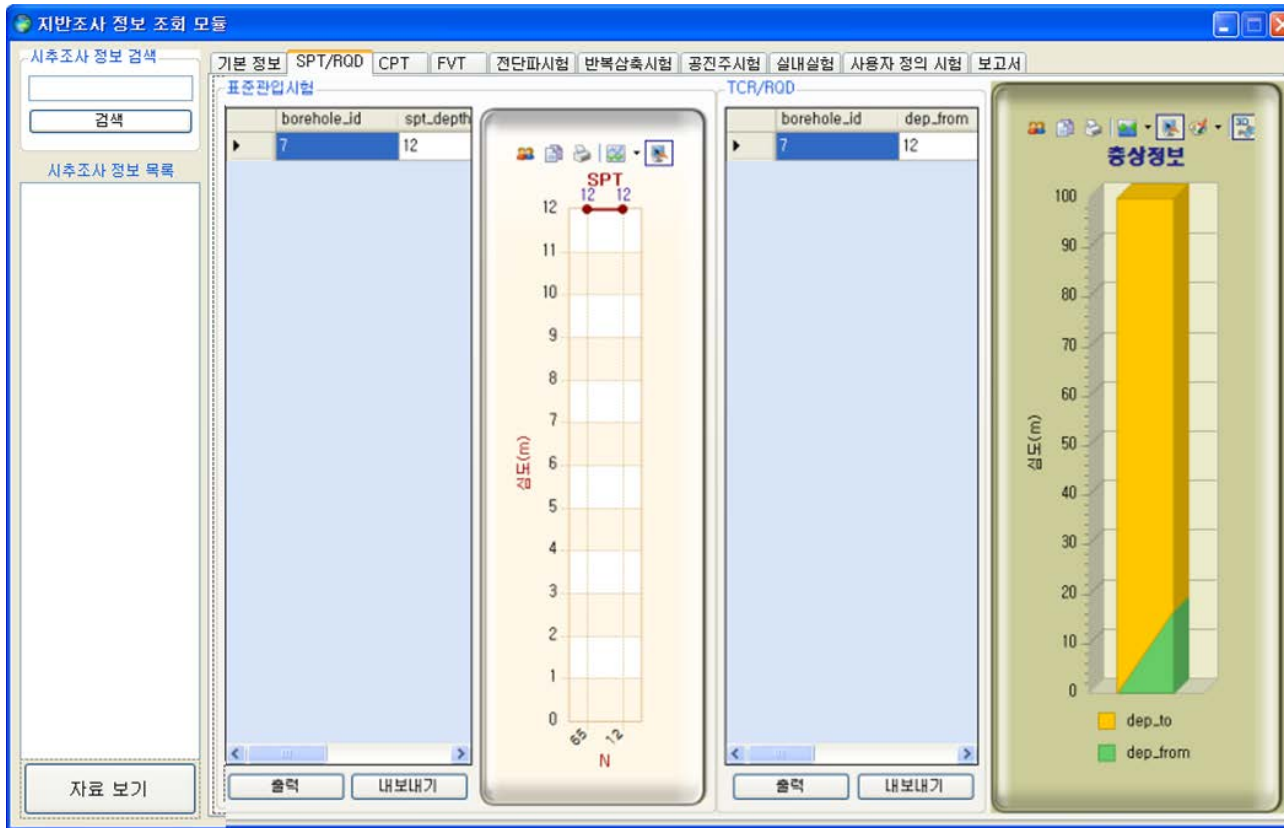


Figure A.2 Management module of geotechnical investigation information–SPT and RQD/TCR information

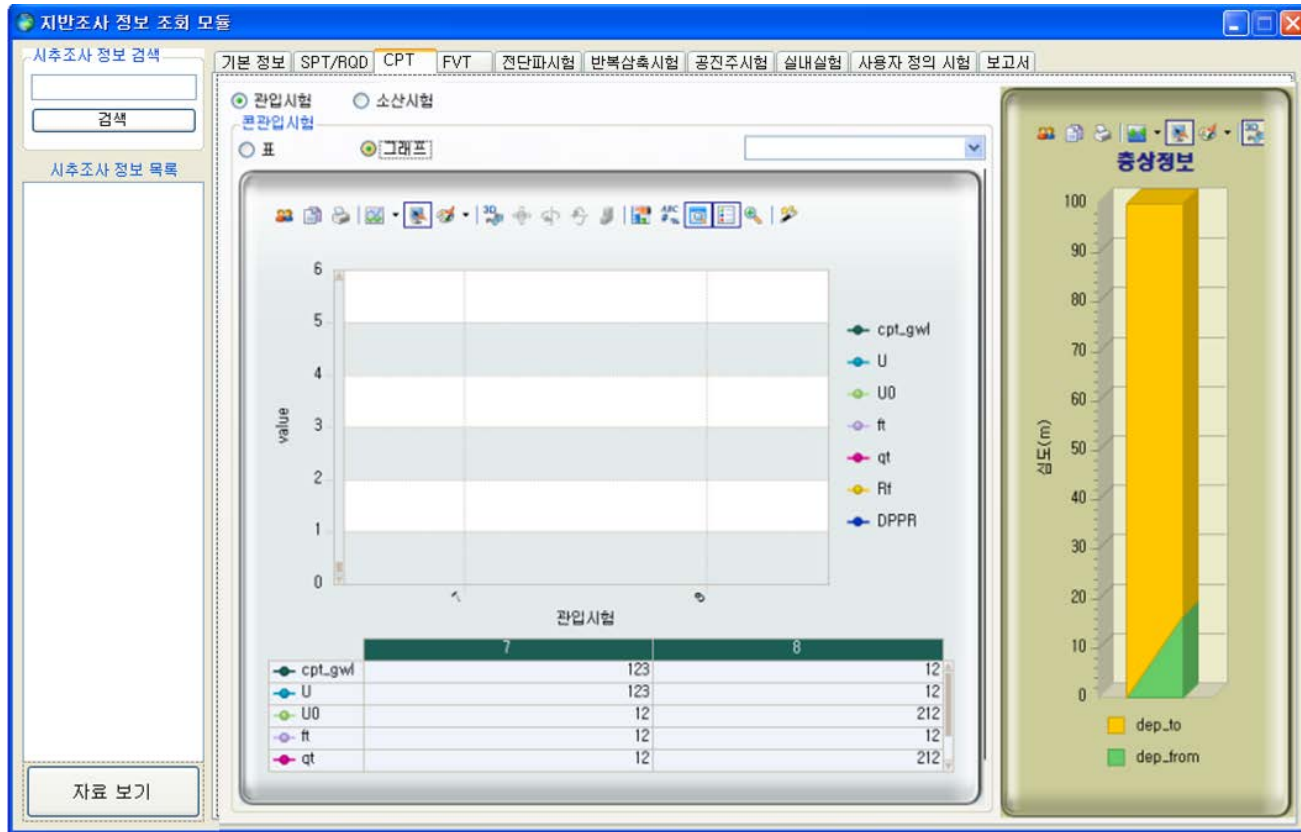


Figure A.3 Management module of geotechnical investigation information–CPT and CPTu information

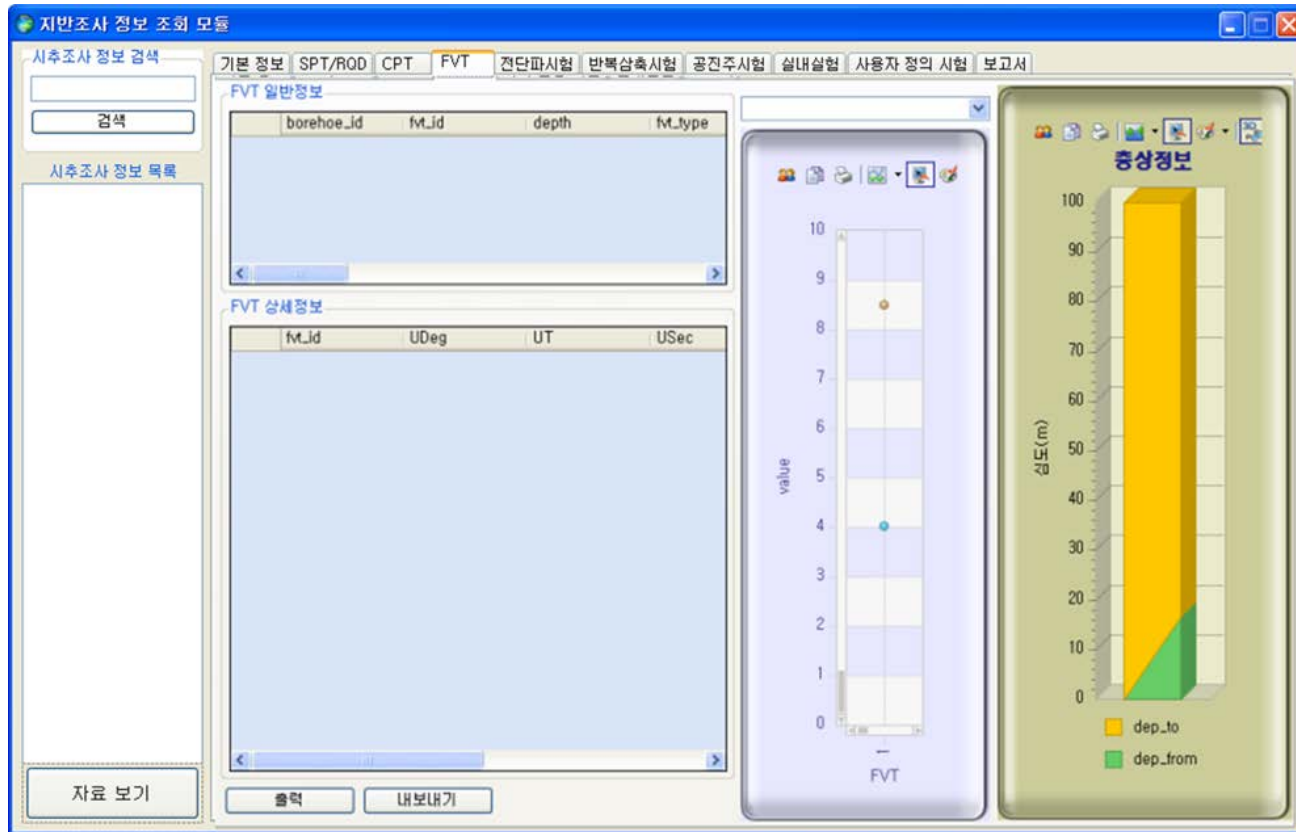


Figure A.4 Management module of geotechnical investigation information–FVT information

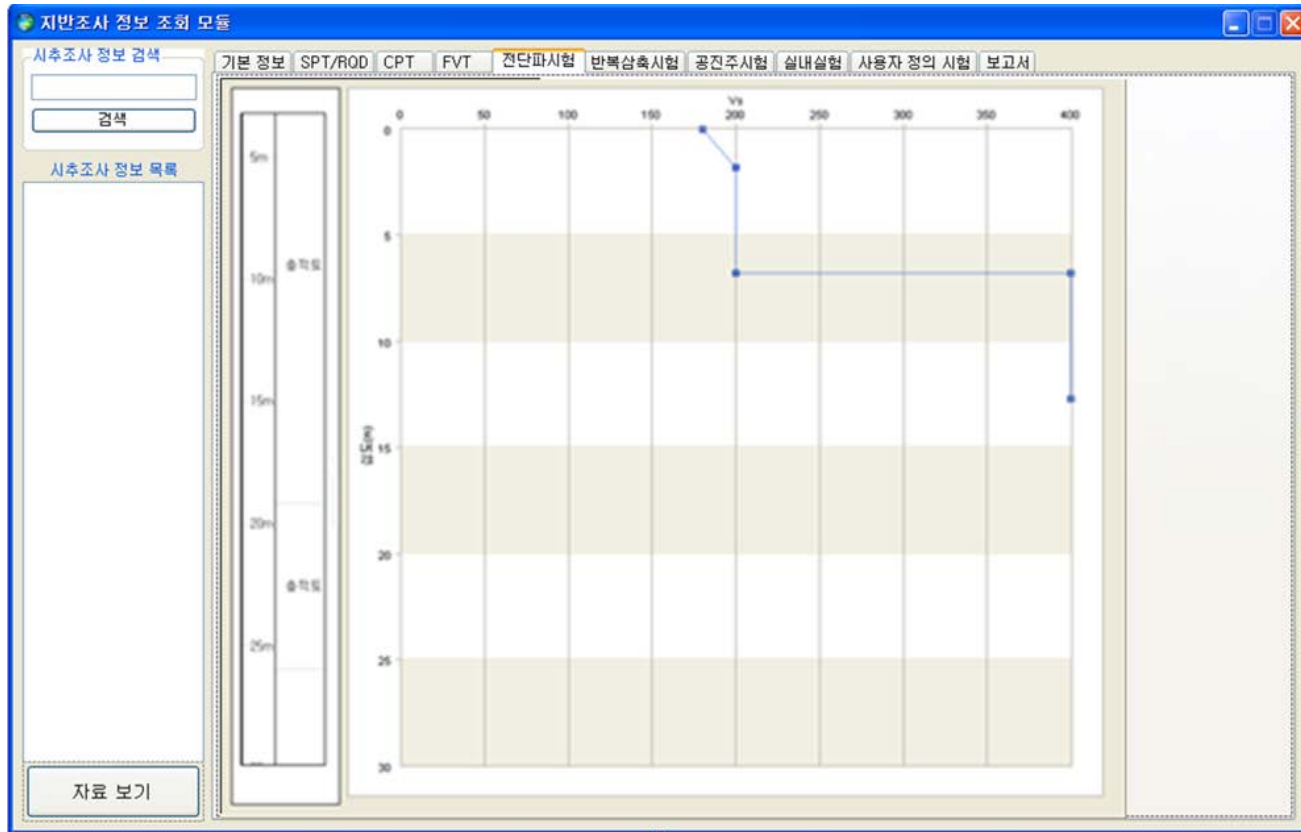


Figure A.5 Management module of geotechnical investigation information–shear wave velocity test information

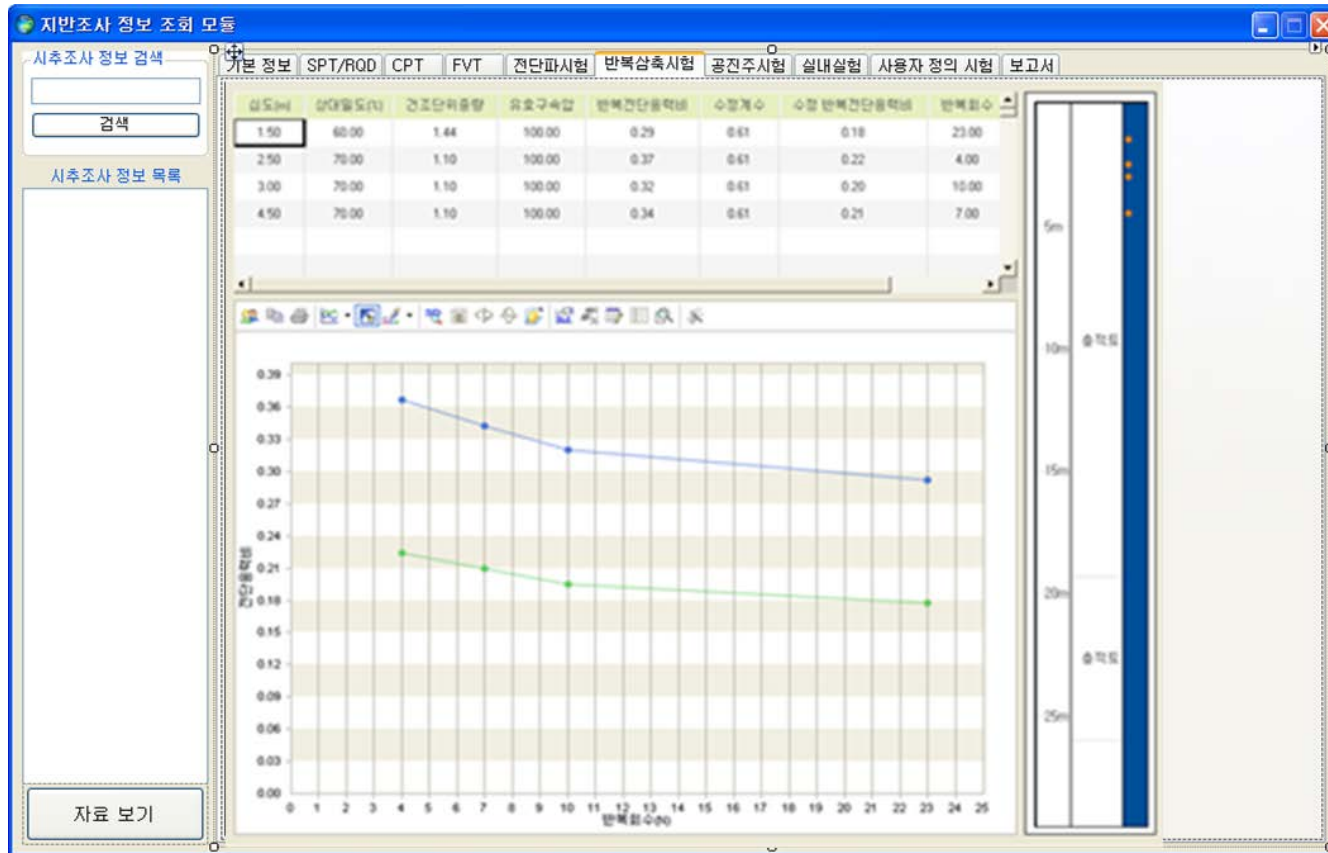


Figure A.6 Management module of geotechnical investigation information–cyclic triaxial test information

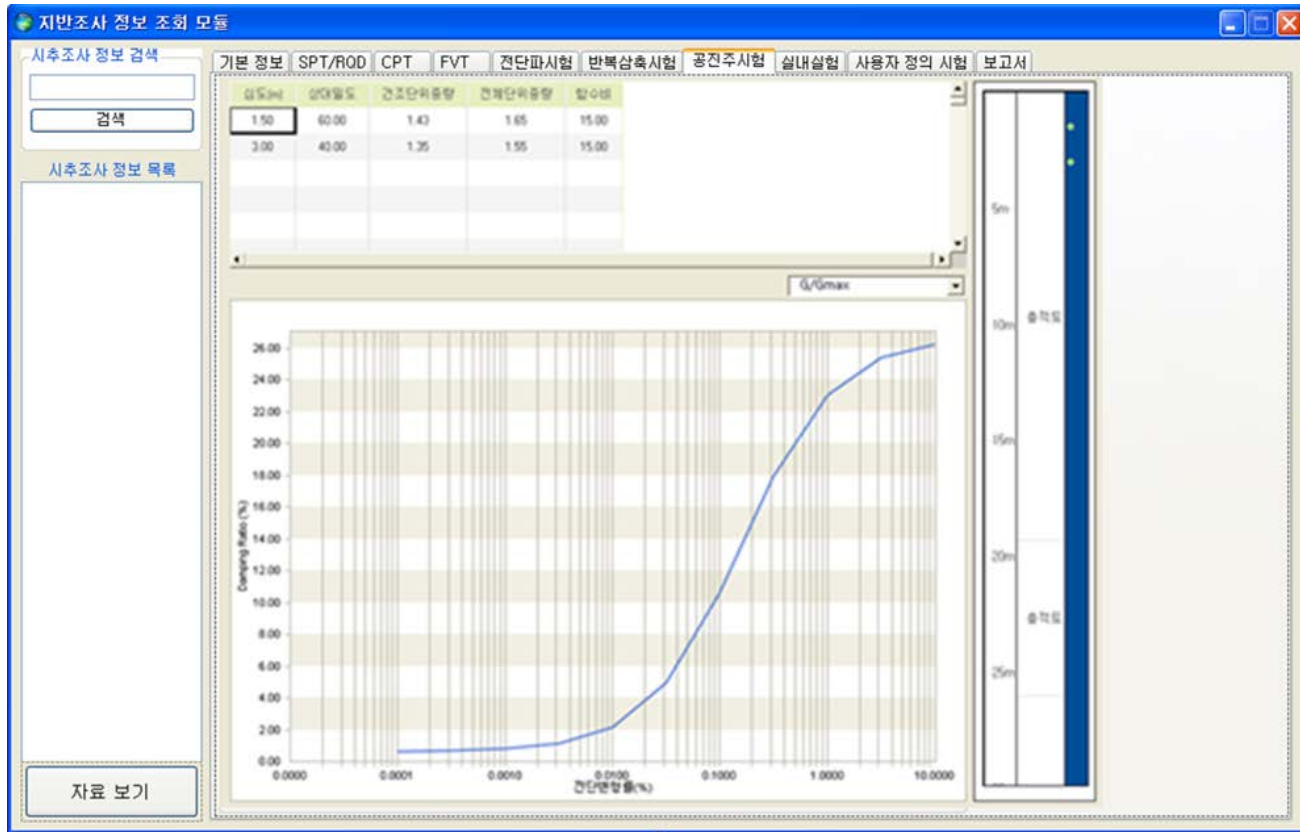


Figure A.7 Management module of geotechnical investigation information–Resonance column test information

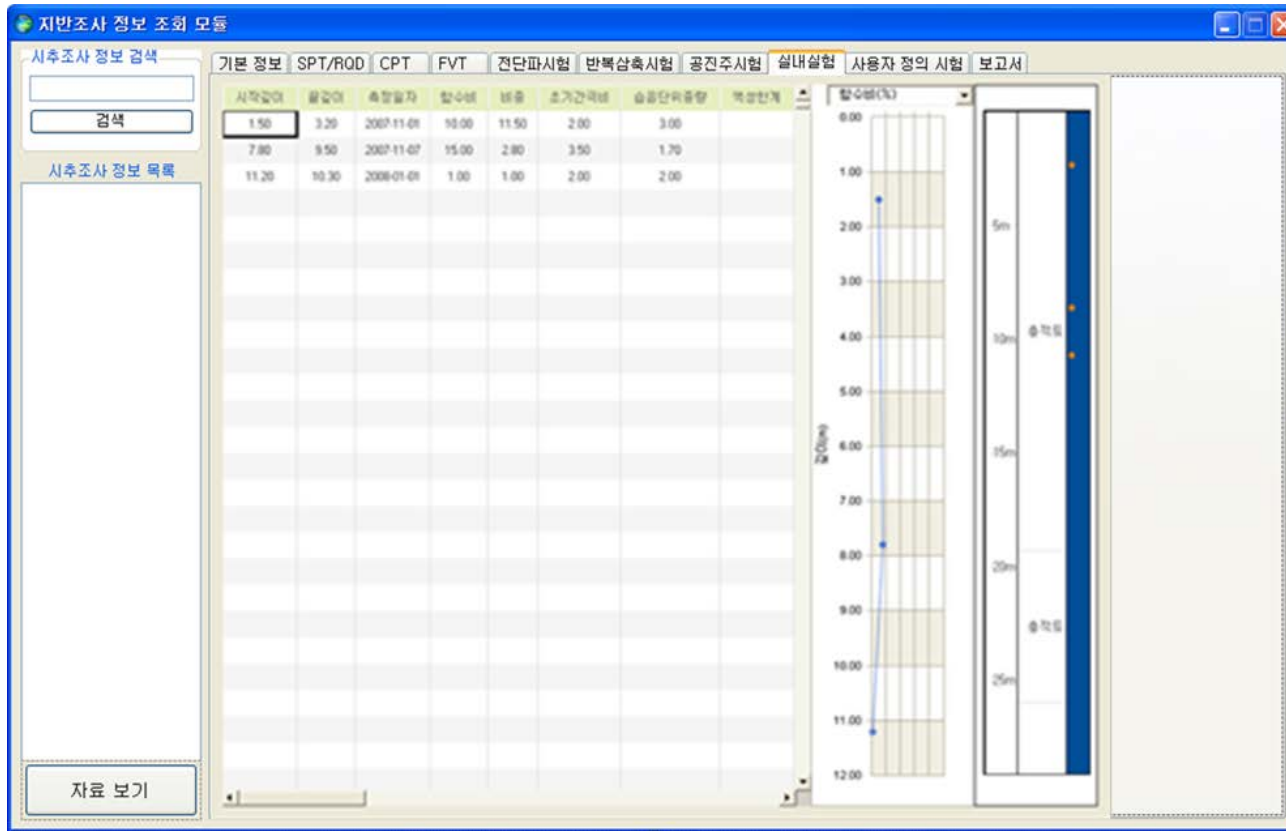


Figure A.8 Management module of geotechnical investigation information–engineering parameters

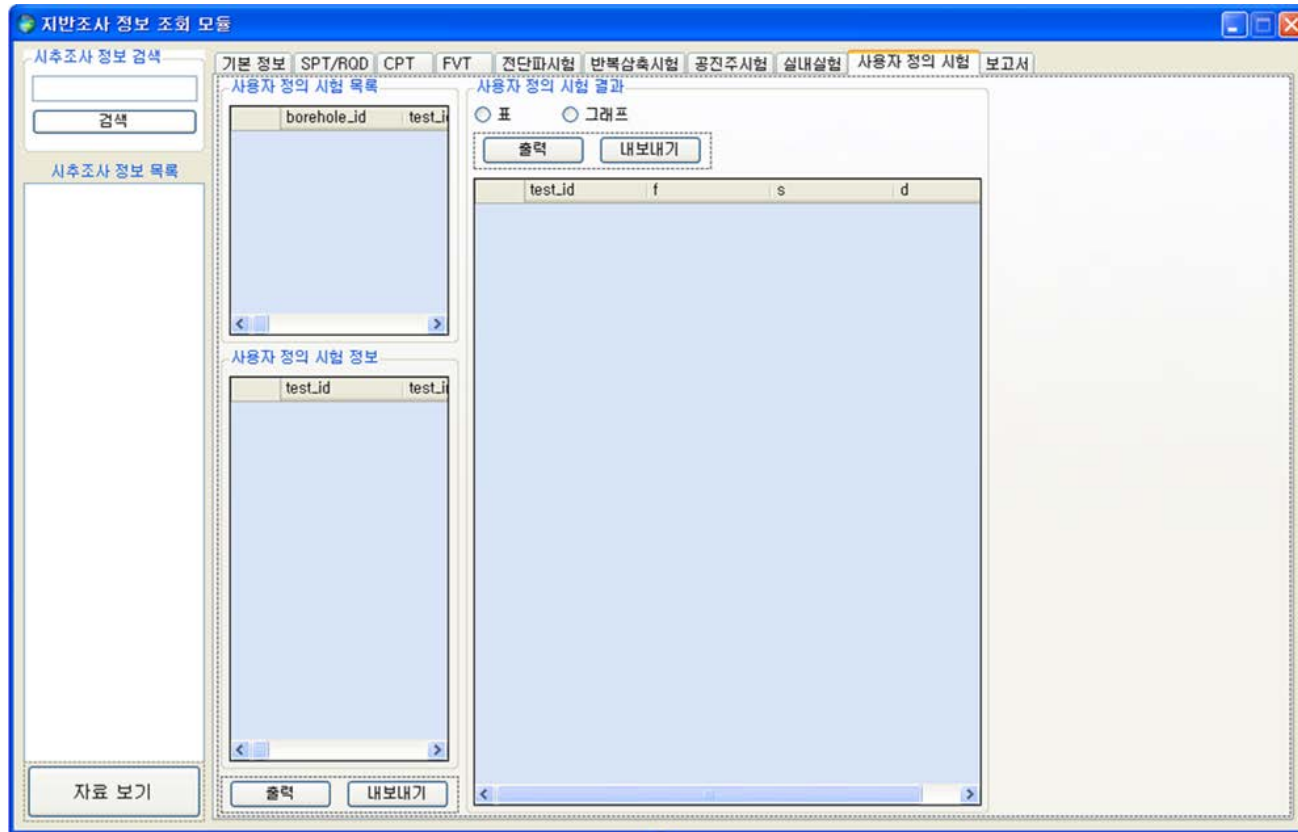


Figure A.9 Management module of geotechnical investigation information–user-defined test information

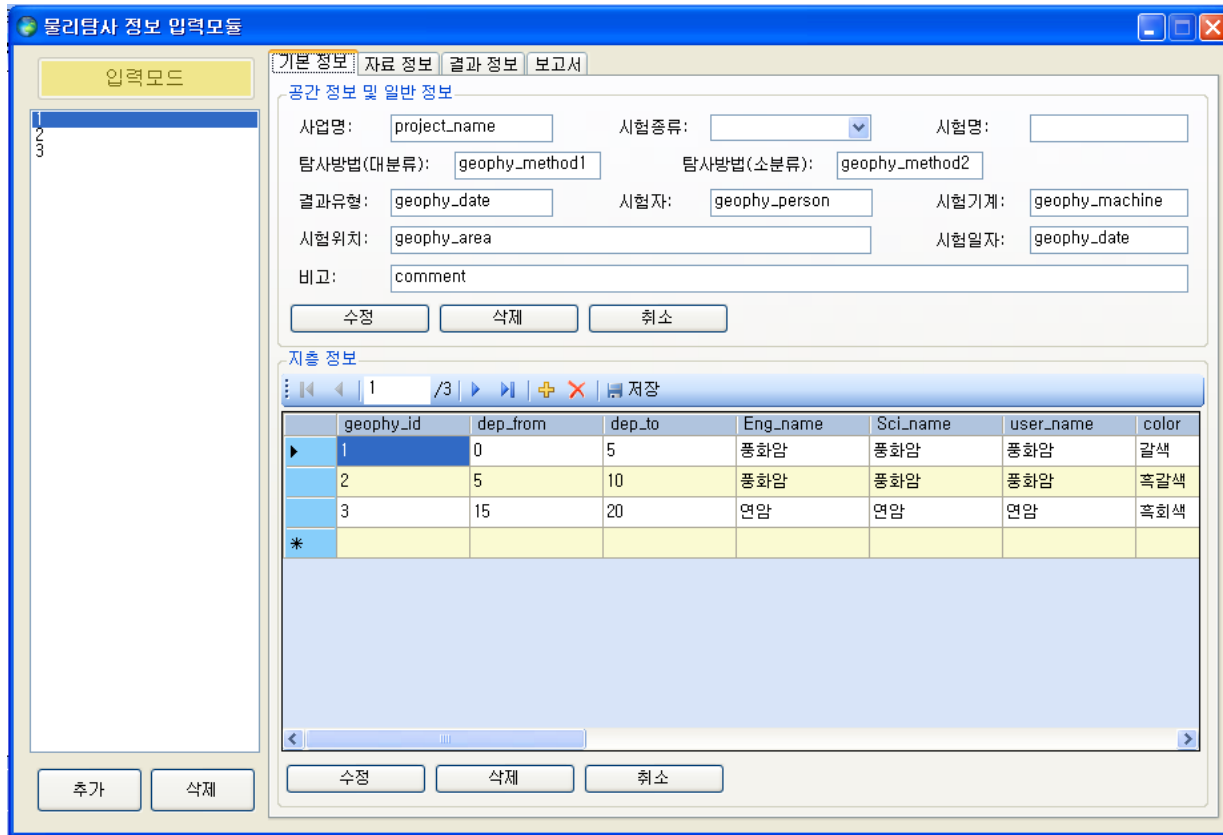


Figure A.10 Management module of geotechnical investigation information–geophysical test condition information

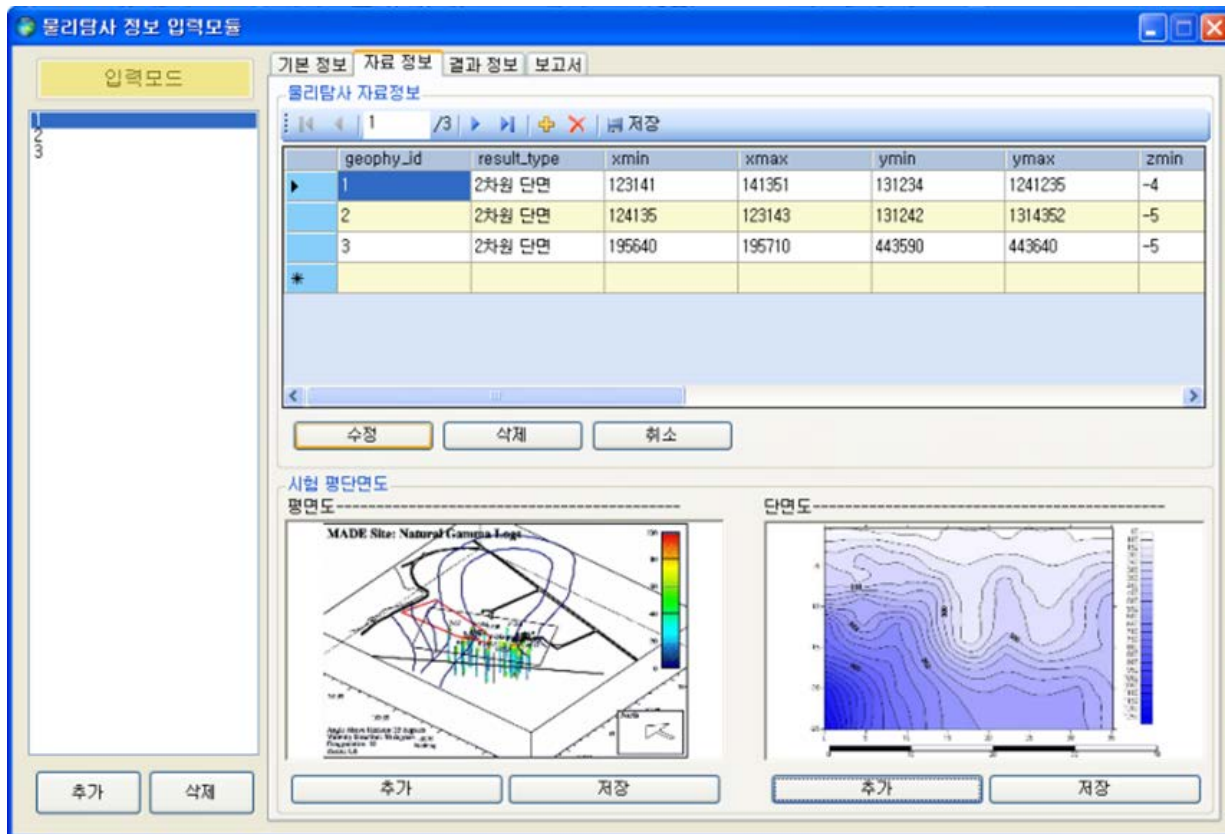


Figure A.11 Management module of geotechnical investigation information–geophysical tomography information

초 록

최근 국내외적으로 지진발생 빈도와 규모가 증가하고 있으며, 이에 따른 지진과 지진재해에 관한 관심과 우려가 증대되고 있다. 이에 따라 구가기반시설을 대상으로 지진발생 및 예상피해 규모를 사전에 예측할 수 있는 시스템의 개발이 시도되고 있다. 그러나 지반과 구조물의 내진 성능을 체계적으로 평가하고, 지진발생 시에 지진계측 정보를 연계함으로써, 지진재해를 실시간으로 예측하는 기술 개발은 미비하다.

본 연구에서는 지진발생 시에 지반공학적 지진재해를 준실시간으로 평가할 수 있는 체계를 수립하고, 이를 바탕으로 GIS기반의 지반공학적 공간그리드 정보를 활용한 지진재해평가 통합정보화 시스템을 개발하였다. 평가 시스템은 데이터베이스(DB)를 중심으로 현장 자료를 표준화하여 DB화할 수 있는 입력 모듈과, 신뢰도가 확보된 3차원의 지반정보를 결정할 수 있는 지구통계학적 3차원 통합분석 모듈, 부지응답 특성을 고려함으로써 액상화와 구조물 취약도를 평가할 수 있는 실시간 지진재해평가 모듈, 그리고 3차원 출력 및 가시화 모듈로 구성된다. 먼저 입력모듈을 통해 지형, 지반, 구조물 정보와, 실시간의 지진계측 정보를 공간정보와 연계하여 DB(geodatabase)에 입력하며, 구축 DB는 국가지진관측망 서버에 탑재되어 운용 중에 있다.

지구통계학적 3차원 통합분석 방법 및 모듈에 따라, 지반정보 중 시추조사 자료의 신뢰도 확보를 위해 이상치 검증기법(교차검증, 극한분포)을 개발하였으며, 이를 이용하여 시추조사 자료를 최적화한다. 최적화된 시추조사 자료와 함께 인접 영역에서 확보한 물리탐사 토모그래피를 통합 활용할 수 있도록 지시자 크리깅 기법을 통한 3차원

통합분석 방법을 개발하였다. 끝으로 지진재해평가 방법과의 연계를 위해 3차원 지반정보를 세분화하여 지반동적 특성값을 부여함으로써 지반공학적 공간그리드를 구축한다.

구축된 3차원의 지반공학적 공간그리드를 바탕으로 준실시간으로 지진재해를 평가할 수 있는 방법 및 모듈을 개발하였다. 대상영역의 부지응답 특성을 고려하기 위해, 계측된 암반가속도를 입력함으로써, 실시간으로 지반의 최대가속도를 결정할 수 있는 방법을 개발하였다. 이후 액상화 가능지수(LPI)를 이용하여 실시간으로 액상화 피해 정도의 공간분포를 평가할 수 있는 방법과 구조물의 취약도 함수와의 연계를 통해 구조물 손상도를 실시간으로 평가할 수 있는 방법을 개발하였다.

수립된 지반공학적 지진재해평가 체계에 따라 지진발생 시에 자동화된 일련의 지진계측 정보 연계 및 신속한 재해평가가 가능하도록 GIS기반의 통합정보화 시스템 프로그램을 개발하였다. 개발시스템의 적용성 검증 차원에서 국내 주요 향만지역(인천향, 부산향, 부산신향)을 대상으로 지진재해 평가 시뮬레이션을 수행하였으며, 즉각적인 재해결과를 예보할 수 있었다. 본 개발 시스템은 국가지진관측망에 탑재되어, 향후 지진발생 시에 지진재해를 선제적이고 즉각적으로 예보함으로써 합리적인 대응 및 복구방안 수립의 기초자료로써 활용되고 있다.

주요어: 통합시스템, GIS, 실시간 지진재해평가, 이상치 검증, 지구통계학적 3차원 통합, 부지응답, 액상화 피해, 구조물 취약도

학번: 2008-21020